Macroevolution across a changing Australian landscape

Ian G. Brennan

Supervised by:
J.Scott Keogh

Division of Ecology & Evolution

Research School of Biology

The Australian National University

A Thesis Submitted

for the Degree of

Doctor of Philosophy

February 2019

The research presented in this thesis is my own original work except where due reference is given. Three of four chapters are co-authored, and unless otherwise noted, the authorship order indicates the intellectual contribution and workload. No part of this thesis has been submitted for any previous degree.

Ian G. Brennan

Acknowledgements

It's easy to get caught up in a PhD and forget to say thanks along the way. Here it goes:

None of this would have been possible without the overwhelming generosity of my supervisor Scott Keogh. For four years, Scott has encouraged nearly every rabbithole I've gone chasing down. He has set an example for me of how to balance work and life, and also how to navigate academia with grace, dignity, and modesty.

Scott also has the amazing ability to build communities, and a magnetic touch for pulling in intelligent, kind, and interesting people. The entire Keogh Lab has been so vital to my success and I want to thank them all for sharing their time. Mitzy Pepper, Damien Esquerre, Carlos Pavon Vazquez, Marta Vidal Garcia, Emma Sherratt—it's been incredible to be surrounded by such smart and driven people. This extends to Moos Blom, Josh Penalba, Leo Tedeschi, Je Fenker Atunes, Ana Silva, Bec Laver, Huw Ogilvie, Christiana McDonald-Spicer, Dan Rosauer, Nick Matzke, Paul Oliver, and Craig Moritz, thanks for welcoming me into your lab, and exposing me to new ideas.

Being in a community as gifted and tight as E&E has other benefits. A number of people in our department have let me ask them lots of questions about ideas, methods, and fields that interested me. Alex Skeels, Rusell Dinnage, and Marcel Cardillo have gracefully fielded a lot of these questions, particularly in the last few months. And what's life without friends? We've turned a sea of international students into a family at ANU. Thank you Regi, Coni, Ili, Pip, Dani, Lalo, Frances, Nina, Liam, Tom, Robyn, and everyone else who helped make this a home. Audra, Jan, Jack, and Wes—they don't call you the *Dream Team* for nothing.

Zoe, there are too many things to thank you for. Most importantly, thank you for joining me on this journey. To my parents and sister, your love and support has kept me warm and content in my time on the other side of the globe. Thank you for giving me this opportunity.

Abstract

Over geological time, the earth's surface and climate have changed, rearranging continental plates and oscillating between a hothouse and snowglobe. These changes have left lasting impressions on the diversity, richness, and distribution of earth's inhabitants. Identifying evolutionary commonalities as a result of these events is one of the main aims of the field of macroevolution. It is also the main theme which unites my thesis: investigating the influence of changes to the Australian climate and landscape on the organisms that call Australia home. Empirically, this has required extenstively sampling Australian vertebrate groups for phylogenetic, distributional, ecological, and morphological trait data. Methodologically, this has required implementing and building phylogenetic comparative methods to better understand the diversity that surrounds us.

As a continent, Australia gained its independence somewhere between 40–30 million years ago when it separated from Antarctica and began drifting north towards Asia. Prior to this, the Australian plate existed alongside South America, Africa, and India, as part of the supercontinent Gondwana. In the intervening millions of years, Australia has remained isolated, and so even comparatively recent immigrant lineages have speciated *in situ*, resulting in a number of iconic endemic terrestrial vertebrate radiations. These radiations are great for comparative studies because they provide replicated groups which have diversified under similar environmental influences. Importantly though, they differ in absolute diversity, ecology, and behavior. My research has investigated how changes due to the isolation of the Australian plate, continental aridification, and grassland expansion have impacted the Australian fauna.

In my opening chapter I discuss how the separation of Australia from Antarctica may have precipitated a mass extinction event in a relatively understudied group of lizards, the pygopodoid geckos. Next I present evidence that the Miocene aridification of Australia likely reduced the rate of phenotypic evolution of terrestrial vertebrates by facilitating allopatric speciation and niche conservatism. In the following chapter I test the

hypothesis that the diversification of macropod marsupials is linked to the Plio-Pleistocene expansion of C_4 grasses. Finally, I present the idea that the immense disparity in body size of Australian varanid lizards is the result of character displacement and competition occurring on a continental scale.

Ultimately, the inferences we can draw about evolutionary changes occurring on deep time scales are exciting because they are often intuitive. In no place else does this seem truer than in Australia, which is a natural laboratory for macroevolutionary studies.

Table of Contents

To my parents and sister.

For always supporting a little herpetologist.

And to Ai

Who taught me weird was cool.

Introduction

Much of biology involves putting the things we see on a daily basis into an appropriate temporal and evolutionary context. We wonder how similar this year's flu will be to the last, how is it possible that chihuahuas and rottweilers belong to the same species, or why birds got feathers and we ended up with hair. We do this for many reasons, but perhaps most genuinely to appreciate the diversity around us. In order to answer these questions, we use different facets of evolutionary biology such as population genetics, phylogenetics, and comparative methods to untangle the branches of the tree of life, working backwards from the leaves to the roots. On deep timescales or above the species level, we refer to this as macroevolution.

The field of macroevolution has been around since at least the 1920's [1], but has expanded enormously since the arrival of phylogenetic comparative methods (PCMs) in the 1980's [2]. PCMs have been a boon to the field because they help us to identify and make sense of evolutionary patterns by linking them with the processes dictating global and local biodiversity. As a result, macroevolutionary methods have also taken off in popularity, and enabled the next generation of evolutionary biologists to approach both new and longstanding questions [3].

Foundational macroevolutionary studies generally focused on trends in richness and phenotypic diversity using the fossil record [4–6]. Recent research has instead turned to patterns and trends in neontological data to describe the tempo and mode of evolution through time [7,8]. This transition came alongside the growth of comparative methods, encouraging many evolutionary questions to account for the relationships among the focal organisms. However, resolving the phylogenetic affinities between organisms is not a trivial task, and is of course itself an entire field of biology. Phylogenetics in turn, has also expanded rapidly as a result of the availibility of genome-scale data, and a shift away from morphological data for inferring species relationships. These new data have their

own difficulties, but have opened new doors in phylogenetics and macroevolution. In this thesis I present a range of phylogenetic resources from Sanger-sequenced mitochondrial, to nuclear exon-capture, and morphological data. I use these data both independently and holistically, implementing a variety of exciting methods that help to take advantage of the overwhelming scale and distinctness of these data types.

After building a stable phylogenetic hypothesis, we can investigate a host of questions regarding the tempo and mode of evolutionary processes and how these relate to observable patterns. Across the globe, shifts in climate and biome turnover have long been linked to diversification trends in organismal groups [9,10]. Identifying these commonalities in response to shared influences strengthens the correlations between patterns and their drivers. Australia, which has been isolated for roughly 40 million years, offers a unique opportunity to look for such trends. As an island continent, Australia has both the geographic scale to look at patterns across a range of habitats, and the diversity necessary to test ideas with sufficient confidence and power. Many Australian organisms belong to iconic radiations which have either rafted with the continent since its days with Gondwana, or more recently emigrated from Asia. This also provides a temporal element, allowing us to compare groups of varied ecologies, richness, and ages.

Here, I present four studies that discuss the macroevolutionary patterns of Australian vertebrates. These cover a broad period of the Australian faunal history, spanning the continent's isolation in the late Oligocene, to Miocene aridification, and Pliocene habitat turnover. Taken together, this thesis examines the phylogenetic, biogeographic, and ecological patterns of some of the continent's most iconic fauna, contributing novel insights into the diversification of these amazing groups. In the process, I also design novel empirical frameworks for macroevolutionary studies, extending available PCMs. My findings contribute to our understanding of the evolution of Australia's unique fauna, and provide a comparison for empirical and theoretical studies elsewhere.

Chapter 1:

Mass turnover and recovery dynamics of a diverse Australian continental radiation

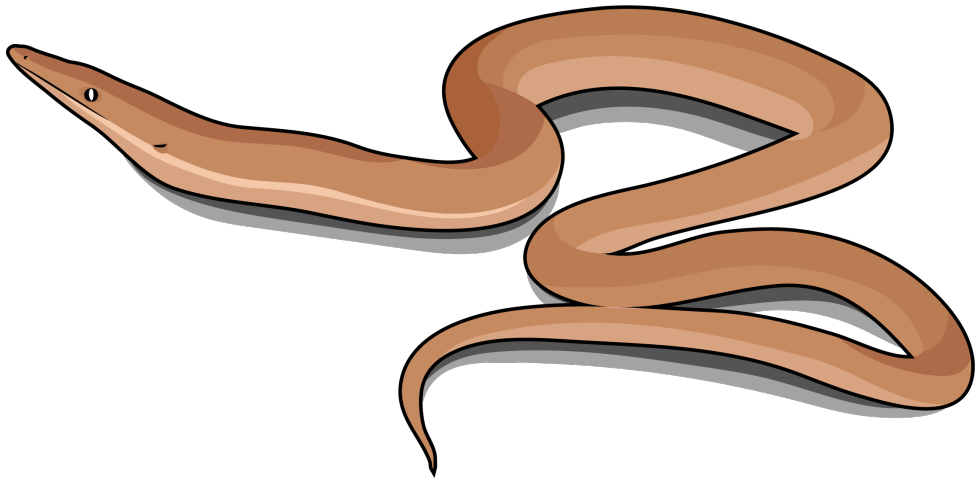

ORIGINAL ARTICLE

doi:10.1111/evo.13207

Mass turnover and recovery dynamics of a diverse Australian continental radiation

Ian G. Brennan[1,2] and Paul M. Oliver[1]

[1]*Division of Ecology and Evolution, Research School of Biology, The Australian National University, Canberra, ACT, Australia*

[2]*E-mail: ian.brennan@anu.edu.au*

Received December 6, 2016
Accepted February 6, 2017

Trends in global and local climate history have been linked to observed macroevolutionary patterns across a variety of organisms. These climatic pressures may unilaterally or asymmetrically influence the evolutionary trajectory of clades. To test and compare signatures of changing global (Eocene-Oligocene boundary cooling) and continental (Miocene aridification) environments on a continental fauna, we investigated the macroevolutionary dynamics of one of Australia's most diverse endemic radiations, pygopodoid geckos. We generated a time-calibrated phylogeny (>90% taxon coverage) to test whether (i) asymmetrical pygopodoid tree shape may be the result of mass turnover deep in the group's history, and (ii) how Miocene aridification shaped trends in biome assemblages. We find evidence of mass turnover in pygopodoids following the isolation of the Australian continental plate ~30 million years ago, and in contrast, gradual aridification is linked to elevated speciation rates in the young arid zone. Surprisingly, our results suggest that invasion of arid habitats was not an evolutionary end point. Instead, arid Australia has acted as a source for diversity, with repeated outward dispersals having facilitated diversification of this group. This pattern contrasts trends in richness and distribution of other Australian vertebrates, illustrating the profound effects historical biome changes have on macroevolutionary patterns.

KEY WORDS: **Aridification, Australia, geckos, extinction, macroevolution.**

The field of macroevolutionary study has grown tremendously as novel analytical methods and ever-larger phylogenies help to reveal patterns of diversity through space and time. Similarly, our rapidly improving understanding of climate history provides the opportunity to link together climatic and evolutionary histories, to directly test the impact of paleoclimate regimes on trends in diversification. The ability to investigate more sophisticated questions across groups of varied species richness, age, and distribution, has revealed consistent macroevolutionary patterns in response to climatic change, including the influence of the tempo and intensity of climatic change (Stadler 2011a; Crottini et al. 2012). Additionally, we can now more accurately test how macroevolutionary mechanisms affect diversification, and compare similar and asymmetrical trajectories of clades under shared climatic histories (Hunter 1998). The accumulating body of evidence suggests that heterogeneity is ubiquitous in phylogenetic, spatial, and temporal diversity. Realizing this, goals have shifted to identifying and testing for the causes of such heterogeneity.

Phylogenetic tree building methods have revealed heterogeneity as imbalance among (phylogenetic) or along (temporal) branches of the tree, initiating questions regarding the intrinsic and extrinsic drivers of such disparity. Imbalance in clade richness is often attributed to intrinsic organismal influences such as ecological differentiation and key innovation (Phillimore and Price 2008; Rabosky 2013; Scantlebury 2013). Conversely, temporal and distributional heterogeneity is frequently explained by extrinsic factors such as geographic and climatic change (Moen and Morlon 2014). Macroevolutionary signature of climatic change however, is highly dependent upon their relative rate and intensity of the variation. For example, rapid perturbation at the K-Pg boundary resulted in global mass extinction of vertebrate groups and unilaterally changed terrestrial assemblages (Halliday et al. 2016). In contrast, protracted environmental changes of the Late Jurassic and Early Cretaceous caused heterogeneous turnover and replacement (Tennant et al. 2016). Together, historical processes of differing scales help explain patterns seen in contemporary diversity.

Rapid cooling and glaciation at the Eocene-Oligocene boundary (EOb, ~34 Ma) has been implicated in considerable biotic turnover globally (Zanazzi et al. 2007; Stadler 2011a; Sun et al. 2014). In Australia, this period demarcates a split from Antarctica and the opening of the circumpolar current, initiating a new period of in-situ diversification (Williams 1984). However, no empirical studies have investigated the impact of rapid (duration <100,000 years) EOb global cooling on the macroevolution of Australian taxa, perhaps due to the paucity of extant radiations that predate the EOb, and limitations of a poor fossil record. Instead, patterns of spatial and phylogenetic richness are more often associated with mid-Miocene continental expansion of arid habitats (Byrne et al. 2008) and contraction of forested systems (Byrne et al. 2011). In contrast to the dramatic cooling of the EOb, the better documented decline of Australian mesic biomes was a more gradual aridification following the Middle Miocene Climatic Optimum ~15 Ma (Martin 2006).

Among biome types, arid climes have traditionally been considered harsh, physiologically exclusive habitats (Axelrod 1967). This has led to the belief that arid regions are species depauperate sinks of diversity (Crisp et al. 2009). Miocene aridification of Australia has been implicated in fracturing and extinction of mesic-adapted terrestrial and aquatic vertebrates (Potter et al. 2012; Unmack et al. 2013; Catullo and Keogh 2014). In contrast, arid biome expansion has been identified as integral in the rapid proliferation of arid-tolerant squamate reptiles (Jennings et al. 2003; Rabosky et al. 2007; Shoo et al. 2008). The variable response of Australian biota to aridification draws attention to the importance of investigating the influence of changing climate on contrasting geographic (global vs continental) and temporal (ancient vs contemporary; rapid vs gradual) scales.

Squamate reptiles represent Australia's most species-rich vertebrate assemblage, comprising more than 1000 species. The varied ages of Australian squamate radiations make them valuable for investigating patterns of continental and island biogeography, invasion, and diversification. Here, we focus on the oldest near-endemic Australian squamate group, pygopodoid geckos, a Gondwanan (crown: 50–70 Ma) suprafamily (families: Carphodactylidae, Diplodactylidae, Pygopodidae) of morphologically and ecologically diverse lizards. Pygopodoids present an ancient set of codistributed sister clades and an ideal system for investigating the variables influencing macroevolutionary trends across closely related radiations.

To address the impact of historical climate change, we have assembled the most complete (>150 Australian spp.; >90% species richness) fossil-calibrated phylogeny of the Pygopodoidea to date. We first investigate the macroevolutionary trajectory of these geckos in the context of global climate change using Bayesian methods to determine if (i) temporal asymmetry in the pygopodoid tree identified by Oliver and Sanders (2009) provides evidence of mass turnover at the EOb, and if so, was (ii) postextinction recovery consistent among families? Second, we question if regional trends in (iii) habitat transitions and (iv) biome-specific diversification rates have been influenced by continental aridification. Our analyses of rates and timing of pygopodoid gecko diversification support a signature of profound turnover near the EOb. Subsequent expansion of arid habitats coincides with elevated diversification in and transition out of this biome, highlighting the influence of continental aridification on Australian macroevolution and contemporary diversity.

Materials and Methods

PHYLOGENETIC AND DISTRIBUTIONAL DATA

We compiled a multilocus dataset of mtDNA (ND2) and nDNA (RAG1, RAG2, C-mos, PDC, ACM4, DYNLL1) markers for 155 ingroup Australian pygopodoid taxa, and 36 outgroup taxa stretching out to *Gallus gallus* (Table S1). Sequences were compiled largely from prior phylogenetic study of Australian geckos (Jennings et al. 2003; Oliver et al. 2007, 2009; Doughty et al. 2010; Oliver et al. 2010; Oliver and Bauer 2011; Pepper et al. 2011; Oliver et al. 2012, 2014; Brennan et al. 2016), and broad-scale investigations into Gekkotan systematics (Gamble et al. 2012, 2015). Taxon coverage among loci varies (Table S1), but is greatest for the mitochondrial locus ND2 (95%), and generally lower for nDNA loci (RAG1–68%, RAG2–65%, PDC–50%, DYNLL1–10%, C-mos–44%, ACM4–42%). Ingroup sampling represents the most inclusive Australian pygopodoid dataset to date (155 spp.; 90.5%), including recognized, molecularly divergent, cryptic lineages, that are likely to be elevated to species level (Doughty et al. 2016; Oliver and Doughty 2016).

For analyses of biome-associated diversification, we partitioned Australia into five discrete biomes that capture both accepted definitions (observed patterns of biological differentiation) and a widely used objective climate classification scheme (modified Köppen-Geiger climate classification; Stern et al. (2000)). Five-region classification is as follows: (i) Savannah—(Equatorial and Tropical in Stern et al. (2000)) and largely corresponding to savannah biome in northern Australia; (ii) Temperate—largely corresponding to the temperate biomes of previous analyses and covering broad areas in south-eastern and south-western Australia; (iii) Subtropical—corresponding to widely isolated areas on the east and west coast of Australia; (iv) Arid—consisting of both arid and surrounding semi-arid regions and "grassland" regions of Stern et al. (2000) and covering the vast majority of Australia (77.8%); (v) Wet forest—highly relictual pockets of generally fire sensitive forest dotted along Australia's east coast (Byrne et al. 2008; Byrne et al. 2011). This fifth category was not captured by Stern et al. (2000), but reflects both present day and historical data that indicate regions of permanently wet

forest have a phylogenetically and ecologically distinctive endemic biota, widely considered to represent the vestiges of a formerly much more widespread mesic adapted biota (e.g., Byrne et al. (2011)). Distributions of all taxa were mapped out against the simplified climate classification using the spatial portal of the Atlas of Living Australia (http://spatial.ala.org.au) and taxa occurring in more than one biome were coded as such. Several genera (*Aprasia*, *Crenadactylus*, arid zone *Oedura*) have members that outwardly code to the arid zone, but likely persist in refugial pockets of mesic habitat (Oliver et al. 2010). To account for the potential for this to bias analyses toward arid biomes, we established a second biome scoring, which incorporates mesic distribution of these taxa, and refer to it as the "mesic refugial" model in downstream biogeographic analyses.

DIVERGENCE TIME ESTIMATION

Divergence dates were estimated in a two-step process using an uncorrelated relaxed molecular clock and birth-death tree prior as implemented in BEAST v.1.8.3 (Drummond et al. 2006; Drummond and Rambaut 2007; Gernhard 2008). An initial BEAST analysis was run on the multilocus nuclear dataset alone, and was constrained by a number of fossil and secondary calibrations (Table S2). We ran two independent analyses for 300 million generations, sampling every 100,000 generations, and upon completion, inspected, and combined the log files using Tracer (Rambaut et al. 2014) and LogCombiner (Rambaut and Drummond 2007) to ascertain that the posterior, likelihood, and all priors reached convergence (ESS>200). Investigations into phylogenetic rate heterogeneity, including mass extinction, are directly linked to divergence-time estimates. Temporal bias in dated trees caused by poorly specified fossil calibrations may be passed on to bias in inference and timing of diversification heterogeneity, so to investigate the robustness of our divergence time estimates to our fossil calibrations, we iteratively removed each calibration and reran the dating analysis. Upon completion, we created a maximum clade credibility (MCC) tree from a set of post burn-in trees for each new dating scheme, and compared key nodes against the nuclear only MCC tree and a set of 100 trees randomly pulled from the posterior using paleotree (function "compareNodeAges") (Bapst 2012).

Exclusion of mtDNA from our initial dating analysis aimed to alleviate the potential for the combination of saturated mtDNA data and old outgroup calibrations to inflate divergence date estimates (Dornburg et al. 2012). From the nuclear only analysis, we extracted the range of generic, intergeneric, and family-level divergence events as 95% CIs from 100 random post burn-in trees via TreeAnnotator. These CIs were applied as secondary calibrations (Table S2) to the combined-locus mtDNA/nDNA analysis, and used in combination with the same fossil calibrations applied previously. Presence and implementation of secondary calibrations were largely dependent upon nuclear sampling, and applied to provide consistent constraint across the pygopodoid tree. All secondary calibrations, with exception of the Archosauria + Lepidosauria split, were implemented with uniform distributions to allow for the high degree of uncertainty of estimates within the 95% CI.

TEMPORAL RATE HETEROGENEITY AND MASS TURNOVER

To test for temporal variation in diversification rates, including Oligocene mass turnover, we used CoMET (May et al. 2015), as implemented in TESS (Höhna et al. 2016). CoMET is a Bayesian statistical method capable of identifying rate heterogeneity along the branches of a phylogeny. We used alternate methods of estimating diversification rates (TreePar, LASER, BAMM) to investigate the robustness of temporal diversification trends across methods, and results are included in Table 1 and Supplemental Materials (Table S4, Supplemental Methods). However, we rely largely upon our TESS results, because this framework is the only currently available method for jointly estimating diversifying rate shifts (λ, μ), and mass extinction (but see Laurent et al. 2015). TESS simultaneously runs simulations across multiple episodically varying birth-death models, and estimates the joint posterior distribution of shifts in rate of speciation (lambda—λ), extinction (mu—μ), and mass extinction events. In the episodic birth-death framework implemented by TESS, rates may change temporally along the tree allowing the timed placement of rate shifts and mass extinction events; however, rates among subclades at any given time remain fixed. Because all phylogenetic diversification analyses are sensitive to the estimated timing of divergence events, we implemented a sequential Bayesian approach to estimating diversification rates and mass extinction, by integrating over 100 trees randomly sampled from the post burn-in posterior distribution of our combined mito-nuclear BEAST analysis.

In TESS, occurrence of mass turnover is estimated as a function of magnitude (probability of survival), and like λ and μ, comparisons between the empirical tree and plausible models are evaluated by simulated reproducibility (Bayes factors and Posterior Probabilities). TESS additionally allows likelihood estimations (functions "tess.likelihood" and "tess.steppingStoneSampling"), to provide comparison across models and analytical programs (results: Table S4). To first investigate if there is phylogenetic support for mass turnover in our set of empirical trees, we constructed two pairs of competing models: (1) a constant-rate birth-death null model ($null_1$), and a constant-rate birth-death model (crbdME) that incorporates mass extinction (see: TESS package vignettes), and (2) a variable-rate birth-death (speciation rate shift $<$ 10 mya) null model ($null_2$), and a variable-rate birth-death (identical speciation rate shift) model with mass extinction (vrbdME). Using the same diversification and turnover parameters, we then estimated

Table 1. Summary of results of diversification and morphological rate analyses.

Macroevolutionary question	Method (function)	References	Settings	Results by taxonomic clade			
				Pygopodoidea	Carphodactylidae	core Diplodactylidae	Pygopodidae
Temporal heterogeneity in diversification (heterotachy)	TreePar (bd.shifts.optim)	(Stadler 2011a)	6 BD nested models, testing 0–5 rate shifts episodically	3 shifts located at 30 (↑), 8 (↓), and 4 (↓) Ma	1 shift (↓) in speciation at 3 Ma	2 shifts in speciation at 16 (↓) and 4 (↓) Ma	1 shift (↓) in speciation at 5 Ma
	TESS (tess.mcmc; tess.likelihood; tess.likelihood. rateshift)	(Höhna et al. 2016)	3 models (constant BD, episodically varying BD, exponentially decreasing BD) implemented with function tess.likelihood	Episodically varying BD, with 2 shifts, located at 7 (↓), and 4 (↓) Ma	Constant rate BD	Constant rate BD	Constant rate BD
	CoMET (tess.analysis)	(May et al. 2015)	rjMCC across episodically varying BD with mass extinction	Mass extinction at 30 Ma, and shifts in speciation rate at 8 (↓) and 4 (↓) Ma	1 shift (↓) in speciation at 3 Ma	2 shifts in speciation at 7 (↓) and 4 (↓) Ma	1 shift (↓) in speciation at 5 Ma
	Gamma statistic: APE (gammaStat)	(Pybus and Harvey 2000; Paradis et al. 2004)	Gamma statistic and two-tailed T test for significance	Diversification has significantly decreased through time	Diversification has significantly decreased through time	Diversification has significantly decreased through time	Diversification has significantly decreased through time
	LASER (pbtree; ltt95)	(Rabosky 2006)	95% CIs of 1000 trees modeled under PB and constant rate BD models	LTT falls below 95CI at 30 Ma for both PB and BD	3 shifts in speciation at 8 (↑), 5 (↓), and 3.3 (↓) Ma	2 shifts in speciation at 9.7 (↓), and 3 (↓) Ma	1 shift (↓) in speciation at 2 Ma
Among clade heterogeneity in diversification	BAMM and BAMMtools (speciation.extinction)	(Rabosky et al. 2014b)	1 model estimating diversification rate heterogeneity	Diversification rates do not differ significantly among subclades	Diversification rates do not differ significantly among subclades	Diversification rates do not differ significantly among subclades	Diversification rates do not differ significantly among subclades
Trait-dependent (biome) heterogeneity in diversification	GeoSSE in diversiTree (find.mle; mcmc; constrain)	(Maddison et al. 2007; FitzJohn et al. 2009; Goldberg et al. 2011)	5 sets (each biome) of 5 nested models testing: equal speciation (eq.div) equal extinction (eq.ext) equal dispersal (eq.disp) no speciation between biomes (no.sAB)	Elevated speciation rate in arid zone	Not tested	Not tested	Not tested

PB, pure birth; BD, birth death; LTT, lineage through time; CI, confidence interval; ↑ increase in rate; ↓ decrease in rate; Ma, million years ago. Table is organized by the macroevolutionary question investigated, the method (R package or C++ program) and functions used (references included), settings applied or models compared, and results by clade.

the marginal likelihoods of the two models sets via stepping-stone-sampling (function "tess.steppingStoneSampling," each run for 10,000 iterations, 1000 discarded as burn-in, 100 stepping stones). After looping through all posterior trees, we compared models via Bayes factors (2 ln Bf). To determine significant difference between focal and null models, we followed Kass and Raftery (1995) and identified BF = 0 to 2 as "not worth more than a bare mention," BF = 2 to 6 as "positive" support, BF = 6 to 10 as "strong" support, and BF > 10 as "very strong" support.

After initial model comparisons, we estimated the timing and intensity of mass extinction with TESS (function "tess.analysis"). The power of methods that use molecular phylogenies to infer mass extinctions (such as TESS/CoMET) is sensitive to the timing of such an event, relative to the total tree depth. Events that occur deep in a group's history are confidently discovered less frequently (see May et al. (2015) for discussion) than those occurring more recently, however, false discovery rates (inferring a mass extinction event when one has not occurred) remain consistently low (8.1–9.9%). As a result, these methods are indirectly restricted to a conservative estimate of the occurrence of mass turnover. We ran the analyses (iterated over 100 post burn-in trees) with the hyper-priors including the time of a mass extinction event ("estimateMassExtinctionTimes") to be estimated empirically from the data, an MCMC length of 200,000 generations, with the first 10% discarded as burnin, a minimum ESS requirement of 500 to determine convergence, and four independent runs each conditioned on taxa and survival. We applied the same Bayes factor significance thresholds as above and as have been used previously (May et al. 2015).

PHYLOGENETIC RATE HETEROGENEITY

To determine if pygopodoid clades have diversified at a similar pace, we used BAMM (Rabosky et al. 2014a), which also estimates λ and μ dynamically, but allows rates among lineages to vary at any given time. This cross-clade comparison results in the ability of contemporary clades to decouple diversification (λ and μ) values among groups. BAMM highlights clades that diverge significantly from background rates of diversification, placing a credible set of shift placements along branches or at nodes. We executed three independent "speciationextinction" analysis runs with BAMM specified priors for 100,000,000 generations, sampling each 100,000 generations, and discarded the first 20% as burn-in. We used BAMMtools (Rabosky et al. 2014b) for postrun statistics and visualization of results, and to compare across runs for convergence. To provide another comparison of diversification rates across groups we also ran clade-specific (Carphodactylidae, Pygopodidae, Diplodactylidae, core Diplodactylidae) TESS analyses, and pairwise chi-square tests to determine significant differences. All methods allowed us to correct for incomplete taxon sampling via clade-specific sampling frequencies.

BIOGEOGRAPHY, AND BIOME TRANSITION AND SPECIATION RATES

Changing global and local climate, particularly aridification, have been implicated in influencing the diversification of most major Australian terrestrial radiations (see Byrne et al. 2011; Table 1). To investigate the evolution of biome distribution in the Pygopodoidea, we used BioGeoBEARS (Matzke 2013) to simultaneously reconstruct ancestral biome states and model biome shifts across the tree. Species were assigned to one or more biomes as outlined in the Materials and Methods. We ran an additional 50 biogeographic stochastic maps to provide a confident estimate of the frequency and directionality of across biome dispersal events, and account for uncertainty in ancestral biome reconstruction and state transitions (Matzke 2016). Transition frequencies and directionality were plotted in ggplot2 (Wickham 2009).

To determine rates of biome-specific diversification and habitat transitions, we applied the geographic extension of the state speciation and extinction model GeoSSE (Goldberg et al. 2011). Inputs were accompanied by phylogenetic sampling corrections to account for our taxonomically incomplete phylogeny (FitzJohn et al. 2009). We used the incorporated maximum likelihood search algorithm to estimate the model parameters and provide a starting point for our Markov Chain Monte Carlo (MCMC) sampling, which was run for two independent chains of 10,000 generations each. To determine best fitting models, we used analysis of variance (ANOVA) and likelihood ratio tests (LRT) to reject poorly supported diversification models, and ANOVA and two-tailed *t*-tests to compare differences in diversification rates among biomes. To check for vulnerability to Type I error in our phylogeny, and reduce the possibility of potentially misleading results from SSE methods (Maddison and FitzJohn 2015), we followed Rabosky and Goldberg (2015) and established a relative significance criterion for neutral traits across our tree. Using phytools (function "sim.char") we executed 100 simulations of a binary, neutral, discrete trait across our phylogeny, as GeoSSE is limited to analyzing binary-only data (Revell 2012). We then estimated the parameter (speciation, extinction, dispersal) rates using the maximum likelihood function ("find.mle") in GeoSSE, and summarized the rates across the 100 independent binary trait simulations. We used this distribution of trait likelihood ratios, as well as the upper and lower means of simulated traits to determine a 95% CI specific to our tree. This simultaneously tested for tendency of null traits to be associated with significant diversification rates, as well as giving us a confidence metric tailored to this dataset.

DATA ACCESSIBILITY

All alignments, divergence dating operator files, biome codings, and analysis scripts have been archived at Data Dryad: http://dx.doi.org/10.5061/dryad.991p6.

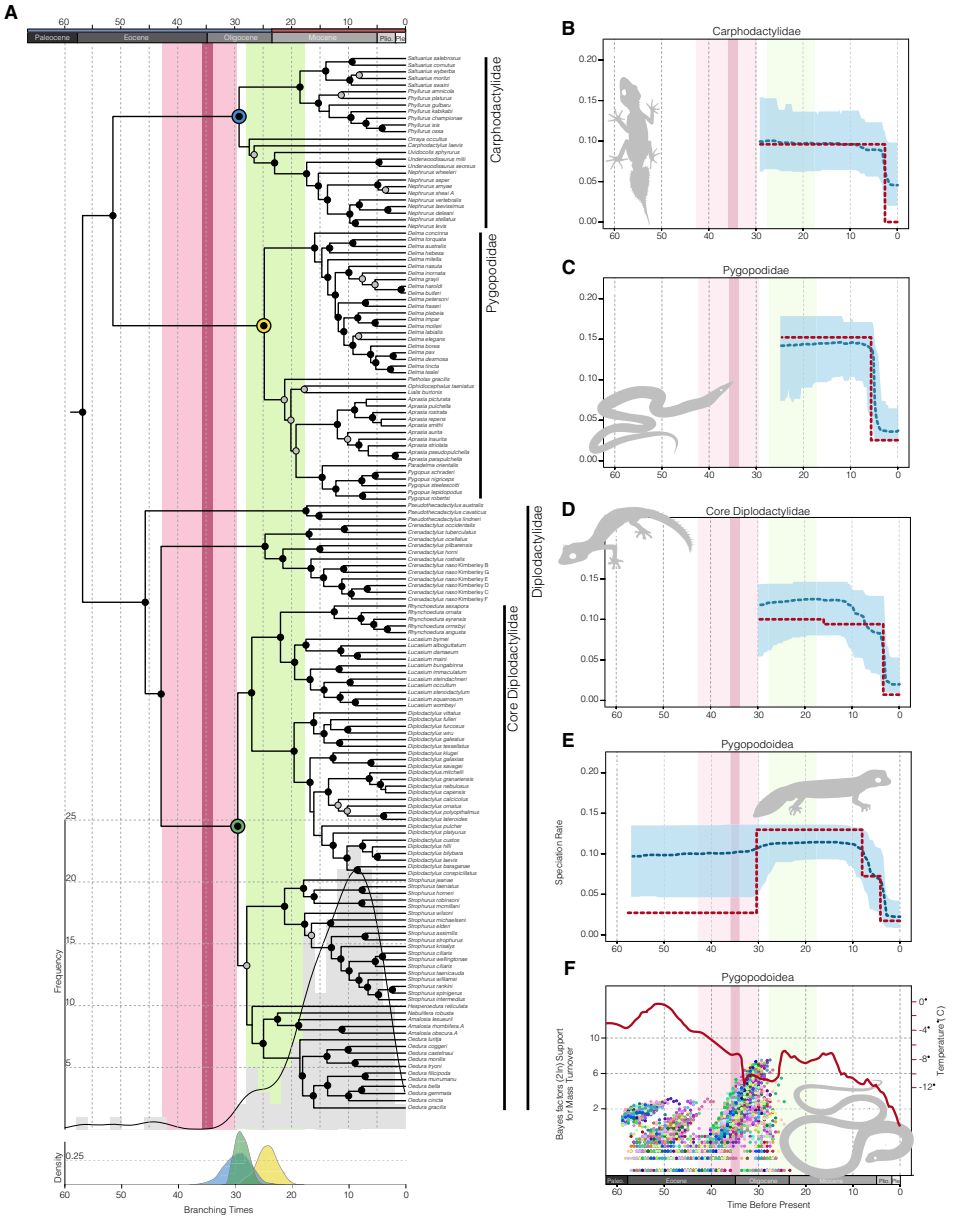

Figure 1. (A) Fossil calibrated phylogeny of the Pygopodoidea, nodes with >95 posterior probabilities are indicated by black circles, gray circles indicate posterior probabilities >80. Vertical pink bar highlights naked stem lineages likely the result of mass turnover at the Eocene-Oligocene boundary, indicated by vertical red bar. Green bar and node age density plots (bottom) draw attention to temporal congruence in crown divergences across all three families, including the diversification of all extant genera save *Crenadactylus* and *Pseudothecadactylus*. Histogram at bottom of tree shows frequency of branching events, which are clustered in the mid and late Miocene. Speciation rate estimates of (B) Carphodactylidae, (C) Pygopodidae, (D) core Diplodactylidae, (E) Pygopodoidea, are shown at right. Rate estimates were determined by TESS (blue dotted line, light blue 95% CI), and TreePar (red dotted line). (F) Shows CoMET results of analysis of mass turnover, across 100 trees as colored circles and support evaluated using Bayes Factors (BF (2ln) $\geq$ 6 is significant). Red line traces the change in mean sea surface temperature, adapted from Zachos et al. (2001). This is used to illustrate coincidence of mass turnover in the Pygopodoidea and dramatic drop in global temperature at the Eocene-Oligocene transition.

Results

DIVERGENCE TIME ESTIMATION

Results of the six locus nuclear BEAST analysis support ($PP \geq 0.98$) the monophyly of all Australian pygopodoid genera and families (Fig. 1). Short internode distances among some genera are associated with phylogenetic uncertainty (Fig. 1, highlighted in green vertical bar), consistent with previous studies (Nielsen et al. 2016; Skipwith et al. 2016; Brennan et al. 2016). Our mean estimate of the crown divergence of Pygopodoidea (57 Mya; 50–64) is slightly younger than previous results, but the 95% CI overlaps with most estimates (56–74 Ma—Skipwith et al. 2016; 65–75 Ma—Gamble et al. 2015; 60–85 Ma—Garcia-Porta and Ord 2013). Investigation of key node ages from alternative fossil calibration schemes yielded dates that did not fall outside confidence intervals of ages estimated from 100 posterior trees of the fully calibrated nuclear BEAST analysis (Fig. S3), and were also consistent with dates from our combined mito-nuclear divergence estimates, indicated no conflict across calibrations and datasets.

DIVERSIFICATION AND RATES, TEMPORAL HETEROGENEITY, AND MASS TURNOVER

Pygopodoid diversification rates reveal a general trend of rate decay consistent with results of Garcia-Porta and Ord (2013). Variable rate models (LASER, TreePar, TESS) applied to the combined MCC tree commonly indicate speciation rate declines occurring within the most recent 10 million years (Table 1; Table S3; Fig. S2). To investigate evidence of, timing, and consistency of support for a mass extinction event, we iterated analyses over 100 trees sampled from the BEAST posterior. TESS model comparison of marginal likelihoods always positively ($2\ln BF > 3$) preferred models including mass extinction (vrbdME, crbdME) to the null ($null_1$, $null_2$) models. However, support for a vrbdME over crbdME model was generally negligible ($2\ln BF < 3$) (Fig. S4). Model support for mass extinction encouraged our investigation into the timing of such an event. Ninety-five percent of trees provide positive ($2\ln BF > 3$) support, and 58% of trees provide strong ($2\ln BF > 6$) support for a mass extinction event occurring between 27 and 32 million years ago, prior to the crown radiations of pygopodids, carphodactylids, and "core" diplodactylids (Fig. 1, Table S3).

AMONG-CLADE DIVERSIFICATION RATE COMPARISONS

BAMM "speciationextinction" analysis does not identify significant heterogeneity in diversification rates among pygopodoid clades, despite similar crown ages, and disparate species richness (Carphodactylidae ~30 Ma, 30 spp.; Diplodactylidae ~30 Ma, 100+ spp.; Pygopodidae ~25 Ma, 46 spp.). Results of clade-specific CoMET analyses identify diversification rates that do not differ significantly among groups (Table S4).

BIOGEOGRAPHY AND TRAIT-ASSOCIATED SPECIATION

BioGeoBEARS analysis identified DEC+j and DIVAlike+j as equally most preferred ($\Delta\text{-}\ln L = -0.1$, $\Delta AIC = 0.3$) models of historical biogeography. Inclusion of the jump parameter "j," is favored considerably over the simpler DEC and DIVA like models ($\Delta\text{-}\ln L = 51.2$), signifying the influence of between-biome founder-event speciation. DEC+j and DIVAlike+j ancestral biome reconstructions are concordant across all nodes with the exception of greater ambiguity in DIVAlike+j results of the interfamilial divergences. Results support a forest origin of the Carphodactylidae, and an arid origin of the Diplodactylidae (Fig. 2). It is necessary to note that biome reconstruction of deep nodes near the crown of Carphodactylidae and Pygopodidae may be confounded by poorly supported intergeneric relationships.

The frequency of outward dispersal events from the arid zone exceeds that of all other biomes combined (mean = 55; 51% of total events), suggesting elevated transition out of arid regions, into more mesic surrounds ("mesic" = savannah, subtropical, temperate, forest; Fig. 3). Outward transitions (source; 55) from the arid zone also double that of incoming events (sink; 22).

GeoSSE was used to test if major Australian biomes show evidence of differing diversification (λ, μ) and transition (q) rates by constraining rates of these three parameters (Table S5). Our analyses established that best-fit models varied across biomes: arid—eq.μ (equal extinction, speciation, and transition rates vary); temperate and savannah—eq.μq (equal extinction and transition rates, speciation may vary), subtropical and forest— eq.$\lambda\mu q$ (all rates equal). When state rates were compared against background rates (all other states combined), we found significant trends in arid (higher), and temperate and savannah (lower) diversification rates. Arid and subtropical zones display a significant elevation in transition rates. Trends identified as significant do not differ between our initial biome scoring and the "mesic refugial" alternative model.

Neutral trait simulations developed a CI for diversification and transition rates in and between two regions ("A" and "B"), giving maximum and minimum mean values built from our phylogeny. After comparison against our summary statistics, estimation of rates of arid zone speciation, and outward dispersal of arid and subtropical taxa remain significantly greater than simulations ($P < 0.05$).

Discussion

Analysis of pygopodoid gecko diversification reveals early Oligocene mass turnover, consistent with fossil and phylogenetic

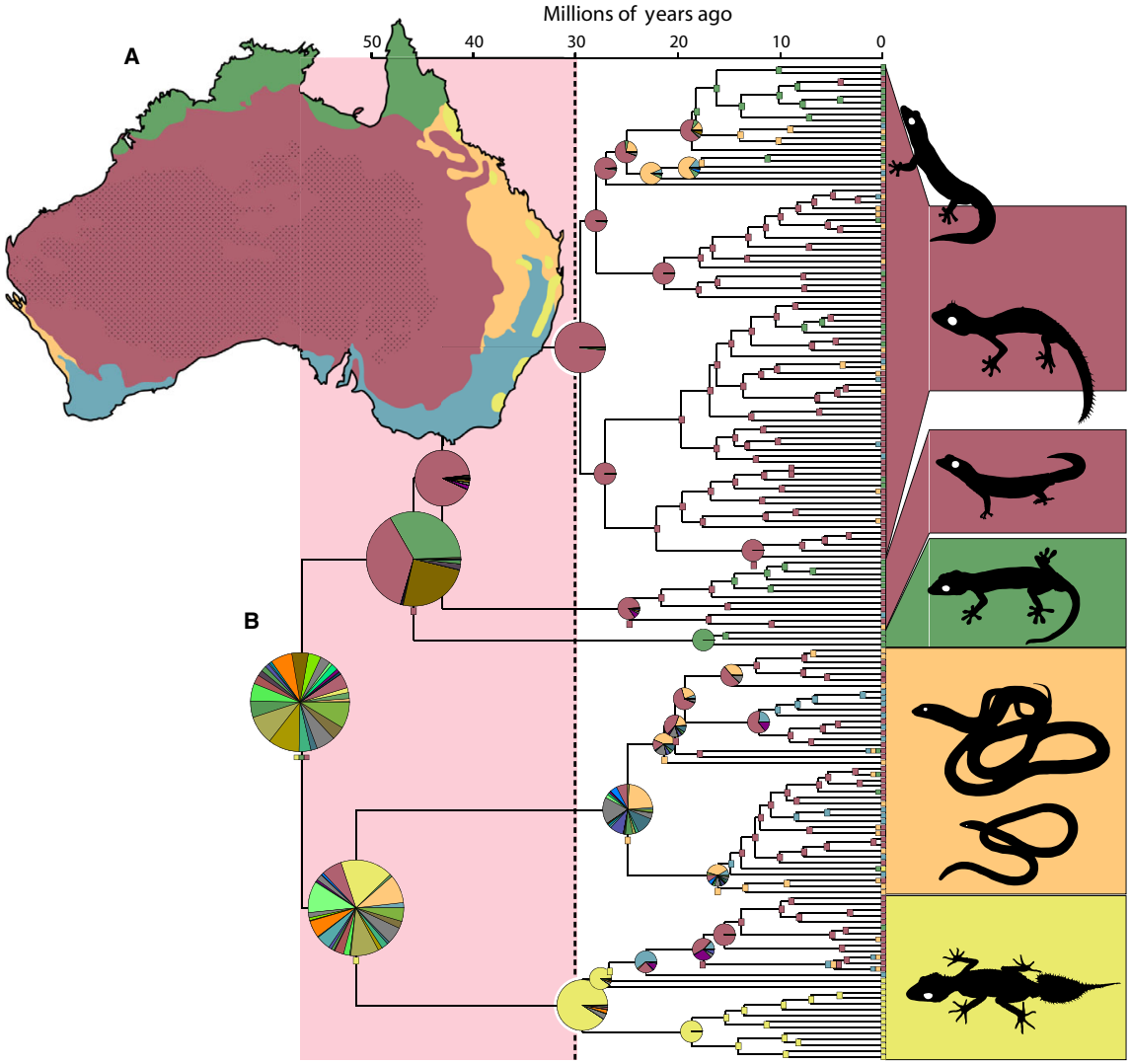

Figure 2. (A) Map of continental Australia as divided by our biome classifications: savannah (green), temperate (blue), subtropical (orange), forest (yellow), arid (red). (B) BioGeoBEARS ancestral state reconstruction under the DEC+j model of biogeographic dispersal. Colors of pie charts correspond to biome types previously mentioned. Pie charts indicate ancestral biome reconstructions of given nodes. Colored boxes below pie charts indicate majority reconstruction of visually ambiguous nodes. Colors present in pie charts but not on the inset Australian biome map indicate shared occurrence in more than one biome. Pink vertical bar indicates period impacted by Eocene-Oligocene turnover, and equivocal reconstructions. Shaded boxes to the right of the tree highlight ancestral biome reconstructions of major clades, from top to bottom: core Diplodactylidae, *Crenadactylus*, *Pseudothecadactylus*, Pygopodidae, Carphodactylidae. Extant pygopodoid diversity is greatest in arid biomes: more than 53% (91 spp.) include arid regions in part of their range, and more than 44% (75 spp.) exist exclusively in the arid zone.

signature of Australian and global contemporaries (Antonelli and Sanmartín 2011; Sun et al. 2014). This period of elevated extinction following dramatic climatic change at the Eocene Oligocene transition, illustrates visible signature of global events on broad phylogenetic groups. Contemporary patterns in species distributions are however, more accurately explained by recent continental, gradual processes, particularly continental aridification. Combining these concepts, the Australian Pygopodoidea likely originated in the Cretaceous and has largely diversified via postextinction response in the Oligocene,

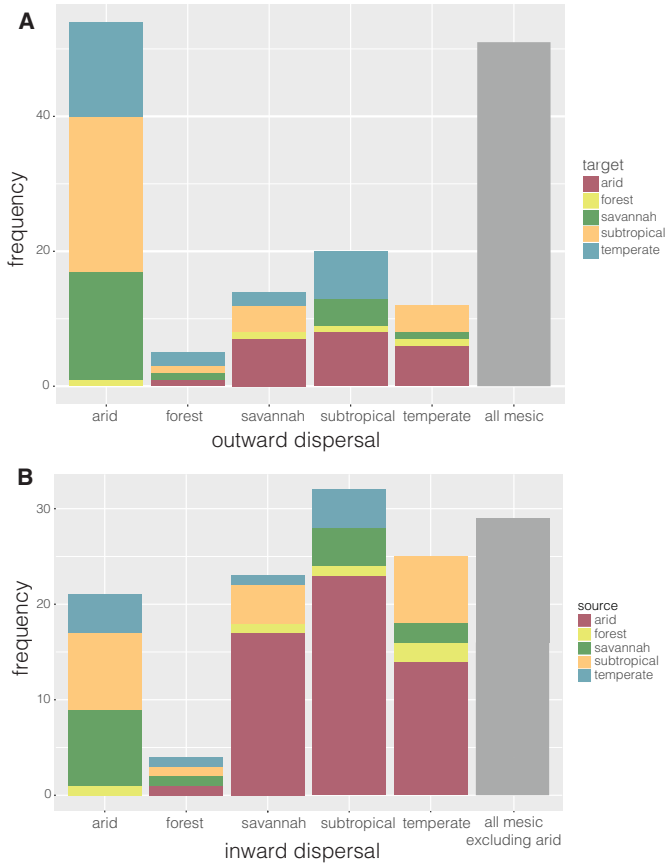

Figure 3. **Directional biome transition frequencies. (A) Histogram showing frequency and composition of outward transitions from five biome types and gray composite bar showing combined outward frequencies from four mesic biomes. Frequency of dispersal out of the arid zone is greater than out of all four mesic biomes combined. (B) Histogram showing frequency and composition of incoming transitions into five biome types, and gray composite bar showing combined incoming frequencies from four mesic biomes, excluding transitions from the arid zone. Dispersal from the arid zone makes up the majority of inward transitions into three of four mesic biomes. All transitions into mesic biomes narrowly exceed that of dispersals into the arid zone.**

flourishing during the protracted Miocene aridification of Australia.

EXTINCTION AND GLOBAL CLIMATE CHANGE

Mass turnover of pygopodoid geckos in the early Oligocene provides an explanation for previously noted (Oliver and Sanders 2009) temporal heterogeneity in the diversification of this group, and homogeneity in crown family divergence ages (Fig. 1). However, molecular phylogenetic signature of such turnover is difficult to reliably identify in the absence of appropriate fossil material (Quental and Marshall 2010). To rely on molecular data alone requires that the group in question both significantly predate and survive a period of mass turnover. Signal of such an event may be further confounded by asymmetrical effects of elevated extinction on different groups (Wilson et al. 2012). To be detectable, signal must generally be consistent among clades, else conflicting trends may smother signature of turnover. Furthermore, without a fossil record, those groups that go completely extinct or survive as relics and fail to subsequently rebound, provide either no molecular signature, or signature largely indistinguishable from long-term low-cladogenic persistence. We provide evidence of just such an exceptional occurrence in Australian pygopodoid geckos.

Diversification dynamics of the Pygopodoidea add to a growing body of evidence supporting mass turnover across broad phylogenetic groups of the late Eocene and early Oligocene (Hooker et al. 2004; Pearson et al. 2008; Sun et al. 2014; Cantalapiedra et al. 2015). The EOb is marked by a period of global climatic

turbulence, including rapid cooling (>5°C in <100,000 years) and aridification (Zachos et al. 2001; Liu et al. 2009). Throughout Southeast Asia and Australia, floristic history provides evidence of contracting rainforest and mesic sclerophyllous habitats (Byrne et al. 2011; Buerki et al. 2013). We suggest that a rapid drop in temperature and contraction of suitable habitat likely outpaced the adaptability of ancestrally mesic pygopodoid geckos. Especially given that most extant taxa are characterized by low vagility and fecundity (Read 1999). This trend in assemblage turnover between the Eocene and Oligocene is potentially also reflected in the radiation and invasion of a number of other Australian squamate lineages, and indicates that climatic change at the EOb ushered in a new era for accumulating Australian diversity.

Congruent crown divergences of Australian pygopodoid families (~25–30 Ma) (Fig. 1), typified by short internode distances and poor resolution of basal intergeneric relationships, is consistent with the theory that, following periods of mass turnover surviving lineages often undergo rapid adaptive radiation. Accelerated postextinction diversification is suggested to be the result of open niche space provided by dramatic loss of standing diversity and opportunity in new or changing habitats (Erwin 2001; Chen and Benton 2012). Here, we suggest similar responses by pygopodoid geckos to the climate and biome turnover of Oligocene Australia. Cooling of the early Oligocene gave way to warming in the late Oligocene, which has been implicated as an important driver of diversity in mammals (Stadler 2011a) and other terrestrial flora and fauna (Sun et al. 2014). This warming trend encapsulates a period of ecological diversification marked by arboreal and terrestrial divergences in carphodactylids and diplodactylids, and diurnal, nocturnal, fossorial, and arboreal clades of pygopodids. Consistent rates of cladogenesis among families indicate a common postextinction response of pygopodoid families following perturbation in the early Oligocene.

DIVERSIFYING DURING CONTINENTAL BIOME CHANGE

In contrast to the relatively rapid climatic change and ensuing turnover of the Oligocene, protracted Miocene aridification of the Australian continent coincides with signal of phylogenetic expansion in pygopodoids. Current understanding of the Australian arid zone has suggested a gradual trend toward aridification throughout the latter half of the Miocene, transitioning from drought-sensitive wet forests to drought-tolerant eucalypts and acacias (Crisp and Cook 2013). Aridification was punctuated by marked mesic pulses in the Pliocene (Sniderman et al. 2016), and Pleistocene (Martin 2006), however the overall trend has continued with the arid zone extending to encompass more than 70% of the continent. The slower tempo of Miocene biome rearrangement suggests that instead of immediate unilateral losses in diversity, there was opportunity for lineages pruned from the phylogeny to be gradually replaced by the proliferation of taxa capable of making the shift to arid biomes (Byrne et al. 2008, 2011). This more recent trend in continental aridification better explains contemporary patterns in distribution and the diversification of extant pygopodoids.

Globally, desert ecosystems have been considered net sinks for diversity (Crisp et al. 2009). Despite the difficulties of persisting in arid biomes, arid climes have had a profound influence on the evolution of plants and animals (Stebbins 1952). In Australia, exceptionally diverse communities of squamate species may be found in sympatry, including closely related lineages (Pianka 1969; Jennings et al. 2003; Goodyear and Pianka 2008). However, the drivers of this arid zone squamate richness have been difficult to pinpoint (Pianka 1989; Powney et al. 2010). The young age of this biome paired with our findings of accelerated rates of arid pygopodoid speciation lend support to the theory that invasion of a novel geographic region or biome is associated with relative rapid diversification (Yoder et al. 2010). Although few other studies have explicitly investigated the speciation dynamics of Australian radiations, predominantly arid zone clades of Australian skinks (*Ctenotus*, *Lerista*) (Rabosky et al. 2014a), *Hylaeus* bees (Kayaalp et al. 2013), and *Triodia* and *Acacia* plants (Crisp and Cook 2013) show elevated rates of speciation, suggesting that this pattern may be widespread.

Elevated arid zone diversification may be attributable to varied intrinsic, extrinsic, and artefactual causes, some of which are likely unique to the Australian continent and focal group. Firstly, the geographic area of the Australian arid zone exceeds that of all other Australian biomes combined, creating a greater platform for speciation and divergence. While primary productivity is low compared to more mesic neighboring biomes, space, and habitat heterogeneity are high. Alternatively, higher arid zone richness may be a consequence of nonrandom extinction. Shrinking mesic biomes have undoubtedly been associated with range restriction and likely elevated extinction of their inhabitants, and so signal from extant taxa may provide an inaccurate representation of historic mesic richness (Bryant and Krosch 2016). Finally, as a group, squamate reptiles are physiologically predisposed to handle heat-stress and evaporative water-loss (Pough 1980; Cox and Cox 2015). In geckos, this preadaptation to arid climes is extended by an ancestral transition to nocturnality, and avoidance of dangerous heat and radiation (Gamble et al. 2015).

Our investigation of biome transitions suggests that arid habitats are a considerable source of Australian continental diversity. Arid zone pygopodoid richness is not trapped exclusively within the arid zone, and elevated diversification rates have resulted in frequent dispersal into peripheral mesic biomes. Though geographic size and perimeter undoubtedly contribute to this, intrinsic factors of ecology may explain elevated transition rates as well. Frequent sympatry of closely related species, and higher local

(alpha) species diversity of squamates in the arid zone (James and Shine 2000; Powney et al. 2010), is likely a result of greater niche differentiation. In this vein, ecological diversity cultivated in the arid zone of Australia may have provided successful transitions back into mesic biomes (Nielsen et al. 2016).

Conclusions

Macroevolutionary studies focusing on broad patterns in diversification may be strengthened by incorporating local (here, continental) mechanisms that may better explain patterns in extant diversity (Vermeij and Leighton 2003). Our investigation of a diverse continental vertebrate radiation is consistent with the understanding that global changes may profoundly and unilaterally impact disparate phylogenetic groups, however subsequent biome assemblages may respond dissimilarly. In these instances, studies of sister-clade dynamics provide valuable insight into such patterns of diversity as they undergo pressure from congruent and contrasting diversifying influences. We provide new evidence of the dramatic impact that rapid (Eocene-Oligocene cooling) climatic change has had on the Australian biotic assemblage. Protracted aridification has also been instrumental in shaping trends in Australian biodiversity (Barker and Greenslade 1982; Cracraft 1986). However, contrary to patterns seen in other Australian radiations, the arid zone has facilitated the diversification of pygopodoid geckos, acting as a source for neighboring habitats. Contrasting signature in response to rapid and gradual climate regimes draw attention to their varied influences on macroevolution, and highlights the necessity of further investigation of historical biogeography among Australian clades. Understanding the importance of the Australian arid zone as a source for continental diversity is paramount to developing a clearer picture of how Australia's regional fauna have been assembled.

AUTHOR CONTRIBUTIONS

I.G.B. conceived and designed the study, and analyzed the data; I.G.B. and P.M.O. collected the data and wrote the article.

ACKNOWLEDGMENTS

We would like to thank J. Scott Keogh, Michael S. Y. Lee, and Joshua V. Peñalba for comments, Nicholas J. Matzke for advice on methods, Zoe K. M. Reynolds for help with scripts, and the Keogh lab group for discussion that greatly improved the quality of this manuscript. Two anonymous reviewers and Dr. Irby Lovette provided immensely helpful critiques and methodological suggestions on a previous version of this manuscript. Thank you to staff of the Australian Museum, Northern Territories Museum, South Australian Museum, Queensland Museum, and Western Australian Museum for access to the tissues that made this work possible. This work has been funded by an Australian Research Council Discovery early career researcher fellowship to P.M.O. Additionally, research by I.G.B. is partially supported by an American Australian Association fellowship. The authors declare no conflict of interest with regards to this manuscript or research.

DATA ARCHIVING

The doi for our data is 10.5061/dryad.991p6.

LITERATURE CITED

Antonelli, A., and I. Sanmartín. 2011. Mass extinction, gradual cooling, or rapid radiation? Reconstructing the spatiotemporal evolution of the ancient angiosperm Genus *Hedyosmum* (Chloranthaceae) using empirical and simulated approaches. Syst. Biol 60:596–615.

Axelrod, D. I. 1967. Drought, diastrophism, and quantum evolution. Evolution 21:201–209.

Bapst, D. W. 2012. paleotree: an R package for paleontological and phylogenetic analyses of evolution. Methods Ecol. Evol. 3:803–807.

Barker, W. R., and P. J. M. Greenslade. 1982. Evolution of the flora and fauna of arid Australia. Peacock Publications, Frewville, South Australia.

Brennan, I. G., A. M. Bauer, and T. R. Jackman. 2016. Mitochondrial introgression via ancient hybridization, and systematics of the Australian endemic pygopodid gecko genus *Delma*. Mol. Phylogenet. Evol. 94:577–590.

Bryant, L. M., and M. N. Krosch. 2016. Lines in the land: a review of evidence for eastern Australia's major biogeographical barriers to closed forest taxa. Biol. J. Linn. Soc. 119:238–264.

Buerki, S., F. Forest, T. Stadler, and N. Alvarez. 2013. The abrupt climate change at the Eocene–Oligocene boundary and the emergence of South-East Asia triggered the spread of sapindaceous lineages. Annals Bot. 112:151–160.

Byrne, M., D. A. Steane, L. Joseph, D. K. Yeates, G. J. Jordan, D. Crayn, K. Aplin, D. J. Cantrill, L. G. Cook, M. D. Crisp, et al. 2011. Decline of a biome: evolution, contraction, fragmentation, extinction and invasion of the Australian mesic zone biota. J. Biogeogr. 38:1635–1656.

Byrne, M., D. K. Yeates, L. Joseph, M. Kearney, J. Bowler, M. A. J. Williams, S. Cooper, S. C. Donnellan, J. S. Keogh, R. Leys, et al. 2008. Birth of a biome: insights into the assembly and maintenance of the Australian arid zone biota. Mol. Ecol. 17:4398–4417.

Cantalapiedra, J. L., M. Hernández Fernández, B. Azanza, and J. Morales. 2015. Congruent phylogenetic and fossil signatures of mammalian diversification dynamics driven by Tertiary abiotic change. Evolution 69:2941–2953.

Catullo, R. A., and J. S. Keogh. 2014. Aridification drove repeated episodes of diversification between Australian biomes: evidence from a multilocus phylogeny of Australian toadlets (*Uperoleia*: Myobatrachidae). Mol. Phylogenet. Evol. 79:106–117.

Chen, Z.-Q., and M. J. Benton. 2012. The timing and pattern of biotic recovery following the end-Permian mass extinction. Nat. Geosci. 5:375–383.

Cox, C. L., and R. M. Cox. 2015. Evolutionary shifts in habitat aridity predict evaporative water loss across squamate reptiles. Evolution 69:2507–2516.

Cracraft, J. 1986. Origin and evolution of continental biotas speciation and historical congruence within the Australasian avifauna. Evolution 40:977–996.

Crisp, M. D., M. T. K. Arroyo, L. G. Cook, M. A. Gandolfo, G. J. Jordan, M. S. McGlone, P. H. Weston, M. Westoby, P. Wilf, and H. P. Linder. 2009. Phylogenetic biome conservatism on a global scale. Nature 458:754–756.

Crisp, M. D., and L. G. Cook. 2013. How was the Australian flora assembled over the last 65 million years? A molecular phylogenetic perspective. Ann. Rev. Ecol. Evol. Syst. 44:303–324.

Crottini, A., O. Madsen, C. Poux, A. Strauß, D. R. Vieites, and M. Vences. 2012. Vertebrate time-tree elucidates the biogeographic pattern of a major biotic change around the K–T boundary in Madagascar. Proc. Natl. Acad. Sci. USA 109:5358–5363.

Dornburg, A., M. C. Brandley, M. R. McGowen, and T. J. Near. 2012. Relaxed clocks and inferences of heterogeneous patterns of nucleotide substitution and divergence time estimates across whales and dolphins (Mammalia: Cetacea). Mol. Biol. Evol. 29:721–736

Doughty, P., R. J. Ellis, and P. M. Oliver. 2016. Many things come in small packages: Revision of the clawless geckos (*Crenadactylus*: Diplodactylidae) of Australia. Zootaxa 4168:239.

Doughty, P., M. Pepper, and J. S. Keogh. 2010. Morphological and molecular assessment of the *Diplodactylus savagei* species complex in the Pilbara region, Western Australia, with a description of a new species. Zootaxa 2393:33–45.

Drummond, A. J., S. Y. Ho, M. J. Phillips, and A. Rambaut. 2006. Relaxed phylogenetics and dating with confidence. PLoS Biol. 4:e88.

Drummond, A. J., and A. Rambaut. 2007. BEAST: Bayesian evolutionary analysis by sampling trees. BMC Evol. Biol. 7:214.

Erwin, D. H. 2001. Lessons from the past: biotic recoveries from mass extinctions. Proc. Natl. Acad. Sci. USA 98:5399–5403.

FitzJohn, R. G., W. P. Maddison, and S. P. Otto. 2009. Estimating trait-dependent speciation and extinction rates from incompletely resolved phylogenies. Syst. Biol. 58:595–611.

Gamble, T., E. Greenbaum, T. R. Jackman, and A. M. Bauer. 2015. Into the light: diurnality has evolved multiple times in geckos. Biol. J. Linn. Soc. 115:896–910.

Gamble, T., E. Greenbaum, T. R. Jackman, A. P. Russell, and A. M. Bauer. 2012. Repeated origin and loss of adhesive toepads in geckos. PLoS ONE 7:e39429.

Garcia-Porta, J., and T. Ord. 2013. Key innovations and island colonization as engines of evolutionary diversification: a comparative test with the Australasian diplodactyloid geckos. J. Evol. Biol. 26:2662–2680.

Gernhard, T. 2008. The conditioned reconstructed process. J. Theor. Biol. 253:769–778.

Goldberg, E. E., L. T. Lancaster, and R. H. Ree. 2011. Phylogenetic inference of reciprocal effects between geographic range evolution and diversification. Syst. Biol. 60:451–465.

Goodyear, S. E., and E. R. Pianka. 2008. Sympatric ecology of five species of fossorial snakes (Elapidae) in Western Australia. J. Herpetol. 42:279–285.

Halliday, T. J. D., P. Upchurch, and A. Goswami. 2016. Eutherians experienced elevated evolutionary rates in the immediate aftermath of the Cretaceous–Palaeogene mass extinction. Proc. R Soc. Lond. B Biol. Sci. 283:1–8.

Harmon, L. J., J. T. Weir, C. D. Brock, R. E. Glor, and W. Challenger. 2008. GEIGER: investigating evolutionary radiations. Bioinformatics 24:129–131.

Höhna, S., M. R. May, and B. R. Moore. 2016. TESS: an R package for efficiently simulating phylogenetic trees and performing Bayesian inference of lineage diversification rates. Bioinformatics 32:789–791.

Hooker, J. J., M. E. Collinson, and N. P. Sille. 2004. Eocene–Oligocene mammalian faunal turnover in the Hampshire Basin, UK: calibration to the global time scale and the major cooling event. J. Geol. Soc. 161:161–172.

Hunter, J. P. 1998. Key innovations and the ecology of macroevolution. Trends Ecol. Evol. 13:31–36.

James, D. C., and R. Shine. 2000. Why are there so many coexisting species of lizards in Australian deserts? Oecologia 125:127–141.

Jennings, W. B., E. R. Pianka, and S. Donnellan. 2003. Systematics of the lizard Family Pygopodidae with implications for the diversification of Australian temperate biotas. Syst. Biol. 52:757–780.

Kass, R. E., and A. E. Raftery. 1995. Bayes factors. J. Am. Stat. Assoc. 90:773–795.

Kayaalp, P., M. P. Schwarz, and M. I. Stevens. 2013. Rapid diversification in Australia and two dispersals out of Australia in the globally distributed bee genus, Hylaeus (Colletidae: Hylaeinae). Mol. Phylogenet. Evol. 66:668–678.

Laurent, S., M. Robinson-Rechavi, and N. Salamin. 2015. Detecting patterns of species diversification in the presence of both rate shifts and mass extinctions. BMC Evol. Biol. 15:1–10.

Liu, Z., M. Pagani, D. Zinniker, R. DeConto, M. Huber, H. Brinkhuis, S. R. Shah, R. M. Leckie, and A. Pearson. 2009. Global cooling during the Eocene-Oligocene climate transition. Science 323:1187–1190.

Maddison, W. P., and R. G. FitzJohn. 2015. The unsolved challenge to phylogenetic correlation tests for categorical characters. Syst. Biol. 64:127–136.

Maddison, W. P., P. E. Midford, and S. P. Otto. 2007. Estimating a binary character's effect on speciation and extinction. Syst. Biol. 56:701–710.

Martin, H. A. 2006. Cenozoic climatic change and the development of the arid vegetation in Australia. J. Arid Environ. 66:533–563.

Matzke, N. J. 2013. Probabilistic historical biogeography: new models for founder-event speciation, imperfect detection, and fossils allow improved accuracy and model-testing. Front. Biogeogr. 5:242–248.

———. 2016. Stochastic mapping under biogeographical models. PhyloWiki BioGeoBEARS Available at http://phylo.wikidot.com/biogeobears#stochastic_mapping.

May, M. R., S. Höhna, and B. R. Moore. 2015. A Bayesian approach for detecting mass-extinction events when rates of lineage diversification vary. bioRxiv:1–47.

Moen, D., and H. Morlon. 2014. Why does diversification slow down? Trends Ecol. Evol. 29:190–197.

Nielsen, S. V., P. M. Oliver, R. J. Laver, A. M. Bauer, and B. P. Noonan. 2016. Stripes, jewels and spines: further investigations into the evolution of defensive strategies in a chemically defended gecko radiation (*Strophurus*, Diplodactylidae). Zool. Scr. 45:481–493.

Oliver, P. M., M. Adams, and P. Doughty. 2010. Molecular evidence for ten species and Oligo-Miocene vicariance within a nominal Australian gecko species (*Crenadactylus ocellatus*, Diplodactylidae). BMC Evol. Biol. 10:1–11.

Oliver, P. M., M. Adams, M. S. Lee, M. N. Hutchinson, and P. Doughty. 2009. Cryptic diversity in vertebrates: molecular data double estimates of species diversity in a radiation of Australian lizards (*Diplodactylus*, Gekkota). Proc. R Soc. Lond. B Biol. Sci. :rspb. 2008.1881.

Oliver, P. M., and A. M. Bauer. 2011. Systematics and evolution of the Australian knob-tail geckos (*Nephrurus*, Carphodactylidae, Gekkota): plesiomorphic grades and biome shifts through the Miocene. Mol. Phylogenet. Evol. 59:664–674.

Oliver, P. M., A. M. Bauer, E. Greenbaum, T. Jackman, and T. Hobbie. 2012. Molecular phylogenetics of the arboreal Australian gecko genus *Oedura* Gray 1842 (Gekkota: Diplodactylidae): another plesiomorphic grade? Mol. Phylogenet. Evol. 63:255–264.

Oliver, P. M., and P. Doughty. 2016. Systematic revision of the marbled velvet geckos (*Oedura marmorata* species complex, Diplodactylidae) from the Australian arid and semi-arid zones. Zootaxa 4088:151–176.

Oliver, P. M., M. N. Hutchinson, and S. J. Cooper. 2007. Phylogenetic relationships in the lizard genus *Diplodactylus* Gray and resurrection of *Lucasium* Wermuth (Gekkota, Diplodactylidae). Aust. J. Zool. 55:197–210.

Oliver, P. M., and K. L. Sanders. 2009. Molecular evidence for Gondwanan origins of multiple lineages within a diverse Australasian gecko radiation. J. Biogeogr. 36:2044–2055.

Oliver, P. M., K. L. Smith, R. J. Laver, P. Doughty, and M. Adams. 2014. Contrasting patterns of persistence and diversification in vicars of a widespread Australian lizard lineage (the *Oedura marmorata* complex). J. Biogeogr. 41:2068–2079.

Paradis, E., J. Claude, and K. Strimmer. 2004. APE: analyses of phylogenetics and evolution in R language. Bioinformatics 20:289–290.

Pearson, P. N., I. K. McMillan, B. S. Wade, T. D. Jones, H. K. Coxall, P. R. Bown, and C. H. Lear. 2008. Extinction and environmental change across the Eocene-Oligocene boundary in Tanzania. Geology 36:179–182.

Pepper, M., P. Doughty, M. N. Hutchinson, and J. S. Keogh. 2011. Ancient drainages divide cryptic species in Australia's arid zone: morphological and multi-gene evidence for four new species of Beaked Geckos (*Rhynchoedura*). Mol. Phylogenet. Evol. 61:810–822.

Phillimore, A. B., and T. D. Price. 2008. Density-dependent cladogenesis in birds. PLoS. Biol. 6:e71.

Pianka, E. R. 1969. Sympatry of desert lizards (Ctenotus) in Western Australia. Ecology 50:1012–1030.

———. 1989. Desert lizard diversity: additional comments and some data. Am. Nat. 134:344–364.

Potter, S., S. J. B. Cooper, C. J. Metcalfe, D. A. Taggart, and M. D. B. Eldridge. 2012. Phylogenetic relationships of rock-wallabies, *Petrogale* (Marsupialia: Macropodidae) and their biogeographic history within Australia. Mol. Phylogenet. Evol. 62:640–652.

Pough, F. H. 1980. The advantages of ectothermy for tetrapods. Am. Nat. 115:92–112.

Powney, G. D., R. Grenyer, C. D. L. Orme, I. P. F. Owens, and S. Meiri. 2010. Hot, dry and different: Australian lizard richness is unlike that of mammals, amphibians and birds. Glob. Ecol. Biogeogr. 19:386–396.

Pybus, O., and P. Harvey. 2000. Testing macro-evolutionary models using incomplete molecular phylogenies. Proc. R Soc. B 267:2267–2272.

Quental, T. B., and C. R. Marshall. 2010. Diversity dynamics: molecular phylogenies need the fossil record. Trends Ecol. Evol. 25:434–441.

Rabosky, D. L. 2006. LASER: a maximuml ikelihood toolkit for detecting temporal shifts in diversification rates from molecular phylogenies. Evol. Bioinform. Online 2:247–250.

———. 2013. Diversity-dependence, ecological speciation, and the role of competition in macroevolution. Ann. Rev. Ecol. Evol. Syst. 44.

Rabosky, D. L., S. C. Donnellan, M. Grundler, and I. J. Lovette. 2014a. Analysis and visualization of complex macroevolutionary dynamics: an example from Australian scincid lizards. Syst. Biol. 63:610–627.

Rabosky, D. L., S. C. Donnellan, A. L. Talaba, and I. J. Lovette. 2007. Exceptional among-lineage variation in diversification rates during the radiation of Australia's most diverse vertebrate clade. Proc. R Soc. Lond. B Biol. Sci. 274:2915–2923.

Rabosky, D. L., and E. E. Goldberg. 2015. Model inadequacy and mistaken inferences of trait-dependent speciation. Syst. Biol. 64:340–355.

Rabosky, D. L., M. Grundler, C. Anderson, P. Title, J. J. Shi, J. W. Brown, H. Huang, and J. G. Larson. 2014b. BAMMtools: an R package for the analysis of evolutionary dynamics on phylogenetic trees. Methods Ecol. Evol. 5:701–707.

Rambaut, A., and A. Drummond. 2007. LogCombiner v.1.6.0. See http://beast.bio.ed.ac.uk/LogCombiner/. Institute of Evolutionary Biology, University of Edinburgh.

Rambaut, A., M. Suchard, W. Xie, and A. Drummond. 2014. Tracer v. 1.6. Institute of Evolutionary Biology, University of Edinburgh.

Read, J. L. 1999. Longevity, reproductive effort and movements of three sympatric Australian arid-zone geckos. Aust. J. Zool. 47:307–316.

Revell, L. J. 2012. phytools: an R package for phylogenetic comparative biology (and other things). Methods Ecol. Evol. 3:217–223.

Scantlebury, D. P. 2013. Diversification rates have declined in the Malagasy herpetofauna. Proc. R Soc. Lond. B Biol. Sci. 280.

Shoo, L., R. Rose, P. Doughty, J. J. Austin, and J. Melville. 2008. Diversification patterns of pebble-mimic dragons are consistent with historical disruption of important habitat corridors in arid Australia. Mol. Phylogenet. Evol. 48:528–542.

Sniderman, J. M. K., J. D. Woodhead, J. Hellstrom, G. J. Jordan, R. N. Drysdale, J. J. Tyler, and N. Porch. 2016. Pliocene reversal of late Neogene aridification. Proc. Natl. Acad. Sci. USA 113:1999–2004.

Stadler, T. 2011a. Mammalian phylogeny reveals recent diversification rate shifts. Proc. Natl. Acad. Sci. USA 108:6187–6192.

———. 2011b. TreePar in R—estimating diversification rates in phylogenies. WWW document Available at http://cran/.r-project.org/web/packages/TreePar/index.html [accessed 4 November 2014].

Stebbins, G. L. 1952. Aridity as a stimulus to plant evolution. Am. Nat. 86:33–44.

Stern, H., G. De Hoedt, and J. Ernst. 2000. Objective classification of Australian climates. Australian Meteorol. Mag. 49:87–96.

Sun, J., X. Ni, S. Bi, W. Wu, J. Ye, J. Meng, and B. F. Windley. 2014. Synchronous turnover of flora, fauna, and climate at the Eocene–Oligocene boundary in Asia. Sci. Rep. 4:7463.

Tennant, J. P., P. D. Mannion, P. Upchurch, M. D. Sutton, and G. D. Price. 2016. Biotic and environmental dynamics through the Late Jurassic–Early Cretaceous transition: evidence for protracted faunal and ecological turnover. Biol. Rev. :1–39.

Unmack, P. J., G. R. Allen, and J. B. Johnson. 2013. Phylogeny and biogeography of rainbowfishes (Melanotaeniidae) from Australia and New Guinea. Mol. Phylogenet. Evol. 67:15–27.

Vermeij, G. J., and L. R. Leighton. 2003. Does global diversity mean anything? Paleobiology 29:3–7.

Wickham, H. 2009. ggplot2: elegant graphics for data analysis. Springer-Verlag, New York.

Williams, M. A. J. 1984. Cenozoic evolution of arid Australia. Pp. 59-78 *in* H. Cogger, and E. E. Cameron, eds. Arid Australia. Australian Museum, Sydney, Australia.

Wilson, G. P., A. R. Evans, I. J. Corfe, P. D. Smits, M. Fortelius, and J. Jernvall. 2012. Adaptive radiation of multituberculate mammals before the extinction of dinosaurs. Nature 483:457–460.

Yoder, J. B., E. Clancey, S. Des Roches, J. M. Eastman, L. Gentry, W. Godsoe, T. J. Hagey, D. Jochimsen, B. P. Oswald, J. Robertson, et al. 2010. Ecological opportunity and the origin of adaptive radiations. J. Evol. Biol. 23:1581–1596.

Zachos, J., M. Pagani, L. Sloan, E. Thomas, and K. Billups. 2001. Trends, rhythms, and aberrations in global climate 65 Ma to present. Science 292:686–693.

Zanazzi, A., M. J. Kohn, B. J. MacFadden, and D. O. Terry. 2007. Large temperature drop across the Eocene-Oligocene transition in central North America. Nature 445:639–642.

Associate Editor: I. Lovette
Handling Editor: M. Noor

Supporting Information

Additional Supporting Information may be found in the online version of this article at the publisher's website:

Table S1. Molecular sampling used in this paper. Data includes the name binomials used in this study, and museum identification numbers.
Table S2. Fossil calibrations collected for this study.
Table S3. Results of temporal and among clade estimates of diversification rate heterogeneity, grouped by analytical program.
Table S4. Diversification rate estimates across the Pygopodoidea, by program.
Table S5. Results of GeoSSE analysis of diversification rates by biome.
Figure S1. Comparison of estimated rates of speciation among taxonomic groups, and analytical programs.
Figure S2. Results of varied analyses of diversification across the Pygopodoidea and subclades.
Figure S3. Results of tests of fossil calibration effects on dating analyses.
Figure S4. Bayes factor comparisons among constant rate (crbd = ConstBD, crbdme = ConstBDME) and variable rate (vrbd = shiftBD, vrbdme = shiftBDME) TESS models investigating support for a mass extinction event.

Supplementary Material:

Table S1. Molecular sampling used in this paper. Data includes the name binomials used in this study, and museum identification numbers. Outgroup taxa used for the BEAST timetree, and excluded from the diversification analyses. Taxon coverage is greatest for the mitochondrial locus ND2 (95%), and generally lower for nDNA loci (RAG1–68%, RAG2–65%, PDC–50%, DYNLL1–10%, C-mos–44%, ACM4–42%).

Genus species	Family	Museum ID
Amalosia lesueurii	Diplodactylidae	AMS R159546
Amalosia obscura	Diplodactylidae	AMS R136124
Amalosia rhombifera	Diplodactylidae	AMS R140413
Aprasia aurita	Pygopodidae	SAMA R43054
Aprasia inaurita	Pygopodidae	SAMA R47087
Aprasia parapulchella	Pygopodidae	MV D66569
Aprasia picturata	Pygopodidae	WAM R131647
Aprasia pseudopulchella	Pygopodidae	SAMA R40729
Aprasia pulchella	Pygopodidae	WAM R8000
Aprasia repens	Pygopodidae	WAM R106018
Aprasia rostrata	Pygopodidae	SAMA R52288
Aprasia smithi	Pygopodidae	SAMA R106018
Aprasia striolata	Pygopodidae	ABTC 6575
Bavayia cyclura	Diplodactylidae (NC)	AMB 7683
Carphodactylus laevis	Carphodactylidae	QMJ8944; AMS R143258 (PDC)
Correlophus ciliatus	Diplodactylidae (NC)	AMS R146595
Crenadactylus tuberculatus	Diplodactylidae	WAM R116913; WAM R132481 (RAG)
Crenadactylus occidentalis	Diplodactylidae	WAM R120918
Crenadactylus horni	Diplodactylidae	ABTC 12583
Crenadactylus rostralis	Diplodactylidae	SAMA R53890
Crenadactylus naso Kimberley B	Diplodactylidae	WAM R108728; WAM R151002 (RAG)
Crenadactylus naso Kimberley C	Diplodactylidae	WAM R106260
Crenadactylus naso Kimberley D	Diplodactylidae	AMS R126186
Crenadactylus naso Kimberley E	Diplodactylidae	WAM R171695; WAM R158040 (RAG)
Crenadactylus naso Kimberley F	Diplodactylidae	WAM R169755
Crenadactylus naso Kimberley G	Diplodactylidae	WAM R171006
Crenadactylus pilbarensis	Diplodactylidae	WAM R127783; WAM R132672 (RAG)
Crenadactylus ocellatus	Diplodactylidae	WAM R114488; WAM R129700 (RAG)
Delma australis	Pygopodidae	SAMA R22784
Delma borea	Pygopodidae	WAM R10881
Delma butleri	Pygopodidae	AMS R130986
Delma concinna	Pygopodidae	WAM R141175
Delma desmosa	Pygopodidae	WAM R114555
Delma elegans	Pygopodidae	WAM R146640

Delma fraseri	Pygopodidae	WAM R141191
Delma grayii	Pygopodidae	WAM R115749
Delma haroldi	Pygopodidae	NTM R16484
Delma hebesa	Pygopodidae	WAM R132154
Delma impar	Pygopodidae	SAMA R43328
Delma inornata	Pygopodidae	AMS R142790
Delma labialis	Pygopodidae	QM J62835
Delma mitella	Pygopodidae	ABTC 58998
Delma molleri	Pygopodidae	SAMA R23137
Delma nasuta	Pygopodidae	SAMA R42914
Delma pax	Pygopodidae	WAM R134068
Delma petersoni	Pygopodidae	WAM R165873
Delma plebeia	Pygopodidae	QM J80132
Delma tealei	Pygopodidae	WAM R153813
Delma tincta	Pygopodidae	WAM R102815
Delma torquata	Pygopodidae	QM J83187
Diplodactylus baraganae	Diplodactylidae	NTM R21395
Diplodactylus bilybara	Diplodactylidae	WAM R102503
Diplodactylus calcicolus	Diplodactylidae	WAM R144224
Diplodactylus capensis	Diplodactylidae	DV.101
Diplodactylus conspicillatus	Diplodactylidae	WAM R110770
Diplodactylus custos	Diplodactylidae	WAM R172675
Diplodactylus fulleri	Diplodactylidae	WAM R157967
Diplodactylus furcosus	Diplodactylidae	SAMA R41131
Diplodactylus galaxias	Diplodactylidae	R132581
Diplodactylus galeatus	Diplodactylidae	SAMA R54738
Diplodactylus granariensis	Diplodactylidae	AMS R151162
Diplodactylus hilli	Diplodactylidae	NTM R17871
Diplodactylus klugei	Diplodactylidae	WAM R120870
Diplodactylus laevis	Diplodactylidae	WAM R172197
Diplodactylus lateroides	Diplodactylidae	WAM R165286
Diplodactylus mitchelli	Diplodactylidae	WAM R152704
Diplodactylus nebulosus	Diplodactylidae	WAM R168640
Diplodactylus ornatus	Diplodactylidae	AMS R140546
Diplodactylus platyurus	Diplodactylidae	AMS R143914
Diplodactylus polyopthalmus	Diplodactylidae	WAM R129887
Diplodactylus pulcher	Diplodactylidae	WAM R146811
Diplodactylus savagei	Diplodactylidae	R108605
Diplodactylus tessellatus	Diplodactylidae	SAMA R30400
Diplodactylus vittatus	Diplodactylidae	AMS R158588
Diplodactylus wiru	Diplodactylidae	SAMA R32052
Hesperoedura reticulata	Diplodactylidae	SAMA R23035

Lialis burtonis	Pygopodidae	JFBM 8
Lucasium alboguttatum	Diplodactylidae	WAM R132945
Lucasium bungabinna	Diplodactylidae	SAMA R32049
Lucasium byrnei	Diplodactylidae	SAMA R52296
Lucasium damaeum	Diplodactylidae	WAM R145933
Lucasium immaculatum	Diplodactylidae	QM J62375
Lucasium maini	Diplodactylidae	AMS R150647
Lucasium occultum	Diplodactylidae	NTM R35008
Lucasium squarrosum	Diplodactylidae	WAM R141462
Lucasium steindachneri	Diplodactylidae	SAMA R42749
Lucasium stenodactylum	Diplodactylidae	AMB 54
Lucasium wombeyi	Diplodactylidae	WAM R157787
Naultinus elegans	Diplodactylidae (NZ)	GU459354
Nebulifera robusta	Diplodactylidae	ABTC 3938
Nephrurus amyae	Carphodactylidae	NTM R18239
Nephrurus asper	Carphodactylidae	QM J54644
Nephrurus deleani	Carphodactylidae	SAMA R47063
Nephrurus laevissimus	Carphodactylidae	SAMA R31893
Nephrurus levis occidentalis	Carphodactylidae	WAM R139548
Nephrurus sheai	Carphodactylidae	WAM R156744 (ND2); QM J57515
Nephrurus stellatus	Carphodactylidae	ABTC 89286
Nephrurus vertebralis	Carphodactylidae	WAM R127566; WAM R146822 (RAG)
Nephrurus wheeleri wheeleri	Carphodactylidae	WAM R137379
Oedodera marmorata	Diplodactylidae (NZ)	AMS R161254
Oedura castelnaui	Diplodactylidae	AMS R143917
Oedura coggeri	Diplodactylidae	AMS R143918
Oedura filicipoda	Diplodactylidae	AMS R126183
Oedura gemmata	Diplodactylidae	SAMA R34170
Oedura gracilis	Diplodactylidae	AMS R136067
Oedura bella	Diplodactylidae	PMO B
Oedura cincta	Diplodactylidae	WAM R154797
Oedura monilis	Diplodactylidae	SAMA R54507
Oedura murrumanu	Diplodactylidae	RL 526
Oedura tryoni	Diplodactylidae	AMS R157247
Ophidiocephalus taeniatus	Pygopodidae	SAMA R44653
Orraya occultus	Carphodactylidae	QM A002513
Paradelma orientalis	Pygopodidae	QM J56089
Phyllurus amnicola	Carphodactylidae	QM J64406
Phyllurus championae	Carphodactylidae	Hoskins 5
Phyllurus gulbaru	Carphodactylidae	Hoskins 1
Phyllurus isis	Carphodactylidae	Hoskins 4
Phyllurus kabikabi	Carphodactylidae	ABTC 5123

Phyllurus ossa	Carphodactylidae	Hoskins 5
Phyllurus platurus	Carphodactylidae	ABTC 51012 (ND2); AMB 42
Pletholax gracilis	Pygopodidae	WBJ 2483
Pseudothecadactylus australis	Diplodactylidae	QM J157120
Pseudothecadactylus cavaticus	Diplodactylidae	WAM R138873
Pseudothecadactylus lindneri	Diplodactylidae	AMB 51; AMB 84 (PDC)
Pygopus lepidopodus	Pygopodidae	WBJ 1206
Pygopus nigriceps	Pygopodidae	AMS R140840; AMB 53 (PDC)
Pygopus robertsi	Pygopodidae	QM J14715
Pygopus schraderi	Pygopodidae	SAMA R54037
Pygopus steelescotti	Pygopodidae	NTM R35022
Rhynchoedura angusta	Diplodactylidae	Gko406
Rhynchoedura eyrensis	Diplodactylidae	Gko422
Rhynchoedura ormsbyi	Diplodactylidae	Gko393
Rhynchoedura ornata	Diplodactylidae	ANWC 6141 (ND2); AMS R155371
Rhynchoedura sexapora	Diplodactylidae	Gko704
Saltuarius cornutus	Carphodactylidae	QM J60629
Saltuarius moritzi	Carphodactylidae	AMS R163012
Saltuarius salebrosus	Carphodactylidae	Hoskins 5
Saltuarius swaini	Carphodactylidae	AMS R143262
Saltuarius wyberba	Carphodactylidae	QM J61542
Strophurus assimilis	Diplodactylidae	AMS R149832
Strophurus ciliaris	Diplodactylidae	AMS R147216
Strophurus elderi	Diplodactylidae	SAMA R29924 (ND2); AMS R130987
Strophurus horneri	Diplodactylidae	NMV D72591
Strophurus intermedius	Diplodactylidae	AMS R132992; AMS R158434 (PDC)
Strophurus jeanae	Diplodactylidae	53.Turree
Strophurus krisalys	Diplodactylidae	QM J83557 (ND2); SAMA R54523
Strophurus mcmillani	Diplodactylidae	68.Bigge.Is
Strophurus michaelseni	Diplodactylidae	WAM R 119199
Strophurus rankini	Diplodactylidae	SAMA R22889 (ND2); AMS R140490
Strophurus robinsoni	Diplodactylidae	Keep.River.NP
Strophurus spinigerus	Diplodactylidae	AMS R179833; AMS R149815 (PDC)
Strophurus strophurus	Diplodactylidae	AMS R179820; AMS R140536 (PDC)
Strophurus taeniatus	Diplodactylidae	246.Victoria.River
Strophurus taenicauda	Diplodactylidae	DV 643
Strophurus wellingtonae	Diplodactylidae	WAM R146819 (ND2); WAM R145495
Strophurus williamsi	Diplodactylidae	QM J76799 (ND2); QM J48398
Strophurus wilsoni	Diplodactylidae	WAM R156206
Underwoodisaurus milii	Carphodactylidae	SAMA R38006
Underwoodisaurus seorsus	Carphodactylidae	ABTC 80807
Uvidocolis sphyrurus	Carphodactylidae	AMS R152381; AMS R152351 (PDC)

Amphisbaena alba	Outgroup: Squamate	CHUNB 38770
Anolis carolinensis	Outgroup: Squamate	GenBank
Aspidocelis tigris	Outgroup: Squamate	TG 00069
Dibamus bouretti	Outgroup: Squamate	ROM 36056
Elgaria kingii	Outgroup: Squamate	TG 00065
Gallus gallus	Outgroup: Archosauria	NM001031188
Heloderma suspectum	Outgroup: Squamate	TG 00068
Plestiodon inexpectatus	Outgroup: Squamate	TG 00792
Podarcis sicula	Outgroup: Squamate	TG 00124
Python molurus	Outgroup: Squamate	NA
Ramphotyphlops braminus	Outgroup: Squamate	AY662612
Rhineura floridana	Outgroup: Squamate	FLMNH 141814
Sphaerodactylus glaucus	Outgroup: Squamate	NA
Sphaerodactylus roosevelti	Outgroup: Squamate	NA
Sphaerodactylus torrei	Outgroup: Squamate	NA
Sphenodon punctatus	Outgroup: Squamate	AY662576
Teratoscincus roborowskii	Outgroup: Squamate	NA
Teratoscincus scincus	Outgroup: Squamate	NA
Tiliqua rugosa	Outgroup: Squamate	JFBM 13685
Triocercos jacksonii	Outgroup: Squamate	FJ984187
Woodworthia maculata	Outgroup: Squamate	NA
Xantusia vigilis	Outgroup: Squamate	TG 00121
Aeluroscalabotes felinus	Outgroup: Eublepharidae	JB 16
Eublepharis macularius	Outgroup: Eublepharidae	TG 00081
Christinus marmoratus	Outgroup: Gekkonidae	AMS R135330
Cyrtodactylus novaeguineae	Outgroup: Gekkonidae	FK 11689
Cyrtodactylus ayeyarwardyensis	Outgroup: Gekkonidae	CAS 216446
Hemidactylus palaichthus	Outgroup: Gekkonidae	LSUMZ 12421
Hemidactylus platyurus	Outgroup: Gekkonidae	JFBM 15815
Phyllodactylus tuberculosus	Outgroup: Phyllodactylidae	KU 289758
Phyllodactylus unctus	Outgroup: Phyllodactylidae	ROM 39002
Sphaerodactylus glaucus	Outgroup: Sphaerodactylidae	JAC 24229
Sphaerodactylus roosevelti	Outgroup: Sphaerodactylidae	TG 691
Sphaerodactylus torrei	Outgroup: Sphaerodactylidae	JB 34
Teratoscincus roborowskii	Outgroup: Sphaerodactylidae	JFBM
Teratoscincus scincus	Outgroup: Sphaerodactylidae	JFBM14252

Table S2. Fossil calibrations collected for this study. The "Used?" column indicates whether we implemented the fossil calibration point in this study. Upper group shows calibrations used on both the nuclear only and combined dating analyses. Lower group shows secondary calibrations acquired from the initial dating analysis, and applied to the combined dating analysis only.

Used?	Name	Split	Calibration Type	Min. Age	Max. Age	Distribution	Citations
Calibrations for nuclear only *and* combined (mtDNA + nDNA) dating analyses							
✓	Root	Lepidosauria + Archosauria	secondary	252	257	normal	Reisz & Müller, 2004
✓	Lepidosauria	Sphenodon + Squamata	fossil calibration of Polysphenodon and Brachyrhinodon	225	ind.	exponential offset=10	Evans, 2003
✓	Anguimorpha	Anguidae + Helodermatidae	fossil calibration of Primaderma nessovi	99	ind.	exponential offset=10	Nydam, 2000
✓	Gekkota	Gekkkota	fossil calibration of Hoburogekko suchanovi	110	ind.	exponential offset=10	Daza, Alifanov & Bauer, 2012
✗	Pygopodidae	Delma + other pygopodids	fossil calibration of Pygopus hortulanus	20	22	exponential offset=10	Hutchinson, 1997
✓	Sphaerodactylus	Crown Sphaerodactylus	fossil calibration of S. dommeli and S. ciguapa	15	ind.	exponential offset=4	Daza & Bauer, 2012
✗	Teratoscincus	T.scincus + T.roborowskii	biogeographic calibration	10		normal	Abdrakhmatov et al., 1996
✗	Serpentes	Scolecophidia + Alethinophidia	fossil calibration of Coniophis sp.	98.3	113	normal	Gardner & Cifelli, 1999; Head, 2015
✗	Alethinophidia	Macrostomata + Anilioidea	fossil calibration of Haasiophis terrasanctus	93.9	100.5		Head, 2015
✗	Anilioidea	Aniliidae + Tropidophiidae	fossil calibration of Australophis anilioides	72.1	ind.		Tchernov et al., 2000; Head, 2015
✗	Boidae	Boinae + Erycinae	fossil calibration of Titanoboa cerrejonensis	58	64		Head, 2015; Woodburne et al., 2014; Jaramillo et al., 2007
✗	Corallus	Corallus + Epicrates group	fossil calibration of Corallus priscus	50.2	64		Rage, 2001; Head, 2015; Woodburne et al., 2014
✗	Epicrates group	Eunectes + Epicrates	fossil calibration of Eunectes stirtoni	12.4	ind.		Head, 2015
✗	Charinidae	Ungaliophiinae + Charininae	fossil calibration of Calamagras weigeli	18.7	ind.		Smith, 2013; Head, 2015
✗	Loxocemidae	Loxocemidae + Pythonidae	fossil calibration of UNSM 125562, as of unnamed	35.2	ind.		Smith, 2013; Head, 2015
✗	Morelia	Morelia+Antaresia	fossil calibration of Morelia riversleighensis	12.5	ind.		Scanlon, 2001; Smith & Plane, 1985; Head, 2015
✗	Xantusidae	Xantusia + Lepidophyma		54			
Additional constraints for combined (mtDNA + nDNA) dating analysis only							
✓	Amalosia	Crown Amalosia	secondary	11.5	20	uniform	This study
✓	Aprasia	Crown Aprasia	secondary	8.5	17	uniform	This study
✓	Carphodactylidae	Crown Carphodactylidae	secondary	21.5	36	uniform	This study
✓	Crendadactylus	Crown Crenadactylus	secondary	14.5	29.5	uniform	This study
✓	Delma	Crown Delma	secondary	14	22.5	uniform	This study
✓	Diplodactylidae	Crown Diplodactylidae	secondary	41	55.5	uniform	This study
✓	Diplodactylus	Dip/Luc/Rhynch Crown Split	secondary	20	29	uniform	This study
✓	Leaftails	Saltuarius/Phyllurus Split	secondary	12	21	uniform	This study
✓	Luc+Rhynch	Lucasium/Rhynchoedura Split	secondary	15	22.5	uniform	This study
✓	Nephrurus	Crown Nephrurus	secondary	8	16	uniform	This study
✓	Oedura	Crown Oedura	secondary	12	19	uniform	This study
✓	Pygopodidae	Crown Pygopodidae	secondary	19.5	29	uniform	This study
✓	Strophurus	Crown Strophurus	secondary	15.5	23	uniform	This study

Table S3. Results of temporal and among clade estimates of diversification rate heterogeneity, grouped by analytical program. Significant (bold) decreasing gamma statistics across all groups show a departure from a pure birth model and general decreasing rates of speciation near the present, across all groups. BAMM analysis recognizes no significant among clade differences in diversification rates. CoMET, TreePar, and LASER identify considerable heterotachy in diversification rates at both deep (30 Ma) and shallow (<10 Ma) scales. Though programs generally agree on the number of shifts, they often disagree in timed placement of recent shifts.

	Gamma Statistic		Program: No. Shifts (shift time)				
	score	*p*-value	BAMM	CoMET	TESS	TreePar	LASER
Pygopodoidea	-6.753	**7.22E-12**	0	3 (30ME, 9, 5)	2 (7, 4)	3 (30, 8, 4)	3 (30, 7.5, 3.3)
Pygopodidae	-3.713	**1.00E-04**	0	1 (5)	0 (constant)	1 (5)	1 (2)
Carphodactylidae	-2.148	**0.015**	0	1 (3)	0 (constant)	1 (3)	3 (8, 5, 3.3)
Diplodactylidae	-6.272	**1.08E-10**	0	2 (9, 4)	not tested	3 (16, 10, 4)	3 (30, 9.6, 3)
core Diplodactylidae	-6.337	**1.17E-10**	0	2 (7, 4)	0 (constant)	2 (16, 4)	2 (9.7, 3)

Table S4. Diversification rate estimates across the Pygopodoidea, by program. CoMET, TreePar, and LASER, the episodic rate-varying models, show a series of constant rates between episodic shifts. BAMM provides a single mean estimate of diversification rate. Rates across all programs generally decrease toward the present.

				Diversification Rates						
	Method	Model Pref.		Rate 1	Rate 2	Rate 3	Rate 4	logLik	#P	AIC
Pygopodoidea Geckos	LASER	yule4rate	λ	0.0288	0.1311	0.0614	0.0126	112.9054	7	-204.5160
			μ	0	0	0	0			
	TESS	**bd2shift +ME**	λ	**0.0988**	**0.0536**	**0.0201**	—	**112.1287**	**9**	**-206.2573**
			μ	**0.0000**	**0.0000**	**0.0000**	—			
	TreePar	bd3shift	λ	0.0271	0.1297	0.0723	0.0173	108.8328	11	-195.6656
			μ	0.0620	0.0000	0.0154	0.0788			
	BAMM	constant	λ	0.0938	—	—	—			
			μ	—	—	—	—			

Table S5. Results of GeoSSE analysis of diversification rates by biome. Analyses were broken down by biome, comparing rates of a single biome (A) against all other biomes combined (B). Available parameters are speciation (sA, sB, sAB—speciation between A and B), extinction (xA, xB), and transition/dispersal between biomes (dA, A→B; dB, B→A). We constrained these parameters in a series of nested models: full—all parameters may vary independently; no.sAB—no speciation between biomes (sAB~0); eq.div—equal speciation in regions A and B (sA~sB); eq.disp—equal dispersal from A→B and B→A (dA~dB). Estimates for extinction were near 0 across all analyses so we dropped those values from this table, and removed the equal extinction model (xA~xB). We compared models using likelihood ratio tests and AIC values, to determine the preferred model for each biome (in **bold**) and the associated estimates of diversification and dispersal rates, and rejected significantly poorer fitting models (*). Confidence intervals established by simulation of neutral characters across 100 trees provided baseline estimates for rates as expected by chance. Rate estimates which exceed our CI (e.g. arid zone speciation and dispersal) are in **bold** and underlined.

		sA	sB	sAB	dA	dB	Df	logLik	AIC	ΔAIC
Arid	**full**	**0.0925**	0.0350	0.2405	**0.0565**	0.0000	7	-685.80	1385.6	—
	no.sAB *	0.1681	0.0360	—	0.0366	0.0000	6	-702.63	1417.3	**31.7**
	eq.div *	0.0539	0.0539	0.2312	0.0419	0.0104	6	-689.79	1391.6	**6**
	eq.disp*	0.0604	0.0485	0.2359	0.0263	0.0263	6	-692.23	1396.5	**10.9**
Arid with Mesic Refugia	**full**	**0.0694**	0.0491	0.1463	**0.0506**	0.0000	7	-669.02	1352.0	—
	no.sAB *	0.1148	0.0491	0.0000	0.0388	0.0000	6	-676.96	1365.9	**13.9**
	eq.div *	0.0584	0.0584	0.1370	0.0490	0.0000	6	-670.88	1353.8	1.8
	eq.disp*	0.0658	0.0579	0.1304	0.0000	0.0000	6	-677.52	1367.0	**15**
Temperate	full	0.0235	0.0720	0.2999	0.0000	0.0092	7	-622.29	1258.6	0.6
	no.sAB *	0.1472	0.0618	—	0.0527	0.0026	6	-632.02	1276.0	**18**
	eq.div *	0.0674	0.0674	0.3277	0.0000	0.0090	6	-626.39	1264.8	**6.8**
	eq.disp	**0.0257**	**0.0716**	0.3219	**0.0087**	0.0087	6	-622.98	1258.0	—
Savannah	**full**	**0.0310**	**0.0720**	0.4286	0.0137	0.0087	7	-620.55	1255.1	—
	no.sAB*	0.1216	0.0704	—	0.0198	0.0088	6	-637.53	1287.1	**32**
	eq.div*	0.0659	0.0659	0.4617	0.0208	0.0089	6	-624.40	1260.8	**5.7**
	eq.disp	0.0303	0.0724	0.3870	0.0092	0.0092	6	-620.64	1253.3	1.8
Subtropical	full	0.0000	0.0725	0.1942	0.0000	0.0142	7	-639.51	1293.0	**5.1**
	no.sAB *	0.1419	0.0557	—	0.0809	0.0044	6	-648.24	1308.5	**20.6**
	eq.div	**0.0521**	0.0521	0.3219	**0.1279**	0.0012	6	-637.94	1287.9	—
	eq.disp	0.0000	0.0720	0.2189	0.0160	0.0160	6	-640.62	1293.2	**5.3**
Forest	full	0.0528	0.0750	0.0231	0.0000	0.0006	7	-565.03	1144.0	1.8
	no.sAB	0.0610	0.0750	—	0.0004	0.0006	6	-565.68	1143.3	1.1
	eq.div	0.0730	0.0730	0.0173	0.0000	0.0006	6	-565.77	1143.5	1.3
	eq.disp	0.0525	0.0750	0.0234	0.0005	0.0005	6	-565.08	1142.2	—
Null Model Simulation	full (highest)	0.0628	0.0107	—	0.0551	0.0101	7			
	full (95%)	0.0603	0.0128	—	0.0505	0.0131	7			

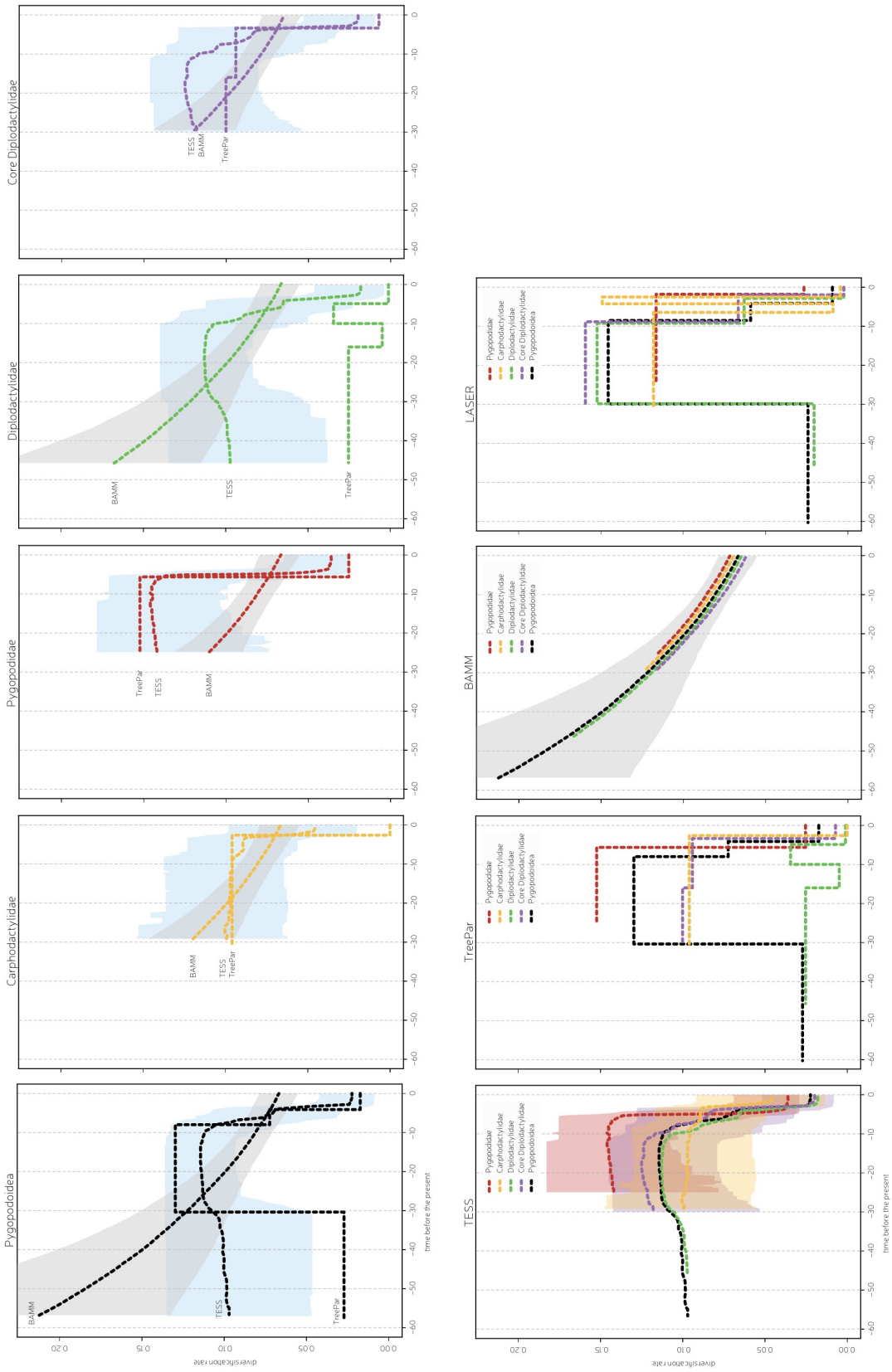
Core Diplodactylidae
Diplodactylidae
Pygopodidae
Carphodactylidae
Pygopodoidea
TESS
BAMM
TreePar
LASER
Pygopodidae
Carphodactylidae
Diplodactylidae
Core Diplodactylidae
Pygopodoidea
diversification rate
time before the present

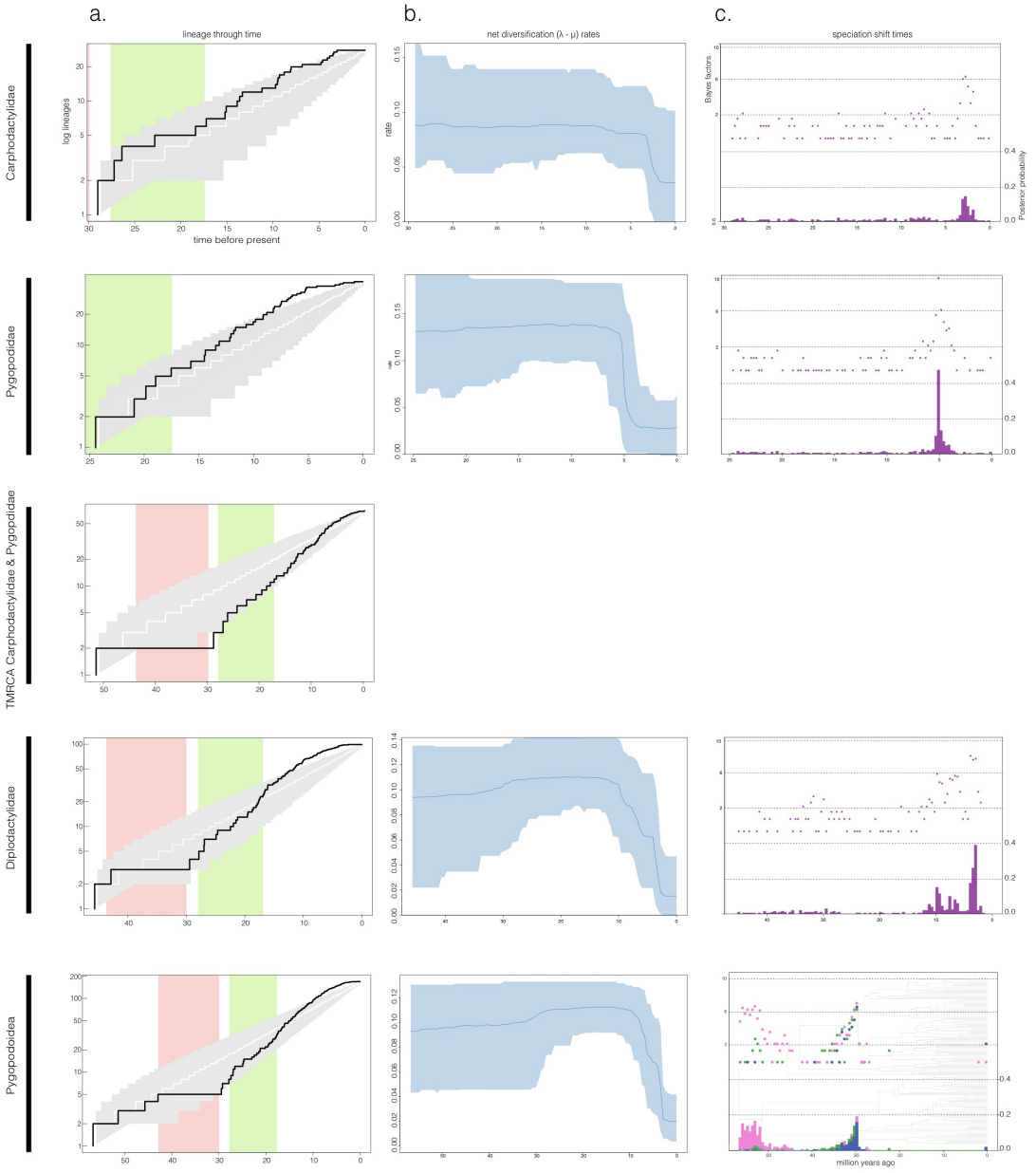
a.
b.
c.
lineage through time
net diversification (λ - μ) rates
speciation shift times
log lineages
rate
Bayes factors
Posterior probability
time before present
million years ago
Carphodactylidae
Pygopodidae
TMRCA Carphodactylidae & Pygopodidae
Diplodactylidae
Pygopodoidea

tree names
No.Archosauria
No.Gekkota
No.Helo.Ang
No.Lepidosaur
No.Sphaerodactylus
Posterior Distribution trees
Crown Pygopodoidea
MRCA Carpho + Pygo
Crown Carphodactylidae
Crown Pygopodidae
All Diplodactylidae
'Crown' Oz Diplodactylidae
Distance (million years) from nuclear MCC tree (0-centered)

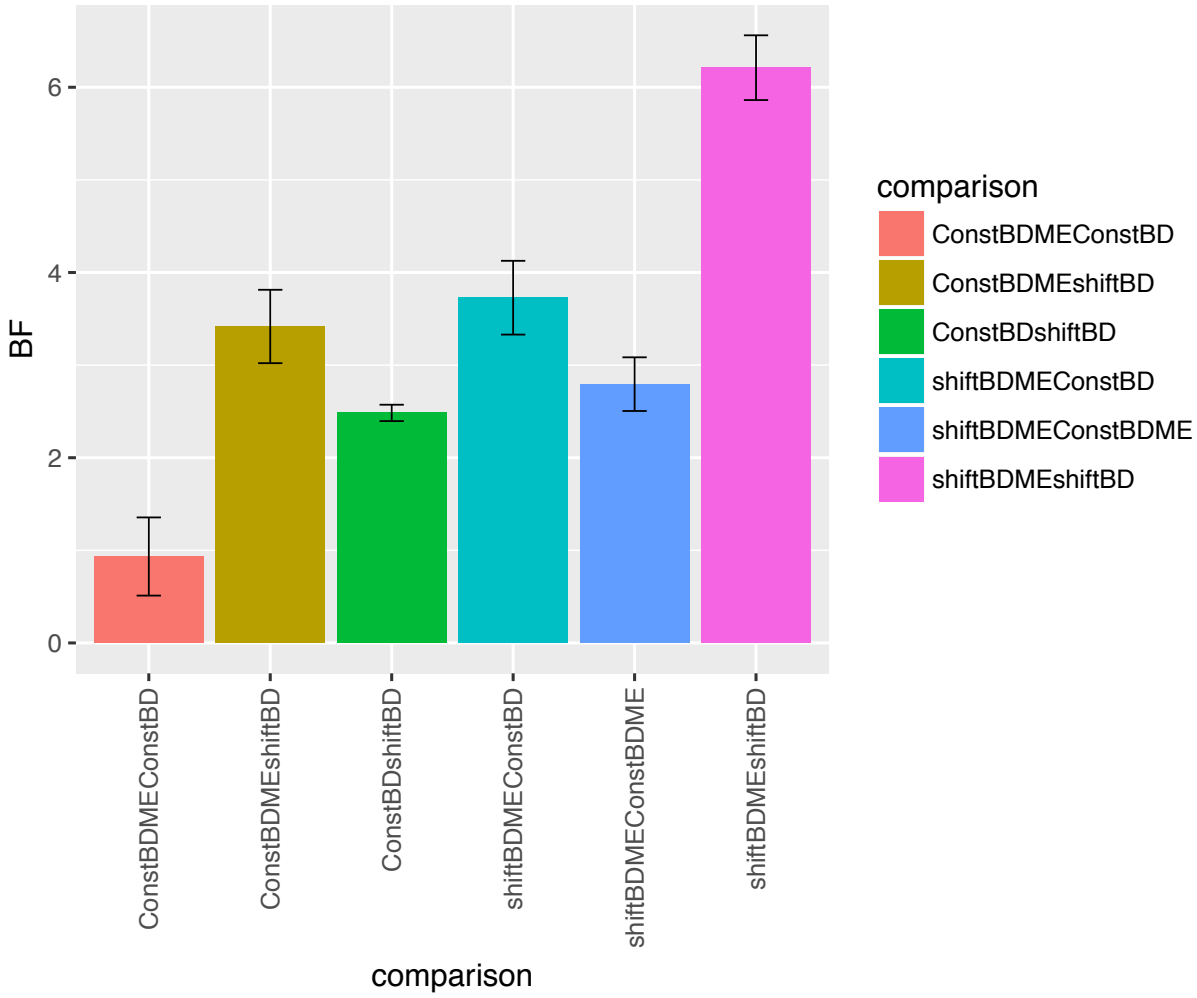
BF
6
4
2
0
ConstBDMEConstBD
ConstBDMEshiftBD
ConstBDshiftBD
shiftBDMEConstBD
shiftBDMEConstBDME
shiftBDMEshiftBD
comparison
comparison
ConstBDMEConstBD
ConstBDMEshiftBD
ConstBDshiftBD
shiftBDMEConstBD
shiftBDMEConstBDME
shiftBDMEshiftBD

Figure S1. Comparison of estimated rates of speciation among taxonomic groups, and analytical programs. Top row shows rates estimated by BAMM, TESS (CoMET), and TreePar, grouped by pygopodoid subclades. Bottom row shows speciation rates as among taxonomic groups, grouped by analytical program. Shaded regions in upper row indicate confidence intervals for rate estimates of BAMM (grey) and TESS (blue) analyses. Shaded regions in lower row indicate confidence intervals as estimated by TESS for the Pygopodidae (red), core Diplodactylidae (purple), and Carphodactylidae (yellow); and BAMM (grey).

Figure S2. Results of varied analyses of diversification across the Pygopodoidea and subclades. Rows correspond to the (1) Carphodactylidae, (2) Pygopodidae, (3) TMRCA Carphodactylidae + Pygopodidae, (4) Diplodactylidae, (5) Pygopodoidea. X-axes all denote the time before present in millions of years. Column (a) shows empirical lineage through time plots (black line) superimposed on top of 95% CI (grey shaded area) constructed from simulated trees conditioned on age and number of taxa. Green and pink shaded vertical bars coincide with identical bars in Fig.1. Column (b) shows the CoMET mean estimates of net diversification rates ($\lambda - \mu$) through time as blue lines, and the 95% CI as a lighter blue shaded area. Column (c) shows temporally placed estimates of shifts in speciation rates, as supported by Bayes Factors (upper portion of graph, left y-axis) and posterior probabilities (lower portion of graph, right y-axis), from CoMET. Column (c) graph for the Pygopodoidea shows temporally placed estimates of mass turnover events conditioned on survival (blue), taxa (green), and time (pink), as supported by Bayes Factors (top portion of graph, left y-axis) and posterior probabilities (lower portion of graph, right y-axis).

Figure S3. Results of tests of fossil calibration effects on dating analyses. Focal nodes are shown along the x axis, and distance (in millions of years) from age estimates of the MCC tree are plotted along the y axis. Fossil removal schemes are shown color coded and listed in the legend to the right, and refer to fossil calibrations listed in Table S2. Results are compared against 100 randomly sampled trees from the posterior distribution of our nuclear-only dating analysis, indicating a concordance in divergence time estimations.

Figure S4. Bayes factor comparisons among constant rate (crbd = ConstBD, crbdme = ConstBDME) and variable rate (vrbd = shiftBD, vrbdme = shiftBDME) TESS models investigating support for a mass extinction event. Y axis shows the difference between the two models in Bayes factors (support for the first model). Models including mass extinction (ME) were always favored over alternatives, however strength of support varied.

Supplemental Methods:

Diversification and Rates

To visualize diversity through time, we used lineage-through-time (LTT) plots generated in the package LASER (Rabosky 2006) as implemented in GEIGER (Harmon et al. 2008). To determine if the accumulation of species richness adheres to a constant rate model, or is punctuated by mass extinction, we simulated two sets of 5,000 rate-constant (pure-birth, PB, extinction = 0; birth-death, BD, speciation = 0.1, extinction = 0.01), null model trees conditioned on the age and species richness of the Pygopodoidea. We repeated this task for an additional set of trees for each of the Pygopodidae, Carphodactylidae, Diplodactylidae, 'core Diplodactylidae' (excluding the relictual lineages *Crenadactylus* and *Pseudothecadactylus*), and the most recent common ancestor (TMRCA) of the Pygopodidae and Carphodactylidae. From our set of simulated trees we harvested 95% CIs, and plotted these against our empirical LTTs to determine if clade diversity has deviated from expected rate constant patterns. Using LASER, we applied the fitDAICrc function which uses the Akaike information criterion (AIC) test statistic to explicitly determine if our tree best fits a model of rate-constant (pure-birth, birth-death) or rate-variable (density dependent, yule-n-rate) evolution.

TreePar (Stadler 2011b) applies a likelihood approach referred to as the 'birth–death–shift' process, and episodic birth-death model in which rates are contemporarily consistent across all lineages, but may be punctuated temporally by shifts in speciation (lambda— λ) or extinction (mu—μ) or both. Using the bd.shifts.optim function, we executed maximum likelihood estimations under differing numbers (0–6) of shifts, and compared models via likelihood ratio tests (LRT) to determine the best fitting model. Although TreePar does allow for the inclusion of mass extinction in models, it is not

currently possible to include speciation rate changes and mass extinction in the same model. To distinguish between a speciation rate increase or a mass extinction event near the Eocene Oligocene boundary (25–35 million years ago), we instead created two competing models. Both optimized speciation and extinction rate estimates, as well as the time of the event, however one inferred a mass extinction and one a rate shift.

Supplemental Results/Discussion:

Visualization of lineage accumulation through time via LASER draw attention to the long, unbranching stem lineages between crown divergence of the Pygopodoidea and crown divergences of the focal families ~30 Ma. LTT plot of the clade including TMRCA of Carphodactylidae and Pygopodidae (Fig.S2) falls below our 95% CI from both sets of simulated trees (PB and BD), indicating a deviation from expected rate constant diversification.

Methods which do not allow for modelling mass extinction (LASER), or do not allow for the simultaneous estimation of rate shifts and mass extinction (TreePar) provide support for a speciation rate shift directly preceding the crown diversification of pygopodoid families ~30 million years ago (Table 1, Table S4). To differentiate between support for a mass extinction event, or speciation rate shift near the Eocene Oligocene boundary, we compared TreePar models for these events. Bayes factor comparison between the models, across the 100 posterior trees, preferred the mass extinction model (91%), however only marginally (2 ln BF < 3). This provides evidence that a speciation rate increase ~30 million years ago is likely an artifact produced by methods/models which cannot directly infer a mass extinction event as an alternative solution.

Chapter 2:

Miocene biome turnover drove conservative body size evolution across Australian vertebrates

PROCEEDINGS B

rspb.royalsocietypublishing.org

Research

Cite this article: Brennan IG, Keogh JS. 2018 Miocene biome turnover drove conservative body size evolution across Australian vertebrates. *Proc. R. Soc. B* **285**: 20181474. http://dx.doi.org/10.1098/rspb.2018.1474

Received: 1 July 2018
Accepted: 26 September 2018

Subject Category:
Evolution

Subject Areas:
evolution

Keywords:
macroevolution, marsupials, reptiles, phenotypic evolution, adaptive radiation, comparative methods

Author for correspondence:
Ian G. Brennan
e-mail: ian.brennan@anu.edu.au

Electronic supplementary material is available online at https://dx.doi.org/10.6084/m9.figshare.c.4255892.

THE ROYAL SOCIETY PUBLISHING

Miocene biome turnover drove conservative body size evolution across Australian vertebrates

Ian G. Brennan and J. Scott Keogh

Division of Ecology and Evolution, Research School of Biology, Australian National University, Canberra, ACT 2601, Australia

IGB, 0000-0002-4416-5224

On deep time scales, changing climatic trends can have a predictable influence on macroevolution. From evidence of mass extinctions, we know that rapid climatic oscillations can indirectly open niche space and precipitate adaptive radiation, changing the course of ecological diversification. These dramatic shifts in the global climate, however, are rare events relative to extended periods of protracted climate change and biome turnover. It remains unclear whether during gradually changing periods, shifting habitats may instead promote non-adaptive speciation by facilitating allopatry and phenotypic conservatism. Using fossil-calibrated, species-level phylogenies for five Australian radiations comprising more than 800 species, we investigated temporal trends in biogeography and body size evolution. Here, we demonstrate that gradual Miocene cooling and aridification correlates with the restricted phenotypic diversification of multiple ecologically diverse vertebrate groups. This probably occurred as species ranges became fractured and isolated during continental biome restructuring, encouraging a shift towards conservatism in body size evolution. Our results provide further evidence that abiotic changes, not only biotic interactions, may act as selective forces influencing phenotypic macroevolution.

1. Introduction

Changes to the global climate can promote macroevolutionary and macroecological turnover by either abiotic or biotic drivers, or both [1]. Climatic changes may proceed over long or short time periods, varying in intensity from mild to extreme, and as a result, changes to macroevolutionary patterns may respond in kind. To date, the overwhelming majority of literature on this topic has been concerned with the effects of rapid climatic change on the pace and process of diversification. As a result of dramatic events, species richness and ecological diversity may first plummet, then swiftly accumulate. This probably occurs due to opening niche space or release from biotic competitive constraint owing to elevated extinction and provides a popular explanation for adaptive radiations that follow periods of climatic flux [2]. However, such extreme events are rare in evolutionary time, and our knowledge of the influence of the much longer intervening periods of gradual climatic change on macroevolution remains limited. Periods of prolonged climatic change are common in palaeoclimatic history and are often defined by more dramatic events which precede and follow them [3,4]. Despite this, identifying signals of the influence of protracted climate change has been difficult. Whereas rapid environmental change may leave obvious fossil and phylogenetic signatures as a result of shifting origination and/or extinction rates, diversification during gradual climate change may outwardly resemble constant-rate processes. This may result in less obvious anagenetic and assemblage changes and provide the appearance of evolutionary stasis [5–7].

The Miocene epoch (23–5.3 Ma) has figured prominently in the diversification of many extant faunal groups. This is largely the result of climatic

instability, fluctuating atmospheric CO_2 concentrations and floral biome turnover [8–11]. Following the Middle Miocene climatic optimum warm phase (17–15 Ma), the latter half of this epoch (12–5.3 Ma) exhibited a global cooling trend (−0.5°C per million years), exemplified by dropping sea surface temperatures and Antarctic glaciation [12,13]. Global cooling coincided with the birth and expansion of arid biomes and contraction of more mesic ones [13]. In Africa and Asia, ecological replacement of C_3 forest and woodland plants with C_4 savannah in the Mid-to-Late Miocene forced an ecological transition in herbivorous mammals from browsers to grazers [5]. Turnover in the Miocene ungulate assemblage also resulted in directional morphological trends, including a general increase in body size [14,15]. This suggests that prolonged change to the global climate may have indirect influences on macroevolutionary trajectories of some groups. But to what extent are morphological changes consistent among coexisting radiations, and are these changes detectable from contemporary data?

The rise of arid habitats in the Miocene, and the impact of these biomes on diversification patterns, provides an ideal opportunity to investigate their influence across ecologically divergent organismal groups. The Miocene climate developed the Gobi and Sahara deserts [16,17], and in Australia, aridification created the red centre of the continent ('outback' Australia). This resulted in the expansion of sclerophyllous vegetation, and shrinking and fracturing of closed and rainforest biomes [18,19]. The growth of the Australian arid zone during this period has been simultaneously implicated in the rapid speciation of some vertebrate groups [20,21], and range restriction and extinction of other, mesic-adapted groups [22–24]. The implications of habitat turnover in the late Miocene for the morphological evolution of Australian vertebrates, however, have not been investigated. Using fossil-calibrated phylogenies and discrete and continuous characters of five Australian vertebrate groups (>800 species), we investigated the influence of protracted Miocene aridification on phenotypic evolution. These focal radiations (agamid lizards, marsupial mammals, meliphagoid birds, pygopodoid geckos, sphenomorphine skinks) cover a diversity of species richness (100–235 spp.), ecology (fossorial to aerial, dietary specialists and generalists) and age (crown 26–60 Ma), to represent a comprehensive sample of extant Australian terrestrial vertebrate biodiversity. More importantly, this sampling enables us to identify the strength and congruence of signatures from multiple independent clades.

To specifically address macroevolutionary change during this period of flux, we focus on body size and historical biogeography. Body size (as body length or mass) is the most commonly used measurement for studies of ecomorphological diversification owing to its ubiquitous influence on life-history traits and ecology [25–27]. Similarly, species' distributions are representative of both their ecological niche (e.g. habitat/biome types), as well as geographical distribution (e.g. explicit proximity or overlap with other species). With recent advances in phylogenetic comparative methods, we can now model changes in morphology and distribution as temporal trends, providing insight into changes both among and along branches of phylogenetic trees.

Given that periods of intense climatic change may precipitate adaptive radiation, we suggest the opposite may be true for periods of gradual change. Whereas ecomorphological radiation follows mass extinction, instead, non-adaptive processes dictate speciation during periods of protracted biome turnover. To address this concept, we started by investigating signature of Miocene biome rearrangement using likelihood methods to determine temporal trends in the geographical mode of speciation, either allopatric or sympatric. We anticipated that changes to the global and Australian climate during this period facilitated an increase in allopatry by fracturing existing mesic habitats. In this case, we consider a strong link between the geographical speciation process of allopatry and the trait evolutionary process of niche conservatism [28,29]. So, we fitted a series of models to the body size data which follow a narrative of increasing late Miocene phenotypic conservatism. These included mode-shifting processes that increasingly retained ancestral body sizes, via declining evolutionary rates and variances in the late Miocene and Pliocene. Our findings are consistent with our hypothesis that prolonged abiotic environmental changes may indirectly constrain phenotypic evolution. These gradual climatic pressures appear to similarly influence the macroevolutionary trajectories of ecologically diverse contemporaneous groups.

2. Material and methods

(a) Phylogenies, and morphological and biogeographic data

Recently developed analytical methods for modelling and visualizing macroevolutionary trends have facilitated the investigation of diversification dynamics of a number of Australian groups [30,31]. Comparatively few studies, however, have looked into the evolutionary tempo of phenotypic evolution in Australian clades [21,32]. We compiled or generated fossil-calibrated phylogenies of Australian radiations spanning squamate reptiles [21,30], birds (honeyeaters) [33] and mammals [34] (see the electronic supplementary material for tree-building details). The breadth of our focal phylogenies (ecology, age, size) aims to analyse a diverse representation of the most conspicuous and abundant Australian vertebrate groups. Though timing and biogeographic patterns of Australian taxa since the Mid-Miocene onset of aridification has been extensively addressed (see [35] for review), we focus on the influence of environmental turnover and biome rearrangement on the tempo and mode of ecomorphological differentiation.

To model body size macroevolution, we collected body size measurements from the literature, relevant to each phylogenetic group: squamate reptiles—snout-vent length (mm); birds—mass (g), mammals—body length (mm) and log-transformed these to normalize data for all analyses. To address biogeographic changes as a result of changing climate and environments, we treated species distributions in two ways. First, by coding occupancy among biomes. Climatic conditions determine the distribution and suitability of biomes largely by influencing the floral assemblage. In Australia, the primary contemporary biome stressor is precipitation and so we partitioned Australia into five discrete biomes that attempt to best encapsulate the intersection of floral community and precipitation. This biome classification system is modified from the widely used objective Köppen–Geiger system [36] and follows Brennan and Oliver [21]. Second, species distributions were described by spatial occurrence data. We downloaded species occurrence records from the Atlas of Living Australia (ALA; www.ala.org.au) then transformed them into spatial data geometries for further analyses (for specifics of data handling, see the electronic supplementary material). Ultimately, both sets of data were used to reconstruct

ancestral occupancy and distribution, to determine pairwise geographical overlap among species.

(b) Analyses of body size evolution

To investigate the tempo and mode of body size evolution, we used maximum-likelihood to fit a series of rate constant, rate variable, mode variable and mode *and* rate variable models to our continuous data. To account for intraspecific variation and trait measurement error (ME) as a potential source of bias in model selection and parameter estimation [37], we jointly estimated ME as an additional parameter during model fitting. We began with Brownian motion (BM) and Ornstein–Uhlenbeck (OU) models as implemented in Geiger [38]; however, our hypothesis of phenotypic evolution focuses on temporal variation in processes and rates. To address this, we also implemented a series of time–variable evolutionary models. These included early burst (EB), multi-era BMOU [39], environmentally dependent [40] and Lévy jump models [41]. We discuss the assumptions and behaviour of these models more extensively in the electronic supplementary material.

During the late Miocene, aridification resulted in the fragmentation of closed forest habitats [22], potentially leading to elevated allopatric speciation, exaggerating niche conservatism and constraining ecomorphological diversification. Morphological conservatism following the Mid-Miocene climatic optimum (MMCO) may be best modelled by a change in the mode of trait evolution, towards a more constrained process akin to OU. To model this indirect environmental constraint on body size evolution, we implement a mode variable BMOU process. We design two models which are methodologically identical to the BMOU and BMOUi models used in mvMORPH [39] and build on the comparative methods literature of time-stratified evolutionary processes [27,42]. These models allow the trait of interest to evolve under BM from the group's origin until t_{shift}, at which point they transition to an OU process with trait evolution constrained by the α parameter. The first, BMOU, estimates only a single rate (σ^2) of trait evolution along the whole tree. The BMOU model fits a narrative where body size evolved unconstrained until a given point in time, after which size evolution became bounded around a stationary peak. The second, BMOUi, is similar to the BMOU; however, the trait evolution rate also changes (σ_0^2 under BM, σ_1^2 under OU), allowing BM and OU processes to independently explain the accumulated variance of trait evolution in different eras (temporal regimes) of the tree. Because joint estimation of ME is not currently incorporated into mvMORPH, we have built this parameter into our BMOU models found in the 'fitContinuous_paleo' script provided in the supplemental material of Slater [27]. This material is available at the GitHub repository for this publication. To determine our ability to recover mode-shifting models and distinguish them from existing models, we performed a series of simulations outlined in the electronic supplementary material.

Advances in macroevolutionary modelling have provided ever-more complex methods which may better describe the idiosyncracies of evolution. We tested the performance of the process and pattern-driven models alongside several recently developed methods. These model trait evolution as jumps across Simpsonian landscapes (models: Jump-Normal, Normal Inverse Gaussian), with varied waiting times between jumps in trait values [41], or trait variance may instead accumulate in response to additional time-sampled variables like global palaeotemperature (model: ENV) or dispersal rates inferred from an external source (model: BGB—dispersal through time as estimated from BioGeoBears), fitted using RPANDA (function 'fit_t_env') [43]. All models in this study were iteratively applied to 100 trees randomly sampled from the post burn-in posterior distribution from dating analyses of each vertebrate clade, as well as the maximum clade credibility tree (MCC) as summarized by TreeAnnotator v. 2.4.2. To compare models against one another, we calculated Akaike information criterion correction (AICc) values from our likelihood scores and the number of parameters in the given model and estimated the AICc weights (AICcWt) as the contribution of the model to the total fit. We combined the AICcWt results across all trees of a given radiation and used this to compute a mean AICcWt and standard error per model, to determine the best fitting models for each radiation. We plotted the results of our iterative model fitting and comparison using ggplot2 [44].

In the process of comparing models for each given tree, we calculated the ΔAICc between each model and the best fitting model (lowest AICc), deeming $\Delta AICc \geq 4$ as significant evidence of model preference and retained all equally plausible models ($\Delta AICc < 4$) following Burnham and Anderson [45]. We then extracted parameter estimates (all applicable: timing of shift, body size optima θ, constraint α, evolutionary rate σ^2, beta) of those preferred (best) models to evaluate the tempo and mode of trait evolution prior to and following the Late Miocene shift at time t_{shift} (electronic supplementary material, figures S3–S6).

(c) Simulating extinction

Macroevolutionary inferences of trait evolution can be improved upon by the inclusion of fossil taxa [46]. This is particularly true on geological time scales, where extinction is considered to be appreciable [47]. Unfortunately, meaningful fossil records are scant for most terrestrial Australian vertebrate groups, save marsupials. Because of this, it is important to take into account that our use of extant-only phylogenies may introduce bias in our inference of trends in biogeographical and body size macroevolution. To directly address the influence of unobserved extinction, we undertook an exercise using our empirical phylogenies to simulate trees and data under a series of plausible extinction scenarios. These assumed extinction throughout the trees to be phylogenetically and temporally (i) stochastic, (ii) elevated in the Pliocene-Pleistocene, or (iii) elevated in the Late Miocene. The specifics of the design and implementation of this extinction exercise are detailed in the electronic supplementary material.

(d) Biogeographic histories

To investigate if the signal of historical biome turnover is detectable and can be modelled from contemporary distributions, we focused on the frequency and timing of cladogenetic dispersal events. We undertook this initially by summarizing species distributions as their occurrence across Australian biomes, then fitting dispersal models using BioGeoBears [48] in R [49] and RStudio [50]. This framework allowed us to account for uncertainty in ancestral distributions using biogeographic stochastic maps, and the ability to simulate data under the generating dispersal model for comparison against empirical results. From this, we summarized the proportion of cladogenetic events deemed allopatric (occurring between biomes) and plotted temporal trends for both the empirical and simulated data (figure 1*b*). Ultimately, clade-specific dispersal trends (figure 3—'proportion of divergence events'; electronic supplementary material, figure S1) were then used as a time-sampled variable to explain body size evolution (model BGB) in our comparative model fitting analyses.

Alternatively, we used spatial records from the ALA to describe species ranges. Using contemporary point data we modelled ancestral distributions using a BM dispersal method implemented in *rase* [51]. This allowed us to determine pairwise overlap among taxa within each tree and plot temporal trends in allopatric and sympatric speciation (figure 3; electronic supplementary material, figure S1). For specifics on our biogeographic methods, see the electronic supplementary material.

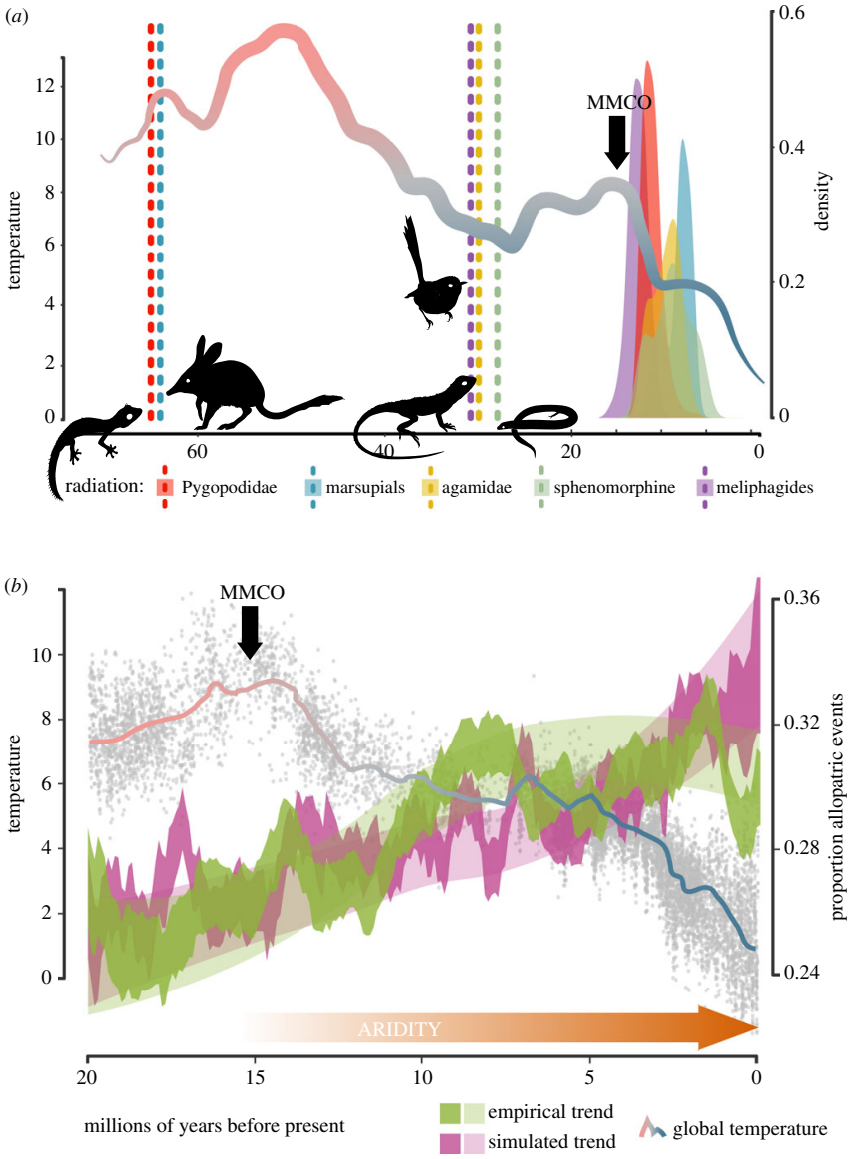

Figure 1. Shifts in evolutionary mode (BM to OU) of body size evolution are temporally clustered in the Late Miocene and congruent with a shift in dispersal histories. (*a*) Dotted vertical lines and density distributions are colour-coded by clade and indicate crown divergences and inferred shift timing of each focal radiation. Shifts between rates or modes (or both) of trait evolution are tightly constrained to the Late Miocene (11–5 Ma). Red-to-blue coloured line shows a global trend in palaeotemperature through the Cenozoic, data from Zachos *et al.* [3]. (*b*) Trends in the dispersal history of Australian radiations from the Early Miocene to present, as inferred from BioGeoBears analyses of empirical and simulated data (i.e. species distributions are observed as biome occurrences). The observed trend in the proportion of allopatric dispersal events (in green) exceeds the expected simulated proportion (purple), in the Late Miocene, coinciding with constraints on body size evolution of select Australian vertebrate clades. Jagged and Loess-smoothed dispersal curves represent two visualization methods of the same trend. Grey dots show palaeotemperature data and the red-to-blue line shows a best fit trend in palaeotemperature data. Note: scales of temperature and time differ between (*a*) and (*b*). MMCO, Mid-Miocene climatic optimum.

(e) Intersecting geographical and phenotypic histories

To investigate body size evolution and determine if conservatism is the result of temporal changes in the prevailing geographical mode of speciation (allopatry or sympatry), we combined our phenotypic and spatial occurrence data. We began by creating a pairwise distance matrix between all tips (terminal nodes) and internal nodes of the tree, representing patristic distances between taxa in millions of years. We repeated this process using trait distances (absolute value of $sp_1 - sp_2$) to determine the amount of phenotypic divergence between species pairs and again using spatial data geometries to ascertain pairwise overlap in distribution (binary: allopatric or sympatric). Unfortunately, shifting species ranges through time, as a result of habitat tracking or evolving niches [52], may erase the signature of the geographical mode of speciation, causing an erroneous signal. To address this, we trimmed these matrices to include only sister pair relationships (terminal node to terminal node, or terminal node to internal node) [53] and plotted the results from 100 trees to visualize temporal trends in phenotypic evolution comparing sympatric to

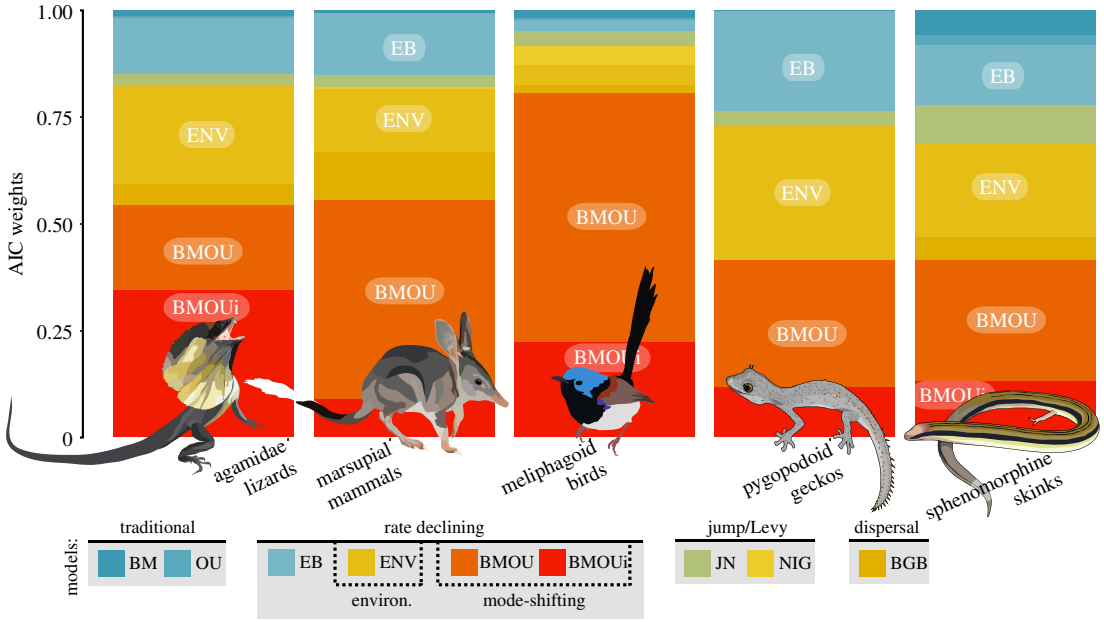

Figure 2. Comparative fit of models to body size data of Australian vertebrate clades finds a preference for rate-declining models (BMOU, BMOUi, EB, ENV). Models are categorized below the plot. BMOU, BMOUi and ENV models are not methodologically explicit rate-declining, but instead, empirical parameter estimates (electronic supplementary material, figures S3,S4,S6) inform this trend. The *y*-axis indicates the relative support for each model as Akaike weights (averaged across 100 posterior trees). The top models which account for a combined more than 0.75 of the AICc weight for each clade are noted on each stacked bar graph.

allopatric species pairs (figure 3, left panel). To further explore the relationship between evolutionary rates and phenotypic variance accumulated between allopatric and sympatric taxa, we mapped range overlap as a binary trait onto our trees and estimated independent evolutionary rates using the BMS model in OUwie [54] (figure 3, right panel). To account for intraspecific variation or error, we provided a uniform value of ME per clade, extracted from the empirical model fits.

3. Results

(a) Body size evolution

The results of comparative model fitting identified three model classes which account for a combined more than 0.75 AICcWt (and up to 0.97) in all five radiations: mode variable (BMOU, BMOUi), global temperature-dependent (ENV) and exponentially declining (EB) (figure 2; electronic supplementary material, figure S2). All four models describe declining evolutionary rates of phenotypic evolution towards the present, with varied intensities and temporal aspects. In the BMOU and BMOUi models, phenotypic variance slows as the evolutionary process shifts in the Mid-to-Late Miocene, with shifts among radiations temporally clustered (11–5 Ma) but not necessarily concurrent (electronic supplementary material, figures S3 and S4). In all focal groups, estimates of beta for the ENV model suggest a positive relationship between Cenozoic temperature fluctuations and body size evolution. As the global temperature dropped following the MMCO, phenotypic rates followed (electronic supplementary material, figure S5). Finally, evolutionary rates decay exponentially (negative beta values) under the EB model, resulting in a considerable slowdown in the accumulation of phenotypic variance towards the tips of the trees (electronic supplementary material, figure S6).

(b) Effects of extinction

In agreement with studies elsewhere [27,46], we find that in the absence of fossil information, false support for non-generating models does increase (electronic supplementary material, figures S7 and S8; for a description of methods, see the electronic supplementary material). In our simulations, this never results in a shift away from the generating model as preferred. This includes the 'worst-case' scenario in which extinction is elevated specifically in the Late Miocene. It is important to note, however, that parameter estimates are dictated by the data provided, and so in the absence of valid fossil information, we rely exclusively on extant taxa for our estimated model values.

(c) Biogeographic histories

Investigating temporal trends in biome dispersal history revealed an increase (5–25% of all events) in the proportion of allopatric events in the Late Miocene. These events, in which sister species (or nodes) do not overlap geographically, increase in relation to sympatric events (figures 1 and 3; electronic supplementary material, figure S1). This result does not appear sensitive to the geographical data used, i.e. if species distributions are coded solely by biome inhabitance (figure 1; electronic supplementary material, figures S1 and S9), or as spatially explicit occurrences (figure 3; electronic supplementary material, figure S1). Elevated trends in allopatric speciation among biomes extend beyond what we would expect from simulations generated under the preferred biogeographic model (always Dispersal Extinction Cladogenesis + jump; see Material and methods). The proportion of allopatric events also increases in a combined analysis across all radiations under both geographical datasets (biome codings and occurrence records).

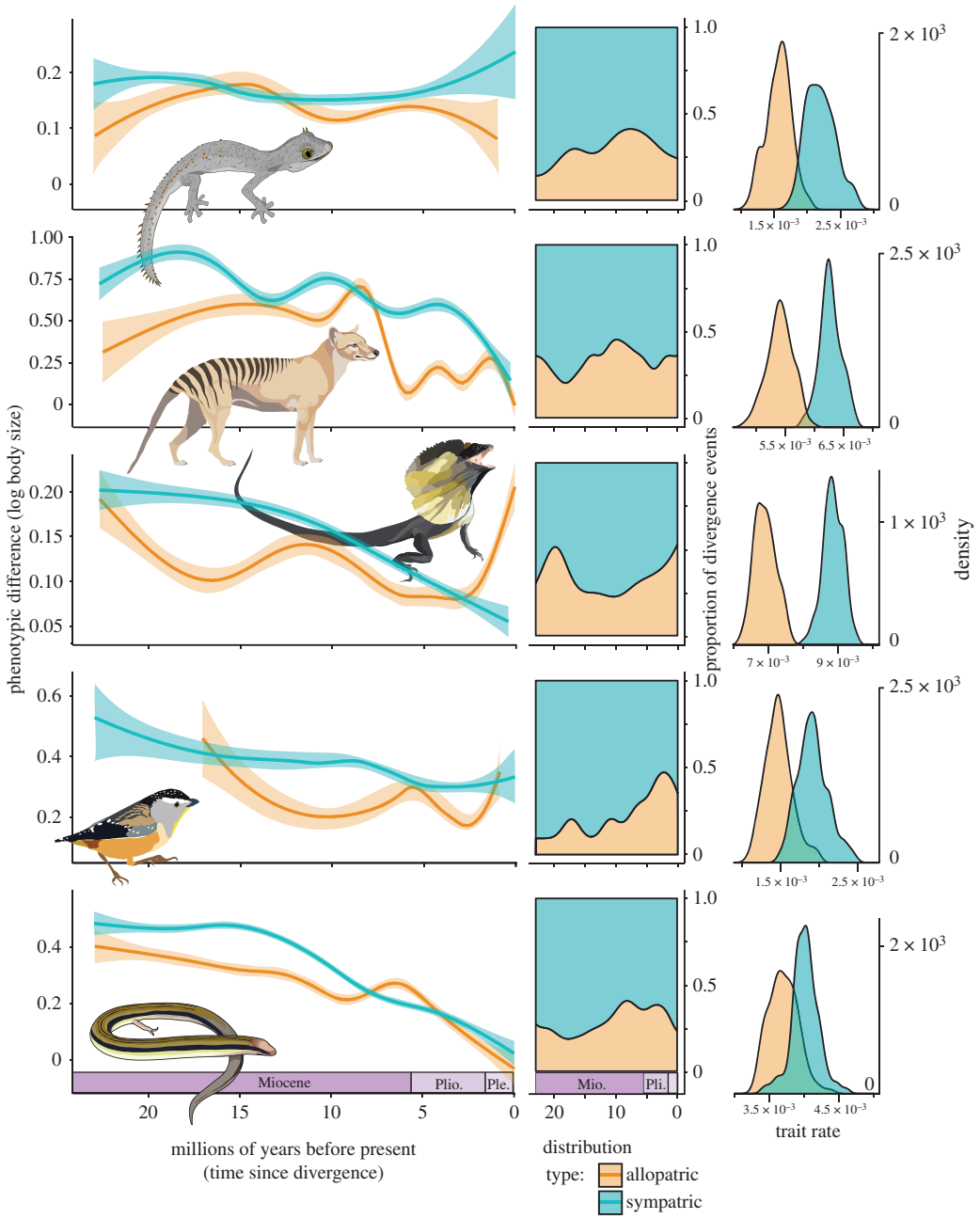

Figure 3. Sympatric and allopatric species pairs display differing trends in body size evolution. Left and centre columns show trends in allopatry and sympatry as inferred using extant species occurrence data and reconstructed ancestral ranges from *rase* [51]. Left column: allopatric species pairs (orange lines) exhibit less phenotypic disparity than sympatric relatives (blue lines) and show more pronounced declines in trait disparity through the Miocene. Centre column: the proportion of divergence events which are allopatric (orange fill) increase through the Miocene in most radiations. These estimates differ slightly from those presented in the electronic supplementary material, figure S1 because of the data used (spatial occurrence records versus biome codings), but see the electronic supplementary material, figure S1 for comparison of trends across all clades using both geographical data. Right column: multi-rate Brownian Motion separate model estimates identify greater evolutionary rates (sigma) for sympatric (blue) sister taxa than allopatric (orange).

(d) Geographical mode of speciation and phenotypic evolution

Using spatial records, trends in body size evolution through time differ between allopatric and sympatric species pairs. Irrespective of time, allopatric taxa exhibit less disparity in body size, and through time, exhibit a greater decrease in disparity in the Late Miocene (figure 3). Lower disparity translates into a lower estimated rate of phenotypic evolution in allopatric taxa in all focal radiations (figure 3, right column). In most cases, the frequency of allopatry as the geographical mode of speciation increases and is temporally consistent with an accelerated decline in phenotypic diversity (figure 3, centre column).

4. Discussion

On deep time scales, ebbs and flows in species richness have generally been attributed to abiotic factors, particularly rapid environmental changes [2,55,56]. In comparison, phenotypic macroevolutionary patterns are most often explained by biotic interactions [57–59]. A growing body of work, however, is beginning to draw attention to the influence of abiotic environmental factors on trait evolution, often across ecologically diverse groups [15,40,60–62]. Here, we investigated the impacts of climate change on body size evolution using an extant continental vertebrate fauna. We first sought to determine if the signal of the process of gradual Miocene biome rearrangement remains detectable from current species distributions by modelling biogeographic histories. Second, we investigated how habitat turnover may have influenced phenotypic evolution. We hypothesized that shifting Miocene habitats may have increased allopatric speciation and by association, reduced rates of body size evolution causing an impression of evolutionary stasis. Our results show that biogeographic dispersal histories across all radiations trend towards increasing allopatry through the Miocene. While it may seem obvious that allopatry is a process independent of trait evolution, it is also a primary cause of niche conservatism, which is not [28,29]. Trends towards increasing allopatry are temporally concordant with a shift towards more conservative body size evolution (decreasing rates and variance). We link these two patterns by observing differing temporal dynamics in the evolution of body size between sympatric and allopatric species. Our results imply a climate-driven shift in the evolution of Australian vertebrate body sizes, and that in the face of changing global climates, macroevolutionary responses across diverse clades may be predictable.

(a) Biome turnover and allopatry

Evidence from palaeontological and neontological data suggest that the Miocene was a period of dramatic climatic and environmental flux across Australia [35,63]. The rise of eucalypts, acacias and chenopods ushered in the birth of modern arid biomes and initiated many common geographical barriers to gene-flow [64]. As habitats shifted, species either shifted their own distribution to track preferable habitat (causing local extinctions) or stayed in place and adjusted to habitat changes (local adaptation), else they went extinct [65]. This resulted in well-documented relictual lineages [22,23,66], particularly in low-vagility groups such as reptiles [67–69] and dasyurid mammals [70,71]. Evidence from the fossil record corroborates this and suggests that habitat tracking may reduce phenotypic variance, promoting morphological stasis and allopatry [52,72]. We observe this in extant allospecies which include exceptional examples of cryptic diversity [68,71,73,74]. These taxa exist in similar habitats, with similar ecologies and morphologies, but are fragmented by suitable habitat and isolated by sometimes tens of millions of years, all hallmarks of conservatism. Broadly across our data, these patterns are consistent: slowdowns in phenotypic evolution are associated with allopatric species pairs, which show less body size disparity than sympatric relatives. It is important to note that there is, however, variation in the intensity and tempo of clade-specific trends, which suggests that environmental pressures may act on intrinsic factors such as ecology to dictate the strength and pace of response.

(b) Declining rates of body size evolution

Australia is home to a number of iconic adaptive radiations that are the result of the continent's extended geographical isolation [75]. These radiations include immense ecological variety, from semelparous carnivorous (*Antechinus*) to gliding herbivorous (*Petaurus*) marsupial mammals, and from arboreal leaf-tailed (Carphodactylidae) to limbless fossorial (Pygopodidae) geckos. To determine the impact of a changing global climate on phenotypic evolution across such diverse groups, we fitted several models which attempt to account for a transition in evolutionary pace and process during the Miocene. Best supported models all suggest declining evolutionary rates over the course of each group's history. This is explained as a result of early accumulation of variance and subsequent decay (EB—electronic supplementary material, figure S6), a positive relationship to cooling global temperatures (ENV—electronic supplementary material, figure S5), or a single shift in process and rate around the Mid-to-Late Miocene time period (BMOU—electronic supplementary material, figure S3, BMOUi—electronic supplementary material, figure S4). Regardless of the specifics, parameter estimates from these models all distinguish between trait evolution occurring at deep and shallower time scales, suggesting differing periods of temporal phenotypic evolution (electronic supplementary material, figure S3–S6).

Outwardly, declining rates result in reduced accumulation of variance and the appearance of periods of morphological stasis [6,7]. To date, the majority of evidence linking phenotypic slowdowns with environmental drivers has been limited largely to fossil data [15,52]. In the absence of reliable fossil records (particularly for squamate reptiles), however, we tentatively suggest the same using molecular and trait data solely from extant taxa. This appearance of stasis may, however, be the result of alternative processes dictating phenotypic evolution. Unpredictable climates might have favoured incremental or gradual steps in trait change (instead of significant jumps), or filtered extreme phenotypes, selecting for generalists. Long-sustained habitats may have also encouraged convergence towards similar trait values, mimicking evolutionary rate declines. Admittedly, all of these are plausible alternatives that are difficult to distinguish with neontological data alone, but present interesting directions for future study. Given existing data and inferred changes to temporal patterns in the process of geographical speciation, we opt to link observed slowdowns in Australian vertebrate trait evolution with gradually shifting global climates and local Australian biome rearrangement.

(c) A changing landscape and phenotypic conservatism

At present, studies investigating periods of protracted climate change are far outnumbered by those studying the effects of dramatic climate turnover. This is probably owing to the more conspicuous diversification and phenotypic shifts which occur following rapid climate change. However, this fails to recognize that periods of gradual climate change predominate geological time. By looking across several cohabiting clades, we find that signature of biome rearrangement may still be readable from extant species, despite the

self-effacing nature of evolution and differing community responses to the expansion of arid habitats [76,77].

Protracted biome rearrangement in Late Miocene Australia has been implicated in allopatric and often cryptic, speciation of mammals [71], reptiles [20], amphibians [78], freshwater fishes [79], spiders [80] and cicadas [23] among others. In some clades (see *Gehyra*, *Diplodactylus*, *Oedura* and *Crenadactylus* geckos; *Ctenotus* and *Lerista* skinks; *Planigale* dasyurids; *Uperoleia* frogs) it is only because of the availability of molecular studies that we have begun to grasp the incredible amount of cryptic diversity that exists. Here, we synthesize trends from several iconic clades to show that conservative phenotypic evolution driven by a cooling global climate and allopatry is a common pattern in Australia. We suggest that for extant taxa, this process is more prevalent than has been previously thought and identify a consistent temporal driver, Miocene climate change. Finally, we find it encouraging that this process is visible on a continental scale, where broad-scale Miocene turnover in terrestrial biomes has accounted for the observed pattern of constrained trait evolution across Australia.

While Australia is unique in its forms of diversity, its biogeographic and phenotypic patterns have probably been shaped by the same processes occurring elsewhere. Changes to the global climate dictate the evolution and succession of biomes, including the expansion of Miocene deserts [16,17]. Though the incredible diversity of body forms of Australian vertebrates appear to have developed early in their evolution, perhaps equally intriguing is the more recent climate-mediated shift towards a non-adaptive process in the Miocene. Results from our study offer evidence that similar processes may have dictated patterns in dispersal history and trait evolution among terrestrial organisms occurring on other continents.

Data accessibility. All data and R code used in this study, as well as supporting materials, results and figures are available on GitHub: https://github.com/IanGBrennan/MioceneAustralia. Details of museum sample numbers and specimen identities can be found in the electronic supplementary material.

Authors' contributions. I.G.B. conceived of the study and collected and analysed the data. I.G.B. and J.S.K. wrote the paper.

Competing interests. We declare we have no competing interests.

Funding. This work has been funded by an Australian Research Council Discovery grant no. (ARC DP150102403) to J.S.K., and an Australian National University International Postgraduate Research Scholarship to I.G.B.

Acknowledgements. We would like to thank the Keogh laboratory group for discussion and comments throughout the development of this project, Rob Lanfear for an unfiltered critique, Alex Skeels for an introduction to spatial data, and Zoe K. M. Reynolds for critical comments and troubleshooting scripts. Thank you to Liam Revell and Graham Slater for help with simulating trait data under varied evolutionary models. Susanne Fritz, Julien Clavel and Michael Landis provided exceptionally thoughtful and constructive suggestions on a previous version of this manuscript. A considerable thank you to the curators and staff of the many Australian Museums and databases (Australian Museum, Northern Territories Museum, South Australian Museum, Queensland Museum, Western Australian Museum, Atlas of Living Australia) for access to tissues and locality data that made this work possible.

References

1. Ezard THG, Aze T, Pearson PN, Purvis A. 2011 Interplay between changing climate and species' ecology drives macroevolutionary dynamics. *Science* **332**, 349–351. (doi:10.1126/science.1203060)
2. Jablonski D. 1989 The biology of mass extinction: a palaeontological view. *Proc. Soc. Lond. B* **325**, 357–368. (doi:10.1098/rstb.1989.0093)
3. Zachos J, Pagani M, Sloan L, Thomas E, Billups K. 2001 Trends, rhythms, and aberrations in global climate 65 Ma to present. *Science* **292**, 686–693. (doi:10.1126/science.1059412)
4. Cramer BS, Miller KG, Barrett PJ, Wright JD. 2011 Late Cretaceous–Neogene trends in deep ocean temperature and continental ice volume: reconciling records of benthic foraminiferal geochemistry (δ18O and Mg/Ca) with sea level history. *J. Geophys. Res. Oceans* **116**, 1–23. (doi:10.1029/2011JC007255)
5. Badgley C, Barry JC, Morgan ME, Nelson SV, Behrensmeyer AK, Cerling TE, Pilbeam D. 2008 Ecological changes in Miocene mammalian record show impact of prolonged climatic forcing. *Proc. Natl Acad. Sci. USA* **105**, 12145–12149. (doi:10.1073/pnas.0805592105)
6. Brett CE, Ivany LC, Schopf KM. 1996 Coordinated stasis: an overview. *Palaeogeogr. Palaeoclimatol. Palaeoecol.* **127**, 1–20. (doi:10.1016/S0031-0182(96)00085-5)
7. Eldredge N *et al.* 2005 The dynamics of evolutionary stasis. *Paleobiology* **31**, 133–145. (doi:10.1666/0094-8373(2005)031[0133:tdoes]2.0.co;2)
8. Hoorn C *et al.* 2010 Amazonia through time: Andean uplift, climate change, landscape evolution, and biodiversity. *Science* **330**, 927–931. (doi:10.1126/science.1194585)
9. Winkler IS, Mitter C, Scheffer SJ. 2009 Repeated climate-linked host shifts have promoted diversification in a temperate clade of leaf-mining flies. *Proc. Natl Acad. Sci. USA* **106**, 18 103–18 108. (doi:10.1073/pnas.0904852106)
10. Pagani M, Freeman KH, Arthur MA. 1999 Late Miocene atmospheric CO_2 concentrations and the expansion of C4 grasses. *Science* **285**, 876–879. (doi:10.1126/science.285.5429.876)
11. Kürschner WM, Kvaček Z, Dilcher DL. 2008 The impact of Miocene atmospheric carbon dioxide fluctuations on climate and the evolution of terrestrial ecosystems. *Proc. Natl Acad. Sci. USA* **105**, 449–453. (doi:10.1073/pnas.0708588105)
12. Savin SM, Abel L, Barrera E, Hodell D, Kennett JP, Murphy M, Keller G, Killingley J, Vincent E. 1985 The evolution of Miocene surface and near-surface marine temperatures: oxygen isotopic evidence. *Geol. Soc. Am. Mem.* **163**, 49–82. (doi:10.1130/MEM163-p49)
13. Herbert TD, Lawrence KT, Tzanova A, Peterson LC, Caballero-Gill R, Kelly CS. 2016 Late Miocene global cooling and the rise of modern ecosystems. *Nat. Geosci.* **9**, 843–847. (doi:10.1038/ngeo2813)
14. Janis C. 2008 An evolutionary history of browsing and grazing ungulates. In *The ecology of browsing and grazing* (eds IJ Gordon, HHT Prins), pp. 21–45. Berlin, Germany: Springer.
15. Vrba SE. 2005 Mass turnover and heterochrony events in response to physical change. *Paleobiology* **31**, 157–174. (doi:10.1666/0094-8373(2005)031[0157:MTAHEI]2.0.CO;2)
16. Caves JK *et al.* 2016 The Neogene de-greening of Central Asia. *Geology* **44**, 887–890. (doi:10.1130/g38267.1)
17. Zhang Z, Ramstein G, Schuster M, Li C, Contoux C, Yan Q. 2014 Aridification of the Sahara desert caused by Tethys Sea shrinkage during the Late Miocene. *Nature* **513**, 401–404. (doi:10.1038/nature13705)
18. Martin HA. 2006 Cenozoic climatic change and the development of the arid vegetation in Australia. *J. Arid Environ.* **66**, 533–563. (doi:10.1016/j.jaridenv.2006.01.009)
19. Crisp MD, Cook LG. 2013 How was the Australian flora assembled over the last 65 million years? A molecular phylogenetic perspective. *Annu. Rev. Ecol.*

Evol. Syst. **44**, 303–324. (doi: 10.1146/annurev-ecolsys-110512-135910)

20. Rabosky DL, Donnellan SC, Talaba AL, Lovette IJ. 2007 Exceptional among-lineage variation in diversification rates during the radiation of Australia's most diverse vertebrate clade. *Proc. R. Soc. B* **274**, 2915–2923. (doi:10.1098/rspb.2007.0924)
21. Brennan IG, Oliver PM. 2017 Mass turnover and recovery dynamics of a diverse Australian continental radiation. *Evolution* **71**, 1351–1365. (doi:10.1111/evo.13207)
22. Bryant LM, Krosch MN. 2016 Lines in the land: a review of evidence for eastern Australia's major biogeographical barriers to closed forest taxa. *Biol. J. Linn. Soc.* **119**, 238–264. (doi:10.1111/bij.12821)
23. Owen CL, Marshall DC, Hill KBR, Simon C. 2017 How the aridification of Australia structured the biogeography and influenced the diversification of a large lineage of Australian cicadas. *Syst. Biol.* **66**, 569–589. (doi:10.5061/dryad.1580p)
24. Cardillo M, Weston PH, Reynolds ZKM, Olde PM, Mast AR, Lemmon EM, Lemmon AR, Bromham L. 2017 The phylogeny and biogeography of Hakea (Proteaceae) reveals the role of biome shifts in a continental plant radiation. *Evolution* **71**, 1928–1943. (doi:10.1111/evo.13276)
25. Peters RH. 1983 *The ecological implications of body size*. Cambridge, UK: Cambridge University Press.
26. Wilson DS. 1975 The adequacy of body size as a niche difference. *Am. Nat.* **109**, 769–784. (doi:10.1086/283042)
27. Slater GJ. 2013 Phylogenetic evidence for a shift in the mode of mammalian body size evolution at the Cretaceous-Palaeogene boundary. *Methods Ecol. Evol.* **4**, 734–744. (doi:10.1111/2041-210X.12084)
28. Wiens JJ. 2004 Speciation and ecology revisited: phylogenetic niche conservatism and the origin of species. *Evolution* **58**, 193–197. (doi:10.1554/03-447)
29. Pyron RA, Costa GC, Patten MA, Burbrink FT. 2015 Phylogenetic niche conservatism and the evolutionary basis of ecological speciation. *Biol. Rev. Camb. Philos. Soc.* **90**, 1248–1262. (doi:10.1111/brv.12154)
30. Rabosky DL, Donnellan SC, Grundler M, Lovette IJ. 2014 Analysis and visualization of complex macroevolutionary dynamics: an example from Australian scincid lizards. *Syst. Biol.* **63**, 610–627. (doi:10.1093/sysbio/syu025)
31. Smissen PJ, Rowe KC. 2016 Repeated biome transitions in the evolution of Australian rodents. *Mol. Phylogenet. Evol.* **128**, 182–191. (doi:10.1016/j.ympev.2018.07.015)
32. Toussaint EFA, Condamine FL, Hawlitschek O, Watts CH, Porch N, Hendrich L, Balke M. 2015 Unveiling the diversification dynamics of Australasian predaceous diving beetles in the Cenozoic. *Syst. Biol.* **64**, 3–24. (doi:10.1093/sysbio/syu067)
33. Marki PZ, Jonsson KA, Irestedt M, Nguyen JM, Rahbek C, Fjeldsa J. 2017 Supermatrix phylogeny and biogeography of the Australasian Meliphagides radiation (Aves: Passeriformes). *Mol. Phylogenet. Evol.* **107**, 516–529. (doi:10.1016/j.ympev.2016.12.021)
34. Mitchell KJ *et al.* 2014 Molecular phylogeny, biogeography, and habitat preference evolution of marsupials. *Mol. Biol. Evol.* **31**, 2322–2330. (doi:10.1093/molbev/msu176)
35. Byrne M *et al.* 2008 Birth of a biome: insights into the assembly and maintenance of the Australian arid zone biota. *Mol. Ecol.* **17**, 4398–4417. (doi:10.1111/j.1365-294X.2008.03899.x)
36. Stern H, De Hoedt G, Ernst J. 2000 Objective classification of Australian climates. *Aust. Meteorol. Mag.* **49**, 87–96.
37. Silvestro D, Kostikova A, Litsios G, Pearman PB, Salamin N, Münkemüller T. 2015 Measurement errors should always be incorporated in phylogenetic comparative analysis. *Methods Ecol. Evol.* **6**, 340–346. (doi:10.1111/2041-210x.12337)
38. Harmon LJ, Weir JT, Brock CD, Glor RE, Challenger W. 2008 GEIGER: investigating evolutionary radiations. *Bioinformatics* **24**, 129–131. (doi:10.1093/bioinformatics/btm538)
39. Clavel J, Escarguel G, Merceron G. 2015 mvmorph: anrpackage for fitting multivariate evolutionary models to morphometric data. *Methods Ecol. Evol.* **6**, 1311–1319. (doi:10.1111/2041-210x.12420)
40. Clavel J, Morlon H. 2017 Accelerated body size evolution during cold climatic periods in the Cenozoic. *Proc. Natl Acad. Sci. USA* **114**, 4183–4188. (doi:10.1073/pnas.1606868114)
41. Landis MJ, Schraiber JG. 2017 Pulsed evolution shaped modern vertebrate body sizes. *Proc. Natl Acad. Sci. USA* **114**, 13 224–13 229. (doi:10.1073/pnas.1710920114)
42. Ree RH, Smith SA. 2008 Maximum likelihood inference of geographic range evolution by dispersal, local extinction, and cladogenesis. *Syst. Biol.* **57**, 4–14. (doi:10.1080/10635150701883881)
43. Morlon H, Lewitus E, Condamine FL, Manceau M, Clavel J, Drury J. 2016 RPANDA: an R package for macroevolutionary analyses on phylogenetic trees. *Methods Ecol. Evol.* **7**, 589–597. (doi:10.1111/2041-210X.12526)
44. Wickham H. 2009 *Ggplot2: elegant graphics for data analysis*. New York, NY: Springer.
45. Burnham KP, Anderson DR. 2002 *Model selection and multimodel inference*, xxvi+488 p. New York, NY: Springer.
46. Slater GJ, Harmon LJ, Alfaro ME. 2012 Integrating fossils with molecular phylogenies improves inference of trait evolution. *Evolution* **66**, 3931–3944. (doi:10.1111/j.1558-5646.2012.01723.x)
47. Jablonski D. 2008 Extinction and the spatial dynamics of biodiversity. *Proc. Natl Acad. Sci. USA* **105**(Supplement 1), 11528–11535. (doi:10.1073/pnas.0801919105)
48. Matzke NJ. 2013 Probabilistic historical biogeography: new models for founder-event speciation, imperfect detection, and fossils allow improved accuracy and model-testing. *Front. Biogeogr.* **5**, 242–248.
49. R Core Team. 2000 *R language definition*. Vienna, Austria: R Foundation for Statistical Computing.
50. R Studio Team. 2017 *RStudio: integrated development environment for R*. Boston, MA: RStudio, Inc.
51. Quintero I, Keil P, Jetz W, Crawford FW. 2015 Historical biogeography using species geographical ranges. *Syst. Biol.* **64**, 1059–1073. (doi:10.1093/sysbio/syv057)
52. Raia P, Passaro F, Fulgione D, Carotenuto F. 2012 Habitat tracking, stasis and survival in Neogene large mammals. *Biol. Lett.* **8**, 64–66. (doi:10.1098/rsbl.2011.0613)
53. Drury JP, Grether GF, Garland Jr T, Morlon H. 2018 An assessment of phylogenetic tools for analyzing the interplay between interspecific interactions and phenotypic evolution. *Syst. Biol.* **67**, 413–427. (doi:10.1093/sysbio/syx079)
54. Beaulieu J, O'Meara B. 2012 OUwie: analysis of evolutionary rates in an OU framework. *R package version* 1. See https://cran.r-project.org/web/packages/OUwie/.
55. Tennant JP, Mannion PD, Upchurch P, Sutton MD, Price GD. 2016 Biotic and environmental dynamics through the Late Jurassic–Early Cretaceous transition: evidence for protracted faunal and ecological turnover. *Biol. Rev.* **92**, 776–814. (doi:10.1111/brv.12255)
56. Jezkova T, Wiens JJ. 2017 What explains patterns of diversification and richness among animal phyla? *Am. Nat.* **189**, 201–212. (doi:10.1086/690194)
57. Weber MG, Wagner CE, Best RJ, Harmon LJ, Matthews B. 2017 Evolution in a community context: on integrating ecological interactions and macroevolution. *Trends Ecol. Evol.* **32**, 291–304. (doi:10.1016/j.tree.2017.01.003)
58. Clarke M, Thomas GH, Freckleton RP. 2017 Trait evolution in adaptive radiations: modeling and measuring interspecific competition on phylogenies. *Am. Nat.* **189**, 121–137. (doi:10.1086/689819)
59. Etienne RS, Haegeman B. 2012 A conceptual and statistical framework for adaptive radiations with a key role for diversity dependence. *Am. Nat.* **180**, E75–E89. (doi:10.1086/667574)
60. Olalla-Tárraga MÁ *et al.* 2011 Climatic niche conservatism and the evolutionary dynamics in species range boundaries: global congruence across mammals and amphibians. *J. Biogeogr.* **38**, 2237–2247. (doi:10.1111/j.1365-2699.2011.02570.x)
61. Condamine FL, Rolland J, Morlon H. 2013 Macroevolutionary perspectives to environmental change. *Ecol. Lett.* **16**, 72–85. (doi:10.1111/ele.12062)
62. Vrba ES. 1993 Turnover-pulses, the Red Queen, and related topics. *Am. J. Sci.* **293**, 418–452. (doi:10.2475/ajs.293.A.418)
63. Byrne M *et al.* 2011 Decline of a biome: evolution, contraction, fragmentation, extinction and invasion of the Australian mesic zone biota. *J. Biogeogr.* **38**, 1635–1656. (doi:10.1111/j.1365-2699.2011.02535.x)

64. Edwards RD, Crisp MD, Cook DH, Cook LG. 2017 Congruent biogeographical disjunctions at a continent-wide scale: quantifying and clarifying the role of biogeographic barriers in the Australian tropics. *PLoS ONE* **12**, e0174812. (doi:10.1371/journal.pone.0174812)
65. Mairal M, Sanmartín I, Pellissier L. 2017 Lineage-specific climatic niche drives the tempo of vicariance in the Rand Flora. *J. Biogeogr.* **44**, 911–923. (doi:10.1111/jbi.12930)
66. Schneider CJ, Cunningham M, Moritz C. 1998 Comparative phylogeography and the history of endemic vertebrates in the wet tropics of Australia. *Mol. Ecol.* **7**, 487–498. (doi:10.1046/j.1365-294x.1998.00334.x)
67. Smith L, Henry J. 1999 *Aprasia picturata* (Squamata: Pygopodidae), a new legless lizard from the interior of Western Australia. *J. R. Soc. West. Aust.* **82**, 75–77.
68. Oliver PM, Adams M, Doughty P. 2010 Molecular evidence for ten species and Oligo-Miocene vicariance within a nominal Australian gecko species (*Crenadactylus ocellatus*, Diplodactylidae). *BMC Evol. Biol.* **10**, 1–11. (doi:10.1186/1471-2148-10-386)
69. Fujita MK, McGuire JA, Donnellan SC, Moritz C. 2010 Diversification and persistence at the arid-monsoonal interface: Australia-wide biogeography of the Bynoe's gecko (*Heteronotia binoei*; Gekkonidae). *Evolution* **64**, 2293–2314. (doi:10.1111/j.1558-5646.2010.00993.x)
70. Garcia-Navas V, Westerman M. 2018 Niche conservatism and phylogenetic clustering in a tribe of arid-adapted marsupial mice, the Sminthopsini. *J. Evol. Biol.* **31**, 1204–1215. (doi:10.1111/jeb.13297)
71. Westerman M, Blacket MJ, Hintz A, Armstrong K, Woolley PA, Krajewski C. 2016 A plethora of planigales: genetic variability and cryptic species in a genus of dasyurid marsupials from northern Australia. *Aust. J. Zool.* **64**, 303. (doi:10.1071/zo16052)
72. Fortelius M, Eronen JT, Kaya F, Tang H, Raia P, Puolamäki K. 2014 Evolution of neogene mammals in Eurasia: environmental forcing and biotic interactions. *Annu. Rev. Earth Planet Sci.* **42**, 579–604. (doi:10.1146/annurev-earth-050212-124030)
73. Oliver PM, Adams M, Lee MS, Hutchinson MN, Doughty P. 2009 Cryptic diversity in vertebrates: molecular data double estimates of species diversity in a radiation of Australian lizards (*Diplodactylus*, Gekkota). *Proc. R. Soc. B* **276**, 2001–2007. (doi:10.1098/rspb.2008.1881)
74. Oliver PM, McDonald PJ. 2016 Young relicts and old relicts: a novel palaeoendemic vertebrate from the Australian Central Uplands. *R. Soc. open sci.* **3**, 160018. (doi:10.1098/rsos.160018)
75. Losos JB. 2010 Adaptive radiation, ecological opportunity, and evolutionary determinism. *Am. Nat.* **175**, 623–639. (doi:10.1086/652433)
76. Lanier HC, Edwards DL, Knowles LL. 2013 Phylogenetic structure of vertebrate communities across the Australian arid zone. *J. Biogeogr.* **40**, 1059–1070. (doi:10.1111/jbi.12077)
77. Powney GD, Grenyer R, Orme CDL, Owens IPF, Meiri S. 2010 Hot, dry and different: Australian lizard richness is unlike that of mammals, amphibians and birds. *Glob. Ecol. Biogeogr.* **19**, 386–396. (doi:10.1111/j.1466-8238.2009.00521.x)
78. Catullo RA, Keogh JS. 2014 Aridification drove repeated episodes of diversification between Australian biomes: evidence from a multi-locus phylogeny of Australian toadlets (*Uperoleia*: Myobatrachidae). *Mol. Phylogenet. Evol.* **79**, 106–117. (doi:10.1016/j.ympev.2014.06.012)
79. Unmack PJ, Bagley JC, Adams M, Hammer MP, Johnson JB. 2012 Molecular phylogeny and phylogeography of the Australian freshwater fish genus *Galaxiella*, with an emphasis on dwarf galaxias (*G. pusilla*). *PLoS ONE* **7**, e38433. (doi:10.1371/journal.pone.0038433)
80. Rix MG, Harvey MS. 2012 Phylogeny and historical biogeography of ancient assassin spiders (Araneae: Archaeidae) in the Australian mesic zone: evidence for Miocene speciation within Tertiary refugia. *Mol. Phylogenet. Evol.* **62**, 375–396. (doi:10.1016/j.ympev.2011.10.009)

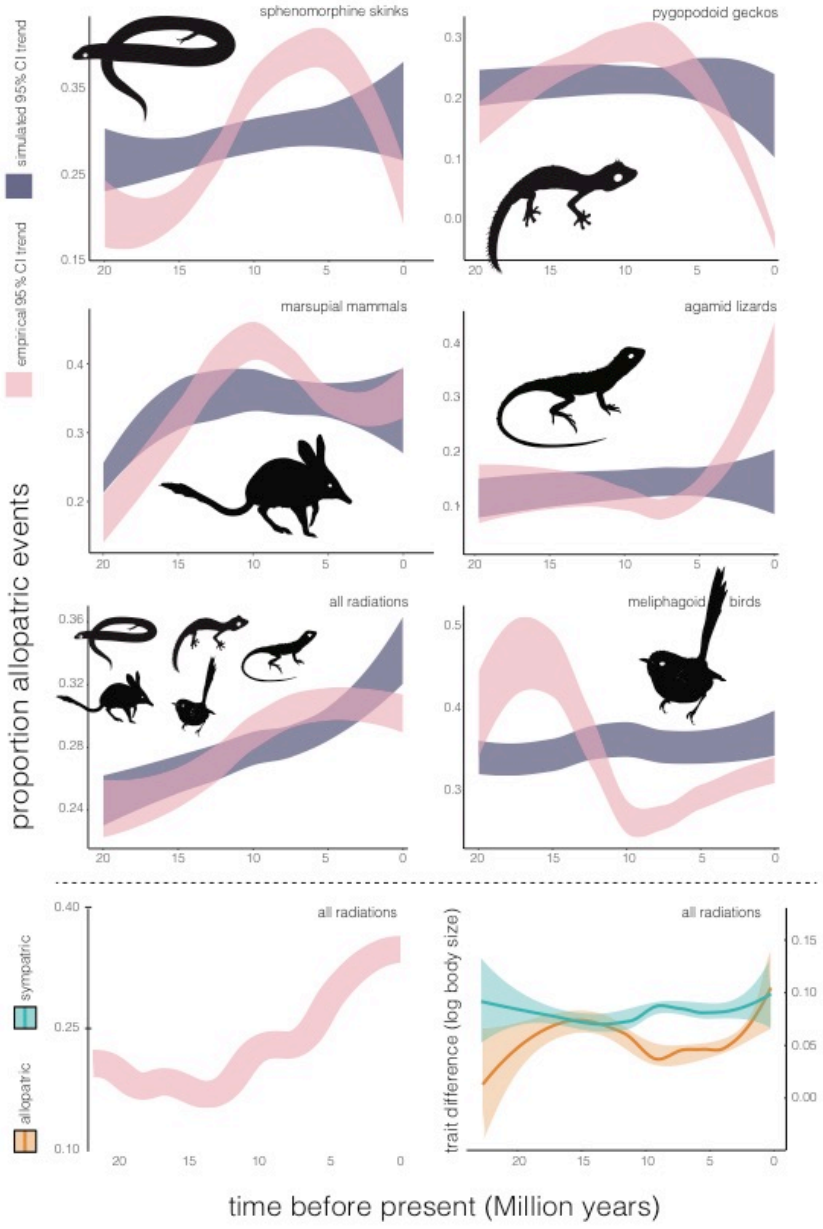

Figure S1. Temporal trends in the proportion of allopatric dispersal events shift in the Late Miocene across all Australian vertebrate radiations studied. Results above the dotted line (top three rows) show trends in allopatry according to BioGeoBEARS analyses using biome codings as distributional data. Bottom row shows trend in allopatry (left) and trends in trait variation among allopatric and sympatric sister pairs, according to explicit occurrence data and ancestral state reconstructions (rase). Combining results of all five radiations (>800 taxa) provides signal of increasing allopatry in the Late Miocene (10–5 Mya) in both geographic data schemes: biomes (left column, second from bottom) and occurrence data (left column, bottom).

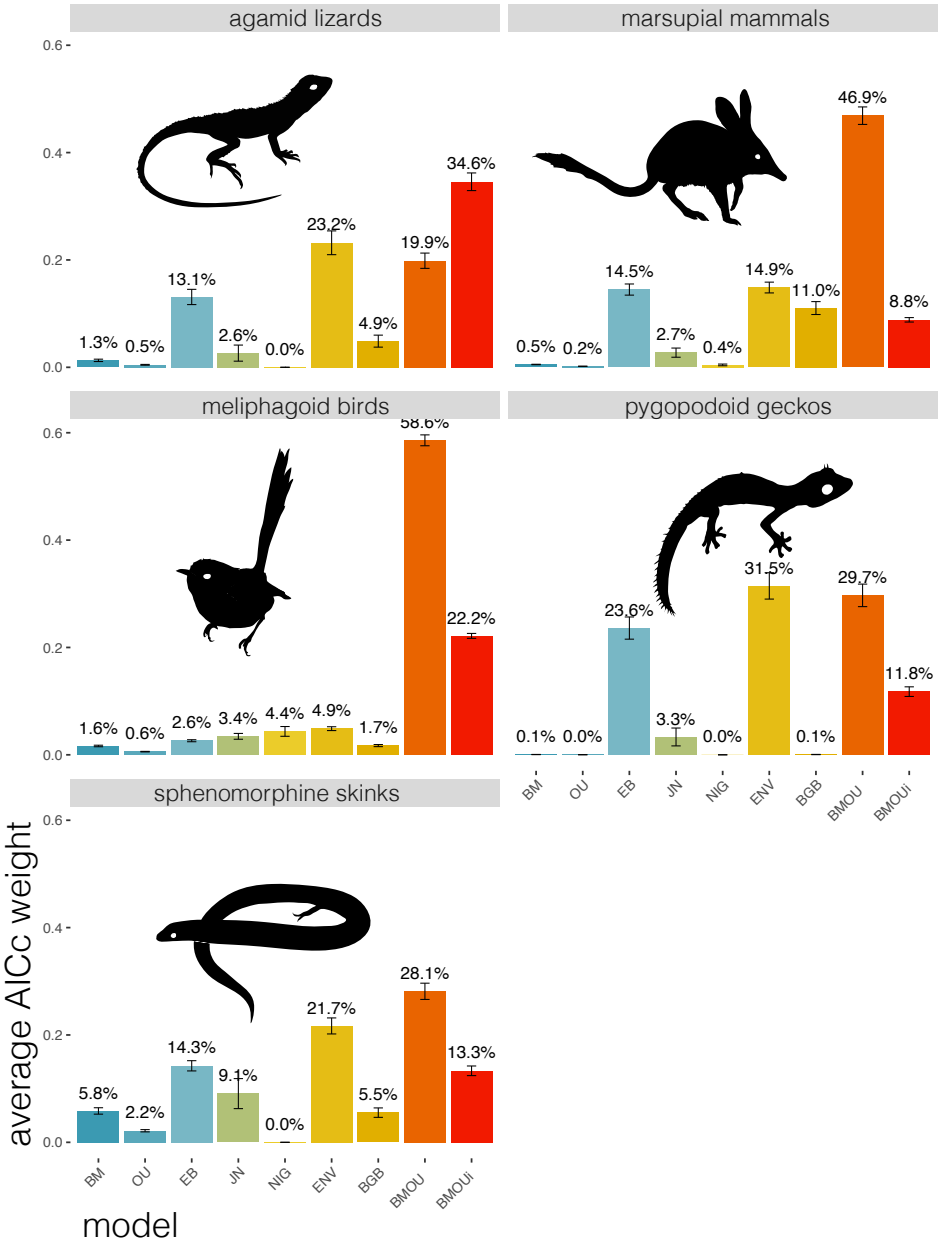

Figure S2. Comparative fit of models to body size evolution data of Australian vertebrate clades finds preference for mode-variable (BMOU, BMOUI), global temperature (ENV), and early burst (EB) models. Models are categorized below the plot, and the y-axis indicates the relative support for each model as Akaike weights (averaged across 100 posterior trees) and noted above each histogram as a percent of the total. Mode-variable models are preferred in every case except pygopodoid geckos, in which ENV and BMOU models are equally favored.

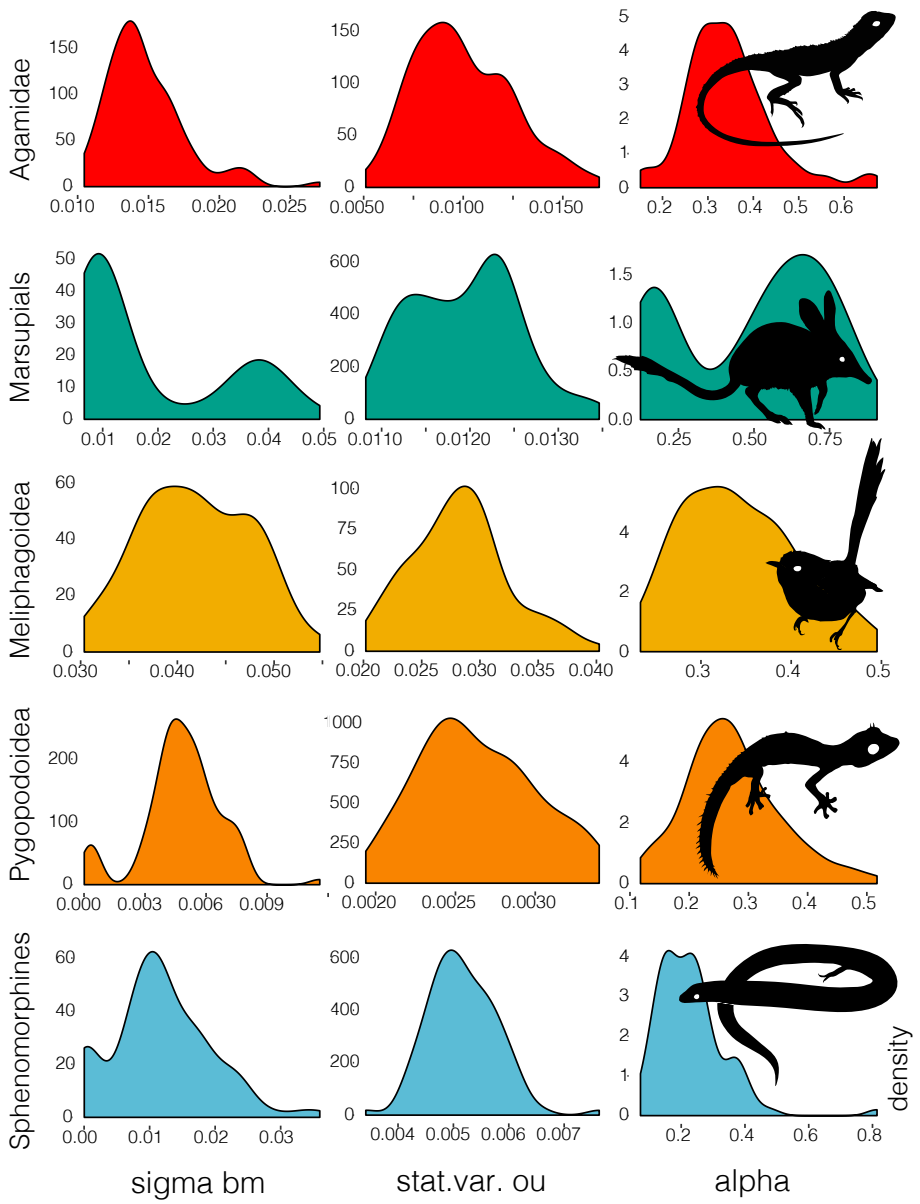

Figure S3. Parameter estimates from the BMOU model indicate declining evolutionary rates in the recent portion of the tree. We present the sigma (rate) value for the BM portion of the tree, and the stationary variance of the OU portion. Because the evolutionary rate of the OU process is an interaction of the sigma and alpha values, we present the stationary variance as $sigma_{OU}/(2*alpha)$. Estimated alpha rates appear biologically reasonable.

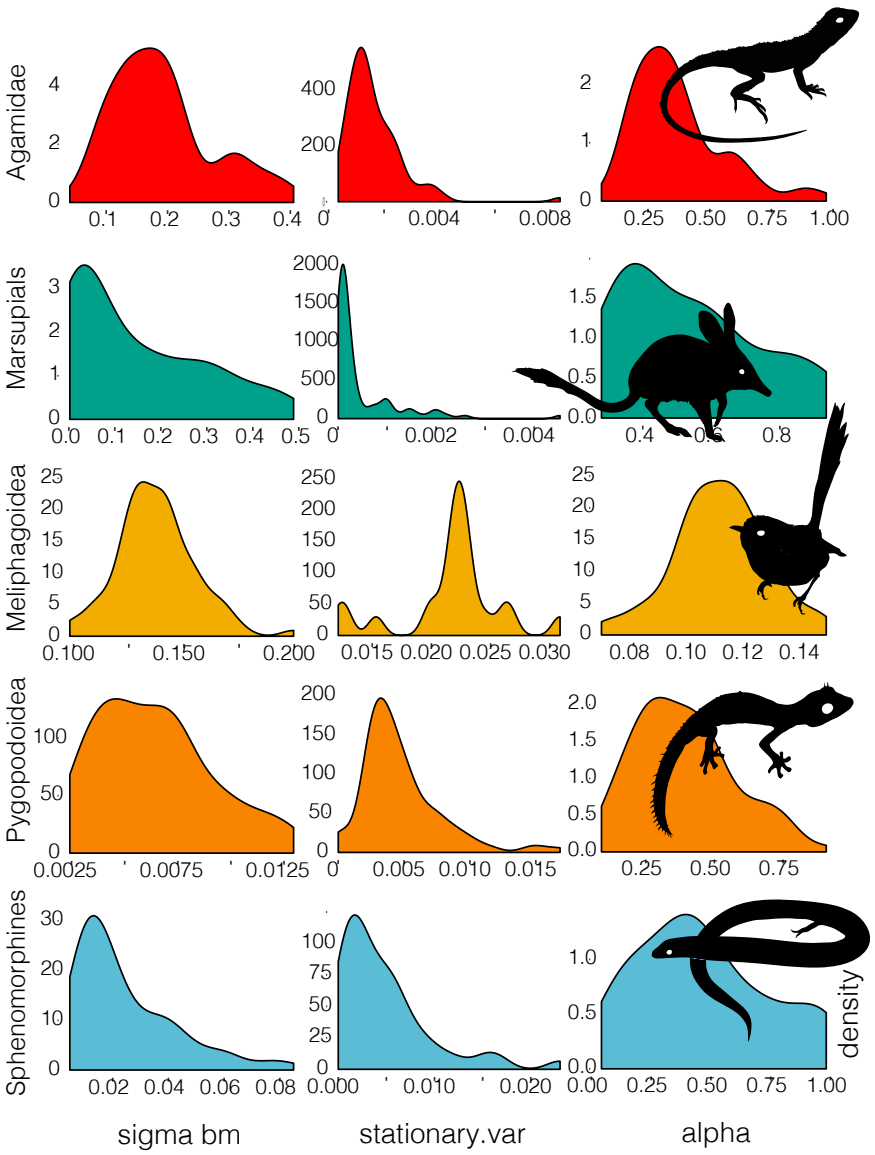

Figure S4. Parameter estimates from the BMOUi model indicate declining evolutionary rates in the recent portion of the tree. We present the sigma (rate) value for the BM portion of the tree, and the stationary variance of the OU portion. Because the evolutionary rate of the OU process is an interaction of the sigma and alpha values, we present the stationary variance as $sigma_{OU}/(2*alpha)$. Estimated alpha rates appear biologically reasonable.

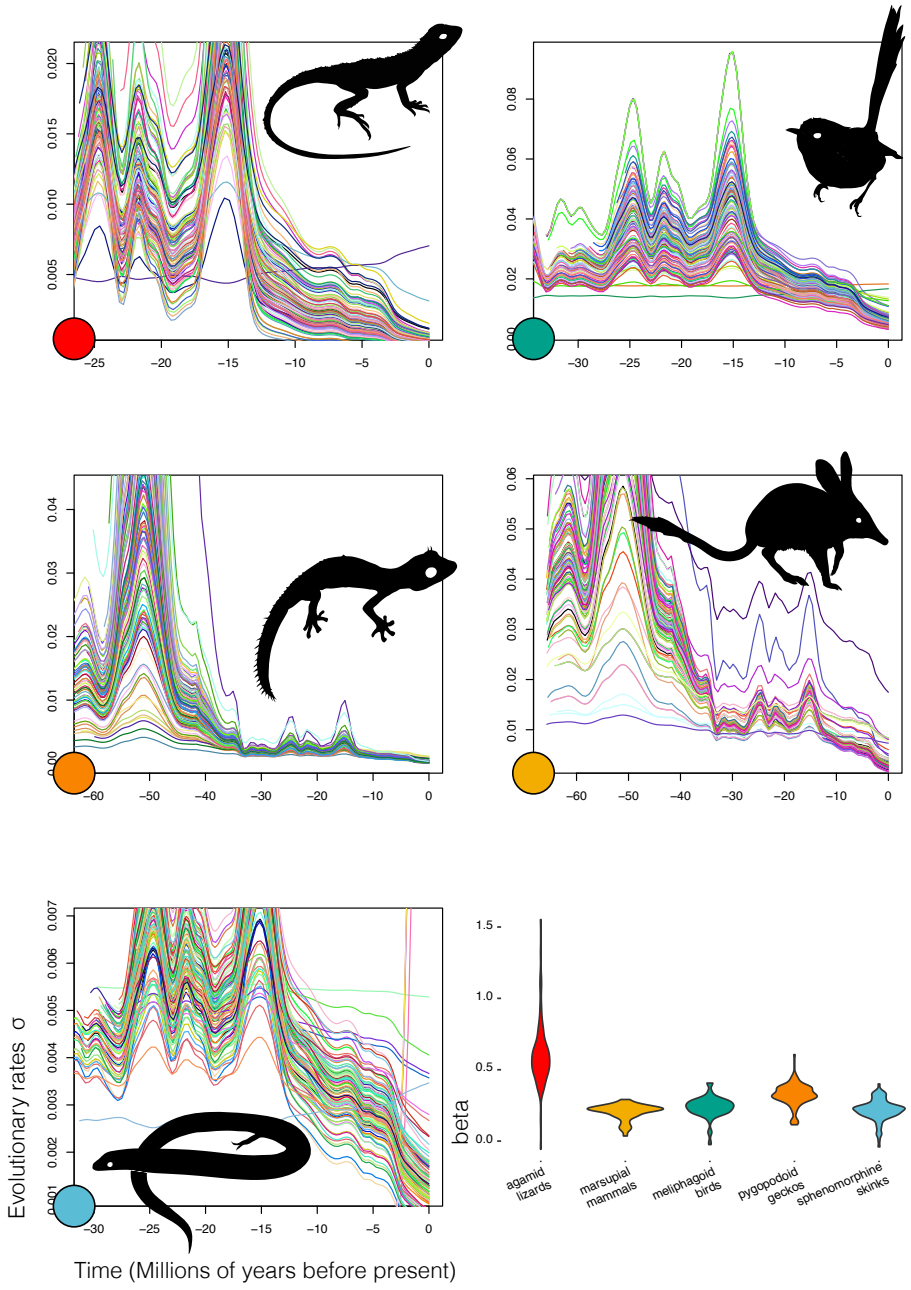

Figure S5. Estimated evolutionary rates under the ENV model respond positively to trends in the global climate. As global temperatures increased, so did evolutionary rates, and as the decreased following the Mid Miocene Climatic Optimum, rates did as well. The beta value for the relation between rates and temperature appear in the bottom right. Beta curve colors were randomly assigned.

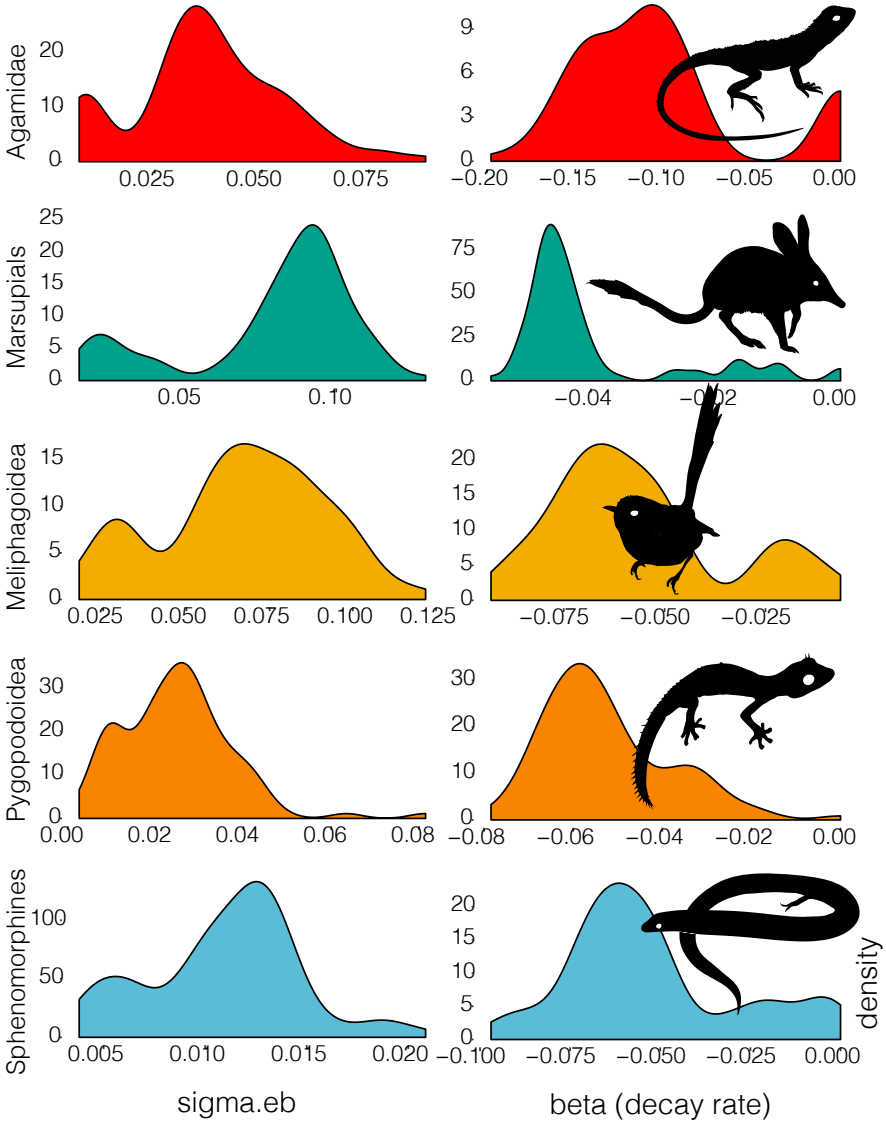

Figure S6. Parameter estimates from the EB model indicate declining evolutionary rates. Evolutionary rates (sigma) decay exponentially (beta) through time.

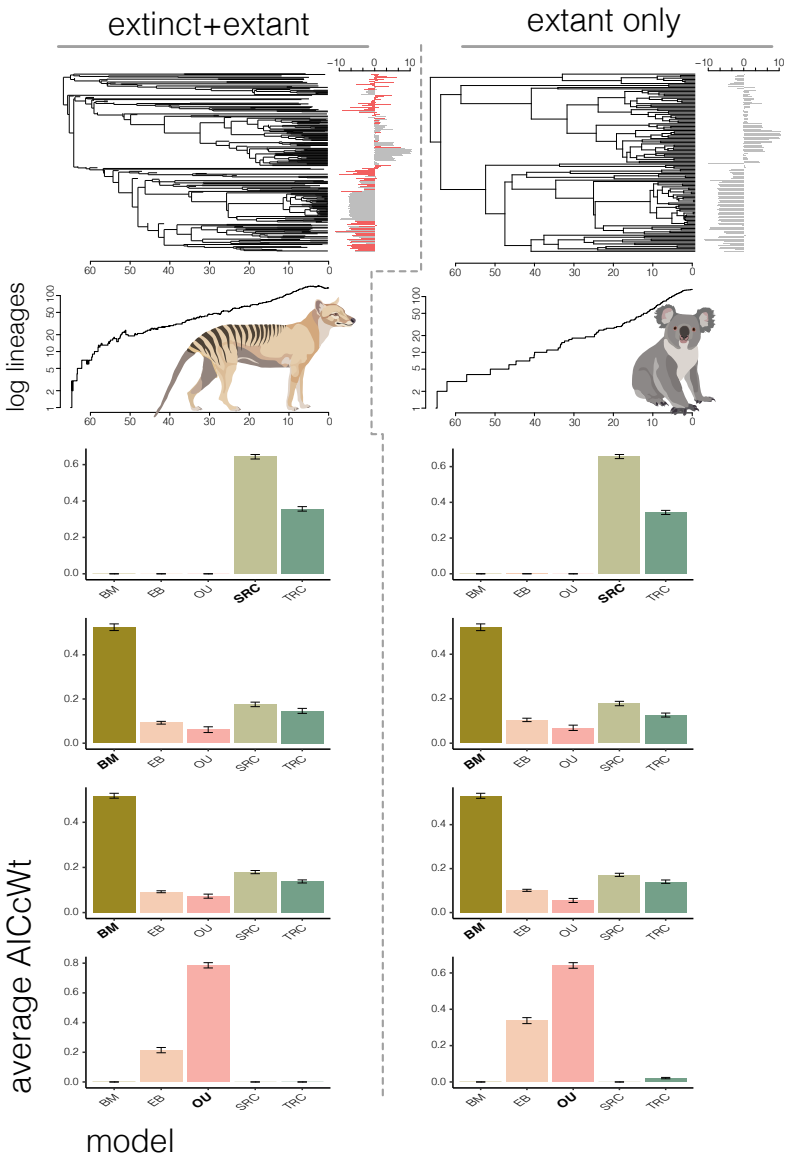

Figure S7. Extinction does not change the preferred model of trait evolution in Australian vertebrates. On the left of the figure (left of the dotted line), a phylogenetic tree including both extinct and extant taxa, with elevated extinction in the Plio-Pleistocene, and the associated distribution of traits adjacent to it (red bars indicate extinct taxa). Below the tree is a lineage through time plot showing the influence of extinction, particularly in the Plio-Pleistocene, and denoted by a Tasmanian tiger *Thylacine*. Below this are results of comparative model fitting, with relative fit denoted by average AICc weights, and the model generating the data indicated in bold. Data was simulated under the novel Single-Rate Constraint model, as well as Brownian Motion (diffusion=0.1), Brownian Motion (diffusion=0.01), and Ornstein-Uhlenbeck processes. On the right of the figure, the same methods after removal of all extinct taxa from the tree and data, resulting in the empirical (extant) tree and data only. In both extinct and extant model fitting, the generating model is always the preferred model, although false support for alternative models does increase slightly when only extant taxa are used.

Miocene
Plio-Pleistocene
Stochastic
Richness (Log Scale)
Time (Before Present)
model
average AICc Weight

Figure S8. Extinction does not change the preferred model of trait evolution in Australian vertebrates. This figure accompanies the Materials and Methods section *Simulating Extinction*. Figure is organized by three regimes estimating alternative hypothetical extinction scenarios, separated by dashed lines: stochastic (time-homogeneous), elevated Plio-Pleistocene, elevated Miocene (mimicking late Miocene macroevolutionary slowdown). Within each scenario, the upper frame shows the phylogeny including extinct lineages, as well as a lineage through time plot to visualize the accumulation of diversity, and histograms of results of comparative model fitting of data simulated under (left to right): Brownian Motion (diffusion=0.1), Brownian Motion (diffusion=0.01), Ornstein-Uhlenbeck, BMOU, BMOUI, and Brownian Motion with a trend (BMtrend) processes (see Supplemental Materials and Methods for specifics on simulation parameters). In the gray panel below are the tree, lineage through time plot, and model fitting results after removing extinct taxa from the tree and data. In both extinct and extant model fitting, the generating model is always the preferred model. In extant only trees/data, false support for alternative models does increase slightly, but not appreciably, except for the case of BMtrend. This occurs because the trend (drift) parameter is not identifiable from trees with extant taxa only, and so the process is most commonly estimated as Brownian Motion.

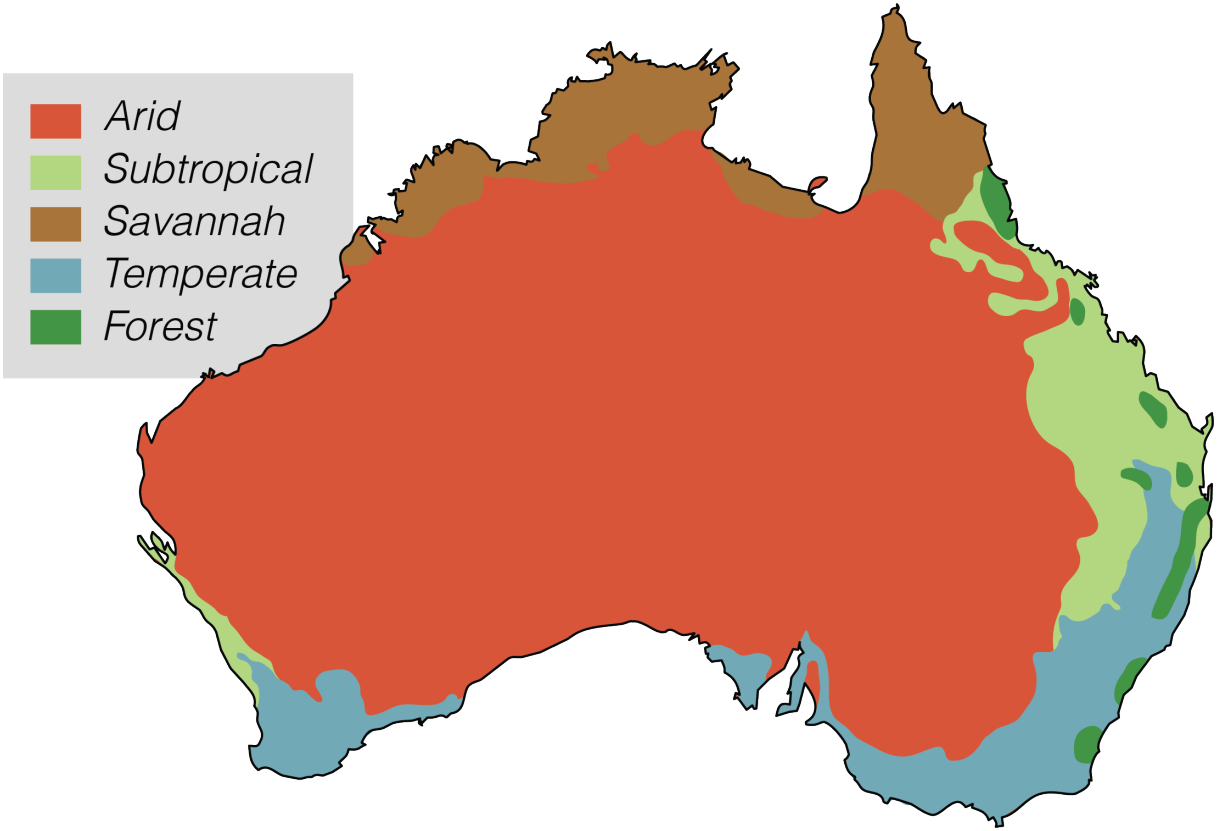

Figure S9. Five biome classification of Australia based on a Köppen-Geiger system, and modified according to Stern, Harvey, Ernst (2000).

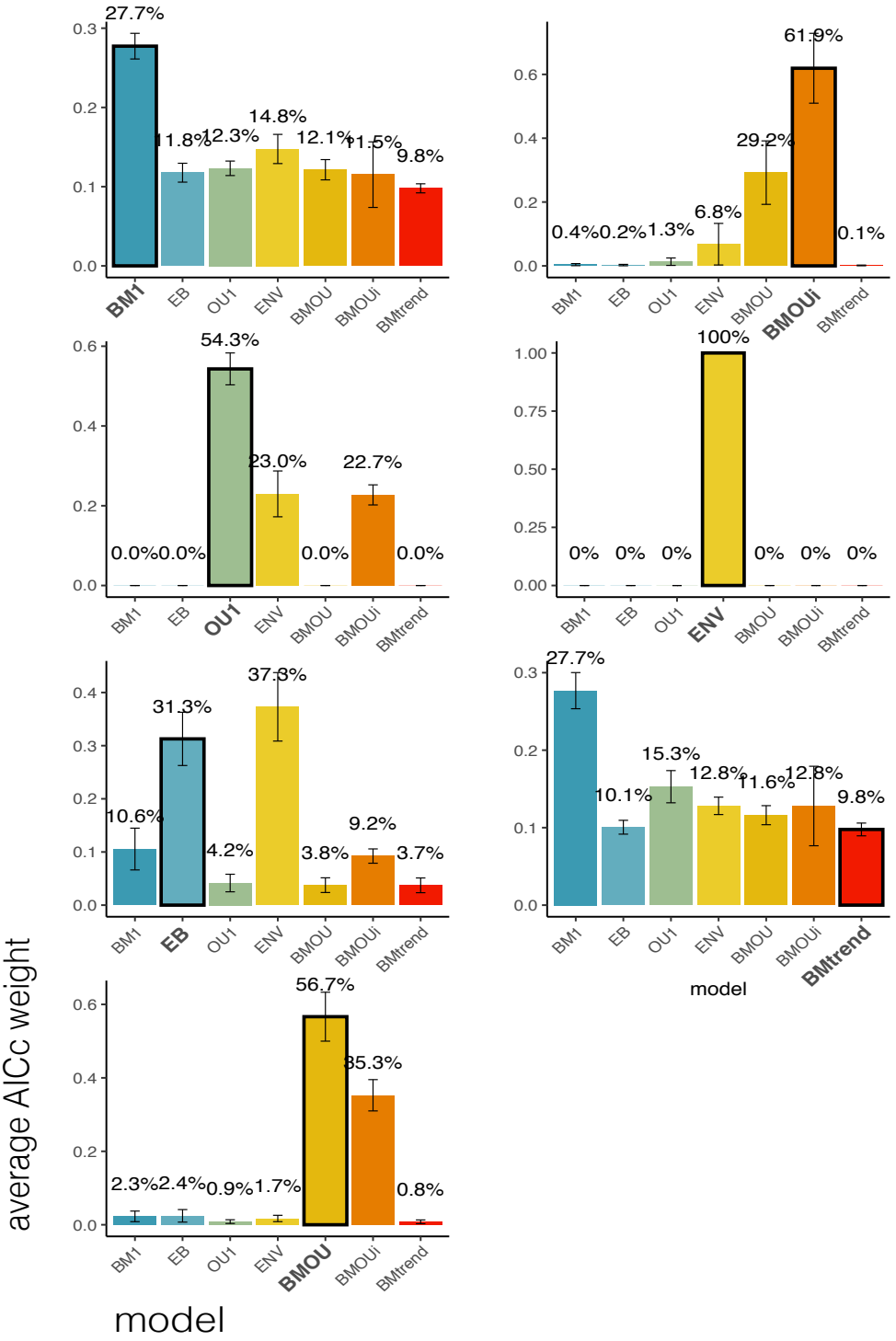
average AICc weight
model
BM1
EB
OU1
ENV
BMOU
BMOUi
BMtrend
27.7%
11.8%
12.3%
14.8%
12.1%
11.5%
9.8%
0.4%
0.2%
1.3%
6.8%
29.2%
61.9%
0.1%
0.0%
0.0%
54.3%
23.0%
0.0%
22.7%
0.0%
0%
0%
0%
100%
0%
0%
0%
10.6%
31.3%
4.2%
37.8%
3.8%
9.2%
3.7%
27.7%
10.1%
15.3%
12.8%
11.6%
12.8%
9.8%
2.3%
2.4%
0.9%
1.7%
56.7%
35.3%
0.8%

Figure S10. Mode-variable models (BMOU and BMOUI) can be accurately recovered using simulated data, and false positive rates remain relatively low. We simulated 100 data sets under (top-to-bottom, left-to-right): BM, OU, EB, BMOU, BMOUI, ENV, and BMtrend models (see **SI** *Materials and Methods—Simulation Tests*), then comparatively fit against the same mode-constant and mode-variable models. Generating models are bolded and their corresponding bar graphs are outlined in black. The BMtrend model is not identifiable from extant-only trees/data, and so is not preferred, even when it is the generating model. One result to note is the preference of the ENV model when the generating model is EB, which is surprising given this behavior is not seen in Clavel and Morlon [1]. This may be a result of the time-frame over which the temporal data (paleotemperature) and response data (body size) were fit. Our simulations were fit to our largest (skinks) and smallest (agamids) trees, which are also coincidentally our youngest trees (both <30 my). It is likely that the trend of paleotemperature from 30mya–present results in pattern indistinguishable from an EB scenario. This may also provide some explanation for their fit to the empirical data for agamid lizards and sphenomorphine skinks.

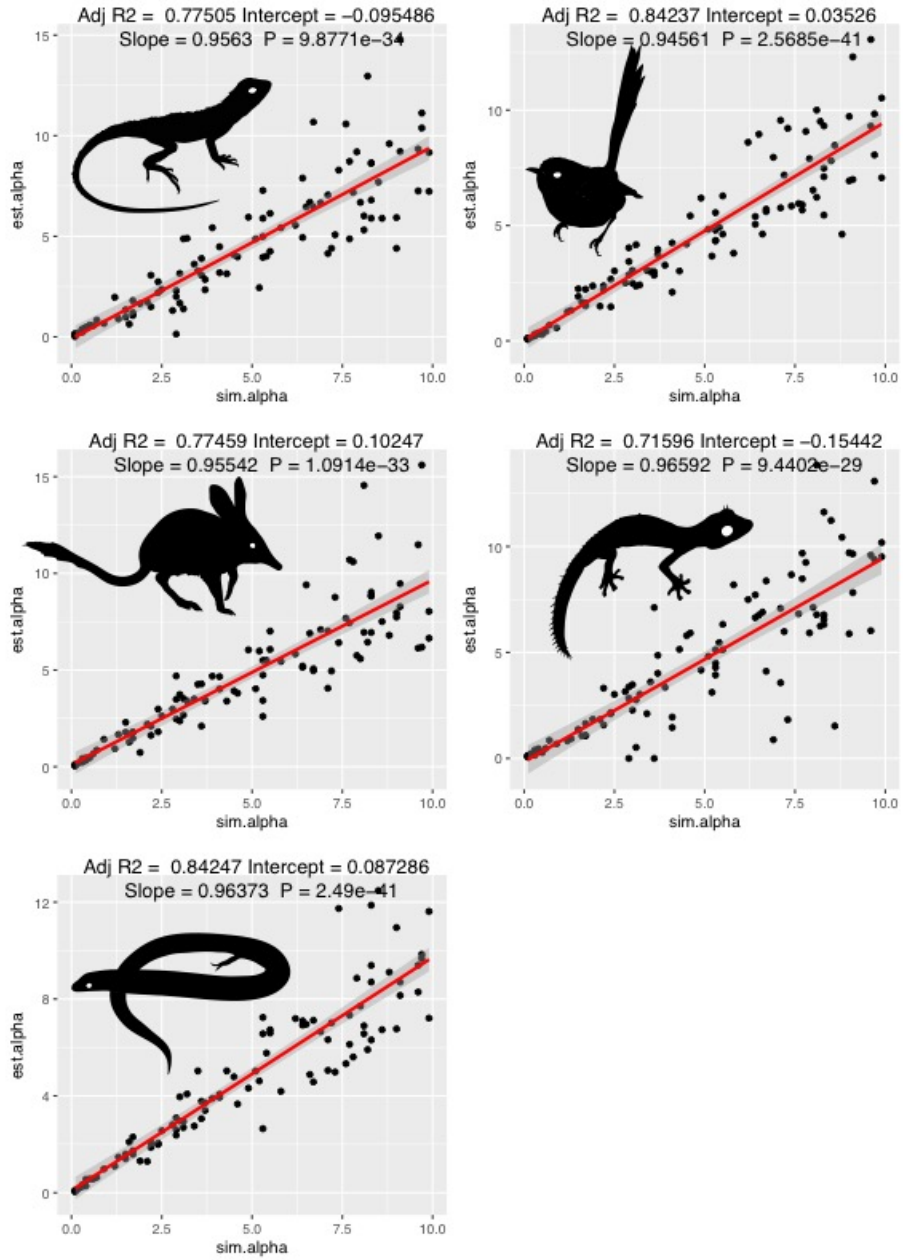

Figure S11. The constraint parameter alpha α can be reliably estimated from phylogenies of varied sizes by the Two Rate Constrained (BMOUI) model. Regression of estimated to simulated (true) alpha values return slopes of 0.945–0.966, showing a strong correspondence between these values, and the ability to estimate them. Relationship between estimated and simulated values are strongest at small values of alpha, and become increasingly difficult to estimate at values >7.

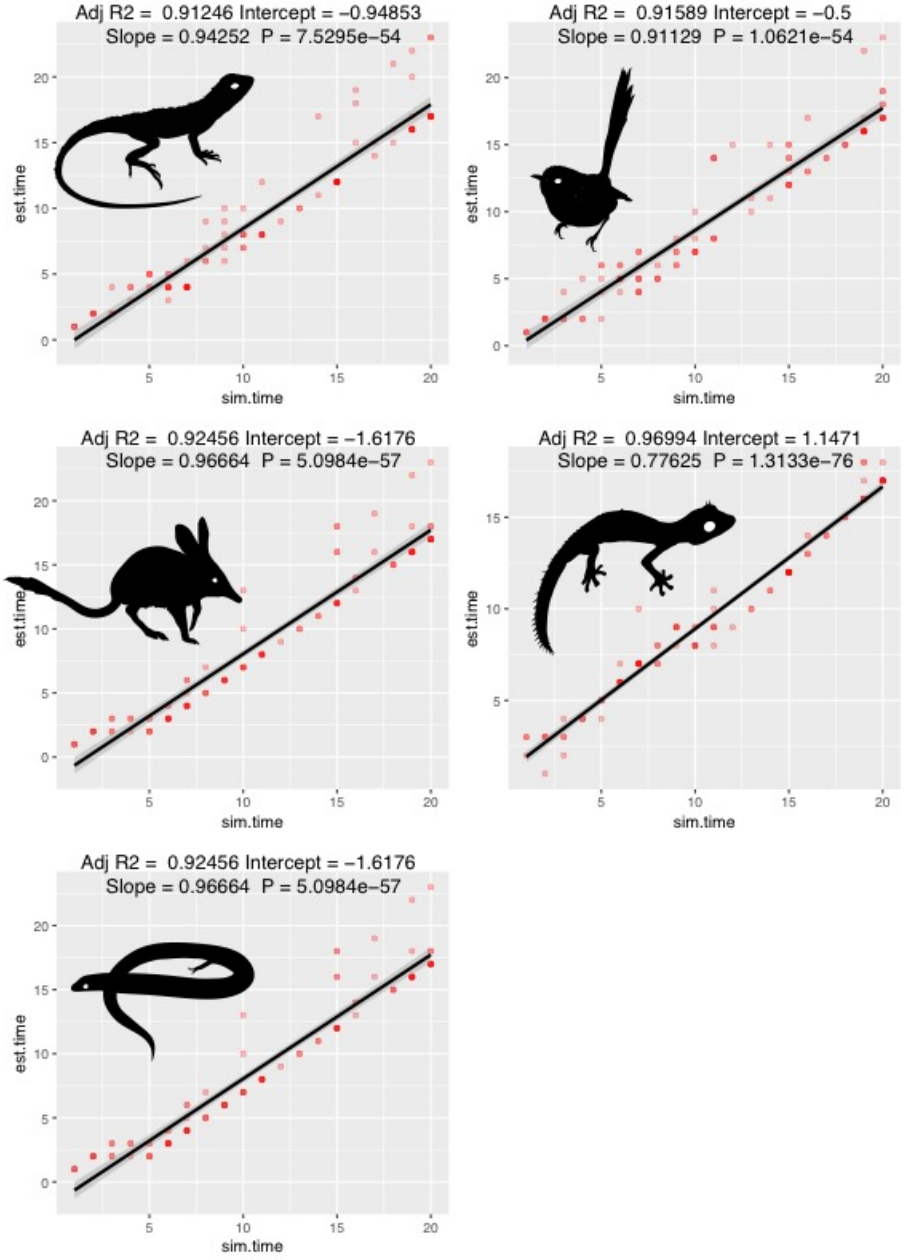

Figure S12. The timing of the shift (t_{shift}) between BM and OU models can be reliably estimated from phylogenies of varied sizes by the Two Rate Constrained (BMOUI) model. Regression of estimated to simulated (true) alpha values return slopes of 0.912–0.969, showing a strong correspondence between these values, and the ability to estimate them. Shift accuracy drops at depths greater than 15 million years. The saturation of each point (pink to red) indicates multiple estimates at that value.

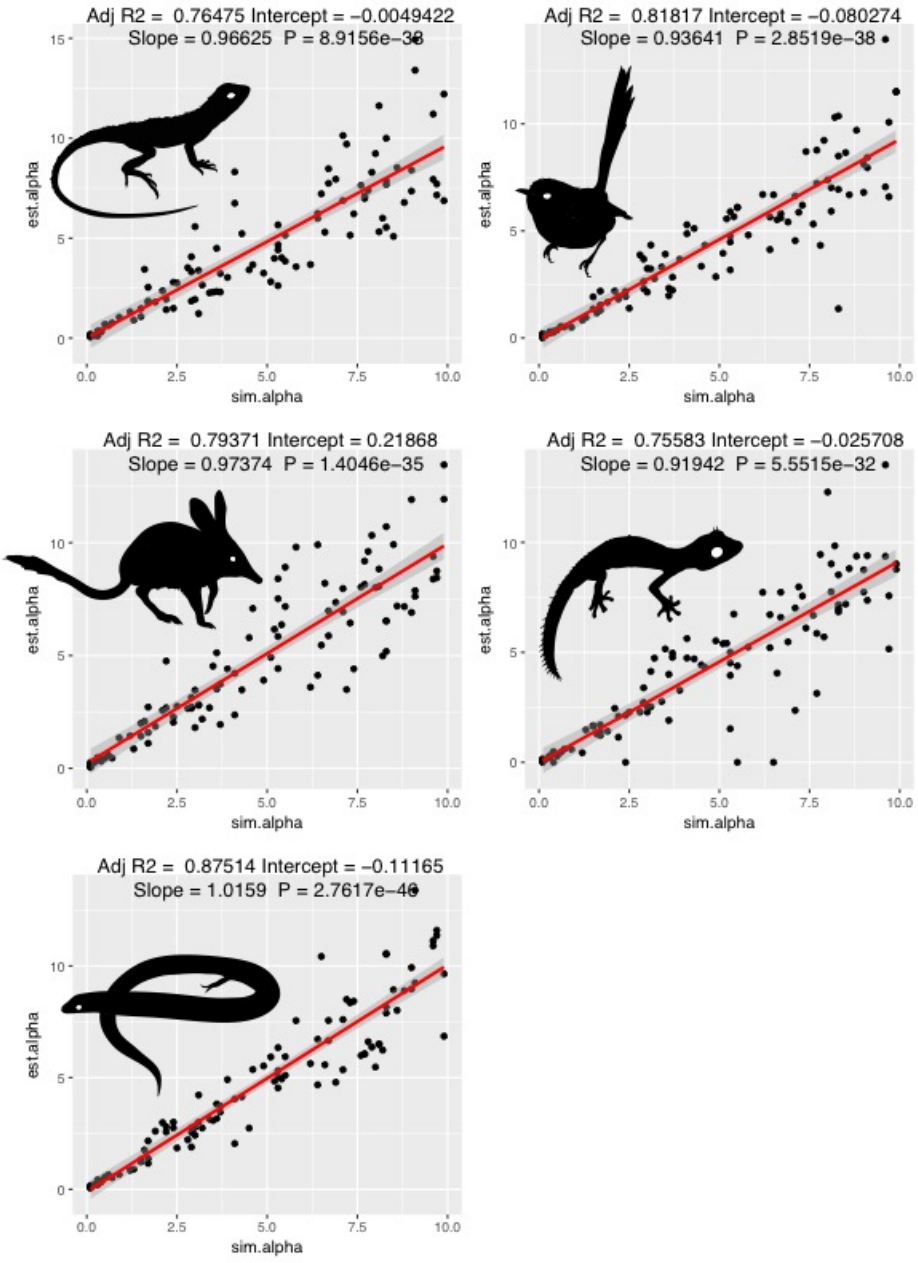

Figure S13. The constraint parameter alpha α can be reliably estimated from phylogenies of varied sizes by the Single Rate Constrained (BMOU) model. Regression of estimated to simulated (true) alpha values return slopes of 0.919–1.016, showing a strong correspondence between these values, and the ability to estimate them. Relationship between estimated and simulated values are strongest at small values of alpha, and become increasingly difficult to estimate at values >5.

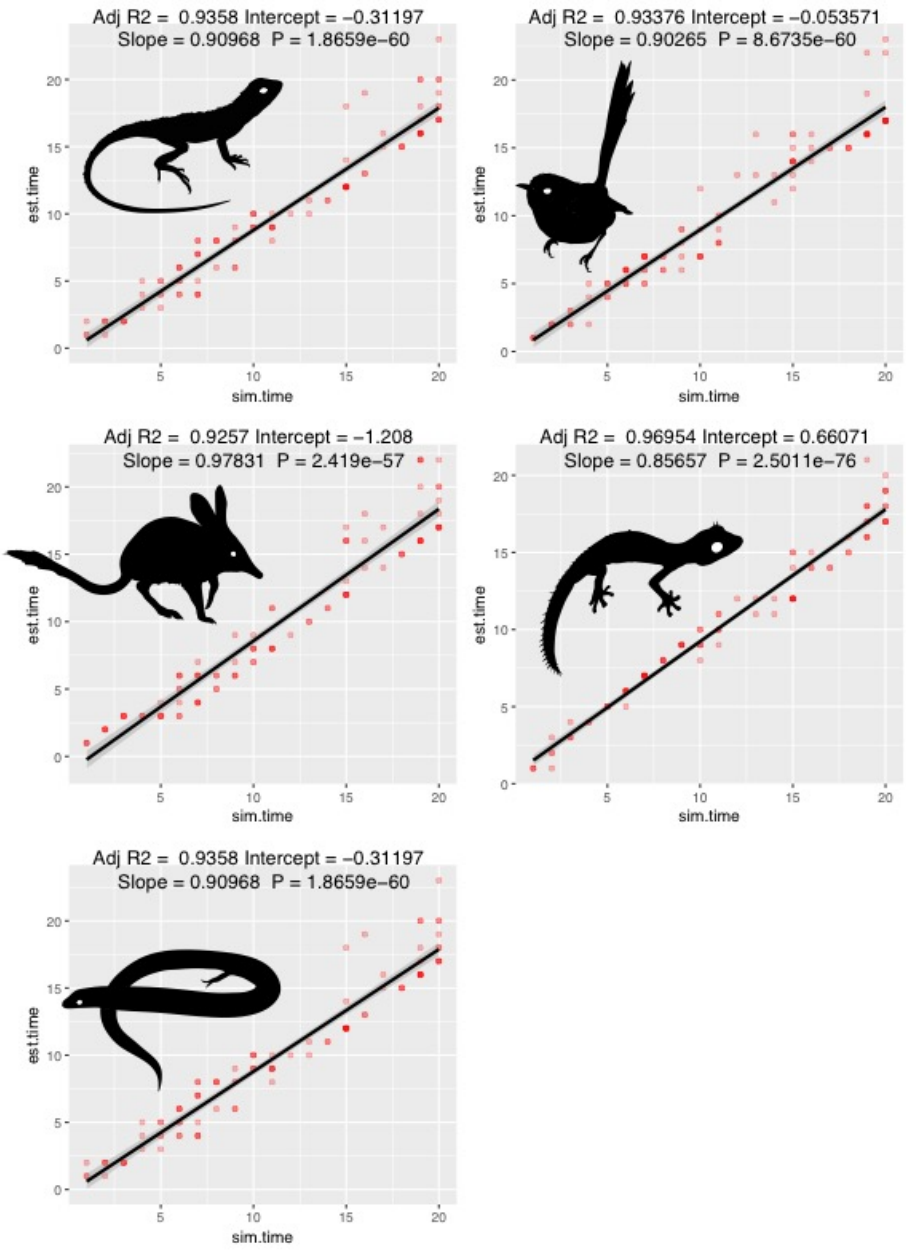

Figure S14. The timing of the shift (t_{shift}) between BM and OU models can be reliably estimated from phylogenies of varied sizes by the Single Rate Constrained (BMOU) model. Regression of estimated to simulated (true) alpha values return slopes of 0.925–0.969, showing a strong correspondence between these values, and the ability to estimate them. Shift accuracy drops at depths greater than 15 million years. The saturation of each point (pink to red) indicates multiple estimates at that value.

Table S1. Fossil and secondary calibrations used for dating estimates of Australian vertebrate radiations.

Tree	No.	Constrained Clade	Calibration Type (placement)	Min Age (My)	Max Age (My)	Distribution	Effective Range Constraint	Oldest Fossil	Comments/References for oldest Fossil & Maximum Age Bounds
Marsupials	1	Peroryctinae + Echymiperinae	Primary (node)	4.36	23.03	Normal prior with mean 13, sigma 5.0	Soft; 95% CI = 3.2-22.8	*cf. Peroryctes; Yarala kida*	Turnbull et al. (2003) reported cf. *Peroryctes* from the Hamilton Local Fauna (minimum age = 4.36 Mya). The Kangaroo Well Local Fauna, which includes Yarala kida (Schwartz 2006), is approximately coeval with the Kutjamarpu Local Fauna of the Wipajiri Formation based on biocorrelation (Schwartz 2006; Megirian et al. 2004). Woodburne et al. (1993) suggested that the Kutjamarpu Local Fauna is correlative with Chron 6Cn, and suggested an age of ~23.8 Mya for the Kutjamarpu Local Fauna. Ogg and Smith's (2004) revision of magnetostratigraphic ages indicates that Chron 6Cn ranges from 22.564 to 23.03 Ma.
Marsupials	2	Peramelemorphia (Dasyuridae + Myrmecobiidae)	Primary (stem)	14.17	54.65	Normal prior with mean 35, sigma 11	Soft; 95% CI = 13.4-54.6	Cf. *Peroryctes; Murgon "Stem perameloid" (2nd outgroup)*	Turnbull et al. 2003 (see comments above). Godthelp et al. 1992, 1999; Archer et al. 1999
Marsupials	3	Dasyuridae + Myrmecobiidae	Primary (stem)	17	54.65	Normal prior with mean 35, sigma 10	Soft; 95% CI = 15.4-54.6	*Barinya wangala; Murgon "Stem perameloid"*	*Barinya* is the oldest dasyurid and is known from Neville's Garden (Riversleigh) (Wroe 1999). This minimum assumes that thylacinids are the sister group to dasyurids + myrmecobiids following Miller et al. (2009). The oldest numbat fossils are from Pleistocene (0.1 Ma) cave deposits (Long et al. 2003). The age of Neville's Garden is Faunal Zone B (~early Miocene) according to Travouillon et al. 2006. Megirian et al. (2010) assigned Neville's Garden to the Wipajirian land mammal age (17-25 Ma). We followed Megirian et al. (2010) and assigned a minimum age of 17 Ma to the common ancestor of Dasyuridae + Myrmecobiidae. Thylacinids are the first outgroup to dasyurids + myrmecobiids (Miller et al. 2009; Wroe 2003). The oldest thylacinid (Badjcinus) is from the White Hunter Site (Muirhead and Wroe 1998). The second outgroup is Peramelemorphia, which includes a "stem perameloid" from Murgon (Godthelp et al. 1992; Archer et al. 1999).
Marsupials	4	Phalangeridae + Burramyidae	Primary (node)	24.6	54.65	Normal prior with mean 39, sigma 8	Soft; 95% CI = 23.3-54.7	*Eocuscus sarastamppi*	*Eocuscus sarastamppi* is known from faunal zone B (Ditjimanka local fauna) of the Edadunna Formation (Case et al. 2009). The age of this fauna is 24.6-24.9 Ma (Megirian et al. 2010).
Marsupials	5	Petauridae to Pseudocheiridae	Primary (node)	24.9	54.65	Normal prior with mean 39, sigma 8	Soft; 95% CI = 23.3-54.7	*Paljara sp. A*	*Paljara* sp. A is known from faunal zone A of the Etadunna Formation (Woodburne et al. 1993). The age of this fauna is 24.9-25.3 Ma (Megirian et al. 2010).
Marsupials	6	Macropodoidea (=Macropodidae + Potoroidae)	Primary (stem)	24.1	54.65	Normal prior with mean 39, sigma 8	Soft; 95% CI = 23.3-54.7	*Bulungamaya*	*Bulungamaya* is known from faunal zone D of the Etadunna Formation (Woodburne et al. 1993). The age of this fauna is 24.1-24.6 Ma (Megirian et al. 2010). Kear et al.'s (2007) cladistics analysis recovered *Bulungamaya* as a stem macropodid.
Marsupials	7	Vombatiformes	Primary (node)	24.9	54.65	Normal prior with mean 39, sigma 8	Soft; 95% CI = 23.3-54.7	*Perikoala*	*Perikoala robusta* is known from faunal zone A of the Etadunna Formation (Woodburne et al. 1993). The age of this fauna is 24.9-25.3 Ma (Megirian et al. 2010).
Marsupials	8	Australidelphia + Didelphimorphia	Primary (node)	65.18	84.2	Normal prior with mean 74, sigma 5	Soft; 95% CI = 64.2-83.8	*Peradectes* (Puercan); *Minoperadectes* (Early Wasatchian)	Horovitz et al. 2009
Marsupials	9	*Antechinus* + *Phascogale*	Primary (node)	4.36	15.97	Normal prior with mean 9, sigma 3	Soft; 95% CI = 3.12-14.9	*Antechinus* sp	*Antechinus* sp. is known from the Hamilton Local Fauna (4.46 +/- 0.1 Ma; Turnbull et al. 2003) and is the oldest described member of the Phascogalini. We used 4.36 Ma as the minimum age for the split between *Antechinus* and *Phascogale*.
Marsupials	10	*Dasyurus* to *Phascolosorex*	Primary (node)	4.36	15.97	Normal prior with mean 10, sigma 2.75	Soft; 95% CI = 4.61-15.4	Cf. *Dasyurus* sp.	Turnbull et al. 2003
Marsupials	11	*Isoodon* to *Perameles*	Primary (node)	3.62	15.97	Normal prior with mean 8, sigma 3	Soft; 95% CI = 2.12-13.9	*Perameles allinghamensis; P. bowensis*	*P. allinghamensis* and *P. bowensis* are known from the early Pliocene Bluff Downs and Bow Local Faunas, respectively (Muirhead et al. 1997; Mackness et al. 2000a). The Bluff Downs Local Fauna is overlain by a basalt flow that has been dated at 3.62 Ma (Mackness et al. 2000b).
Marsupials	12	Australasian marsupials	Primary (stem)	54.55	65.8	Normal prior with mean 59, sigma 3	Soft; 95% CI = 53.1-64.9	Murgon "stem perameloid"; Peradectes (Puercan)	Godthelp et al. 1992; Archer et al. 1999; Meredith et al. 2008. Microbiotheres are the first outgroup to Australasian marsupials. The oldest putative microbiothere is Khasia from the early or middle Paleocene (see Beck 2008), although the affinities of this taxon with Microbiotheria have been questioned (Wroe et al. 2000). Djarthia is a putative stem australidelphian (Beck et al. 2008) and is the second outgroup to crown Australasian marsupials. Djarthia is known from Murgon and is younger than Khasia (Beck et al. 2008).
Marsupials	13	Dasyuromorpha	Primary (node)	24.7	54.65	Normal prior with mean 39, sigma 8	Soft; 95% CI = 23.3-54.7	Badjcinus turnbulli	Meredith et al. (2009); Campbell (1976a,b). We also included a 13th calibration for Dasyuromorpha from Meredith et al. (2009). Specifically, we used a minimum age of 24.7 Myr for this clade based on Badjcinus turnbulli, which is the oldest known thylacinid fossil. This minimum age also conforms to the inferred place- ment of Apoktesis cuspis as the most ancient dasyurid (sensu Campbell, 1976a, b). The maximum age was changed to 54.65 Myr rather than the more conserva- tive 65 Myr used previously.
Sphenomorphinae	1	Australian sphenomorphines	Secondary (node)	24	36	Normal prior with mean 30 and s.d. 3.0	Soft, 95% CI 24.12-35.88		Calibration with 95% ci spanning values in Skinner et al. 2013, Pyron & Burbrink 2014, Zheng Wiens 2016
Sphenomorphinae	2	Australian sphenomorphines	Primary (node)	20	NA	Uniform, 20 to 200 (effectively unbounded upper limit)	Hard minimum of 20		~20Ma based on faunal/stratigraphic analysis of a range of Riversleigh sites, Hutchinson 1992. This calibration has little effect due to the above calibration for the same clade also being used.
Pygopodoidea	1	Pygopodoidea (all)	Secondary (node)	48	77	Normal prior with mean 62.65 and s.d. 7.12	Soft, 95% CI 48.7-76.6		Calibration with 95% ci spanning the 3 estimates in Mulcahey et al. 2012 Appendix E and the (generally older) estimates in Zheng & Wiens 2016 Fig. S3
Pygopodoidea	2	Pygopodidae	Secondary (node)	20	39	Normal prior with mean 29.805 and s.d. 4.595	Soft, 95% CI 20.8-38.81		Calibration with 95% ci spanning the 3 estimates in Mulcahey et al. 2012 Appendix E and the (generally older) estimates in Zheng & Wiens 2016 Fig. S3
Pygopodoidea	3	Diplodactylidae	Secondary (node)	30	62	Normal prior with mean 45.965 and s.d. 7.94	Soft, 95% CI 30.4-61.53		Calibration with 95% ci spanning the 3 estimates in Mulcahey et al. 2012 Appendix E and the (generally older) estimates in Zheng & Wiens 2016 Fig. S3
Pygopodoidea	4	Core Diplodtylids, stem	Primary (node)	16	NA	Uniform, 16 to 200 (effectively unbounded upper limit)	Hard minimum of 16		Based on faunal/stratigraphic analysis of St Bathans, Lee et al. 2009
Pygopodoidea	5	*Pygopus,* stem	Primary (node)	18	NA	Uniform, 18 to 200 (effectively unbounded upper limit)	Hard minimum of 18		18Ma based on radiometric dating of Nevilles Garden, Riversleigh.
Agamidae	1	Australian agamids	Secondary (node)			Normal prior with mean 30.22 and s.d. 3.938			Calibration with 95% ci spanning estimates in Townsend et al. 2011, Hugall et al. 2008, Zheng & Wiens 2016 Fig. S3.
Agamidae	2	*Intellagama,* stem	Primary (stem)	18	NA	Uniform, 18 to 200 (effectively unbounded upper limit)	Hard minimum of 18		Based on radiometric dating of Nevilles Garden, Riversleigh by Woodhead et al. 2016
Meliphagoid	1	Acanthizidae	Primary (node)	16.24	NA	Uniform, 16.24 to 51	Hard; min. of 16.24		Crown acanthizid from early Miocene deposit from the Riversleigh World Heritage Area, Australia, (Nguyen, in prep.), dated by Woodhead et al. 2016
Meliphagoid	2	Meliphagidae	Primary (node)	14.17	NA	Uniform 16.24 to 51	Hard; min of 14.17		Crown meliphagid from middle Miocene deposit at Riversleigh World heritage Area, Australia, (Boles, 2005), dated by Woodhead et al. 2016
Meliphagoid	3	Meliphagidae	Secondary (node)	37	65	Normal prior with mean 53, s.d. 5	Soft; 95% CI = 37-65		Secondary calibration from Prum et al. (2015) to estimate the divergence between *Acanthasitta* and all other passerines.

REFERENCES CITED

Archer, M., et al., *Aust. Mammal.* **21**, 1 (1999).
Beck, R.M.D., Godthelp, H., Weisbecker, V., Archer, M., Hand, S.J. Australia's oldest marsupial fossil and their biogeographic implications. PLoS One https://doi.org/10.1371/journal.pone.0001858
Case, J.A., R. W. Meredith, J. Person, *Mus. No. Ariz. Bull.* **65**, 659 (2009).
Godthelp, H., M. Archer, R. Cifelli, S. J. Hand, C. F. Gilkeson, *Nature* **256**, 514 (1992).
Horovitz, I., et al., *PLoS One* **4**, e8278 (2009).
Hugall AF et al 2008. Phylogeny of Australasian agamid lizards based on nuclear and mitochondrial genes: implications for morphological evolution and biogeography. Biol. J. Linn. Soc. 93: 343-358.
Hutchinson MN. 1992. Origins of the Australian scincid lizards: A preliminary report on the skinks of Riversleigh. Beagle - Records of the Museums and Art Galleries of the Northern Territory 9: 61-69
Kear, B.P., B. N. Cooke, M. Archer, T. F. Flannery, *J. Paleontol*. **81**, 1147 (2007)
Kear, B.P., N. S. Pledge, *Aust. J. Zool.* **55**, 331 (2008).
Lee MSY et al. 2009. Miocene skinks and geckos reveal long-term conservatism of New Zealand's lizard fauna. Biology Letters 10.1098/rsbl.2009.0440
Long, J., M. Archer, T. F. Flannery, S. J., *Hand Prehistoric Mammals of Australia and New Guinea: One Hundred Million Years of Evolution (Univ. New South Wales Press, Sydney, 2002).*
Mackness, B.S., Whitehead, P.W., McNamara, G.C. New potassium-argon basalt data in relation to the Pliocene Bluff Downs Local Fauna, northern Australia. Australian Journal of Earth Sciences 47(4): 807-811 (2000b)
Mackness, B.S., Wroe, S., Muirhead, J., Wilkinson, C., Wilkinson, D. First fossil bandicoots from the Pliocene. Australian Mammalogy 22(2): 133-136 (2000a)
Megirian, D., P. Murray, L. Schwartz, C. von der Borch, *Aust. J. Earth. Sci.* 51, 701 (2004).
Meredith, R.W., *et al*., *J. Mammal. Evol*. **15**, 1 (2008).
Meredith, R.W., M. Westerman, M. S. Springer, *Mol. Phylogenet. Evol*. **51**, 554 (2009).
Miller, W., et al., Genome Res. 19, 213 (2009).
Muirhead, J., Wroe, S. A new genus and species, *Badjcinus turnbulli* (Thylacinidae: Marsupialia), from the late Oligocene of Riversleigh, northern Australia, and an investigation of thylacinid phylogeny. *Journal of Vertebrate Paleontology* **18**(3): 612-626 (1997)
Pyron RA, Burbrink FT. 2014. Early origin of viviparity and multiple reversions to oviparity in squamate reptiles. Ecology Letters 17:13-21.
S. Wroe, in *Predators with Pouches: The Biology of Marsupial Carnivores* , M. Jones, C. Dickerman, M. Archer, Eds. (CSIRO, Collingwood, Australia, 2003), pp. 102-123.
Schwartz, L.R.S., *Palaeontol*ogy **49**, 991 (2006).
Skinner A et al. 2013. Phylogeny and Divergence Times of Australian Sphenomorphus Group Skinks (Scincidae, Squamata). Mol Phylogenet Evol. 69: 906-918.
Townsend TM et al. 2011. Phylogeny of iguanian lizards inferred from 29 nuclear loci, and a comparison of concatenated and species-tree approaches for an ancient, rapid radiation. Mol Phylogenet Evol. 61: 363-380.
Travouillon, K.J., M. Archer, S. J. Hand, H. Godthelp, *Alcheringa* **Special Issue 1**, 323 (2006).
Turnbull, W.D., E. L. Lundelius, Jr., M. Archer, Bull. Am. Mus. Nat. Hist. 279, 513 (2003).
Woodburne, M.O. et al., *J. Vertebr. Paleontol*. **13**, 483 (1993).
Woodhead, J. et al. 2014. Developing a radiometrically-dated chronologic sequence for Neogene biotic change in Australia, from the Riversleigh World Heritage Area of Queensland. Gondwana Research 29: 153–167
Woodhead, J., et al., Developing a radiometrically-dated chronologic sequence for Neogene biotic change in Australia, from the Riversleigh World Heritage Area of Queensland. Gondwana Res. 29:153-167 (2016)
Wroe, S., in *Predators with Pouches: The Biology of Marsupial Carnivores* , M. Jones, C. Dickerman, M. Archer, Eds. (CSIRO, Collingwood, Australia, 2003), pp. 102-123.
Wroe, S., *Palaeontology* **42**, 501 (1999).
Zheng Y, Wiens JJ. 2016. Combining phylogenomic and supermatrix approaches, and a time-calibrated phylogeny for squamate reptiles (lizards and snakes) based on 52 genes and 4162 species. Mol Phylogenet Evol. 94: 537-47.

Table S1. Fossil and secondary calibrations used for dating estimates of Australian vertebrate radiations.

SI. Materials and Methods

Data Availability

All data and R code used in this study, as well as supporting materials, operator files, results, and figures are available on GitHub at https://github.com/IanGBrennan/MioceneAustralia.

Molecular Taxon Sampling and Alignments

Molecular sampling for this paper is largely built off of previous systematic investigations into Australian vertebrate groups. We would like to acknowledge the importance of the many molecular studies which contributed data, and colleagues who made this work possible. Our sampling comprises near-complete species-level phylogenies of the five most species-rich terrestrial Australian vertebrate radiations, with the notable exception of Anuran amphibians (Myobatrachidae, Hylidae). These radiations account for more than 800 taxa distributed across the continent (Sphenomorphine skinks—240 taxa; pygopodoid geckos—189 taxa; meliphagoid birds—149 taxa; marsupial mammals—133 taxa; agamid lizards—99 taxa). To abide by assumptions of the birth-death model of Stadler [2], we included one exemplar per species, or species-level candidate lineage. Alignments and trees for the three reptile radiations were built under the same directions as Oliver, Brennan [3], and so we have reproduced the process of their construction below.

Agamidae Lizards: Initial molecular sampling was collated from Hugall, Foster [4] and Chen, Stuart-Fox [5], comprising a single mitochondrial (ND2) and three nuclear loci (MOS, BDNF, RAG1). To this we added recently published data for species of *Ctenophorus* [6] and *Tympanocryptis*. Final alignment consists of 3,538 bp, across 99 taxa comprising 92 recognized species and 7 candidate species, including outgroup New Guinea lineages.

Pygopoidodea Geckos: The basis for molecular sampling of geckos was that of Brennan and Oliver [8]. We added a number of deeply divergent lineages in the genera *Amalosia*, *Oedura*, and *Strophurus* from published [9-11] and in-review materials [12, 13], as well as new sequences for recently described species *Strophurus congoo*, and divergent lineages in the genera *Lucasium* and *Pygopus*. Final alignment consists of 3,756 bp, across 189 taxa comprising 157 recognized species and 32 OTUs.

Sphenomorphine Skinks: We started with the 6 locus alignment of Rabosky, Donnellan [14], which comprises 4 mitochondrial genes (12S, 16S, cyt-b, ND4) and 2 nuclear introns (LDLR, ATP synthetase), to which we added of 3 nuclear exons: (CMOS, BDNF, PTPN12). CMOS from Skinner, Hutchinson [15] and Pyron, Burbrink [16]; BDNF from Pyron, Burbrink [16]; and PTPN12 from Skinner, Hutchinson [15]. Final alignment consists of 7,537 bp, across 240 taxa comprising 235 recognized Australian species and 5 candidate lineages.

Meliphagoid Birds: Dr. Petter Marki provided 1000 post burn-in trees sampled from the posterior distribution of the fossil-calibrated analysis presented in Marki, Jonsson [17]. These trees are based on alignments of five mitochondrial genes (12S, cyt-b, COI, ND2, ND3), two nuclear introns (Fib-5, GAPDH) and two nuclear exons (RAG1, RAG2), and account for 286 of 289 recognized species, including all 149 Australian taxa.

Marsupial Mammals: The basis for marsupial molecular sampling was collated from Mitchell, Pratt [18], with molecular markers pruned down to three mitochondrial genes (12S, 16S, cyt-b) and five nuclear introns/exons (APO8, BRCA1, IRBP, RAG1, vWF). To this, we added recent dasyuromorph sequences from Westerman, Krajewski [19], to create the most extensive molecular representation of Australasian marsupials to date, comprising 232 recognized taxa, of which 133 are Australian.

Phylogenetic Inference and Chronogram Calibrations

We estimated phylogenetic relationships and dated our trees using Bayesian methods as implemented in BEAST v1.8.4 [20] or BEAST2 [21]. We used PartitionFinder [22] to determine the most appropriate molecular partitioning schemes and substitution models. Ultimately, all loci across all four datasets (geckos, skinks, agamids, mammals) were partitioned separately. For protein-coding loci, first and second codon positions were partitioned together (1+2; GTR+I+Γ) and third codon positions separately (GTR+I+Γ). Nuclear introns were not partitioned by codon, and were modelled under GTR+I+Γ as well. All analyses were run under a Birth Death speciation process, with a relaxed uncorrelated log-normal clock distribution, and unlinked site, clock, and tree models.

For all radiations, following phylogenetic estimation, extralimital taxa (non-Australian, and non-continental Australian, with the exception of Tasmania) were pruned from trees in R [23], using RStudio [24] (package: APE [25]; function: 'drop.tip') prior to macroevolutionary analyses.

BEAST and BEAST2 divergence date estimates were informed by fossil and secondary calibrations routinely used in molecular divergence studies, and are detailed in Table S1. Due to the paucity of available informative fossils for Australian lizards, we cautiously used secondary calibrations on root ages where necessary.

Biogeographic Data

For analyses of historical biome dispersal patterns and trends, we partitioned Australia into five discrete biomes that capture both accepted definitions (observed patterns of biological differentiation) and a widely used objective climate classification scheme (modified Köppen-Geiger climate classification [26]). Five regions were classified as followed (Fig.S9):

Arid: consisting of both arid, and surrounding semi-arid and grassland regions of Stern, De Hoedt [26], and covering the vast majority of Australia (77.8%).

Subtropical: corresponding to widely isolated areas of the east and west coast of Australia.

Savannah: equatorial and tropical, largely corresponding to the savannah biome of northern Australia, including monsoonal grassland habitats.

Temperate: cool climate, highly seasonal temperate biomes of the south eastern and south-western coast of Australia.

Forest: consists of highly relictual pockets of generally fire sensitive forest dotted along Australia's east coast [27, 28]. This fifth category was not capture by the basis of our climate classification scheme [26], but reflects both present day and historical data which indicate regions of permanently wet forest have a phylogenetically and ecologically distinctive endemic biota of their own. This is widely considered to represent the vestiges of a formerly widespread mesic-adapted biota.

The distributions of all taxa were mapped out against our five biome classification using the spatial portal of the Atlas of Living Australia (http://spatial.ala.org.au). Taxa with distributions in two or more biomes were scored accordingly, with multiple states. We then modeled the biogeographic history of each group using BioGeoBEARS. For empirical tests, we used the MCC tree and 100 trees randomly sampled from the post burn-in distribution from dating analyses of each clade to account for phylogenetic and dating estimate uncertainty. Macroevolutionary analyses such as BioGeoBEARS are sensitive to the parsimonious state reconstruction of ancestral nodes, and so to account for uncertainty in ancestral biome reconstruction, state transitions, and dispersal frequencies, we ran an additional 50 biogeographic stochastic maps (BSM) on each of the 101 trees [29]. For comparison against empirical results, we iterated across 100 alternative biogeographic

histories created by simulating tip states (5 states) onto the focal tree using the preferred dispersal model (always DEC+j), following Matzke [30], and simulated 50 BSMs per iteration, comprising a total of 5,000 alternative scenarios per group. To summarize empirical and simulated results, we created a sliding window with width 1 million years and moved it through our BSM results at 0.1 million year intervals, starting at current time and working backwards to the extent of the tree depth. Within each window, we noted the number of total cladogenetic dispersal events (num.total), and the number of vicariance (v) and founder (j) events (together: num.vj), then calculated the ratio of vicariance/founder events to all events within that time period (num.vj/num.total = ratio.vj), with the1q2 remainder assumed to have occurred in sympatry. For each radiation, for both empirical and simulated biogeographic histories, we combined results from each of the 100 iterations, and calculated the 95% confidence interval (CI) at each time period, to create an overall estimate through time of the proportion of dispersal events which are founder or vicariance events given our tree and the DEC+j model. We then used ggplot2 [31] to plot the empirical and null confidence intervals to visualize periods in which the proportion of empirical vicariance/founder events deviated from an expected biogeographic history (Fig.S1). To determine the trend across all radiations together, we followed the same approach, combining the num.vj across all lineages at each given time window, doing this for both simulated and empirical data, and similarly for all dispersal events (num.total), then calculated the ratio (num.vj/num.total) in each window, and estimated a 95% CI across all trees, followed by plotting the observed and simulated trends (Fig.1B—"proportion allopatric events").

We also considered species distributions using explicit occurrence data. We started by downloading spatial records for all available taxa found in our trees. We cleaned data by inspecting species point distributions for outliers, comparing against expert field guides. For each species we translated spatial records into spatial points objects using the R package *sp* [32], then collated spatial points into buffered polygons using the 'gBuffer' function in the package *rgeos* [33] with width set to 1. To account for ancestral distributions, we applied a Brownian Motion dispersal method, rase [34]. Using contemporary distribution data, we ran two MCMC chains for 100,000 generations (function 'rase'), logging every 100 generations. We inspected the chains for stasis, discarded the first 20% of each chain, and visually compared inferred distributions for consistency in ancestral range reconstructions. Again, we translated ranges (this time, of nodes) from spatial points to spatial polygons, and determined pairwise range overlap using the *rgeos* function 'gOverlaps'.

Model Comparison and Statistical Analyses

Advances in macroevolutionary methods by Landis and Schraiber [35] have provided us the means to test if traits evolve following a Simpsonian evolutionary landscape with multiple peaks, and jumps among them. We implemented two Lévy process "jump" models (JN, NIG) using the R scripts 'pulsR'. These models aimed to determine if the considerable shifts in trait values of some clades are the result of numerous small, or fewer large, evolutionary jumps.

Phenotypic divergence across the evolution of each group may best be explained by changes in global climate or dispersal patterns. To test this, we used the 'fit_t_env' function in the R package RPANDA [36]. To investigate if trends in global temperature predict trait evolution, we used the temperature curve estimated from Zachos, Pagani [37] supplied in RPANDA as 'InfTemp' data. This model has provided an equivocal fit for Australian marsupials, with results largely dependent upon the topology and branch lengths of the provided tree. Some results indicate a positive relationship between declining global temperatures and increasing rate of body size evolution in macropods, while others show a poor fit to body size evolution of dasyurids [1]. In our model fitting, we call this the "ENV"

model. Alternatively, to test a strictly niche conservatism hypothesis that body size evolution is dictated by the relative frequency of vicariant dispersal events among biomes, we provided the mean estimate of the proportion of vicariant dispersal events, specific to each group, through time, as our data (model: BGB). We anticipated an inverse relationship between these factors, such that as the proportion of vicariant events increases, the rate of body size evolution would decrease.

Simulation Tests

To test the power to detect shifts in the mode and rate of trait evolution along our trees, and investigate the ability to recover mode-shifting models, we performed a series of simulations. The ability to fit more complex models, such as those with parameter values differing among regimes, may be limited by the number of tips present in the tree and total tree depth [38]. To address this, we used our empirical Australian vertebrate phylogenies which vary in composition (100–240 tips) and age (crown: 26-60 Mya), and focused on the ability to distinguish between two previously untested models, BMOU and BMOUi. We began by simulating data under BM, OU, EB, ENV, and BMtrend models using mvMORPH [39] and RPANDA [36]. For the BMOU and BMOUi models, we provide an explanation of how to simulate this data as we did, however, it is worth noting that this can be done using the mvSIM function in mvMORPH. We simulated traits across each phylogeny under BMOU and BMOUi models by first splitting the variance-covariance (vcv) matrix, simulating a shift at time *t* (vcv_1 before *t*, vcv_2 after *t*). We then transformed the recent vcv matrix (vcv_2) by applying a defined (empirical) alpha value, and left alone the ancient vcv matrix (vcv_1) akin to a Brownian Motion process (alpha=0). For the BMOU model, which estimates a single rate (sigma.sq) we then recombined the matrices, and drew our simulated data from a multivariate normal distribution, with an appropriate root state value applied. For the BMOUi model, prior to recombining the matrices, we applied a post-shift scalar to the rate of trait evolution in the younger matrix, then recombined the two matrices, and drew our simulated data from a multivariate normal distribution. Parameter bounds for simulation were extracted from our empirical estimates, α (0.01–0.5), σ^2_0 (0.01–0.5) , σ^2_1 (0.001–0.4). Data simulated under additional models (BM, OU, EB, ENV, BMtrend) were created using parameter bounds from the empirical estimates, and are detailed in the *Simulating Extinction* section..

We first sought to determine the recoverability (true positive rate) of our models via simulated trait data. Because the ability to recover the correct model may be dependent upon the number of tips in the tree, we simulated data and fit models to the smallest (agamid lizards–100 tips) and largest (sphenomorphine skinks–240 tips) phylogenies, and iteratively fit a set of standard (BM, EB, OU), shifting (alpha, variance, or both; BMOU, BMOUi), and other (ENV, BMtrend) models. We then calculated AICcWt, and used this to compute mean AICcWt as a measure of model recovery.

Estimates of the timing of shifts (t_{shift}), as well as the strength of the constraint parameter alpha (α) are paramount to the conclusions of this study (top panel, Fig.1). To assess the accuracy of these parameter estimates we simulated trait data on each phylogeny (one maximum clade credibility tree per) under randomly sampled values (t_{shift} = 1–20; α = 0–10). We repeated this procedure for both BMOU and BMOUi models.

Simulating Extinction

To directly address the influence of unobserved but ubiquitous extinction, we undertook a simulation exercise. We started by sampling a set of 100 trees composed of 20 randomly chosen dated trees of each vertebrate radiation. To avoid confounding model fitting with phylogenetic tree shape, we used our empirical phylogenies as the basis for our simulation exercises, integrating the branching topologies of these real taxa. We then

simulated extinction by building extinct taxa onto our empirical trees under three broad scenarios. The first scenario assumed extinction to be a stochastic process. We added 50-100% of the number of extant taxa back onto the tree as extinct tips (e.g. for a tree with 100 extant tips, 50-100 extinct tips were added, resulting in a tree with 150-200 total tips). Extinct tips had randomly sampled phylogenetic positions, branch lengths, and extinction ages. The second scenario focused on exaggerated extinction in the Plio-Pleistocene [40-42]. We took trees created under the stochastic process above, then added an additional 50% of all taxa onto the tree as tips that went extinct in the Plio-Pleistocene (5.3–0.25 Mya). These additional tips were also placed in randomly sampled phylogenetic positions, with branch lengths randomly chosen to allow their extinction in the Plio-Pleistocene. The final extinction process was designed to simulate a worst-case scenario for our preferred Miocene mode-variable models. From our new set of 100 trees, we added an additional 50-100% of the number of extant tips back onto the trees as tips that went extinct in the late Miocene (10–5 Mya). This aimed to simulate extinctions as a result of shifting biome distributions, and the shrinking of mesic forests. These extinct tips were randomly placed throughout the phylogeny, with randomly sampled branch lengths sufficient to allow them to go extinct between 10–5 million years ago (all scenarios are shown in Fig.S8).

After building trees for each extinction scenario, we simulated data under four models of trait evolution. Two were simulated under Brownian Motion (BM) with varied rates of the diffusion parameter σ^2 (high $\sigma^2 = 0.1$, low $\sigma^2 = 0.01$). The third set of data were simulated under an Ornstein-Uhlenbeck process (OU) with variable α (0.1–5) and σ^2 (0.01–0.5) parameters. The fourth set of data were simulated under the BMOU mode-variable model, with variable α (0.01–0.9) and σ^2 (0.01–0.5) parameters pulled from directly from our empirical estimates, but a single σ^2 parameter across any given tree. Data simulated under the BMOUI model used variable α (0.01–0.5) and σ^2_0 (0.01–0.5) parameters, as well as a second rate parameter σ^2_1 (0.001–0.4) pulled from our empirical estimates. The final dataset was simulated under a Brownian Motion process with a trend towards increasing trait values (mu=0.1–0.5). We then fit a series of five models (BM, OU, EB, BMOU, BMOUI, BMtrend) to the data and tree, and collected model fit statistics in the same manner as with the empirical trees. To test the affect of extinction on model inference, we removed all extinct taxa from the trees and data (functions ‘is.extinct’ and ‘drop.extinct’ in geiger), and refit the same models to the extant only data and trees. Finally, we summarized the model fits across the 100 trees and data sets in each extinction scenario, and plot the extinct and extant model fits using ggplot2 (Fig.S8). We anticipated the elevated late Miocene extinction scenario may prove particularly insightful for our inference of mode-variable temporal models (BMOU, BMOUI). Data simulated under low diffusion BM or high α OU processes on trees with elevated Miocene extinction may mimic the application of the α constraint parameter of BMOU or BMOUI processes once extinct taxa are dropped from the tree.

Intersecting Geographic and Phenotypic Histories

To explore the relationship between phenotypic change and geographic mode of speciation, we compared variances (Fig.3, left column) and rates (Fig.3, right column) between sympatric and allopatric taxa. For the methods outlined in the main text we present the comparison only of observable sister taxa (terminal node to terminal node, or terminal node to internal node). However the same comparison could be made between all nodes in the tree. To estimate the distributions of ancestral nodes, we used the R package *rase* [34].

For our comparison of rates, we used the ‘makeSimmap’ function of phytools [43], to stochastically map characters to the tree, or the ‘paintBranches’ function to paint regimes only on sister taxa (leaving a third estimated regime for deeper branches). The ‘makeSimmap’ function (including all node comparisons) tends to overwhelmingly assign

deep branches in the trees (including the root), to be sympatric taxa, potentially resulting in undesirable bias towards high variances, or if the tree depth is appreciable, low rates of evolution. Our results indicate that rates of phenotypic evolution fit using the BMS model consistently estimate greater rates for sympatric taxa compared to allopatric, regardless of the method (all nodes, or solely sister taxa) used.

SI. Results and Discussion

Phylogenetic Reconstructions

Phylogenetic trees are broadly concordant in topology, support, and divergence dating with those from the literature, from which their sampling is based. To account for topological and dating estimate variation, we iterated all analyses across a distribution of 100 trees for each radiation.

Simulations Results

The ability to accurately recover the correct (generating) process is essential to any study of which seeks to explain observations using models. We find consistent support for the accurate assignment and preference of generating models in our simulation study (Fig.S7, S8, S10). This provides evidence that we can appropriately infer a change in the mode of trait evolution, but also a shift in the rate (BMOUI vs. BMOU).

Late Miocene constraint on variance of body sizes highlights a transition in evolutionary modes, and suggests an indirect pressure to maintain ancestral body size. For both t_{shift} and α, generated under both BMOU and BMOUI models, the relationship between estimated and simulated (true) values are highly similar (Fig.S11–S13). We find that for the alpha parameter, when simulated values approach ~7, accurate recovery of this parameter begins to fade. Similarly, as the timing of a shift in the evolutionary mode exceeds 15 Mya, estimates begin to stray from the simulated time. Because our study is focused on a younger time scale (Late Miocene: 12–5 Mya), and empirically estimated values of alpha are far lower, we believe that we can accurately recover both of these parameters.

Body Size Evolution and Model Fitting

Instead of directly modelling the evolution of a given trait without an *a priori* hypothesis about what is driving it, we could instead directly address the influence of a measured external variable on trait evolution [1]. Using this approach, previous study has found that body size in birds and mammals is tightly linked to fluctuations in Cenozoic climate. Interestingly, meliphagid birds (a family within the Meliphagoidea) show declining rates which are correlated with declining global temperatures. The basis of this model allows for the investigation of the relationship between the evolutionary rate of a trait of interest (σ^2) and any other variable with time-sampled data. This provided us the opportunity to directly test if body size evolution is correlated with the Miocene fracturing of mesic biomes, and an increase in the relative proportion of allopatric dispersal events. We replaced global temperatures through the Cenozoic with our sliding-window dispersal estimates as our variable (*Materials and Methods*), but again, this model (BGB) provided a poor fit to all radiations, perhaps as a result of insufficient cladogenetic events and exaggerated dispersal proportions deep in our phylogenies.

SI References

1. Clavel J., Morlon H. 2017 Accelerated body size evolution during cold climatic periods in the Cenozoic. *Proc Natl Acad Sci U S* **114**(16), 4183-4188. (doi:10.1073/pnas.1606868114).
2. Stadler T. 2010 Sampling-through-time in birth-death trees. *J Theor Biol* **267**(3), 396-404. (doi:10.1016/j.jtbi.2010.09.010).
3. Oliver P.M., Brennan I.G., Lee M.S.Y. in review Arid biomes as species pumps boosting continental biodiversity. *Nature*.
4. Hugall A.F., Foster R., Hutchinson M., Lee M.S.Y. 2008 Phylogeny of Australasian agamid lizards based on nuclear and mitochondrial genes: implications for morphological evolution and biogeography. *Biol J Linn Soc* **93**, 343-358.
5. Chen I.P., Stuart-Fox D., Hugall A.F., Symonds M.R. 2012 Sexual selection and the evolution of complex color patterns in dragon lizards. *Evolution* **66**(11), 3605-3614. (doi:10.1111/j.1558-5646.2012.01698.x).
6. Edwards D.L., Melville J., Joseph L., Keogh J.S. 2015 Ecological Divergence, Adaptive Diversification, and the Evolution of Social Signaling Traits: An Empirical Study in Arid Australian Lizards. *Am Nat* **186**(6), E144-161. (doi:10.1086/683658).
7. Doughty P., Kealley L., Shoo L.P., Melville J. 2015 Revision of the Western Australian pebble-mimic dragon species-group (Tympanocryptis cephalus: Reptilia: Agamidae). *Zootaxa* **4039**(1), 85-117. (doi:10.11646/zootaxa.4039.1.3).
8. Brennan I.G., Oliver P.M. 2017 Mass turnover and recovery dynamics of a diverse Australian continental radiation. *Evolution*. (doi:10.1111/evo.13207).
9. Oliver P.M., Doughty P. 2016 Systematic revision of the marbled velvet geckos (*Oedura marmorata* species complex, Diplodactylidae) from the Australian arid and semi-arid zones. *Zootaxa* **4088**(2), 151-176.
10. Oliver P.M., McDonald P.J. 2016 Young relicts and old relicts: a novel palaeoendemic vertebrate from the Australian Central Uplands. *R Soc Open Sci* **3**(10). (doi:10.1098/rsos.160018).
11. Oliver P.M., Smith K.L., Laver R.J., Doughty P., Adams M. 2014 Contrasting patterns of persistence and diversification in vicars of a widespread Australian lizard lineage (the *Oedura marmorata* complex). *J Biogeogr* **41**(11), 2068-2079.
12. Laver R.J., Doughty P., Oliver P.M. in review Origins and patterns of endemism in two specialised lizard lineages from the Australian Monsoonal Tropics (*Oedura*). *J Biogeogr*.
13. Laver R.J., Nielsen S.V., Oliver P.M., Moritz C. in review Trans-biome diversity in Australian grass-specialist lizards (Diplodactylidae: *Strophurus*). *Mol Phylogenet Evol*.
14. Rabosky D.L., Donnellan S.C., Grundler M., Lovette I.J. 2014 Analysis and visualization of complex macroevolutionary dynamics: An example from Australian scincid lizards. *Syst Biol* **63**(4), 610-627. (doi:10.1093/sysbio/syu025).
15. Skinner A., Hutchinson M.N., Lee M.S. 2013 Phylogeny and divergence times of Australian Sphenomorphus group skinks (Scincidae, Squamata). *Mol Phylogenet Evol* **69**(3), 906-918. (doi:10.1016/j.ympev.2013.06.014).
16. Pyron R., Burbrink F., Wiens J. 2013 A phylogeny and revised classification of Squamata, including 4161 species of lizards and snakes. *BMC Evol Biol* **13**(1), 1-54. (doi:10.1186/1471-2148-13-93).
17. Marki P.Z., Jonsson K.A., Irestedt M., Nguyen J.M., Rahbek C., Fjeldsa J. 2017 Supermatrix phylogeny and biogeography of the Australasian Meliphagides radiation (Aves: Passeriformes). *Mol Phylogenet Evol* **107**, 516-529. (doi:10.1016/j.ympev.2016.12.021).
18. Mitchell K.J., Pratt R.C., Watson L.N., Gibb G.C., Llamas B., Kasper M., Edson J., Hopwood B., Male D., Armstrong K.N., et al. 2014 Molecular phylogeny, biogeography, and

habitat preference evolution of marsupials. *Mol Biol Evol* **31**(9), 2322-2330. (doi:10.1093/molbev/msu176).
19. Westerman M., Krajewski C., Kear B.P., Meehan L., Meredith R.W., Emerling C.A., Springer M.S. 2016 Phylogenetic relationships of dasyuromorphian marsupials revisited. *Zool J Linn Soc* **176**(3), 686-701. (doi:10.1111/zoj.12323).
20. Drummond A.J., Rambaut A. 2007 BEAST: Bayesian evolutionary analysis by sampling trees. *BMC Evol Biol* **7**, 214.
21. Bouckaert R., Heled J., Kühnert D., Vaughn T., Wu C.-H., Xie D., Suchard M.A., Rambaut A., Drummond A. 2014 BEAST2: A software platform for Bayesian evolutionary analysis. *PLoS Computational Biology* **10**(4), e1003537. (doi:10.1371/journal.pcbi.1003537).
22. Lanfear R., Calcott B., Ho S.Y.W., Guindon S. 2012 PartitionFinder: Combined Selection of Partitioning Schemes and Substitution Models for Phylogenetic Analyses. *Mol Biol Evol* **29**(6), 1695-1701. (doi:10.1093/molbev/mss020).
23. R Core Team. 2000 R language definition. In *Vienna, Austria: R foundation for statistical computing* (
24. R Studio Team. 2017 RStudio: integrated development environment for R. RStudio, Inc., Boston, MA. (
25. Paradis E., Claude J., Strimmer K. 2004 APE: Analyses of phylogenetics and evolution in R language. *Bioinformatics* **20**(2), 289-290. (doi:10.1093/bioinformatics/btg412).
26. Stern H., De Hoedt G., Ernst J. 2000 Objective classification of Australian climates. *Aust Meteorol Mag* **49**(2), 87-96.
27. Byrne M., Steane D.A., Joseph L., Yeates D.K., Jordan G.J., Crayn D., Aplin K., Cantrill D.J., Cook L.G., Crisp M.D., et al. 2011 Decline of a biome: evolution, contraction, fragmentation, extinction and invasion of the Australian mesic zone biota. *J Biogeogr* **38**(9), 1635-1656. (doi:10.1111/j.1365-2699.2011.02535.x).
28. Byrne M., Yeates D.K., Joseph L., Kearney M., Bowler J., Williams M.A.J., Cooper S., Donnellan S.C., Keogh J.S., Leys R., et al. 2008 Birth of a biome: insights into the assembly and maintenance of the Australian arid zone biota. *Mol Ecol* **17**(20), 4398-4417. (doi:10.1111/j.1365-294X.2008.03899.x).
29. Matzke N.J. 2016 Stochastic mapping under biogeographical models. (PhyloWiki BioGeoBEARS website http://phylo.wikidot.com/biogeobears#stochastic_mapping.
30. Matzke N.J. 2014 Model Selection in Historical Biogeography Reveals that Founder-Event Speciation Is a Crucial Process in Island Clades. *Syst Biol* **63**(6), 951-970. (doi:10.1093/sysbio/syu056).
31. Wickham H. 2009 *ggplot2: Elegant Graphics for Data Analysis*. New York, Springer-Verlag.
32. Bivand R.S., Pebesma E.J., Gómez-Rubio V., Pebesma E.J. 2008 *Applied spatial data analysis with R*, Springer.
33. Bivand R., Rundel C. 2013 rgeos: interface to geometry engine-open source (GEOS). *R package version 03-2*.
34. Quintero I., Keil P., Jetz W., Crawford F.W. 2015 Historical Biogeography Using Species Geographical Ranges. *Syst Biol* **64**(6), 1059-1073. (doi:10.1093/sysbio/syv057).
35. Landis M.J., Schraiber J.G. 2017 Pulsed evolution shaped modern vertebrate body sizes. *Proc Natl Acad Sci U S*. (doi:10.1073/pnas.1710920114).
36. Morlon H., Lewitus E., Condamine F.L., Manceau M., Clavel J., Drury J. 2016 RPANDA: an R package for macroevolutionary analyses on phylogenetic trees. *Methods Ecol Evol* **7**(5), 589-597. (doi:10.1111/2041-210X.12526).

37. Zachos J., Pagani M., Sloan L., Thomas E., Billups K. 2001 Trends, Rhythms, and Aberrations in Global Climate 65 Ma to Present. *Science* **292**(5517), 686-693. (doi:10.1126/science.1059412).
38. Beaulieu J.M., Jhwueng D.-C., Boettiger C., O'Meara B.C. 2012 Modeling stabilizing selection: Expanding the Ornstein-Uhlenbeck model of adaptive evolution. *Evolution* **66**(8), 2369-2383. (doi:10.1111/j.1558-5646.2012.01619.x).
39. Clavel J., Escarguel G., Merceron G. 2015 mvmorph: anrpackage for fitting multivariate evolutionary models to morphometric data. *Methods Ecol Evol* **6**(11), 1311-1319. (doi:10.1111/2041-210x.12420).
40. Werdelin L., Lewis M.E. 2005 Plio-Pleistocene Carnivora of eastern Africa: species richness and turnover patterns. *Zool J Linn Soc* **144**(2), 121-144. (doi:10.1111/j.1096-3642.2005.00165.x).
41. Grayson D.K. 1991 Late Pleistocene mammalian extinctions in North America: Taxonomy, chronology, and explanations. *Journal of World Prehistory* **5**(3), 193-231. (doi:10.1007/bf00974990).
42. Jablonski D. 2008 Extinction and the spatial dynamics of biodiversity. *Proc Natl Acad Sci U S* **105**(Supplement 1), 11528-11535. (doi:10.1073/pnas.0801919105).
43. Revell L.J. 2012 phytools: an R package for phylogenetic comparative biology (and other things). *Methods Ecol Evol* **3**(2), 217-223. (doi:10.1111/j.2041-210X.2011.00169.x).

Chapter 3:

Incorporating uncertainty is essential to macroevolutionary inferences: Grass, grit, and the evolution of kangaroos

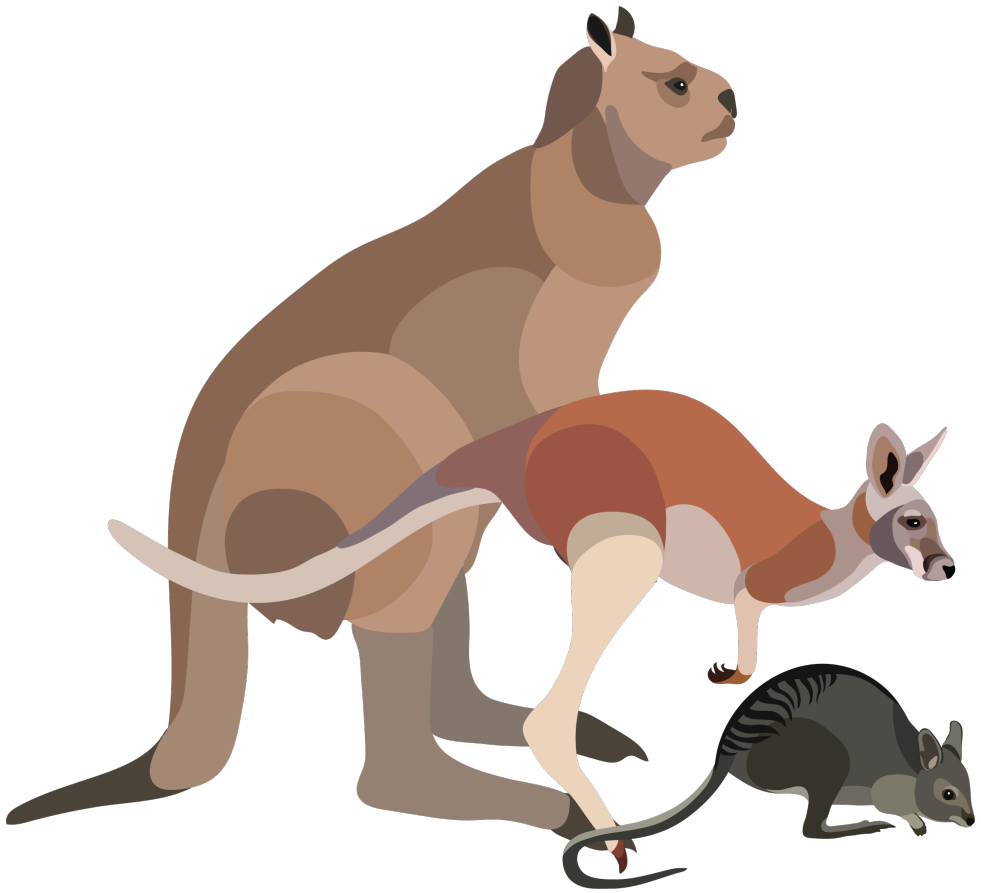

Incorporating uncertainty is essential to macroevolutionary inferences: Grass, grit, and the evolution of kangaroos

Ian G. Brennan[*1]

[1]*Division of Ecology & Evolution, Research School of Biology, Australian National University, Canberra, ACT 2600 Australia*

[*]Corresponding author: ian.brennan@anu.edu.au

Authorship: IGB designed the study, performed the analyses, and wrote the article.

Short Title: Incorporating uncertainty in macroevolution

Acknowledgements: I would like to thank J.Scott Keogh, Marcel Cardillo, and Zoe K.M. Reynolds for discussion and comments on this manuscript. A considerable thank you to the paleontologists and marsupial phylogeneticists who collected the data used in this project, without whom this work would have been impossible.

Data availability: All data and code have been deposited on Github: https://github.com/IanGBrennan/FossilUncertainty

Abstract

Studying organismal ecology and evolution on deep timescales provides us opportunities to identify the processes driving patterns in diversity and forms. These macroecological studies are often built atop a number of preconceived hypotheses regarding phylogenetic relationships, divergence times, and environmental trends. However, many studies fail to account for sources of variation in these data, potentially biasing findings. Here I test several common sources of uncertainty and address their influences on downstream macroevolutionary inferences. Using data from Australian macropod marsupials (kangaroos and allies), I find that assumptions about fossil age and phylogenetic position can dramatically affect divergence date estimates. Variation in inferred divergence dates may then strongly influence our understanding of the links between trait evolution, ecology, and environmental change, including the drivers of kangaroo diversification across Australia. Iterating over uncertainty may ameliorate some issues, but this highlights the importance of testing the assumptions inherent in our data and the methods.

Keywords: comparative methods, phylogenetics, kangaroos, trait evolution.

Introduction

Macroevolutionary and macroecological studies help us to link observable patterns in diversity, form, and function, with the processes dictating them. The methods they involve often rely on phylogenetic and/or phenotypic hypotheses on deep time scales, incorporating little fossil evidence, requiring us to do a delicate dance around uncertainty. To mitigate error, it is first important to recognize the sources, and identify how variation in our data can affect downstream analyses and inferences (Silvestro *et al.* 2015; Title & Rabosky 2016). However, many macroevolutionary studies either ignore this uncertainty or do little to address its potential impacts. Unfortunately, this may lead to more *precise* but potentially less *accurate* inferences that ignore the complex nature of evolution over deep time.

Most macroevolutionary studies include a temporal element, and this—alongside phylogenetic estimation—is arguably one of the most common sources of uncertainty. Fossil ages may not always be confidently known and this can influence divergence time estimates, which can in turn impact inferred evolutionary rates (Beck & Lee 2014; Renner *et al.* 2016; Dos Reis *et al.* 2018). Patterns in these rates can further be attributed to a number of abiotic or biotic processes, which may require testing the relationship between **many** possible factors and their response variables (often organismal traits, genetic diversity, or species richness). Each of these variables may themselves then introduce additional sources of known and unknown error. Here I show how some of these sources of error can be addressed, by demonstrating the influence of fossil age estimates on divergence times and trait evolution in macropod marsupials.

The timing of the radiation of modern kangaroos remains a topic of debate. Most recently it has been suggested that kangaroos speciated rapidly in response to the expansion of C_4 grasses in the Pliocene (Couzens & Prideaux 2018; Nilsson *et al.* 2018). This hypothesis conflicts with a number of molecular and morphological dating studies (Phillips *et al.* 2013; Mitchell *et al.* 2014; Brennan & Keogh 2018; Cascini *et al.* 2018; Celik *et al.* 2019), and relies predominantly on secondary node calibrations and the absence of Miocene fossil evidence to instead infer a considerably younger crown age of the group. In Australia and elsewhere, climate and habitat-driven shifts have often been invoked to explain the diversification of

organismal groups (Kürschner *et al.* 2008; Ezard *et al.* 2011). Changes in species richness may also be accompanied by changes in individual or suites of traits, as with increasing body size and molar tooth height in Miocene Asian and African herbivores as grasslands expanded (Badgley *et al.* 2008). A similar climate-driven narrative in Australia has related the radiation of arid-adapted lineages to late-Miocene continental aridification (for review see (Byrne *et al.* 2008)). These global and local patterns however, are at odds with a much more recent hypothesis of Pliocene radiation and transition to grazing in the Macropodini: kangaroos, wallabies, and their allies.

To investigate macropodoid evolution and test how incorporating uncertainty influences our interpretations, I bring together molecular and morphological data from extant and extinct macropod species in a combined-evidence framework. Current extensions to divergence dating analyses mean we can now estimate phylogenetic relationships, species divergence times, fossil ages, and macroevolutionary parameters jointly (Heath *et al.* 2014; Gavryushkina *et al.* 2017; Ogilvie *et al.* 2018; Barido-Sottani *et al.* 2019). The implementation of these methods in a flexible Bayesian framework (BEAST2) (Bouckaert *et al.* 2018) further allows us to address uncertainty in inferred parameters and relationships, and their influence on macroevolutionary inferences. I explore potential drivers of the evolution of Macropodinae molar tooth height, an important trait suggested to have evolved in response to increasing grazing behavior. Ultimately, I demonstrate that accounting for aspects of uncertainty in (**1**) fossil taxa ages, (**2**) phylogenetic resolution, (**3**) divergence time estimation, and (**4**) mechanistic drivers of macroevolution provides a more encompassing view of the diversification of modern kangaroos. These methods are relatively easy to implement, and I encourage members of the evolutionary biology community to consider them as well.

Materials and Methods

Data

Recent advances in phylogenetic reconstruction methods have facilitated better integration of molecular sequence data with fossil ages (Lee *et al.* 2009; Heath *et al.* 2014) and data (Pyron 2011; Ronquist *et al.* 2012; Beck & Lee 2014; Gavryushkina *et al.* 2017), incorporating

morphological information of both extant and extinct taxa—called "**Total Evidence Dating**" or "**Combined Evidence Dating**." I compiled molecular and/or morphological data for 69 living and extinct macropodoid marsupials (Table 1). Molecular data were collected from GenBank (mostly from (Meredith *et al.* 2008; Mitchell *et al.* 2014; Eldridge *et al.* 2018)), comprising three mitochondrial (*16S*, *12S*, *CytB*) and seven nuclear (*APOB*, *BRCA1*, *IRBP*, *Pro1*, *RAG1*, *TRSP*, *vWF*) loci. Morphological data were collected from (Butler *et al.* 2016) which collated data matrices from (Kear & Pledge 2008; Prideaux & Warburton 2010), and comprise 186 characters focusing on cranial and dental elements, of which 149 characters are variable.

Combined Evidence Analysis: Integrating Data Types

I reconstructed the phylogeny of living and extinct macropodoids using the Fossilized Birth-Death Multi-Species Coalescent model (FBD-MSC) implemented in StarBEAST2 (Ogilvie *et al.* 2018), allowing fossil taxa to be identified as direct ancestors using the Sampled Ancestors package (Gavryushkina *et al.* 2014). In divergence dating analyses fossil information may be included using node priors (generally hard minimum bounds with diffuse upper bounds) or as tip dates (an estimate of the fossil sampling time) (Ho & Phillips 2009). Where data is available, combining node– and tip-dating may provide an advantage over using either method independently (Beck & Lee 2014; O'Reilly & Donoghue 2016). This provides the opportunity to co-estimate the phylogeny and divergence times, while providing structured priors on nodes which may otherwise be driven to unrealistic deep or shallow values. One shortcoming of nearly all implementations of tip-dating however, is the requirement of fixing fossil ages to a single value (Heath *et al.* 2014; Barido-Sottani *et al.* 2019). Except where radiometrically dated, fossil age estimates are rarely precise enough to fit this expectation, and so we often arbitrarily use the median value or a bio-correlated guess within a fossil's age interval. This practice can lead to biased inferences when values nearer maximum or minimum ages are consistently applied, or when an age is randomly assigned (Barido-Sottani *et al.* 2019). Fixed fossil ages also ignore the persistence of lineages for potentially long periods of time, summarizing an extinct taxon to a single point estimate. This discards useful temporal information about fossil occurrences and sampling, which can be incorporated as

"stratigraphic ranges" for extinct taxa (Stadler *et al.* 2018).

To counter these shortcomings, I incorporated uncertainty in fossil ages by sampling from informed priors for both node *and* tip calibrations. In both simulated and empirical data, this process has been shown to provide divergence estimates more consistent with those using known fossil ages. I started by collecting data on fossil taxa occurrences, assemblages, and ages from Couzens and Prideaux (2018) and the Fossilworks database (www.fossilworks.org). I assigned fossil taxa ages based on their most recent (youngest) stratigraphic occurrence. I then set fossil tip dates as either (**1**) fixed values (maximum, mean, or minimum stratigraphic age) or (**2**) sampled from a uniform prior ranging between maximum and minimum stratigraphic age estimates. Extant taxa were coded with age "0". Five node calibrations (*Supplemental Material* Table 3) were also applied as uniform priors, and to address the influence of fossil information incorporated as node priors, I systematically removed each to determine its affect on divergence estimates (Near & Sanderson 2004). The partitioning scheme and models for molecular data were determined using Partitionfinder (Lanfear *et al.* 2012) and are detailed in *Supplemental Material* Table 4.

Morphological data were modelled under the Mkv model, a special case of the Mk model (Lewis 2001)—the most commonly used model for discrete morphological data. The Mk model operates under the assumption that each character may exhibit k states, and can transition among states at equal frequencies/rates. Because different characters may exhibit differing numbers of states, I applied the partitioning strategy of Gavryushkina et al. (2017), which partitions the morphological data based on the number of observed states of each character. Traditionally, invariant characters are either not coded, or stripped from discrete morphological alignments, resulting in an ascertainment bias for variable characters. The Mkv model (Lewis 2001) was proposed to account for this.

Sampling for the combined evidence analyses included nine extinct Macropodinae taxa, however, this certainly underrepresents the true evolutionary diversity of this group. For example, the genus *Macropus* comprises 13 living species, but we are aware of at least as many described extinct taxa. To account for this disparity between the sampled and known diversity of the Macropodinae, I also ran analyses incorporating all fossil macropodin taxa included in the trait data of Couzens and Prideaux (2018). These 38 taxa (Table 2) were incorporated

as tips by including them in all molecular and morphological alignment files, and scored as missing data for all characters. They were then restricted to a clade via monophyletic constraints based on taxonomy, or where available, existing systematic knowledge (Dawson & Flannery 1985). Finally I imposed similar uniform priors on the ages of the tips between their maximum and minimum stratigraphic ages. This provided the inclusion of these fossil taxa, but allowed their absolute age and phylogenetic position to vary within reasonable temporal and topological bounds.

All analyses were run for four independent chains under uncorrelated relaxed lognormal (UCLN) molecular clocks (Table 4) for 1 billion generations and sampled each 5x10^5 generations, to assess convergence among runs. I inspected the MCMC chains for stationarity (ESS > 200) using Tracer v1.7.0 (Rambaut *et al.* 2018), and discarded the first 10-40% of each run as burn-in as necessary before combining runs.

Fossil Taxa as Sampled Ancestors

Fossil taxa are almost always assumed to represent terminal tips that have since gone extinct. To test whether there is signal for some taxa to instead be sampled ancestors, I calculated Bayes factors (BF) for each fossil taxon. Given that I can hypothesize a taxon to be either a tip H_1 or an ancestor H_2, I can estimate the posterior probability for either hypothesis $P(H_1)$, $P(H_2)$, provided the molecular and morphological data (D), the joint estimation of the phylogeny and divergence times (τ), and a model (M) of the molecular and morphological evolution. I can go on to sample exclusively from both the prior and posterior of StarBEAST2 analyses (Gavryushkina *et al.* 2014), and then calculate the Bayes factors using the probabilities of the competing hypotheses. I log transformed the BFs and used a threshold of log(BF) > 1 to identify sampled ancestors, log(BF) < -1 to recognize terminal taxa, and -1 < log(BF) < 1 taxa were categorized as equivocal.

$$BF = \frac{P(H_1|D,\tau,M)P(H_2|\tau,M)}{P(H_2|D,\tau,M)P(H_1|\tau,M)} = \frac{P(Posterior_{ancestor})P(Prior_{tip})}{P(Posterior_{tip})P(Prior_{ancestor})}$$

The Evolution of Hypsodonty

In mammals, molar crown height is correlated with dietary preferences (Williams & Kay 2001; Butler *et al.* 2014; Janis *et al.* 2016). In particular, hypsodonty, very high-crowned teeth, is associated with grazing and browsing on abrasive grasses and shrubs. Because of this, the convergent evolution of high-crowned teeth across many groups has traditionally been associated with the global expansion of grasslands in the Miocene (Badgley *et al.* 2008). This idea has also been applied to macropods, in which high-crowned molars have been suggested to have developed alongside the expansion of C_4 grasses and a transition to grazing in the Pliocene (Couzens & Prideaux 2018). However, the relationship between increasing crown height and endogenous (fiber, silica) dietary abrasives has more recently been disputed. Instead, the argument has been made in ungulates and rodents, that exogenous (dust, grit) abrasives more likely influence the evolution of tooth height (Jardine *et al.* 2012; Strömberg *et al.* 2013; Semprebon *et al.* 2019). Few experimental studies have aimed to disentangle these effects, and so a more holistic view of increasing crown height as a result of endogenous *and* exogenous properties of ingested food items is perhaps currently warranted (Williams & Kay 2001; Hummel *et al.* 2011). In macropods, the evolution of this trait, however, has not been investigated in a proper comparative phylogenetic framework, and so I aimed to do so here.

To better understand the evolutionary pattern and process of hypsodonty in macropodoids, I used phylogenetic comparative methods to test for correlation with a number of time-sampled variables. From the posteriors of the four dating schemes (minimum, mean, maximum, estimated fossil ages) and two sampling strategies (sampled with data, sampled with data and age priors for additional extinct taxa) I extracted Macropodinae trees by sampling uniformly between the minimum and maximum estimated crown ages. This aimed to represent the breadth of inferred ages from all dating schemes (~7–12 MYA). I calculated the Hypsodonty Index (HI) for each sample by dividing tooth height by width ($Height\ Hypoconid\ /Talonid\ Width$), then summarized HI data to species means (**Fig.1**). Intraspecific trait variation is yet another source of data uncertainty, and to account for this I estimated measurement error following (Silvestro *et al.* 2015). Taxa with only a single HI

measurement were scored as NA, and error was estimated jointly during the model fitting. I then fit models of trait evolution using standard stochastic and deterministic (Brownian Motion–**BM**; Early Burst–**EB**; Brownian Motion with a trend–**TREND**; implemented in *geiger* (Pennell *et al.* 2014)), and correlative ("fit_t_env" implemented in *RPANDA* (Morlon *et al.* 2016)) models. For the correlative scenarios, I estimated the rate of trait evolution as a function of temporal variation in palaeotemperature (**ENV**) (Zachos *et al.* 2001), aeolian dust flux (**FLUX**) (Andrae *et al.* 2018), or C_4 plant cover ($\mathbf{C_4}$) (Andrae *et al.* 2018). I fit correlative models as both exponential and linear functions, but collapsed support into a single value for each dataset (ENV, FLUX, C_4). I then fit all six model groups to the data, using trees of varying ages. Because the correlative models are identical to Brownian Motion when $\beta = 0$, I collapsed model fits with $\beta \leq 0.001$ into the Brownian Motion model estimate, as this correlation is unlikely to be biologically meaningful. For each tree, I calculated the relative weight of each model to the total fit (AICc Weight), and plotted this to visualize model support as a function of increasing Macropodinae crown age.

Taxon sampling in many macroevolutionary studies is biased towards including extant taxa. This may be further exaggerated by uneven sampling at the tips of the tree, ultimately affecting downstream macroeovolutionary inferences (Heath *et al.* 2008). To test how this may influence this study, I applied the comparative models described above to three additional phylogenetic and trait datasets. The first involved including a number of fossil taxa which lack morphological or molecular assessment, but are represented in the tooth trait data (n = 38). These were included in dating analyses using uniform priors on their tip age, and taxonomic phylogenetic constraints to produce a set of posterior trees. To these fossil trees and the focal trees (sampling only lineages with molecular or morphological data), I further removed 10–30% of extant tips to simulate extant taxa undersampling, resulting in two additional tree and trait datasets. Each of the four datasets comprises 500 trees.

To investigate the relationship between tree height (age), topology, and model support, I created pairwise matrices for all analyzed trees comparing (**1**) Macropodinae crown height (Δ Crown Age), (**2**) topological similarity, and (**3**) absolute difference in model support (Δ AICcWeight). I used the quartet distance metric (Estabrook *et al.* 1985; Brodal *et al.* 2013) implemented in *Quartet* (Sand *et al.* 2014; Smith 2019) to distinguish topological

differences instead of alternative methods (Robinson-Foulds, Subtree Prune Regraft) because of its sensitivity. I then plotted Δ AICcWeight as a function of Δ Crown Age, and quartet distance to visualize the relationship between these variables.

Molar crown height may not be the only way to understand temporal patterns and the influence of dietary and extra-dietary abrasives on the dental evolution of macropod marsupials. Patterns of dental macrowear—changes to the tooth surface—may also provide information regarding the onset of dietary or environmental changes. Previous interpretation of macropodoid macrowear data suggested that macrowear increased alongside the transition towards increasing grazing activity (Couzens & Prideaux 2018). These trends are based on estimated fossil ages, and do not account for the variance in fossil age estimates. I instead sampled trends in both crown height and macrowear from plausible fossil age scenarios. I first assumed that all fossils from a given "assemblage" had the same age (though this may not be accurate), and that the age of these fossils may be distributed uniformly between the minimum–maximum stratigraphic bounds. For each assemblage (and so for each fossil), I then randomly chose an age from within its bounds, then repeated this exercise 1000 times, plotting the trends for each iteration. For the three main groups of interest (Macropodinae, Sthenurinae, Lagostrophinae), I also summarized the 1000 simulations and plotted the mean trends, accompanied by the trends using expert estimated ages for each fossil (from Couzens and Prideaux 2008).

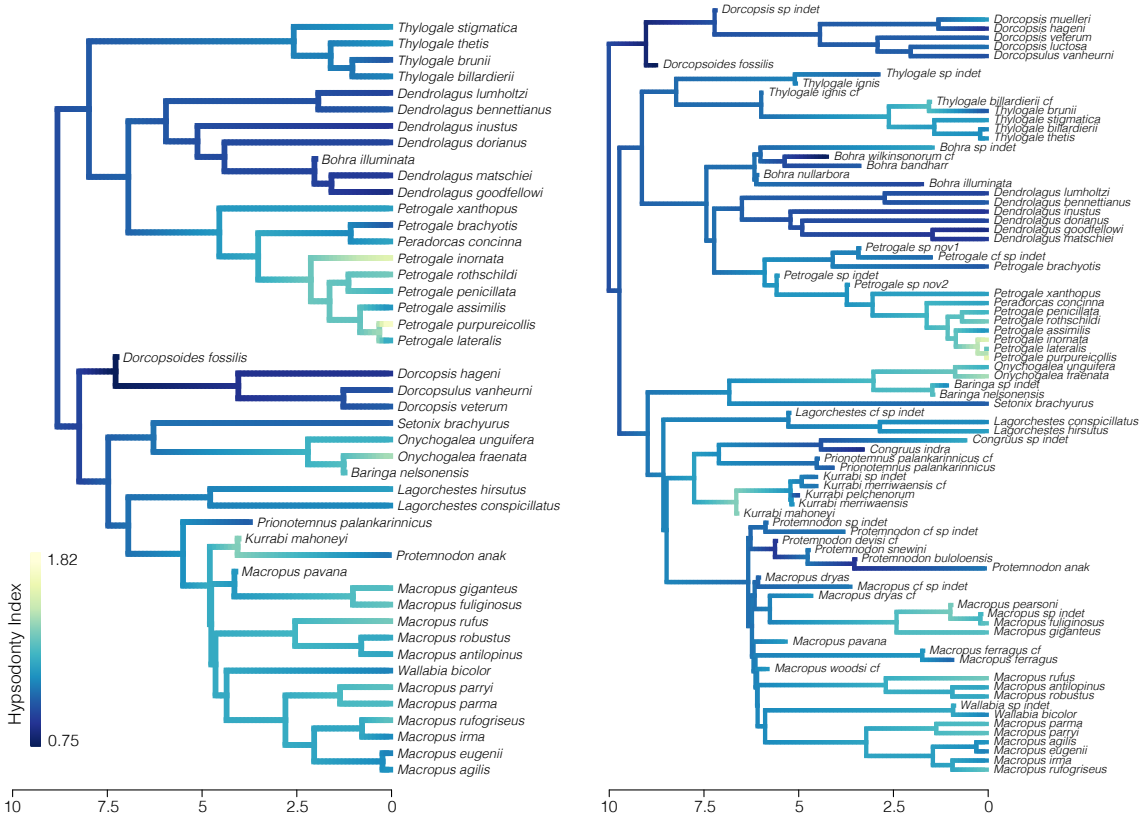

Figure 1: Highly hypsodont molars have evolved multiple times across the Macropodinae. The Hypsodonty Index mapped as a continuous character using 'contMap' in *phytools*, which estimates states at internal nodes by using the contrast algorithm of Felsenstein (1985). On the left is a single tree from the posterior of the tip dating analysis using prior ages on extinct taxa and molecular and morphological data. On the right, a single tree from the posterior of the tip dating analysis using prior ages on extinct taxa, and molecular and morphological data in addition to stratigraphic age data for taxa not sampled in the morphological or molecular data.

Results

Kangaroo Phylogeny

Combined evidence analyses of the macropodoids suggests conflict among current divergence estimates, molecular and morphological data, and fossil information (Cascini *et al.* 2018). Perhaps the most obvious inconsistencies are among divergence date estimates occurring as a result of varied fossil age assignments (**Fig.2**). Fossil ages fixed at minimum, mean, and maximum values return incongruent divergence dates suggesting that the data and results are not robust to the influence of fixed tip ages. Divergence dates estimated from fossils

with tip age priors are broadly overlapping with those of mean and maximum fixed ages, often fall between estimates from those dating schemes, and do not solely return prior values (**Fig.S11**).

Divergence analyses using fossil tips and all five node priors result in date estimates which are at odds with recent molecular results (Dodt *et al.* 2017; Couzens & Prideaux 2018; Nilsson *et al.* 2018; Celik *et al.* 2019). This is primarily driven by the hard minimum prior age of *Ganguroo bilamina* which limits the divergence of the Lagostrophinae and Macropodinae to 17.79 MYA (Neville's Garden Site (Woodhead *et al.* 2016)), and to a lesser extent, the minimum prior age of *Ngamaroo archeri* (**Fig.S1**–**S2**). These node priors cause a dramatic increase in the height of the macropodoid tree, including pulling the Lagostrophinae—Macropodinae split from 12 to 19 MYA. Concerningly, the phylogenetic position of *Ganguroo* has also varied among studies (Prideaux & Warburton 2010; Butler *et al.* 2016, 2018), suggesting its affinities are equivocal, and as such, the hard minimum node prior should be considered carefully.

Removing *Ganguroo* and *Ngamaroo* node priors results in divergence estimates from combined evidence analyses (with priors on extinct taxa ages) which are generally in agreement with another recent phylogenetic assessment of this group (Celik *et al.* 2019). This places the crown divergences of the Macropodinae at 7.8–10 MYA, Dendrolagini 6–8.5 MYA, Dorcopsini 6.5–9 MYA, and Macropodini 6.5–9.5 MYA, slightly older than another molecular-only estimate (Nilsson *et al.* 2018) (**Fig.2**). Because the dates inferred using *Ganguroo* and *Ngamaroo* fossil node calibrations differ so considerably from estimates in the literature, I removed them from further analyses, and consider divergence estimates and macroevolutionary inferences using trees that do not include these node calibrations.

Phylogenetic placement of fossil taxa is largely in agreement with previous investigations (Prideaux & Warburton 2010; Butler *et al.* 2016; Cascini *et al.* 2018), and nearly all fossil taxa are reasonably assigned to appropriate clades. A few fossil Macropodinae taxa (*Congruus*, *Kurrabi*, *Prionotemnus*) however, show unresolved intraclade positions, most likely due to incomplete molecular and morphological sampling. The method for determining support for the position of fossil taxa as terminals or sampled ancestors appears sensitive to the tip-dating method implemented (**Fig.3**). Only two taxa (*Simosthenurus*, *Protemnodon*) are

confidently returned as a terminal taxon in both static and prior informed dating schemes (**Fig.3**), though this is expected given that they are also sampled for molecular data. Two more taxa are considered tips in the prior informed scheme, but not in the fixed age scheme (*Prionotemnus*, *Drocopsoides*). Two others are considered tips in the fixed age scheme, but not in the prior informed scheme (*Baringa*, *Congruus*). The remaining fossil taxa are considered equivocal under both dating methods (*Bohra*, *Kurrabi*, *Macropus pavana*). Estimating fossil taxa ages jointly with the phylogeny and divergence times results in age estimates which do not simply return the uniform priors applied (**Fig.2**). Most distributions of fossil ages appear roughly normal, and fall within and not at the prior bounds (**Fig.3, S10**).

Macropod Tooth Evolution

Trends in molar crown height and macrowear are both temporally and phylogenetically variable (**Fig.4**). In the Macropodinae, Sthenurinae, and Lagostrophinae, macrowear increases or peaks in the early-to-mid Pliocene, decreases rapidly, and then increases again in the late Pliocene to early Pleistocene. This pattern is mirrored in tooth crown height (HI) trends, and occurs alongside increasing C_4 grass estimates and dust flux levels. The timing and confidence in these trends is sensitive to the age assigned to each fossil, and differs slightly from the previous presentation of these data (Couzens & Prideaux 2018). Trend lines based on expert estimated fossil ages, always fall inside the simulated envelopes, however, it is important to highlight the variability in the onset and timing of molar crown height evolution and macrowear.

Comparative phylogenetic analyses favor a relationship between the rate of tooth height evolution and C_4 grass expansion across the Australian continent (**Fig.5**). These results however are sensitive to the age of the input tree (**Fig.S3–S5**), and show that for scenarios in which the crown Macropodini split is between 6–9 Ma, C_4 plant cover is the best predictor of the rate of crown height evolution ($\beta>0$; positive relationship) (**Fig.5; S6–S8**). For scenarios in which the crown split is between 9–11 Ma, support shifts towards a model where the rate of tooth crown height evolution is correlated with aeolian dust flux ($\beta>0$; positive relationship), and shifts again >11 Ma to the ENV model ($\beta<0$; negative relationship). Sampling additional extinct taxa results in a modest decrease in support for the C_4 model. Undersampling extant

taxa however, dramatically alters the macroevolutionary result, shifting support to the aeolian dust flux model instead (**Fig.5**).

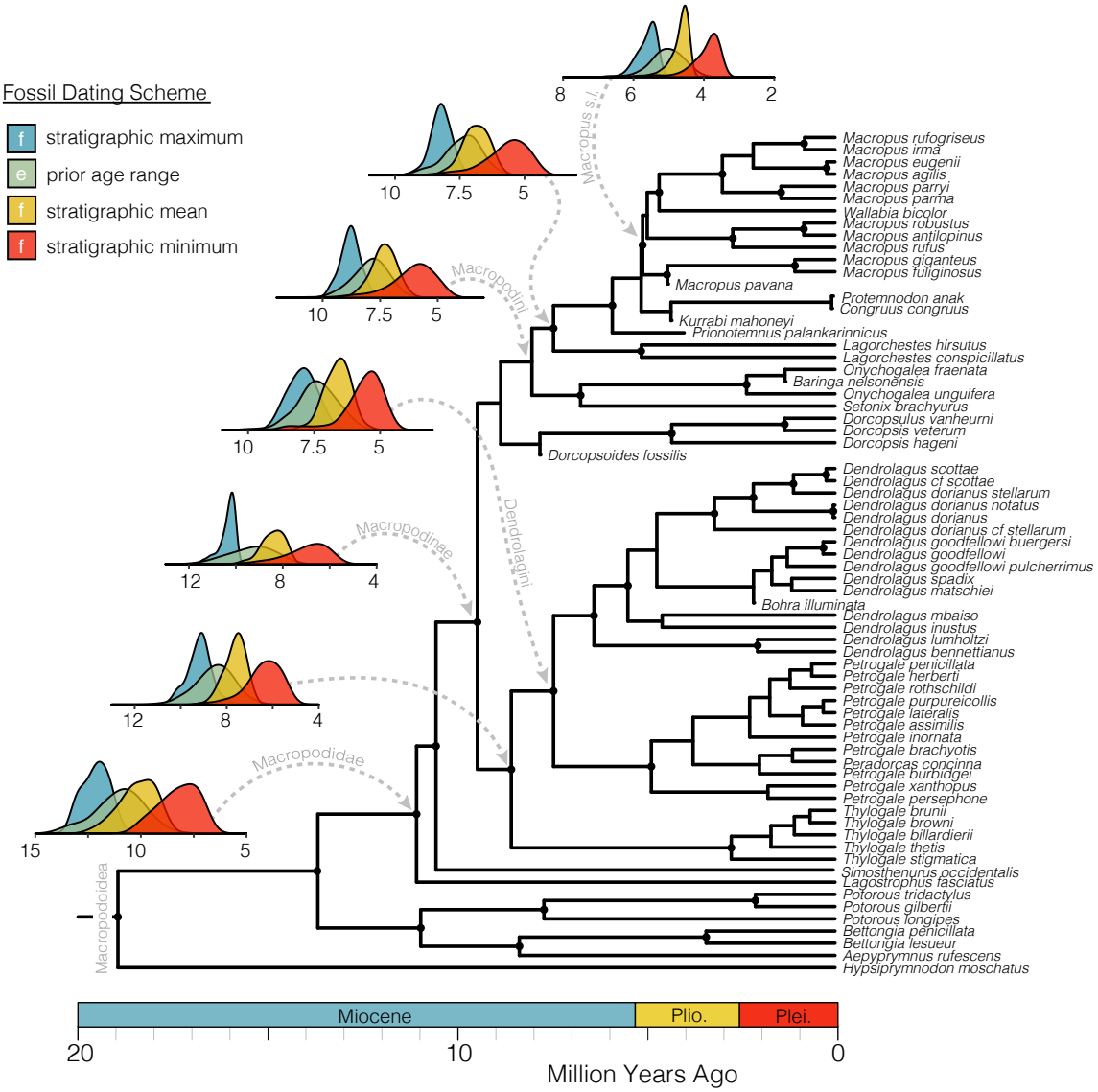

Figure 2: Divergence date estimates vary widely as a result of differing fossil age schemes. The phylogeny shown is the maximum clade credibility tree of the combined evidence analysis of the Macropodoidea, estimating fossil ages jointly with the phylogeny. Nodes denoted by a black circle are supported by posterior probabilities >0.85, nodes with lower support are considered equivocal and their support values are not shown. I highlight the variation in ages of several key nodes. Distributions are estimated ages of a given node from 500 trees pulled from the posterior of all dating analysis schemes. Colors denote the dating methodology used, 'f' designating fixed date schemes, 'e' designating ages estimated from within a prior range.

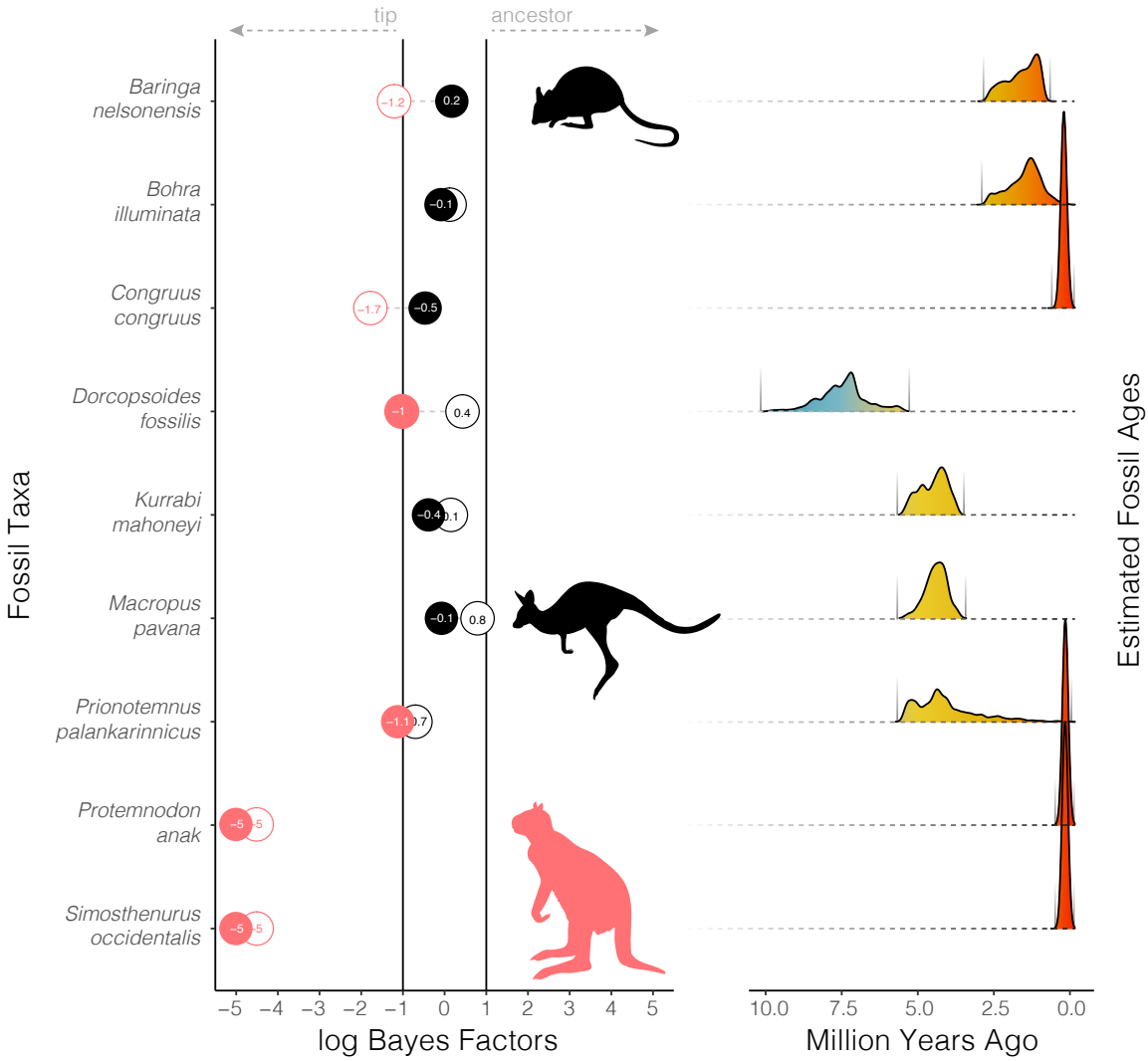

Figure 3: Bayes Factor support for fossil taxa as tips or sampled ancestors may vary when different methods of fossil age assignment are used. Filled circles represent fossil states estimated under the tip-dating prior age method using minimum and maximum fossil ages. Empty circles represent fossil states estimated under the standard tip-dating method using mean ages. Pink circles are strongly supported as terminal taxa, black circles denote equivocal assignment. Very high and very low log BF scores (taxa *always* sampled as ancestors or terminals) are reported arbitrarily as 5 or -5 to facilitate visualization. To the right, estimated fossil ages are shown as distributions pulled from 200 trees from the posterior of the combined evidence analysis using priors on extinct tips. Estimated ages fall within—and not at the bounds.

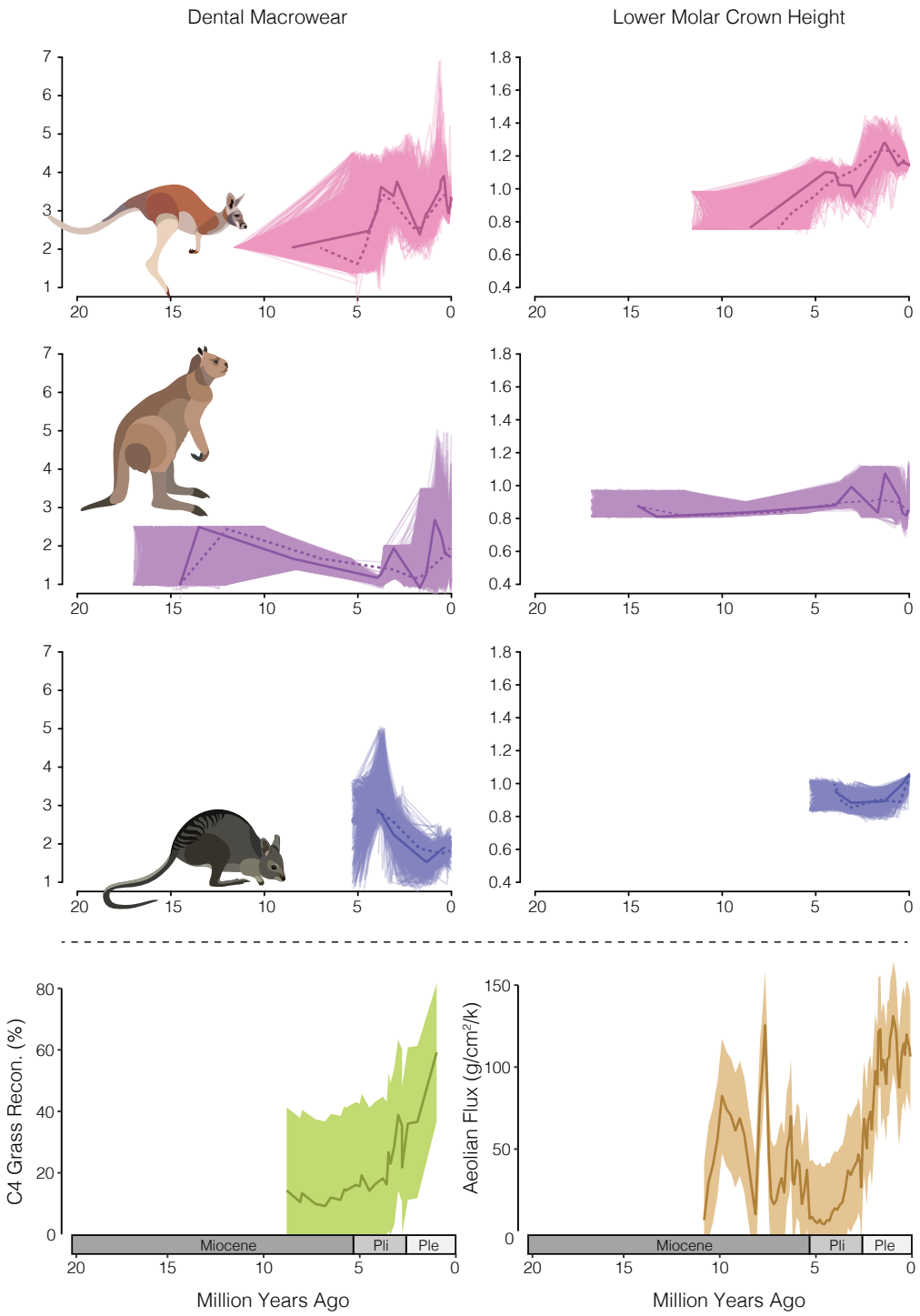

Figure 4: Temporal trends in macropodoid molar crown macrowear and height vary under different fossil age estimates. On the left, macrowear trends, and on the right, the hypsodonty index. The top row is trends in the Macropodini, below the Sthenurinae, and finally the Lagostrophinae. The bottom row shows temporal trends in C_4 grass reconstruction and dust flux across the Australian continent.

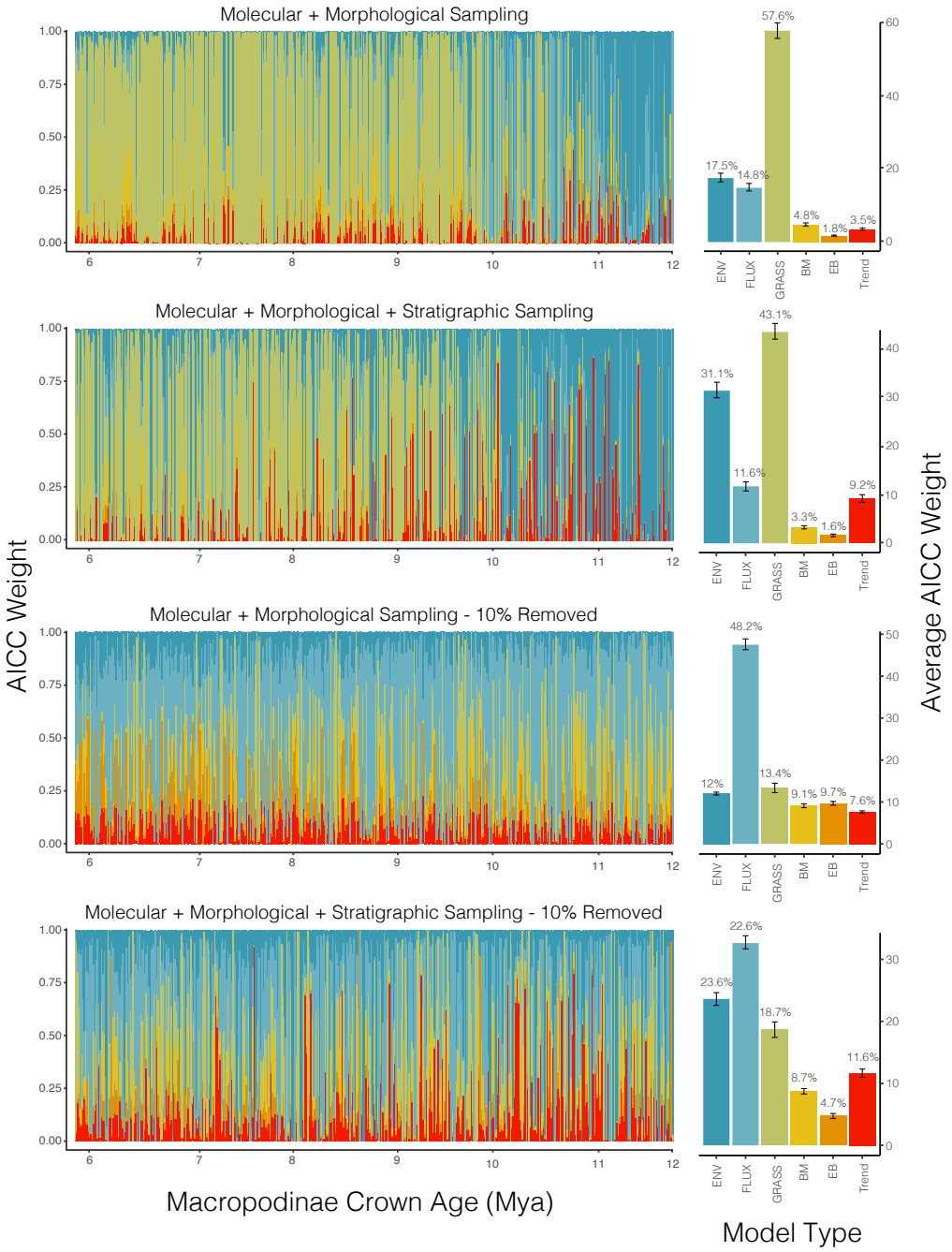

Figure 5: The preferred model of molar crown height (HI) evolution among the Macropodinae differs depending on estimated fossil taxa ages and divergence times. Each vertical bar represents relative AICc weights of all models for a single tree pulled from the dating posteriors, with crown age of the Macropodinae noted below. In the right column, the average AICc weight across all 500 trees. Each row corresponds to a different set of 500 trees sampled: row 1 includes trees built including taxa sampled in both morphological and molecular data matrices; row 2 includes trees built including molecular and morphologically sampled taxa, as well as 38 additional extinct taxa incorporated into the phylogenies using priors on their age; row 3 are the trees used in row 1 with 10–30\% of extant taxa randomly removed in each tree; row 4 are the trees used in row 2 with 10–30\% of extant taxa randomly removed from each tree.

Discussion

Inferences from evolutionary and phylogenetic studies on deep time scales require a healthy amount of skepticism from both researchers and audiences alike. Unfortunately, in the quest for precision, sources of bias and uncertainty are often ignored, unintentionally sacrificing accuracy. The sources of data uncertainty are many, and it may be unreasonable to account for them all, but I provide some suggestions for incorporating fossil uncertainty and understanding its influence on our inferences of the macroevolution of modern kangaroos.

Combined Evidence Analyses and Divergence Dating

Incorporating fossil information into divergence dating analyses can often feel like black magic. In the case of macropodoids, perhaps the first consideration is the application of fossil information to macropodoid clades. Fossil ages for two extinct taxa *Ganguroo bilamina* and *Ngamaroo archeri* are often used as node priors to calibrate marsupial trees. *Ngamaroo* is generally used to provide a late Oligocene (24.7 Mya) or early Miocene (16 Mya) minimum bound on the divergence between the Hypsiprymnodontidae and the group including potoroids, macropodids, and all other related taxa. This clade is most frequently referred to as the "Macropodoidea" (Den Boer & Kear; Kear et al. 2007; Kear et al. 2008; Burk & Springer; Black 2012; Black 2014; Bates 2014; Janis 2016) (Kear & Pledge 2008; Janis *et al.* 2016; Couzens & Prideaux 2018), but is alternatively called the "Macropodiformes" (Phillips *et al.* 2013; Cascini *et al.* 2018; Celik *et al.* 2019). Morphological phylogenetic analyses however, tend to place this taxon within the clade comprising Potoroidae and Macropodidae (Prideaux & Warburton 2010; Butler *et al.* 2016, 2018). This suggests a disconnect between the phylogenetic position of the taxon and the implementation of a fossil age prior. Applying this minimum bound to the potoroid–macropodid split ultimately dramatically increases divergence date estimates across the macropodoid tree (**Fig.S1,S2**), pulling dates outside of reasonable estimates. Similarly, *Ganguroo* is typically used to provide an early-to-mid Miocene minimum (17.79) (Woodhead *et al.* 2016) on the Potoroidae–Macropodidae split (Cascini *et al.* 2018; Celik *et al.* 2019). This taxon alternately falls within the potoroid–macropodid crown, or the *Lagostrophus*–Macropodinae clade. Applying this minimum bound

to the *Lagostrophus*–Macropodinae split also tends to inflate divergence estimates. This highlights the difficulty in implementing fossil information from extinct taxa with ambiguous phylogenetic affinities (Near & Sanderson 2004).

One step in simplifying this process may be instead to remove node priors based on these ambiguous taxa, and instead estimate their phylogenetic position, divergence times, and fossil ages jointly. By implementing this process in dating analyses, I recovered divergence estimates that are broadly concordant with recent node-calibrated molecular based studies (Celik *et al.* 2019) and interpretations from the fossil record (Couzens & Prideaux 2018). These divergence estimates differ considerably from analyses implementing fixed fossil ages (as minimum, mean, or maximum stratigraphic bounds), including another tip-dating study (Cascini *et al.* 2018), and generally fall between estimates from mean and maximum fixed dates (**Fig.2**). This exercise suggests that signal in the morphological and molecular clocks can contribute to fossil age information, and is consistent with other recent study in this area suggesting that fixing tip ages should be avoided (Barido-Sottani *et al.* 2019). Though it is important to note that in divergence dating analyses focused on intraspecific sampling implementing a strict molecular clock, divergence estimates may not differ between fixed and prior-informed tip ages (Molak *et al.* 2013). This raises the question of if fixed and prior-informed tip ages may differently affect analyses using intraspecific versus interspecific sampling, and strict versus relaxed molecular clocks.

Interestingly, the decision to fix fossil tip dates or jointly estimate their age may also have an impact on the recovery of fossil taxa as terminals or sampled ancestors, as well as the overall tree topology. Fixed and estimated fossil tip age methods applied to these data differ in their assignment of some fossil taxa (**Fig.3**). I anticipate that the ability to accurately recover taxa as ancestors is likely correlated to the number and quality of sampled traits, though there is evidence that fossil occurrences and models of morphological evolution are certainly a concern (Goloboff *et al.* 2018; Luo *et al.* 2018). While our knowledge of the homology, rate, and process of molecular evolution is considerable, it has been much more difficult to adequately model morphological data. In contrast to molecular sites or loci, morphological characters are likely more often correlated (Billet & Bardin 2018), nonhomologous (Baum & Donoghue 2002), or evolving under dramatically different mechanisms (Goloboff *et al.* 2018),

and may disrupt our best efforts at reconstructing phylogeny, divergence times, and rates of evolution. This difficulty is exaggerated on deep time scales and highlights important caveats to consider in the application of combined– or total-evidence methods (Puttick *et al.* 2017; Luo *et al.* 2018).

The Evolution of Hypsodonty

Uncertainty in divergence dates and sampling may directly compound uncertainty in macroevolutionary inferences. In the case of kangaroos and their allies, the cause of increasing tooth crown height is most likely related to the emergence and expansion of C_4 vegetation. In both the focal trees and those including additional fossil taxa, I find greatest support for models in which the rate of tooth height evolution is positively correlated with Australian grassland reconstructions from the late Miocene–present (**Fig.5**). These rates are greatest from the Pleistocene–present, but exhibit a gradual increase from the late Miocene to Pliocene (**Fig.S6–S8**). Undersampling fossil macropodines does appear to affect model support, but does not change away from the C_4 model as preferred, instead increasing support for the paleotemperature model. In contrast, undersampling extant Macropodinae species shifts the preferred model class from the dietary model (C_4) to the exogenous grit model (FLUX). Frighteningly, this is exacerbated by excluding additional fossil taxa, and suggests that sampling biases may compound one another in contributing to error in evolutionary inferences.

It is important of course to note that correlative models are just that, correlative, and their inferences should be interpreted carefully. Because these models estimate the relationship between evolutionary rates and a time sampled variable, it is not surprising to see that model support varies with tree age (**Fig.5, S3–S5**). This *is* concerning however, given that divergence estimates of the Macropodinae and Macropodini have varied considerably among published studies, as well as among the tip dating fossil age schemes presented here (**Fig.2**). This should give us reason to pause and consider the relative influence of our divergence dating methods and results on the downstream macroevolutionary inferences we use them to obtain. Interestingly, while model support varies with age, in this case it does not appear to vary consistently with topology (**Fig.S5**).

In the case of kangaroos, the transition in preferred model of tooth height evolution as a result of varying crown age, highlights the difficulty in identifying processes driving macroevolution. In macropods, it is likely that an increase in molar tooth height is a direct result of increasing grazing activity, spurred by the expansion of Australian grasslands. It remains possible however, depending on the estimated age of kangaroos, that taller molar crowns are **also** the result of either greater abrasion from increasing atmospheric dust, or some undetermined correlate with paleotemperature. As the late Miocene marked a dramatic turn towards cooler temperatures and increasing aridity, airborne abrasives increased, and groundcover shrank as arid habitats expanded (Hill 2004; Martin 2006). Support for the dust flux and paleotemperature models in some cases may make it tempting to question the correlation between hypsodonty and grazing activity. There remains disagreement around whether the more herbivorous feeding ecologies (browsing, mixed feeding, grazing) can accurately be distinguished solely by dental proportions such as the Hypsodonty Index (HI) (Janis 1990; Couzens & Prideaux 2018) (**Fig.S9**), but there may be functional reasons for this. Bilophodont molars, such as those in macropodoid marsupials, are structurally limited in the extent of their hypsodonty by the cutting action of the teeth, and masticatory movements (Janis 1990). As bilophodont teeth wear down, they become less efficient, and so to address this, grazing macropods have added transverse cross links between the main lophs to increase integrity and relief (Sanson 1980). These limitations and adaptations may explain an upper ceiling on hypsodonty in kangaroos, and overlap in the trait measured here (HI) among macropod diet guilds. However, this does not entirely explain elevated macrowear scores and hypsodonty prior to the Plio–Pleistocene expansion of C_4 grasses. Perhaps more realistically, the evolution of high-crowned teeth is the result of some interaction among these forces (exogenous and endogenous dietary properties).

Overall, I infer that the diversification of modern kangaroos and their allies and the onset of increasing molar crown heights may have occurred earlier than an explosive Plio–Pleistocene model suggests. Rapid divergences among the Macropodini genera *Macropus*, *Notamacropus*, *Osphranter*, and *Wallabia* appear to precede the Pliocene, in which case the distribution of feeding ecologies suggest multiple independent transitions towards mixed feeding and grazing (**Fig.S9**). While this goes against parsimony, it suggests that the transition towards

increasing herbivory—including associated dental changes and foregut fermentation—early in the Macropodinae history truly paved the way for kangaroos to take advantage of the increasing aridity and grass cover (Dawson 2006).

Conclusion

Observational evolutionary studies, particularly those on deep time scales, will always be hampered by limited data. Dating the radiation of Macropodinae marsupials presents a particularly interesting challenge because of conflicting intrinsic (molecular, morphological) and extrinsic (environmental, habitat, diet) signals. In addition, resolving the relationships among kangaroo groups and species has been complicated by evidence of ancient and recent introgression (Potter *et al.* 2012; Phillips *et al.* 2013; Nilsson *et al.* 2018). While we work to find more accurate and more complete answers to these questions, we would be better served by recognizing current limitations and ambiguities, rather than ignoring them. In macroevolutionary studies, this means incorporating aspects of uncertainty that are a direct result of phylogenetic estimation, fossil and divergence dating, and intraspecific variation.

Supplemental Material

Additional files, including phylogenetic trees, fossil age data, and molecular and morphological alignments are available at https://github.com/IanGBrennan/FossilUncertainty

Table 1. Taxon sampling across molecular and morphological datasets.

Sampled Taxon	Molecular Data	Morphological Data	Stratigraphic Data
Aepyprymnus rufescens	Yes	No	Yes
Baringa nelsonensis	No	Yes	Yes
Bettongia lesueur	Yes	No	Yes
Bettongia penicillata	Yes	Yes	Yes
Bohra illuminata	No	Yes	Yes
Bulungamaya delicata	No	Yes	Yes
Congruus congruus	No	Yes	Yes
Dendrolagus dorianus	Yes	Yes	Yes
Dendrolagus goodfellowi	Yes	No	Yes
Dendrolagus lumholtzi	Yes	No	Yes
Dendrolagus matschiei	Yes	Yes	Yes
Dorcopsis hageni	Yes	No	Yes
Dorcopsis veterum	Yes	Yes	Yes
Dorcopsoides fossilis	No	Yes	Yes
Dorcopsulus vanheurni	Yes	Yes	Yes
Ganguroo bilamina	No	Yes	Yes
Hadronomas puckridgi	No	Yes	Yes
Hypsiprymnodon moschatus	Yes	Yes	Yes
Kurrabi mahoneyi	No	Yes	Yes
Lagorchestes conspicillatus	Yes	Yes	Yes
Lagorchestes hirsutus	Yes	Yes	Yes
Lagostrophus fasciatus	Yes	Yes	Yes
Macropus agilis	Yes	No	Yes
Macropus antilopinus	Yes	No	Yes
Macropus eugenii	Yes	Yes	Yes
Macropus fuliginosus	Yes	Yes	Yes
Macropus giganteus	Yes	No	Yes
Macropus irma	Yes	No	Yes
Macropus parma	Yes	No	Yes
Macropus parryi	Yes	No	Yes
Macropus pavana	No	Yes	Yes
Macropus robustus	Yes	Yes	Yes
Macropus rufogriseus	Yes	No	Yes
Macropus rufus	Yes	No	Yes
Ngamaroo archeri	No	Yes	Yes
Onychogalea fraenata	Yes	No	Yes
Onychogalea unguifera	Yes	Yes	Yes
Peradorcas concinna	Yes	No	Yes
Petrogale assimilis	Yes	No	Yes
Petrogale brachyotis	Yes	Yes	Yes
Petrogale burbidgei	Yes	No	Yes
Petrogale herberti	Yes	No	Yes
Petrogale inornata	Yes	No	Yes

Sampled Taxon	Molecular Data	Morphological Data	Stratigraphic Data
Petrogale lateralis	Yes	No	Yes
Petrogale penicillata	Yes	No	Yes
Petrogale persephone	Yes	No	Yes
Petrogale purpureicollis	Yes	No	Yes
Petrogale rothschildi	Yes	No	Yes
Petrogale xanthopus	Yes	No	Yes
Potorous gilbertii	Yes	No	Yes
Potorous longipes	Yes	No	Yes
Potorous tridactylus	Yes	Yes	Yes
Prionotemnus palankarinnicus	No	Yes	Yes
Procoptodon goliah	No	Yes	Yes
Protemnodon anak	No	Yes	Yes
Setonix brachyurus	Yes	Yes	Yes
Simosthenurus occidentalis	No	Yes	Yes
Sthenurus andersoni	No	Yes	Yes
Thylogale billardierii	Yes	Yes	Yes
Thylogale browni	Yes	No	Yes
Thylogale brunii	Yes	No	Yes
Thylogale stigmatica	Yes	No	Yes
Thylogale thetis	Yes	No	Yes
Troposodon minor	No	Yes	Yes
Wallabia bicolor	Yes	Yes	Yes
Wanburoo hilarus	No	Yes	Yes

Table 2. Taxon sampling across extinct species in trait datasets.

Fossil Taxon	Molecular Data	Morphological Data	Stratigraphic Data
Baringa sp indet	No	No	Yes
Bohra bandharr	No	No	Yes
Bohra nullarbora	No	No	Yes
Bohra sp indet	No	No	Yes
Bohra wilkinsonorum cf	No	No	Yes
Congruus indra	No	No	Yes
Congruus sp$_i$ndet	No	No	Yes
Dorcopsis luctosa	No	No	Yes
Dorcopsis muelleri	No	No	Yes
Dorcopsis sp indet	No	No	Yes
Kurrabi merriwaensis cf	No	No	Yes
Kurrabi merriwaensis	No	No	Yes
Kurrabi pelchenorum	No	No	Yes
Kurrabi sp indet	No	No	Yes
Lagorchestes cf sp indet	No	No	Yes
Macropus cf sp indet	No	No	Yes
Macropus dryas cf	No	No	Yes
Macropus dryas	No	No	Yes
Macropus ferragus cf	No	No	Yes
Macropus ferragus	No	No	Yes
Macropus pearsoni	No	No	Yes
Macropus sp indet	No	No	Yes
Macropus woodsi cf	No	No	Yes
Petrogale cf sp indet	No	No	Yes
Petrogale sp indet	No	No	Yes
*Petrogale sp nov*1	No	No	Yes
*Petrogale sp nov*2	No	No	Yes
Prionotemnus palankarinnicus cf	No	No	Yes
Protemnodon buloloensis	No	No	Yes
Protemnodon cf sp indet	No	No	Yes
Protemnodon devisi cf	No	No	Yes
Protemnodon snewini	No	No	Yes
Protemnodon sp indet	No	No	Yes
Thylogale billardierii cf	No	No	Yes
Thylogale ignis cf	No	No	Yes
Thylogale ignis	No	No	Yes
Thylogale sp indet	No	No	Yes
Wallabia sp indet	No	No	Yes

Table 3. Node prior information. All node calibrations were applied as lognormal priors.

Fossil Taxon	Minimum Age	Maximum Age C	lade
Thylogale ignis	4.36	14.22	Dendrolagini + Thylogale
Dendrolagus Mt. Etna	3.6	14.22	Dendrolagini
Macropus Hamilton Fauna	4.46	14.22	Macropodini
Ngamaroo archeri	15.97	30	Potoroidae + Macropodidae
Ganguroo bilamina	17.79	35	Lagostrophus + Macropodinae

Table 4. Molecular data partitioning scheme for StarBEAST2 analyses. "..." indicates a parameter partition linked with the above partition.

Locus	Site Model	Clock Model	Tree
12S	GTR+G	12S	mtDNA
16S	GTR+G	...	...
Cytb	GTR+G	...	...
APO8	HKY+G	APOB	APOB
IRBP	HKY+G	...	IRBP
Pro1	HKY+G	...	Pro1
RAG1	HKY+G	...	RAG1
TRSP	HKY+G	...	TRSP
vWF	HKY+G	...	vWF
BRCA1	HKY+G	...	BRCA1

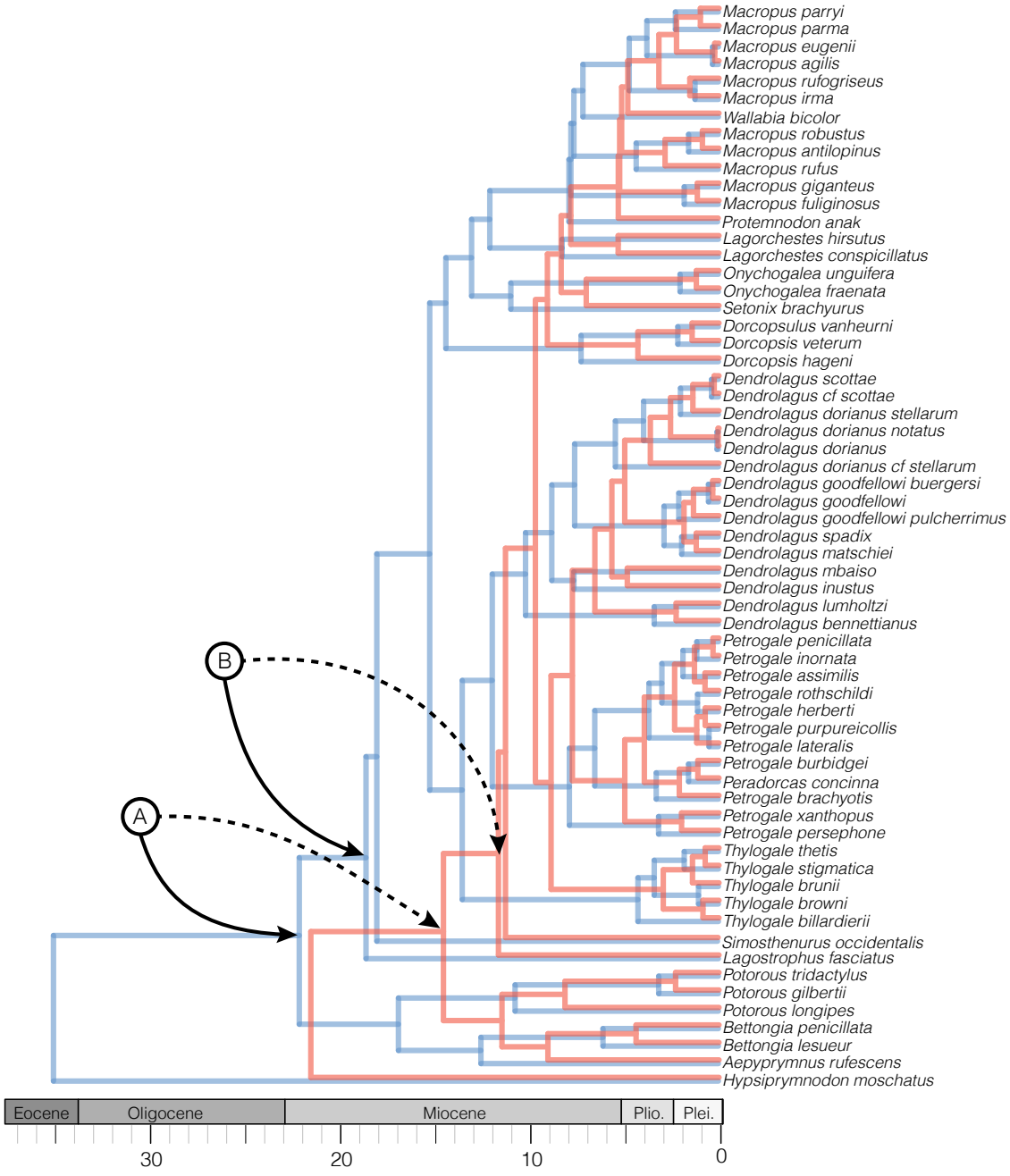

Figure S1: Macropodoid divergence estimates are strongly influenced by the inclusion of information from two fossil taxa. Incorporating these taxa as extinct tips, or as node calibration priors dramatically inflates divergence times across the tree. The two trees presented are the result of combined evidence analyses including molecular, morphological, and stratigraphic data. (A) denotes the position of fossil information of *Ngamaroo archeri* and (B) for *Ganguroo bilamina*. Solid arrows identify the placement of these nodes in the tree (blue) which includes these calibrations. Dashed arrows indicate the same nodes in the tree (orange) without these priors applied.

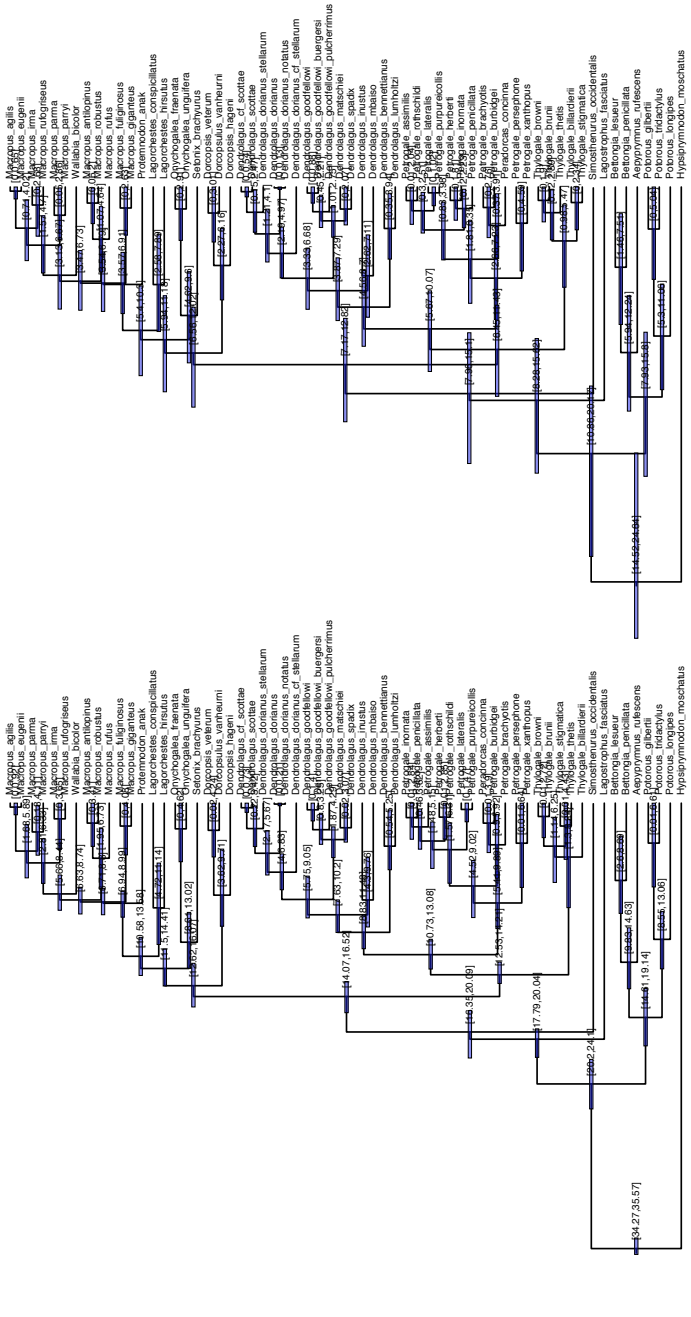

Figure S2: Macropodoid divergence estimates are strongly influenced by the inclusion of information from two fossil taxa, *Ngamaroo archeri* and *Ganguroo bilamina*. Incorporating these taxa as node calibration priors dramatically inflates divergence times across the tree. The two trees presented are the result of molecular tip dating analyses. The tree on the left includes five node calibrations (A–E), including those for *Ngamaroo* and *Ganguroo*. The tree on the right includes three node calibrations (A–C). Information on the application of fossil information as node priors is included in Table 2.

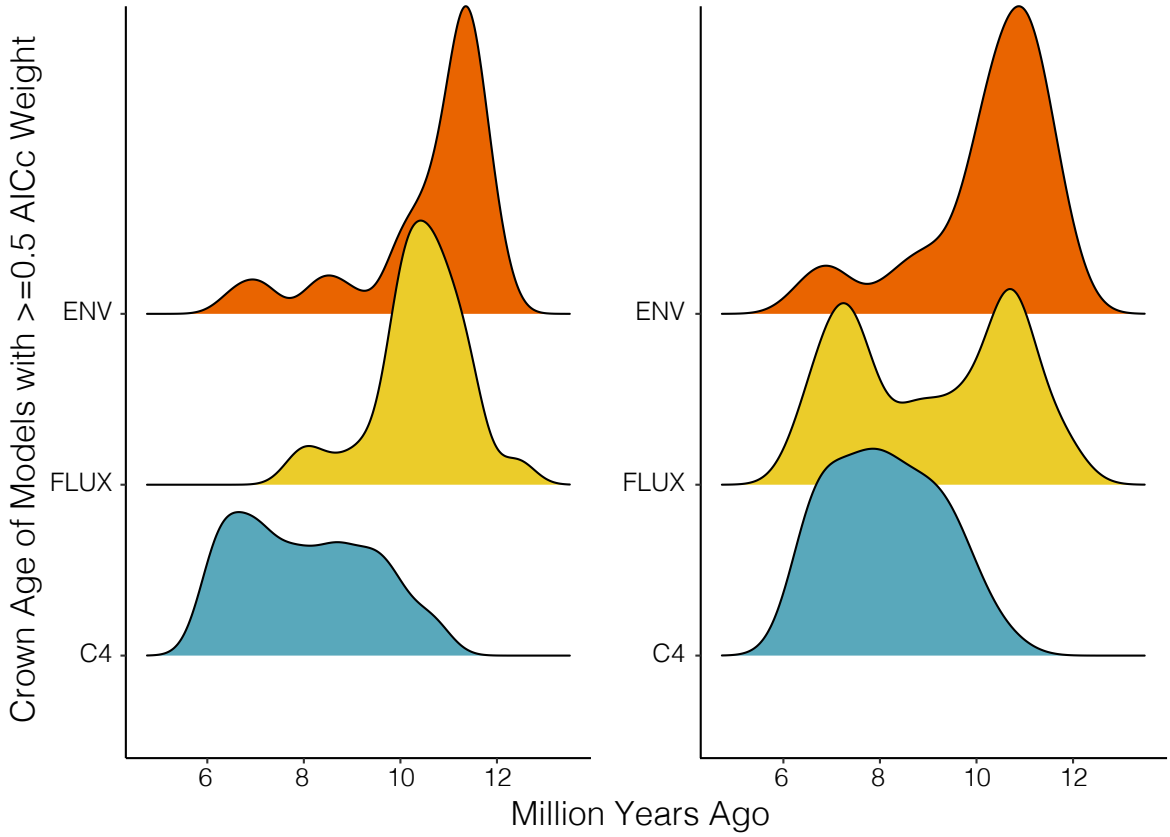

Figure S3: Model support is influenced by the age of the input tree. Results from focal trees (left) and fossil trees (right) indicate that model support varies as a function of tree age. Younger trees (6–10 Mya) provide show strong evidence for the C_4 model, and older trees (10–12 Mya) provide support for dust flux and environmental models.

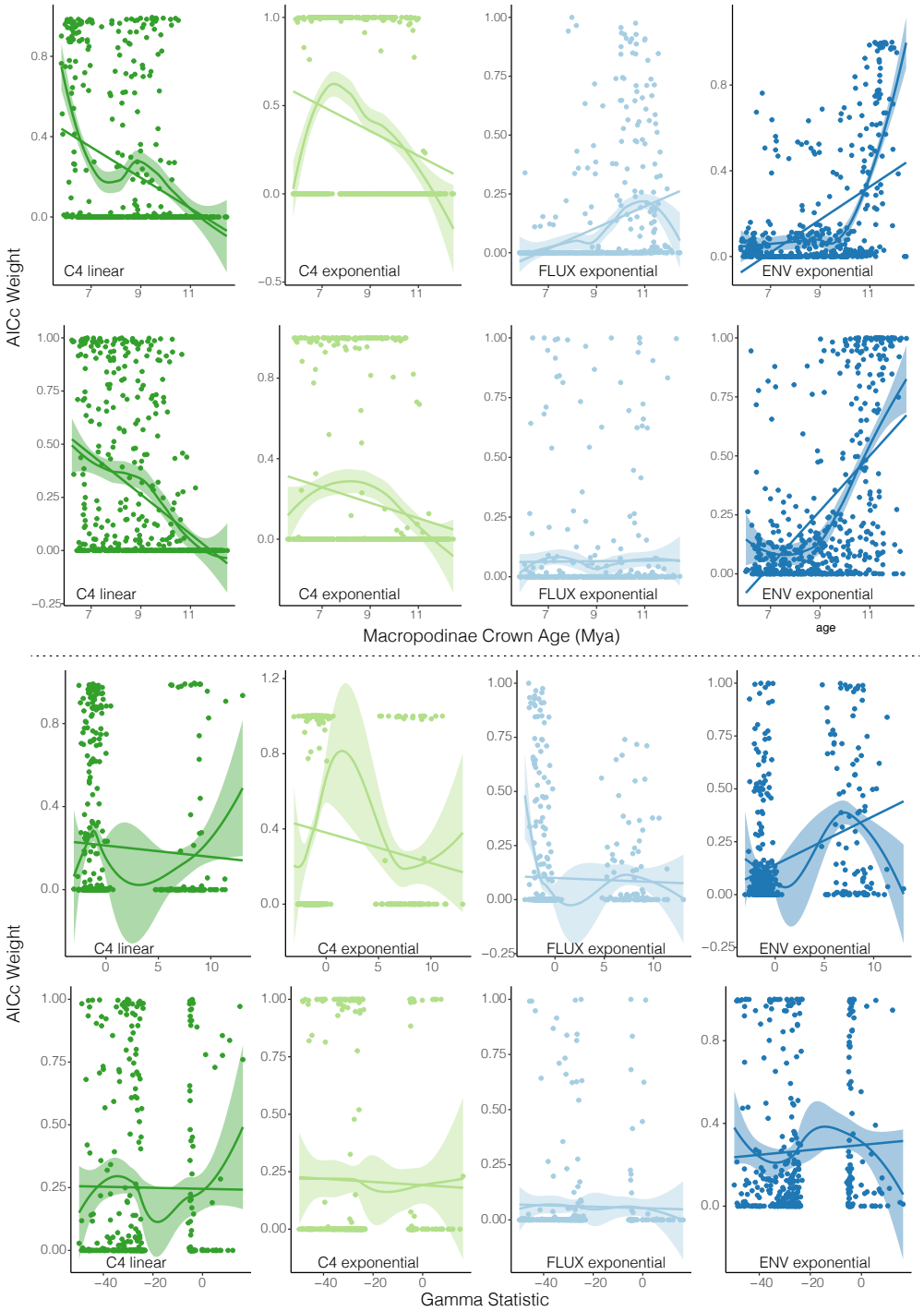

Figure S4: Model fit (AICc Weight) is influenced by the age of the input tree, and only moderately by the gamma statistic. Results from focal trees (top row) and fossil trees (bottom row) indicate that model support varies as a function of tree age. Support for the C_4 models (linear and exponential) decrease with increasing tree age, and the dust flux (FLUX) and paleotemperature (ENV) models (both exponential) increase with increasing tree age. Relationships are visualized as Loess smoothings (with confidence envelopes) and linear models.

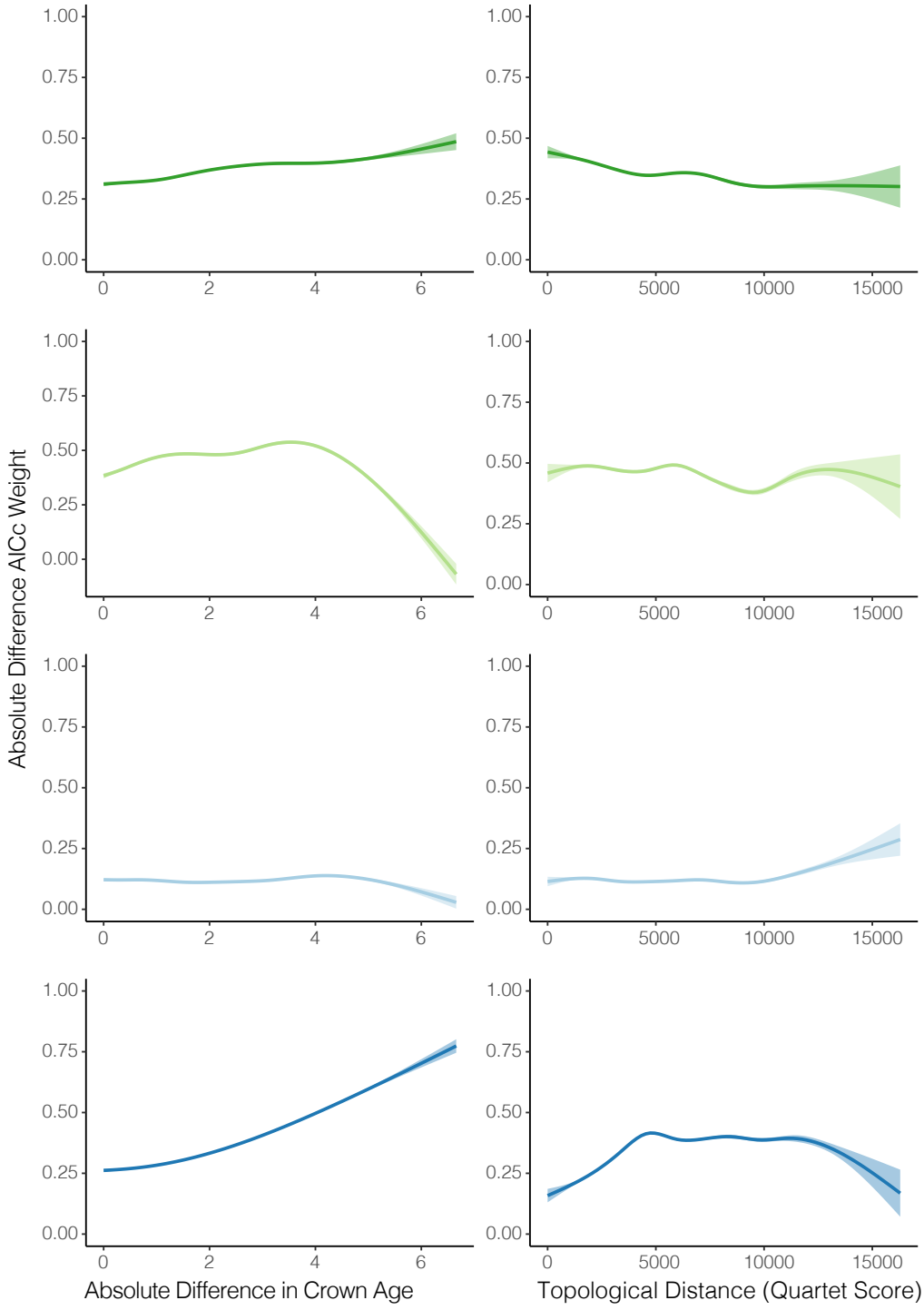

Figure S5: Model fit (AICc Weight) is influenced to a degree by differences in tree ages and topology. Plots represent all pairwise comparisons among focal trees, showing AICc Weight differences as a function of increasing age differences or topological distances. Toplogical differences among trees (right column) alone can not explain preference for a given model.

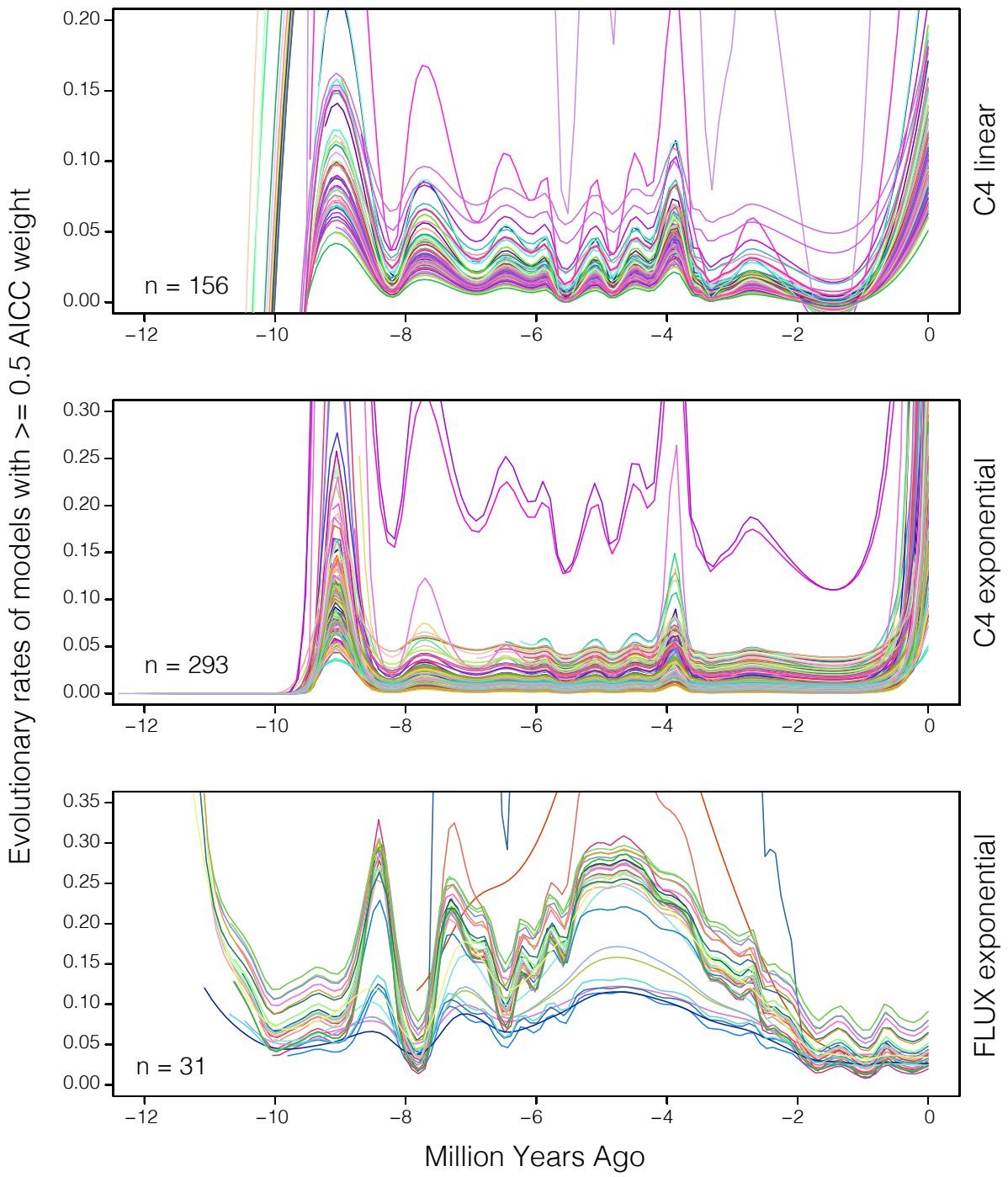

Figure S6: Rates of tooth height evolution estimated under different macroevolutionary models on the focal trees (taxa sampled for molecular or morphological data; n=49). Each line represents the evolutionary rate estimated from a model with >= 0.5 AICC weight for a given tree. The macroevolutionary model is listed to the right of the plot, and the number of lines and hence the number of times the model was the preferred model (AICC weight >= 0.5) is noted in the bottom left of each plot.

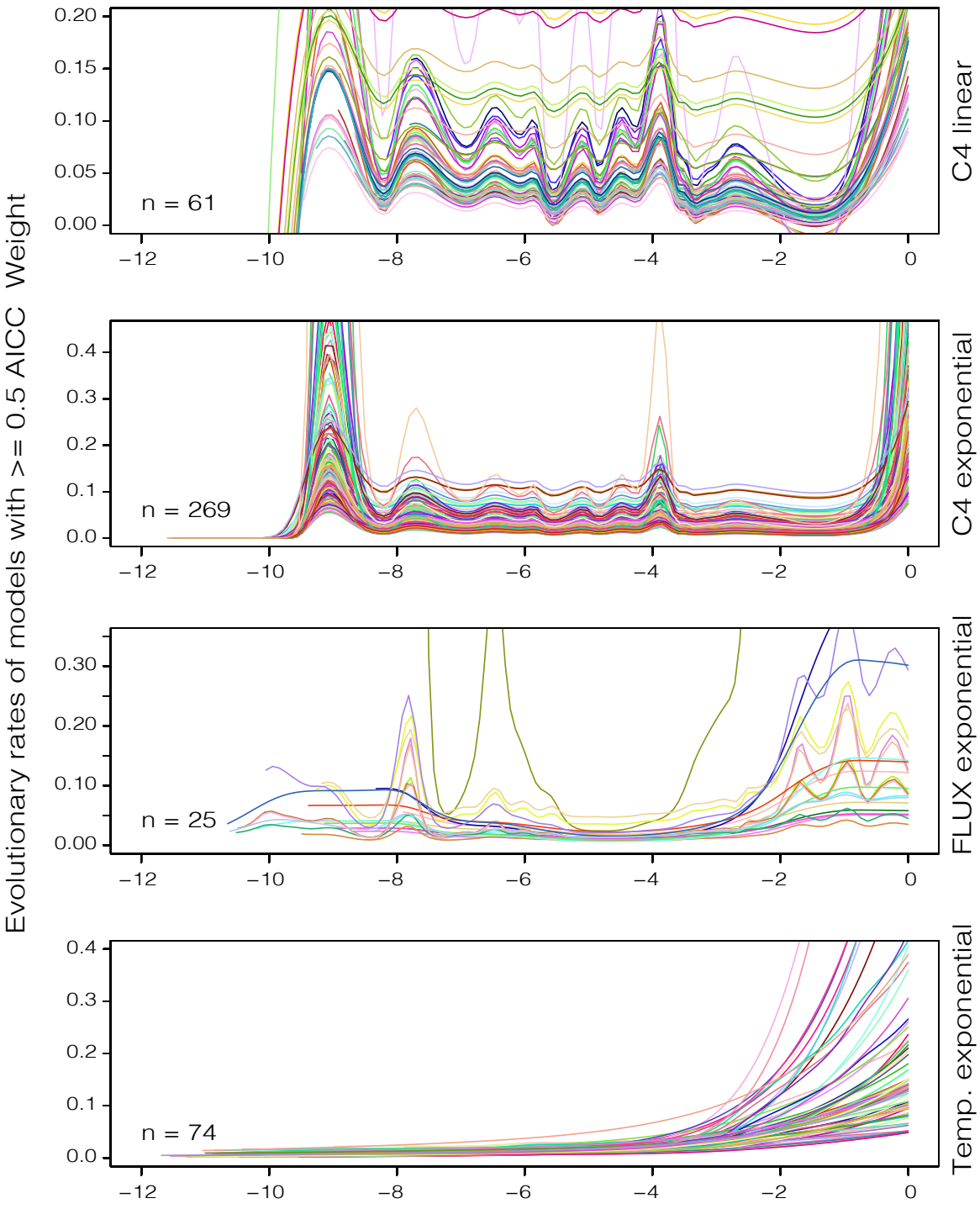

Figure S7: Rates of tooth height evolution estimated under different macroevolutionary models on the fossil trees (taxa sampled for molecular, morphological, or stratigraphic data; n=84). Each line represents the evolutionary rate estimated from a model with >= 0.5 AICC weight for a given tree. The macroevolutionary model is listed to the right of the plot, and the number of lines and hence the number of times the model was the preferred model (AICC weight >= 0.5) is noted in the bottom left of each plot.

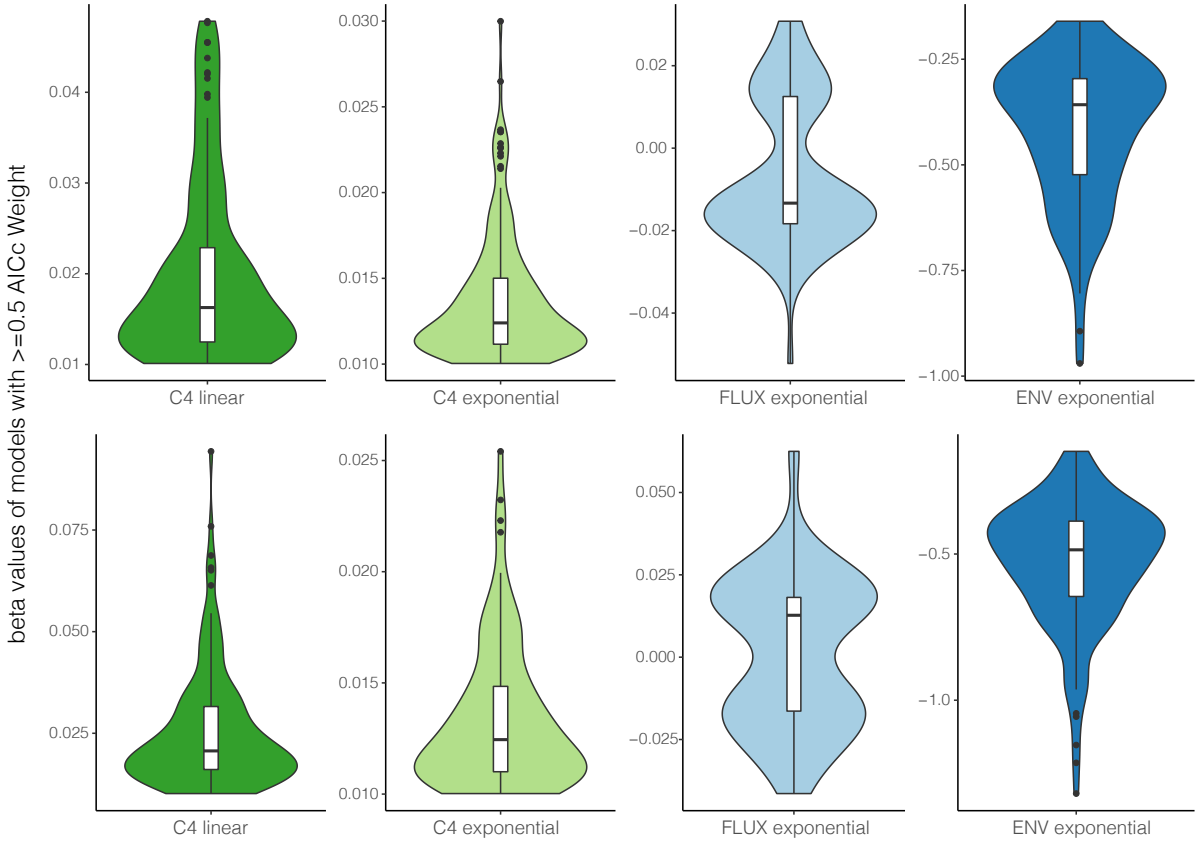

Figure S8: β (beta) parameter estimates from focal trees (top row) and fossil trees (bottom row), these correspond to results in the top two rows of Fig.5. β values indicate the strength and direction of the relationship between the rate of trait evolution and the time sampled variable. Positive values indicate a positive relationship, negative values indicate a negative relationship, and greater absolute values of *beta* indicate stronger relationships. The bimodal distribution of β values in the FLUX model corresponds roughly to the age of the input tree, with postive *beta* associated with trees of crown age 8–10 Mya, and negative *beta* associated with trees of crown age 10–11 Mya.

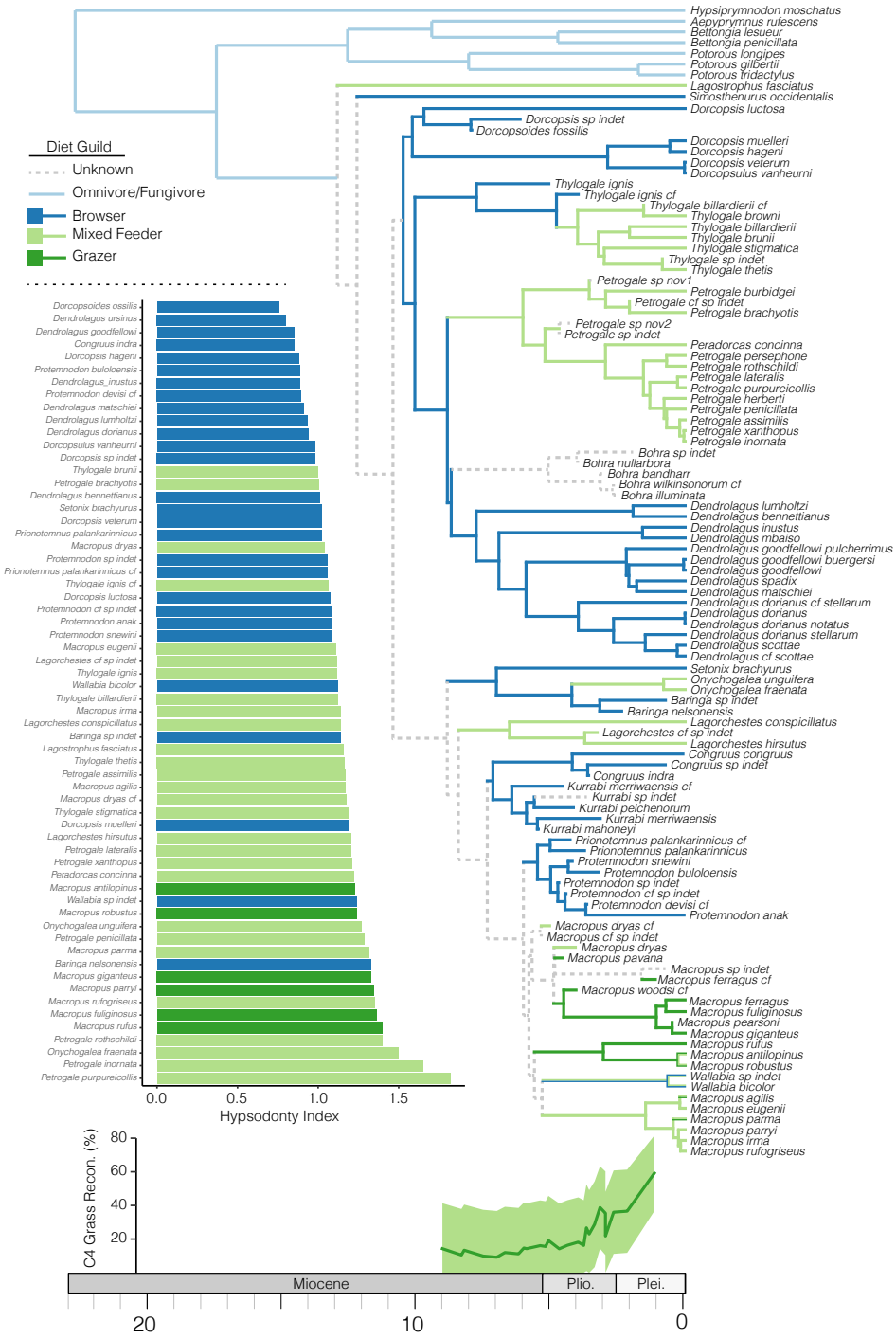

Figure S9: The distribution of grazing and mixed feeding ecologies is not consistent with a single transition coincident with the expansion of Plio–Pleistocene grasslands. (A) This representation of the distribution of feeding ecologies across living and extinct macropodoids presents only a single SIMMAP reconstruction of diet as a discrete character. Mapping the characters in this fashion highlights potentially multiple transitions to grazing or mixed feeding among macropodoids, and considerable lability in this trait in the macropodines. (B) Comparing Hypsodonty Index scores color coded by feeding ecology shows the difficulty in determining diet guild based solely on tooth proportions.

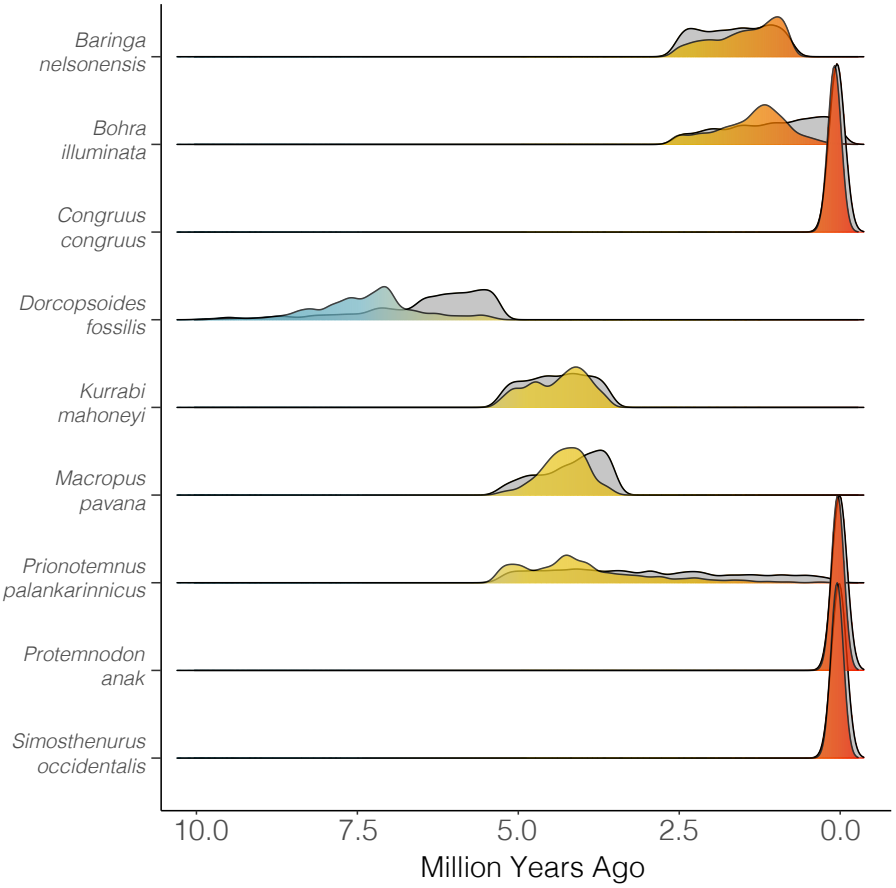

Figure S10: Estimating fossil taxa ages jointly with the phylogeny and divergence times results in age estimates which do not simply return the uniform priors applied. Most distributions of fossil ages appear roughly normal, and fall within and not at the prior bounds.

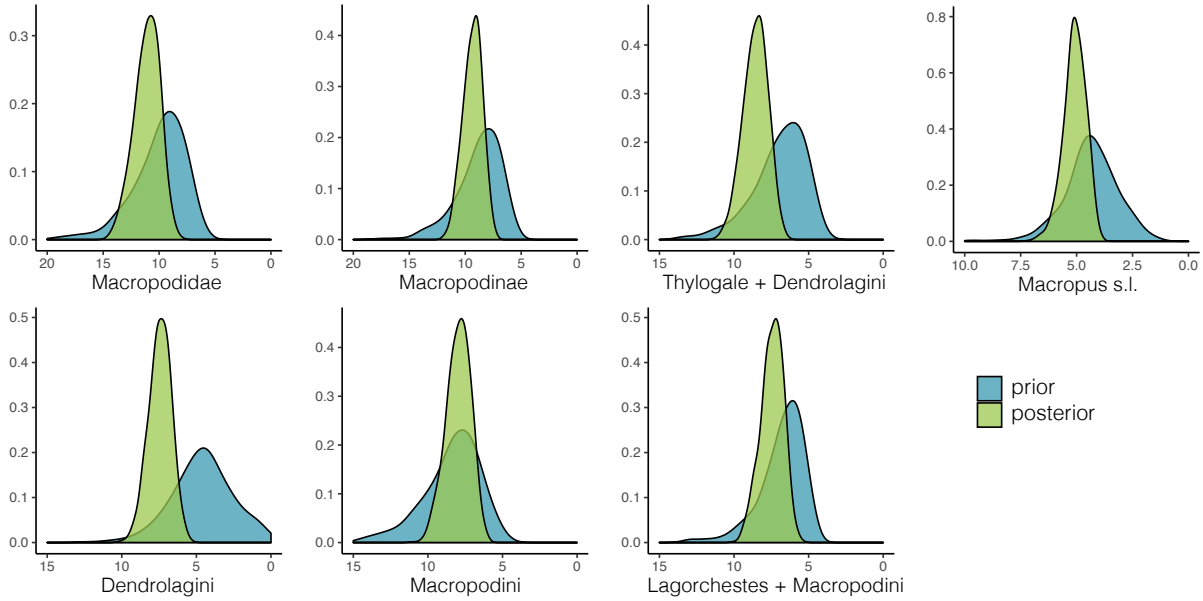

Figure S11: Divergence dates estimated from fossils with tip age priors are broadly overlapping with those of mean and maximum fixed ages, often fall between estimates from those dating schemes, and do not solely return prior values.

References

Andrae, J.W., McInerney, F.A., Polissar, P.J., Sniderman, J.M.K., Howard, S. & Hall, P.A. *et al.* (2018). Initial expansion of C4 vegetation in Australia during the Late Pliocene. *Geophysical Research Letters*, 45, 4831–4840.

Badgley, C., Barry, J.C., Morgan, M.E., Nelson, S.V., Behrensmeyer, A.K. & Cerling, T.E. *et al.* (2008). Ecological changes in Miocene mammalian record show impact of prolonged climatic forcing. *Proceedings of the National Academy of Sciences*, 105, 12145–12149.

Barido-Sottani, J., Aguirre-Fernandez, G., Hopkins, M.J., Stadler, T. & Warnock, R. (2019). Ignoring stratigraphic age uncertainty leads to erroneous estimates of species divergence times under the fossilized birth-death process. *Proc Biol Sci*, 286, 20190685.

Baum, D.A. & Donoghue, M.J. (2002). Transference of function, heterotopy and the evolution of plant development. *SYSTEMATICS ASSOCIATION SPECIAL VOLUME*, 65, 52–69.

Beck, R.M. & Lee, M.S. (2014). Ancient dates or accelerated rates? Morphological clocks and the antiquity of placental mammals. *Proc Biol Sci*, 281.

Billet, G. & Bardin, J. (2018). Serial Homology and Correlated Characters in Morphological Phylogenetics: Modeling the Evolution of Dental Crests in Placentals. *Systematic Biology*, 68, 267–280.

Bouckaert, R., Vaughan, T.G., Barido-Sottani, J., Duchene, S., Fourment, M. & Gavryushkina, A. *et al.* (2018). BEAST 2.5: An advanced software platform for bayesian evolutionary analysis. *bioRxiv*.

Brennan, I.G. & Keogh, J.S. (2018). Miocene biome turnover drove conservative body size evolution across australian vertebrates. *Proceedings of the Royal Society B: Biological Sciences*, 285.

Brodal, G.S., Fagerberg, R., Mailund, T., Pedersen, C.N.S. & Sand, A. (2013). Efficient algorithms for computing the triplet and quartet distance between trees of arbitrary degree. SODA '13, 1814–1832.

Butler, K., Louys, J. & Travouillon, K. (2014). Extending dental mesowear analyses to australian marsupials, with applications to six plio-pleistocene kangaroos from southeast queensland. *Palaeogeography, Palaeoclimatology, Palaeoecology*, 408, 11–25.

Butler, K., Travouillon, K.J., Price, G.J., Archer, M. & Hand, S.J. (2016). Cookeroo, a new genus of fossil kangaroo (marsupialia, macropodidae) from the oligo-miocene of riversleigh, northwestern queensland, australia. *Journal of Vertebrate Paleontology*, 36.

Butler, K., Travouillon, K., Price, G., Archer, M. & Hand, S. (2018). Revision of oligo-miocene kangaroos, ganawamaya and nambaroo (marsupialia: Macropodiformes, balbaridae). *Palaeontologia Electronica*, 1–58.

Byrne, M., Yeates, D.K., Joseph, L., Kearney, M., Bowler, J. & Williams, M.A.J. *et al.* (2008). Birth of a biome: Insights into the assembly and maintenance of the Australian arid zone biota. *Molecular Ecology*, 17, 4398–4417.

Cascini, M., Mitchell, K.J., Cooper, A. & Phillips, M.J. (2018). Reconstructing the evolution of giant extinct kangaroos: Comparing the utility of dna, morphology, and total evidence. *Syst Biol*.

Celik, M., Cascini, M., Haouchar, D., Van Der Burg, C., Dodt, W. & Evans, A.R. *et al.* (2019). A molecular and morphometric assessment of the systematics of the macropus complex clarifies the tempo and mode of kangaroo evolution. *Zoological Journal of the Linnean Society*, 186, 793–812.

Couzens, A.M.C. & Prideaux, G.J. (2018). Rapid Pliocene adaptive radiation of modern kangaroos. *Science*, 362, 72–75.

Dawson, L. (2006). An ecophysiological approach to the extinction of large marsupial herbivores in middle and late pleistocene australia. *Alcheringa: An Australasian Journal of Palaeontology*, 30, 89–114.

Dawson, L. & Flannery, T. (1985). Taxonomic and phylogenetic status of living and fossil kangaroos and wallabies of the genus macropus shaw (macropodidae: Marsupialia), with a new subgeneric name for the larger wallabies. *Australian Journal of Zoology*, 33, 473–498.

Dodt, W.G., Gallus, S., Phillips, M.J. & Nilsson, M.A. (2017). Resolving kangaroo phylogeny and overcoming retrotransposon ascertainment bias. *Sci Rep*, 7, 16811.

Dos Reis, M., Gunnell, G.F., Barba-Montoya, J., Wilkins, A., Yang, Z. & Yoder, A.D. (2018). Using phylogenomic data to explore the effects of relaxed clocks and calibration strategies on divergence time estimation: Primates as a test case. *Syst Biol*, 67, 594–615.

Eldridge, M.D.B., Potter, S., Helgen, K.M., Sinaga, M.H., Aplin, K.P. & Flannery, T.F. *et al.* (2018). Phylogenetic analysis of the tree-kangaroos (dendrolagus) reveals multiple divergent lineages within new guinea. *Mol Phylogenet Evol*, 127, 589–599.

Estabrook, G.F., McMorris, F.R. & Meacham, C.A. (1985). Comparison of undirected phylogenetic trees based on subtrees of four evolutionary units. *Systematic Biology*, 34, 193–200.

Ezard, T.H.G., Aze, T., Pearson, P.N. & Purvis, A. (2011). Interplay between changing climate and species' ecology drives macroevolutionary dynamics. *Science*, 332, 349–351.

Felsenstein, J. (1985). Phylogenies and the comparative method. *The American Naturalist*, 125, 1–15.

Gavryushkina, A., Heath, T.A., Ksepka, D.T., Stadler, T., Welch, D. & Drummond, A.J. (2017). Bayesian total-evidence dating reveals the recent crown radiation of penguins. *Syst Biol*, 66, 57–73.

Gavryushkina, A., Welch, D., Stadler, T. & Drummond, A.J. (2014). Bayesian inference of sampled ancestor trees for epidemiology and fossil calibration. *PLOS Computational Biology*, 10, e1003919.

Goloboff, P.A., Pittman, M., Pol, D. & Xu, X. (2018). Morphological Data Sets Fit a Common Mechanism Much More Poorly than DNA Sequences and Call Into Question the Mkv Model. *Systematic Biology*, 68, 494–504.

Heath, T.A., Huelsenbeck, J.P. & Stadler, T. (2014). The fossilized birth–death process for coherent calibration of divergence-time estimates. *Proceedings of the National Academy of Sciences*, 111, E2957–E2966.

Heath, T.A., Zwickl, D.J., Kim, J. & Hillis, D.M. (2008). Taxon Sampling Affects Inferences of Macroevolutionary Processes from Phylogenetic Trees. *Systematic Biology*, 57, 160–166.

Hill, R.S. (2004). Origins of the southeastern australian vegetation. *Philosophical Transactions of the Royal Society B: Biological Sciences*, 359, 1537–1549.

Ho, S.Y.W. & Phillips, M.J. (2009). Accounting for calibration uncertainty in phylogenetic estimation of evolutionary divergence times. *Systematic Biology*, 58, 367–380.

Hummel, J., Findeisen, E., Sudekum, K.H., Ruf, I., Kaiser, T.M. & Bucher, M. *et al.* (2011). Another one bites the dust: Faecal silica levels in large herbivores correlate with high-crowned teeth. *Proc Biol Sci*, 278, 1742–7.

Janis, C. (1990). Why kangaroos (marsupialia: Macropodidae) are not as hypsodont as ungulates (eutheria). *Australian Mammalogy*, 13, 49–53.

Janis, C.M., Damuth, J., Travouillon, K.J., Figueirido, B., Hand, S.J. & Archer, M. (2016). Palaeoecology of oligo-miocene macropodoids determined by craniodental and calcaneal data. *Memoirs of Museum Victoria*, 74, 209–232.

Jardine, P.E., Janis, C.M., Sahney, S. & Benton, M.J. (2012). Grit not grass: Concordant patterns of early origin of hypsodonty in great plains ungulates and glires. *Palaeogeography, Palaeoclimatology, Palaeoecology*, 365-366, 1–10.

Kear, B.P. & Pledge, N.S. (2008). A new fossil kangaroo from the oligocene-miocene etadunna formation of ngama quarry, lake palankarinna, south australia. *Australian Journal of Zoology*, 55, 331–339.

Kürschner, W.M., Kvaček, Z. & Dilcher, D.L. (2008). The impact of Miocene atmospheric carbon dioxide fluctuations on climate and the evolution of terrestrial ecosystems. *Proceedings of the National Academy of Sciences*, 105, 449–453.

Lanfear, R., Calcott, B., Ho, S.Y.W. & Guindon, S. (2012). PartitionFinder: Combined selection of partitioning schemes and substitution models for phylogenetic analyses. *Molecular Biology and Evolution*, 29, 1695–1701.

Lee, M.S.Y., Oliver, P.M. & Hutchinson, M.N. (2009). Phylogenetic uncertainty and molecular clock calibrations: A case study of legless lizards (pygopodidae, gekkota). *Molecular Phylogenetics and Evolution*, 50, 661–666.

Lewis, P.O. (2001). A likelihood approach to estimating phylogeny from discrete morphological character data. *Systematic Biology*, 50, 913–925.

Luo, A., Duchêne, D.A., Zhang, C., Zhu, C.-D. & Ho, S.Y. (2018). A simulation-based evaluation of total-evidence dating under the fossilized birth-death process. *bioRxiv*.

Martin, H.A. (2006). Cenozoic climatic change and the development of the arid vegetation in australia. *Journal of Arid Environments*, 66, 533–563.

Meredith, R.W., Westerman, M. & Springer, M.S. (2008). A phylogeny and timescale for the living genera of kangaroos and kin (macropodiformes: Marsupialia) based on nuclear dna sequences. *Australian Journal of Zoology*, 2008, 395–410.

Mitchell, K.J., Pratt, R.C., Watson, L.N., Gibb, G.C., Llamas, B. & Kasper, M. *et al.* (2014). Molecular phylogeny, biogeography, and habitat preference evolution of marsupials. *Molecular Biology and Evolution*, 31, 2322–30.

Molak, M., Lorenzen, E.D., Shapiro, B. & Ho, S.Y. (2013). Phylogenetic estimation of timescales using ancient dna: The effects of temporal sampling scheme and uncertainty in sample ages. *Mol Biol Evol*, 30, 253–62.

Morlon, H., Lewitus, E., Condamine, F.L., Manceau, M., Clavel, J. & Drury, J. (2016). RPANDA: An r package for macroevolutionary analyses on phylogenetic trees. *Methods in Ecology and Evolution*, 7, 589–597.

Near, T.J. & Sanderson, M.J. (2004). Assessing the quality of molecular divergence time estimates by fossil calibrations and fossil-based model selection. *Philosophical Transactions of the Royal Society B: Biological Sciences*, 359, 1477–1483.

Nilsson, M.A., Zheng, Y., Kumar, V., Phillips, M.J. & Janke, A. (2018). Speciation generates mosaic genomes in kangaroos. *Genome Biol Evol*, 10, 33–44.

Ogilvie, H.A., Vaughan, T.G., Matzke, N.J., Slater, G.J., Stadler, T. & Welch, D. *et al.*

(2018). Inferring species trees using integrative models of species evolution. *bioRxiv*.

O'Reilly, J.E. & Donoghue, P.C. (2016). Tips and nodes are complementary not competing approaches to the calibration of molecular clocks. *Biol Lett*, 12.

Pennell, M.W., Slater, G.J., Eastman, J.M., Uyeda, J.C., Brown, J.W. & Harmon, L.J. *et al.* (2014). Geiger v2.0: An expanded suite of methods for fitting macroevolutionary models to phylogenetic trees. *Bioinformatics*, 30, 2216–2218.

Phillips, M.J., Haouchar, D., Pratt, R.C., Gibb, G.C. & Bunce, M. (2013). Inferring kangaroo phylogeny from incongruent nuclear and mitochondrial genes. *PLoS One*, 8, e57745.

Potter, S., Cooper, S.J.B., Metcalfe, C.J., Taggart, D.A. & Eldridge, M.D.B. (2012). Phylogenetic relationships of rock-wallabies, petrogale (marsupialia: Macropodidae) and their biogeographic history within australia. *Molecular Phylogenetics and Evolution*, 62, 640–652.

Prideaux, G.J. & Warburton, N.M. (2010). An osteology-based appraisal of the phylogeny and evolution of kangaroos and wallabies (macropodidae: Marsupialia). *Zoological Journal of the Linnean Society*, 159, 954–987.

Puttick, M.N., O'Reilly, J.E., Tanner, A.R., Fleming, J.F., Clark, J. & Holloway, L. *et al.* (2017). Uncertain-tree: Discriminating among competing approaches to the phylogenetic analysis of phenotype data. *Proc Biol Sci*, 284.

Pyron, R.A. (2011). Divergence time estimation using fossils as terminal taxa and the origins of lissamphibia. *Systematic Biology*, 60, 466–481.

Rambaut, A., Drummond, A.J., Xie, D., Baele, G. & Suchard, M.A. (2018). Posterior summarization in bayesian phylogenetics using tracer 1.7. *Systematic Biology*, 67, 901–904.

Renner, S.S., Grimm, G.W., Kapli, P. & Denk, T. (2016). Species relationships and divergence times in beeches: New insights from the inclusion of 53 young and old fossils in a birth-death clock model. *Philos Trans R Soc Lond B Biol Sci*, 371.

Ronquist, F., Klopfstein, S., Vilhelmsen, L., Schulmeister, S., Murray, D.L. & Rasnitsyn, A.P. (2012). A total-evidence approach to dating with fossils, applied to the early radiation of the hymenoptera. *Systematic Biology*, 61, 973–999.

Sand, A., Holt, M.K., Johansen, J., Brodal, G.S., Mailund, T. & Pedersen, C.N.S. (2014). TqDist: A library for computing the quartet and triplet distances between binary or general trees. *Bioinformatics*, 30, 2079–2080.

Sanson, G. (1980). The morphology and occlusion of the molariform cheek teeth in some macropodinae (marsupialia : Macropodidae). *Australian Journal of Zoology*, 28, 341–365.

Semprebon, G.M., Rivals, F. & Janis, C.M. (2019). The role of grass vs. Exogenous abrasives in the paleodietary patterns of north american ungulates. *Frontiers in Ecology and Evolution*, 7.

Silvestro, D., Kostikova, A., Litsios, G., Pearman, P.B., Salamin, N. & Münkemüller, T. (2015). Measurement errors should always be incorporated in phylogenetic comparative analysis. *Methods in Ecology and Evolution*, 6, 340–346.

Smith, M.R. (2019). Quartet: Comparison of phylogenetic trees using quartet and bipartition measures.

Stadler, T., Gavryushkina, A., Warnock, R.C.M., Drummond, A.J. & Heath, T.A. (2018). The fossilized birth-death model for the analysis of stratigraphic range data under different speciation modes. *J Theor Biol*, 447, 41–55.

Strömberg, C.A., Dunn, R.E., Madden, R.H., Kohn, M.J. & Carlini, A.A. (2013). Decoupling the spread of grasslands from the evolution of grazer-type herbivores in south america. *Nat Commun*, 4, 1478.

Title, P.O. & Rabosky, D.L. (2016). Do macrophylogenies yield stable macroevolutionary inferences? An example from squamate reptiles. *Systematic Biology*.

Williams, S.H. & Kay, R.F. (2001). A comparative test of adaptive explanations for hypsodonty in ungulates and rodents. *Journal of Mammalian Evolution*, 8, 207–229.

Woodhead, J., Hand, S.J., Archer, M., Graham, I., Sniderman, K. & Arena, D.A. *et al.* (2016). Developing a radiometrically-dated chronologic sequence for neogene biotic change in australia, from the riversleigh world heritage area of queensland. *Gondwana Research*, 29, 153–167.

Zachos, J., Pagani, M., Sloan, L., Thomas, E. & Billups, K. (2001). Trends, rhythms, and aberrations in global climate 65 ma to present. *Science*, 292, 686–693.

Chapter 4:

Phylogenomics of monitor lizards and the role of competition in dictating body size disparity

Phylogenomics of monitor lizards and the role of competition in dictating body size disparity

Ian G. Brennan[*1], *Emily Moriarty Lemmon* [2], *Alan Lemmon* [2], *Luke Welton* [3], *Daniel M. Portik* [4], *Valter Weijola* [5], *J.Scott Keogh* [1], *Stephen Donnellan* [3,4]

[1]*Division of Ecology & Evolution, Research School of Biology, Australian National University, Canberra, ACT 2601 Australia*

[2]*Department of Biological Science, Florida State University, Tallahassee, FL 32306, USA*

[3]*Univeristy of Kansas Biodiversity Institute & Natural History Museum, 1345 Jayhawk Blvd, Lawrence, KS 66045 USA*

[4]*Department of Ecology and Evolution, University of Arizona, Biosciences West Rm 310, 1041 E. Lowell St, Tucson, AZ 85745 USA*

[5]*Biodiversity Unit, University of Turku, Turku, Finland*

[6]*School of Biological Sciences, The University of Adelaide, Adelaide, SA 5005, Australia*

[7]*South Australian Museum, North Terrace, Adelaide SA 5000 Australia*

Abstract

Monitor lizards (*Varanus*) are an exceptional radiation of squamate reptiles which range from Africa, through the middle East and Indian subcontinent, and across Southeast Asia into AustraloPapua. Among living vertebrates, monitors exhibit the greatest size disparity within a single genus, varying in orders of magnitude between the colossal Komodo Dragon *Varanus komodoensis* and the smallest Australian dwarf goannas. While it is easy to appreciate this variety, little research has attempted to explain it. Here we test the hypothesis that size variation among Australian *Varanus* has been driven by character displacement among sympatric monitor species. We use a phylogenomic approach to first estimate the relationships among living and extinct varaniforme lizards, incorporating both

*Corresponding author: iangbrennan@gmail.com

exon-capture molecular and morphological datasets. Biogeographic and dating analyses suggest that monitor lizards originated in late Cretaceous or early Paleocene Eurasia, and dispersed into Africa, Southeast Asia, and Australia—where they reached their greatest diversity. We extend existing phylogenetic comparative methods which consider lineage interactions to account for dynamic biogeographic history, and apply these methods to Australian monitors and marsupial predators. Our results suggest that communities of Australian *Varanus* show high functional diversity as a result of continent-wide interspecific competition with other monitors. This study highlights the amazing diversity of *Varanus* lizards, and demonstrates the value of incorporating biogeography and lineage interactions into comparative models of trait evolution.

Keywords: comparative methods, phylogenetics, *Varanus*, trait evolution.

Organismal interactions provide an important selective force for evolution (Darwin 1859). On macroevolutionary time scales, interspecific interactions help drive the accumulation and distribution of diversity (Benton 1987). Perhaps the most commonly invoked type of interaction—competition—has frequently been used to explain the distribution of species, and how communities assemble (Sepkoski Jr 1996). Because ecological communities are built on diversity, competition should therefore also drive ecomorphological differentiation through **character displacement** (Brown and Wilson 1956). This claim has been repeatedly used in the case of insular adaptive radiations like Darwin's finches, Caribbean anoles, and Lake Victoria cichlids, where young clades have rapidly diverged into many available phenotypes (Schluter et al. 1985; Losos 1990; Grant and Grant 2006). While insular systems account for only a fraction of the earth's biodiversity, it has been much more difficult to quantify the influence of competition on continental scales (Drury et al. 2018b). Where it *has* been tested, biogeography has been incorporated at a discrete scale, but this fails to take into account that species ranges may be a temporally dynamic patchwork (of allopatry and sympatry) across the landscape (Drury et al. 2016, 2018b). We therefore know little about how competition between organisms may influence the (broad patterns in the) evolution of traits and distribution of species on continental scales.

Perhaps the most obvious axis for differentiation between organisms is absolute size (Peters and Peters 1986). In animals, body size is often used as a proxy for guild, and because it dramatically affects life-history traits and ecology, it is the most commonly used measurement in macroevolutionary studies (Wilson 1975). Among vertebrates, monitor lizards *Varanus* exhibit the greatest variation in body size within a single genus (Pianka 1995). Extant monitors include island giants like the Komodo dragon *V.komodoensis* (up to 3 m long and 100 kg), and desert dwarves like the short-tailed goanna *V.brevicauda* (0.2 m and 0.016 kg), which vary by orders of magnitude. Though there are roughly 80 described monitors, the greatest morphological diversity is concentrated in the 30 or so Australian species. Nearly all Australian monitors are hypothesized to constitute a single radiation that likely dispersed from Sundaland into Sahul, though the timing and biogeographic history of this group remains uncertain. Such considerable diversity in body size and forms begs the question, what has driven it?

Over the years, researchers have suggested that this disparity is the result of habitat partitioning (Collar et al. 2011), or release from competition with carnivoran mammals (Pianka 1995; Sweet and Pianka 2007). However, no one has yet investigated whether variation in monitor body sizes is instead the result of character displacement through competition, either with other *Varanus* or

mammalian carnivores. This is likely due to the fact that probabilistic trait evolutionary models largely remain ignorant of such interactions, even those these type of interactions are ubiquitous. Only recently have methods for modelling continuous traits attempted to take into account the influence of lineages on one another (Drury et al. 2016; Manceau et al. 2017; Adams and Nason 2018).

In order to address these macroevolutionary questions on the origins and diversity of varanid lizards, it is absolutely essential to first construct a reliable time-scaled phylogeny. Relationships among *Varanus* have been reconstructed historically through a number of morphological and molecular methods, but subgeneric relationships have been notoriously inconsistent (Conrad et al. 2012; Lin and Wiens 2017). We generated a nuclear exon capture dataset and combine it with existing morphological data to build a comprehensive phylogenetic hypothesis for *Varanus* in a **combined evidence** framework, incorporating fossil and extant taxa. We use this to reconstruct the global biogeographic history of varaniforme lizards, then focus on the evolution of body size among Australian taxa. To address the influence of competition on size evolution, we extend a series of novel comparative phylogenetic models. These include models which integrate continental biogeographic history (not just contemporary distribution), and the possibility of competition with another group of highly diverse Australian carnivores: dasyuromorphian marsupials.

Methods

Molecular Sampling

We collected tissue from 103 *Varanus* specimens, representing 61 of 80 currently recognized species. This sampling covers all nine subgenera and major clades of *Varanus*, as well as recognized subspecies, and known divergent populations. We also included four additional non-varanoid anguimorphs (*Elgaria*, *Heloderma*, *Shinisaurus*, *Xenosaurus*), a skink (*Plestiodon*), and tuatara (*Sphenodon*) as outgroups. Nuclear exons were targeted and sequenced using the Anchored Hybrid Enrichment approach (Lemmon et al. 2012). Sequencing, filterting, and alignment details are provided in the *Supplementary Material*.

Morphological Sampling

In addition to the molecular data, we also include morphological data collected by Conrad et al. (Conrad et al. 2011). We chose to exclude a number of characters added to this matrix in Conrad

(Conrad et al. 2012) because of extensive missing data and uncertain homology. We filtered the data matrix using an allowance of 50% missing data per character, excluding characters above this threshold, and removed taxa with greater than 70% missing data, as we found these samples to be disruptive in exploratory analyses. Finally, we removed invariant characters from the remaining data to conform to assumptions of the MKv model, resulting in a final morphological matrix comprising 303 characters. Disruptive samples—often called 'rogues'—are not limited to those with large amounts of missing data. So, to identify if rogue taxa are causing topological imbalances in our phylogenetic hypotheses, we applied RogueNaRok (Aberer et al. 2012) to initial total evidence analyses, identified rogues, and removed them for downstream analyses. Morphological sampling includes 55 extant *Varanus*, as well as the extinct *V.priscus*. A number of extant and fossil outgroups are included to sample the closely related groups Helodermatidae (*H.suspectum*), Lanthanotidae (*L.borneensis*), Paleovaranidae (formerly Necrosauridae) (*P.cayluxi*, *P.giganteus*) (Georgalis 2017), Shinisauridae (*S.crocodilurus*), and uncertain varaniforme lizards.

Phylogenetic Analyses

To generate a molecular species tree, we started by reconstructing individual genealogies for each of the 388 recovered loci. To estimate individual geneaologies for each locus we used IQ-TREE (Schmidt et al. 2014), and allowed the program to automatically pick the best fitting model of molecular evolution using PartitionFinder (Lanfear et al. 2012), then perform 1,000 ultrafast bootstraps (Haeseler et al. 2013). As a preliminary step, we also used IQ-TREE to infer the phylogeny from a concatenated alignment, with individual partitions assigned by PartitionFinder. To estimate a species tree, coalescent methods have been shown more accurate than concatenation (Kubatko and Degnan 2007), and so we used the shortcut coalescent method ASTRAL III (Zhang et al. 2017), with all our IQ-TREE gene trees as input. We estimated local posterior probabilities in ASTRAL and gene concordance factors (gCF) to address node support.

Preliminary analysis of genealogies indicated some strongly conflicting topologies between *Varanus* subgenera. To address gene-tree incongruence and investigate possible conflicting signals in our data, we used multidimensional scaling (MDS) to approximate the relative distances between gene tree topologies (Hillis et al. 2005), following the methodology of Duchene et al. (Duchene et al. 2018). To prepare the data, we trimmed down gene trees to a single representative of each subgenus (except *Papuasaurus*—*V.salvadorii*) as well as the outgroup *Xenosaurus*, and discarded loci missing any taxa, leaving us with 340 loci. We then calculated the pairwise distances between

all gene trees using the Robinson-Foulds metric, in the R package APE (Paradis et al. 2004). We projected the tree distances into two and three dimensions (representing tree topology space) using MDS, as visualizing and interpreting any more dimensions becomes difficult. To test if gene trees are uniformly distributed throughout tree space, or clustered, we used the partitioning around medoids algorithm as implemented in the R package CLUSTER (Maechler et al. 2018). We chose the optimum number of clusters (k), using the gap statistic, calculated for each k = 1–10. Clusters of gene trees represent similar topologies, and so we then summarized each cluster using ASTRAL, to identify consistent differences in topology.

As a complementary strategy to estimating *Varanus* relationships using ASTRAL, we also estimated a species tree using the full multispecies coalescent (MSC) model implemented in StarBEAST2 (Ogilvie et al. 2016). Computational requirements limit the number of loci we can realistically use under the MSC, and so we summarized per-locus informativeness using AMAS (Borowiec 2016). We then used custom scripts to sort the loci sequentially by (*i*) MDS cluster (determined above), (*ii*) missing taxa per alignment, (*iii*) number of variable sites, and (*iv*) AT content [**Fig.SX**]. Given this order, we then chose the first three sets of twenty loci (1–20; 21–40; 41–60) as representatives of the most informative and complete loci, and used them to build our phylogeny.

Advances in phylogenetic reconstruction methods have sought to better integrate molecular sequence data with fossil ages and morphological data (Lee et al. 2009; Pyron 2011; Ronquist et al. 2012; Beck and Lee 2014; Heath et al. 2014; Gavryushkina et al. 2017). Incorporating these lines of information in a **combined evidence** approach has provided more accurate phylogenetic estimation, and timing of divergence events. We reconstructed the phylogeny of living and extinct varaniforme lizards using the **Fossilized Birth-Death Multi-Species Coalescent** implemented in starBEAST2 (Ogilvie et al. 2018). In divergence dating analyses fossil information may be included using node priors (generally hard minimum bounds with diffuse upper bounds) or as tip dates (an estimate of the fossil sampling time) (Ho and Phillips 2009). Where data is available, combining node– and tip-dating may provide an advantage over using either method independently (Beck and Lee 2014; O'Reilly and Donoghue 2016). This provides the opportunity to co-estimate the phylogeny and divergence times, while providing structured priors on nodes which may otherwise be driven to unrealistic deep or shallow values. In most implementations of tip-dating fossil ages are fixed to a single value—most often this is the median value between upper and lower bounds. To avoid unintentional bias in choosing exact fossil ages, we instead incorporate uncertainty by sampling from informed uniform priors allowing the fossil ages to be jointly estimated (Barido-Sottani et

al. 2019). Morphological data were modelled under the Mkv model, a special case of the Mk model (Lewis 2001)—the most commonly used model for discrete morphological data. The Mk model operates under the assumption that each character may exhibit k states, and can transition among states at equal frequencies/rates. Because different characters may exhibit differing numbers of states, I applied the partitioning strategy of Gavryushkina et al. (2017), which partitions the morphological data based on the number of observed states of each character. Traditionally, invariant characters are either not coded, or stripped from discrete morphological alignments, resulting in an ascertainment bias for variable characters. The Mkv model (Lewis 2001) was proposed to account for this. All analyses were run for four independent chains under uncorrelated relaxed lognormal (UCLN) and strict molecular clocks (Table 4) for 1 billion generations and sampled each $5x10^5$ generations, to assess convergence among runs. We inspected the MCMC chains for stationarity (ESS $>$ 200) using Tracer v1.7.0 (Rambaut et al. 2018), and discarded the first 10-40% of each run as burn-in as necessary before combining runs.

Morphological and molecular phylogenies of living and extinct monitor lizards have previously provided conflicting results regarding the relationships between the major clades and subgenera of *Varanus*. Inconsistencies among these data types may partially be due to difficulties in accurately modelling morphological evolution (Goloboff et al. 2018). While our knowledge of the homology, rate, and process of molecular evolution is considerable, it has been much more difficult to adequately model morphological data. In contrast to molecular sites or loci, morphological characters are likely more often correlated (Billet and Bardin 2018), nonhomologous (Baum and Donoghue 2002), or evolving under dramatically different mechanisms (Goloboff et al. 2018), and may disrupt our best efforts at reconstructing phylogeny, divergence times, and rates of evolution. This difficulty is exaggerated on deep time scales and highlights important caveats to consider in the application of combined– or total-evidence methods (Puttick et al. 2017; Luo et al. 2018). To address this, we also estimated divergence dates for *Varanus* and outgroup anguimorphs using MCMCTree (Yang 2007). We used 50 loci, and applied three secondary node calibrations as truncated Cauchy distributions with 2.5% above and below the designated bounds to the splits between (*i*) Rhynchocephalia and Lepidosauria (lower=210, upper=270), (*ii*) Scincoidea and Anguimorpha (lower=150, upper=200), and (*iii*) the crown divergence of Anguimorpha (lower=60, upper=160). We ran two analyses to determine if they had converged on similar estimates, each for 2,000 burn-in generations, and then until another 20,000 samples had been collected.

Fossil Taxa as Sampled Ancestors

Fossil taxa are almost always assumed to represent terminal tips that have since gone extinct. To test this assumption, we allowed fossil taxa to be identified as terminal or stem lineages using the **Sampled Ancestors** package implemented in starBEAST2. After running our full analyses, we also ran prior-only analyses for each dataset and used these to calculate Bayes factors (BF) for each fossil taxon to test competing hypotheses. Given that we place a prior on the age of each taxon (τ) and are jointly estimating their position among the phylogeny, including a model (M) of the molecular and morphological evolution, we can sample exclusively from both the prior and posterior of our starBEAST2 analyses (*Supplementary Material*). We used a threshold of log(BF) > 1 to identify sampled ancestors, log(BF) < -1 to recognize terminal taxa, and -1 < log(BF) < 1 taxa were categorized as equivocal.

Biogeographic History

Varanus lizards have been variously hypothesized to have originated in Asia (Keast 1971; Estes 1983; Fuller et al. 1998; Jennings and Pianka 2004; Amer and Kumazawa 2008; Vidal et al. 2012; Conrad et al. 2012), Africa (Holmes et al. 2010), or Gondwana (Schulte et al. 2003) with conclusions largely based on which taxa were included, and the timing of varanid divergence events. To infer the biogeographic history of varanids and their allies, we used *BioGeoBEARS* (Matzke 2014). Because of the broad distribution of living and extinct monitors, we divided their range into seven major regions relevant to this group: North America, Europe, Sundaland/Wallacea, Australo-Papua, Africa/Arabia, West Asia (Indian subcontinent and surrounds), and East Asia (China, Mongolia, mainland Southeast Asia). We used as input our maximum clade credibility tree from the total evidence dating analysis in order to incorporate the geographic history of fossil taxa. Because of the deep evolutionary history of this group we took plate tectonic history into account by correcting dispersal probability as a function of distance between areas. We estimated distances between areas and continents through time at five million year intervals from 0–40 million years ago, then ten million year intervals from 40–100 million years, using latitude and longitude positions from GPlates (Boyden et al. 2011), and calculated pairwise distance matrices using the R package *geosphere* (Hijmans 2016). Additionally, we limited the model-space by providing information about area adjacency. For each time period, we removed unrealistic combinations of ranges (e.g. North America + AustraloPapua), with the aim of recovering more realistic biogeographic scenarios. We undertake

the exercise of reconstructing the biogeographic history of this group fully recognizing that the observation of current (or fossilized) ranges of terminal taxa provide little information about the processes that got them there (Ree and Sanmartín 2018). Recognizing this, we implement only the dispersal-extinction-cladogenesis model (DEC) and the jump extension of this model (DEC+j), and compare models with and without dispersal-distance-penalties. Further, we acknowledge the DEC model's proclivities for inflating the importance of cladogenetic dispersal, and consider its conclusions cautiously.

To further understand the spatial evolution of *Varanus*, we used a Bayesian method to model the dispersal of monitors across the Australian landscape. The R package *rase* (Quintero et al. 2015) assumes a Brownian motion diffusion process, using point data instead of discrete areas to infer geographic ranges which may be irregular or discontinuous. We started by downloading occurrence records for all continental Australian *Varanus* species from the Atlas of Living Australia (ala.org) (), curating the data for erroneous records, then trimmed our input tree down to just Australian taxa. We ran *rase* for 10,000 generations, sampling each 10th generation, then discarded the first 10% (100 samples) as burn-in, leaving 900 samples. We inspected the traces of the MCMC chains for stationarity using *coda* (Plummer et al. 2006).

Signature of Character Displacement

Ecological communities are generally thought to assemble under opposing processes of habitat filtering and interlineage competition. Filtering is suggested to select for species with similar phenotypes, resulting in conservatism or convergence, whereas competition is expected to result in greater phenotypic disparity. These expectations can be tested by investigating the functional diversity of communities across the landscape. We divided the Australian continent into half-degree cells, and created a site by species matrix using the ALA distribution data for (**i**) monitor lizards and again for (**ii**) monitors and dasyuromorphian marsupials together. We estimated the functional diversity for the two data sets using the package *FD* (Laliberté et al. 2014) and Rao's Quadratic, using body size as the trait of interest. We then estimated functional diversity for each inhabited cell 100 times using a dispersal null metric model which sampled from nearby cells assuming a probability proportional to the inverse of the distance from the focal cell. To compare observed and simulated functional diversities, we calculated standardized effect sizes (SES) for each cell, and a mean SES across the continent with 95% confidence intervals.

Modelling Body Size Evolution with Competition

Only within the past few years have phylogenetic comparative methods (PCMs) begun to account for the interaction of lineages on trait evolution. Building off conceptual work by Nuismer & Harmon (Nuismer and Harmon 2015), Drury et al. (Drury et al. 2016) and Manceau et al. (Manceau et al. 2017) elegantly integrated a system of ordinary differential equations in RPANDA (Morlon et al. 2016) for estimating the effect of competition on trait evolution in a maximum likelihood framework. This methodology allows us to estimate a parameter S which describes the strength of the interaction, as well as the polarity: negative values of S indicate competition or repulsion, positive values indicate attraction towards common values. In its most simplistic form (the Phenotypic Matching **PM**, or Matching Competition **MC** model), the S parameter interacts with the mean trait values of all other lineages (vector X_t), to reflect their relationship (*Supplementary Material* Equation 1). To take into account changes through evolutionary time, the S parameter further interacts with the evolutionary rate (σ), and drift (d), to dictate the trajectory of trait evolution. This model however, assumes that *all* lineages in a tree are sympatric and interact with one another. To address this, Drury et al. (Drury et al. 2018b) extended the model by incorporating interaction matrices (P) that dictate which taxa interact with one another to more realistically estimate S (equation 1).

In natural ecosystems, many different organisms compete for the same resources, so accounting for competition only within a single group is perhaps unrealistic. To address this issue, we consider the influence of another broadly distributed group of like-sized carnivores, dasyuromorphian marsupials, on the size evolution of Australian monitor lizards. Dasyuromorphians cover a similar breadth in range and body size, inhabiting deserts and closed forests, ranging from the tiny *Antechinus* up to the recently extinct canine-convergent *Thylacine*. There is evidence to believe that these lineages may compete both directly and indirectly for resources (Wroe 2002). To test this hypothesis we begin by trimming the marsupial phylogeny of Brennan & Keogh (Brennan and Keogh 2018) down to just the faunivorous clade, from which we also dropped *Myrmecobius* because of its unusual ecology. We collected body size (mm) information for marsupials from Pantheria (Jones et al. 2009), and monitors from the literature (Wilson and Swan 2013). Manceau et al. (Manceau et al. 2017) introduced a framework for estimating the effect of one clade on the trait evolution of another, incorporating two phylogenetic trees, referred to as the Generalist Matching Mutualism **GMM** model. This is essentially a two-clade extension of the **PM** model, which makes the assumption that the evolution of trait values in clade A are the result of interactions *only* with lineages in

clade B, and vice versa. We present a graphical description of this and additional models below (Fig.1). The **GMM** model however makes two very basic assumptions that we expect do not fit our data: (**1**) interactions between phenotypes are limited to interclade (between trees) matching or competition, meaning there is no influence of intraclade (within tree) interactions, and (**2**) that all contemporaneous lineages are interacting, regardless of geographic distribution. To address these assumptions, we develop a series of models that expand on the interaction parameter S, and incorporate biogeography, to hopefully provide more realistic models of trait evolution. We briefly summarize and illustrate those models here, but discuss their behavior more extensively in the *Supplementary Material*.

PM (Nuismer and Harmon 2015) *or* **MC** (Drury et al. 2016): the basis for PCMs incorporating interactions between lineages. S is estimated from the interaction of *all* contemporaneous lineages, irrespective of geography. $\mathbf{PM_{geo}}$ *or* $\mathbf{MC_{geo}}$ (Drury et al. 2016): geographic extension to the PM/MC model. Only sympatric lineages interact (determined in P matrices), influence the estimation of S. **GMM** (Manceau et al. 2017): the two tree extension of the PM/MC model. S is estimated from the interaction of *all* contemporaneous lineages *between* trees, but not within. $\mathbf{GMM_{all}}$: extends the GMM model to estimate S from interactions between *all* contemporaneous lineages both within and between trees. **CoEvo**: a geographic extension of the GMM model, accounting for interactions among geographic co-occurring lineages *between* trees (as with the original GMM model). $\mathbf{CoEvo_{all}}$: a geographic extension of the GMM_{all} model, accounting for interactions among geographic co-occurring lineages both within *and* between trees. $\mathbf{CoEvo_{split}}$: as with the $\text{CoEvo}_{\text{all}}$ model, this is an extension of the GMM_{all} model, accounting for interactions among geographic co-occurring lineages. Separate S parameters are estimated for interactions among lineages in different trees (S_1) and within a given tree (S_2). **CoPM**: This is a joint estimation of the PM/MC model for two trees. It estimates a single interaction (S) and rate (σ) value across both trees, but S is estimated solely from intra-clade interactions (no interaction between trees). $\mathbf{CoPM_{geo}}$: This is an extension of the CoPM model. It estimates a single interaction (S) and rate (σ) values across both trees, but S is estimated solely from intra-clade interactions (no interaction between trees). **JointPM**: This is a joint estimation of the PM model for two trees. It differs from the CoPM model by estimating separate interaction values for each clade (tree1 = S_1; tree2 = S_2). All lineages in a tree are assumed to interact with ALL other lineages in that tree. $\mathbf{JointPM_{geo}}$: This is a joint estimation of the PM/MC model for two trees. It differs from the CoPM_{geo} model by estimating separate interaction values for each clade (tree1 = S_1; tree2 = S_2). Like the CoPM_{geo}

(unlike JointPM) it correctly estimates the interaction parameters (S_1, S_2) for only geographic overlapping taxa. Those models which do not incorporate geographic history (GMM, GMM_{all}, CoPM, JointPM) are logical and cohesive models, but inappropriate for application to our data. This is because they operate under the assumption that **all** contemporaneous lineages interact, which we know is not true for our Australian animals, and is unlikely to be valid for most circumstances. Because of this, we restrict our exercise to geographically-informed models, though we present results of all models in the *Supplementary Materials*.

Existing and new models described here allow us to test a number of hypotheses regarding the evolution of varanid body size. We focus on those that incorporate dasyuromorphian marsupials as well, because this provides a more holistic view of the macroevolution of two iconic groups of Australian vertebrates. Using these models we first test the idea that the evolution of varanid and dasyuromorphian body size has been dictated by competition with congeners, between clades, or both. We then test whether the strength of intraclade competition is equivalent in the two groups, and if the inclusion of geography via coexistence matrices improves model fit. Finally, we can ask if size evolution is instead dictated by non-ecological processes, by implementing standard models of trait evolution, Brownian Motion **BM** and Ornstein Uhlenbeck **OU**. Using these traditional null models, we can again ask if monitor and dasyuromorphian size has evolved under similar or independent rates using *ratebytree* in *phytools*, though we also provide implementations of shared BM and OU models in the *RPANDA* framework—**CoBM** and **CoOU**.

To incorporate historical and contemporary biogeography, we started by extending our *rase* analyses to marsupials with data collected from the ALA. We designed a number of custom scripts and functions to process the spatial data and model objects including extensions of the 'CreateGeoObject' of *RPANDA*. Our functions 'CreateGeoObject_SP' and 'CreateCoEvoGeoObject_SP' produce *RPANDA* GeoObjects that take as input a tree, spatial distribution data in latitude/longitude format, and a post-processed *rase* object. Internally, these functions use the packages *sp* and *rgeos* to translate spatial data into spatial polygons representative of species distributions. Then, at each cladogenetic event, we determine the pairwise overlap of all contemporaneous lineages to construct our GeoObject (see Fig.S1). The 'CreateCoEvoGeoObject_SP' function has adapted this process for two trees, to be applied to GMM-type models.

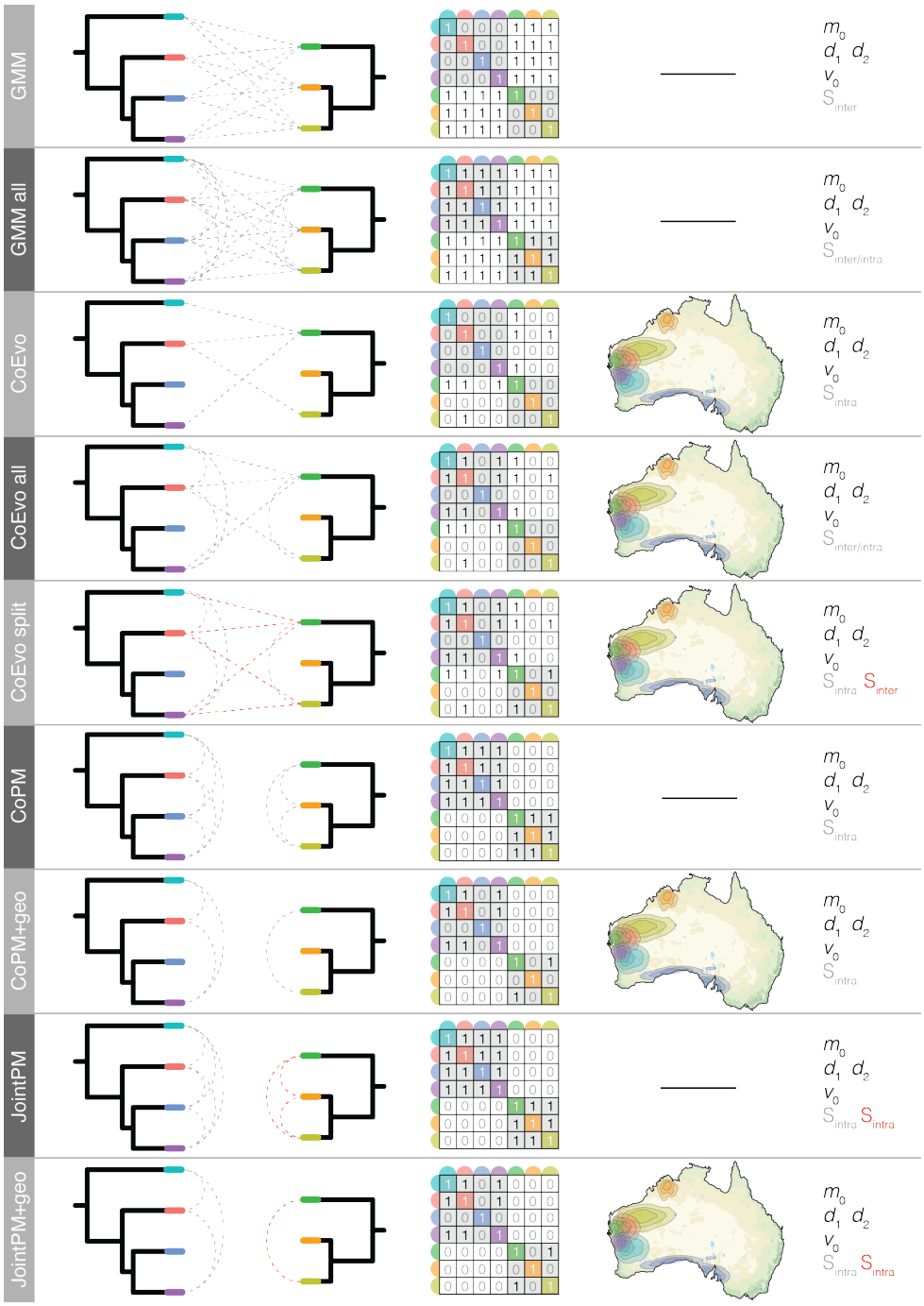

Figure 1: Schematic components of various GMM-type models of evolution including two clades. Each model name is listed at left, followed by a diagram of the two trees with interlineage interactions allowed under the given model designated by dashed grey lines. If more than one interaction parameter S is estimated, it is denoted by red dashed lines. The contemporary summary of these interactions are presented in the interaction matrix P, and the estimated parameters are listed at the far right. If the interaction matrix is geographically informed, a map showing species ranges is shown to the right of the interaction matrix.

Model Behavior and Identifiability

The ability to identify competition and estimate associated parameters using process-based models has been tested extensively previously (Drury et al. 2016, 2018a, 2018b). From this we know that the ability to recover competitive models and estimate the interaction parameter S—when it is the generating process—is strongly linked to the absolute value of S, and to a lesser degree the size of the phylogeny. Parameter estimate and recovery of S can also be highly influenced by the incorporation of stabilizing selection (ψ or α), with the two parameters working agonistically in instances of competition (-S), and synergistically in mutualistic circumstances (+S).

To ensure that we can accurately identify our models and estimate parameter values, we undertook a focused simulation exercise. Following the advice of Manceau et al. (Manceau et al. 2017), we simulated data directly onto our Australian monitor and marsupial trees under the same models we fit to our empirical data: BM_{shared}, OU_{shared}, CoEvo, $CoEvo_{all}$, $CoEvo_{split}$, $JointPM_{geo}$, and $CoPM_{geo}$. We used the *RPANDA* function 'simulateTipData' to simulate body size data under all specified models, keeping the empirical biogeography constant. Specifics of the generating parameter values are noted in the Table S3. We then iteratively fit the models to our simulated data, and compared fit using AICc and plotted AICc weights. To determine the ability to accurately recover parameter values, we then compared estimated to simulated values under each model.

Historical Models of Monitor Size Evolution

To test our hypothesis of character displacement as a driving force of *Varanus* size disparity, we also fit standard stochastic (Brownian Motion) and stabilizing (Ornstein-Uhlenbeck–OU) models of trait evolution, and a multi-optima (OUM) model following Collar et al. (2011). This multi-OU (OUM) model explains size evolution as a result of differing selective optima correlated with habitat use. These models were implemented and fit using *geiger* (Pennell et al. 2014) and *OUwie* (Beaulieu et al. 2012).

Results

Phylogenetic Analyses

We successfully captured and sequenced 388 loci, with an average coverage of 350 loci per sample (min = 112, max = 373) (**Fig.S2**). One ingroup sample *Varanus komodoensis* had low sequence coverage

and quality, and so we replaced the sample with sequences extracted from the Komodo dragon genome (Lind et al. 2019). Phylogenetic hypotheses of molecular samples across ASTRAL and starBEAST2 coalescent analyses are broadly in agreement (Figs.2,3). Both support the monophyly of *Varanus* and anguimorphs, and unite the Shinisauridae with the Helodermatidae, Anguidae, and Xenosauridae along a short internal branch. The varanidae is sister to this group. They also agree on the placement of the engimatic monitor *V.spinulosus* as sister to the Asian and Pacific clade, and *V.gleboplama* as sister to the rest of *Odatria*. The position of these last two taxa have not been recorded elsewhere, but both are strongly supported. Perhaps as expecteds, ASTRAL and starBEAST2 disagree on the interspecific relationships of the water monitors *V.salvator* complex, which occur across a number of extremely short and unstable branches. Remaining intraclade relationships are congruent between analyses.

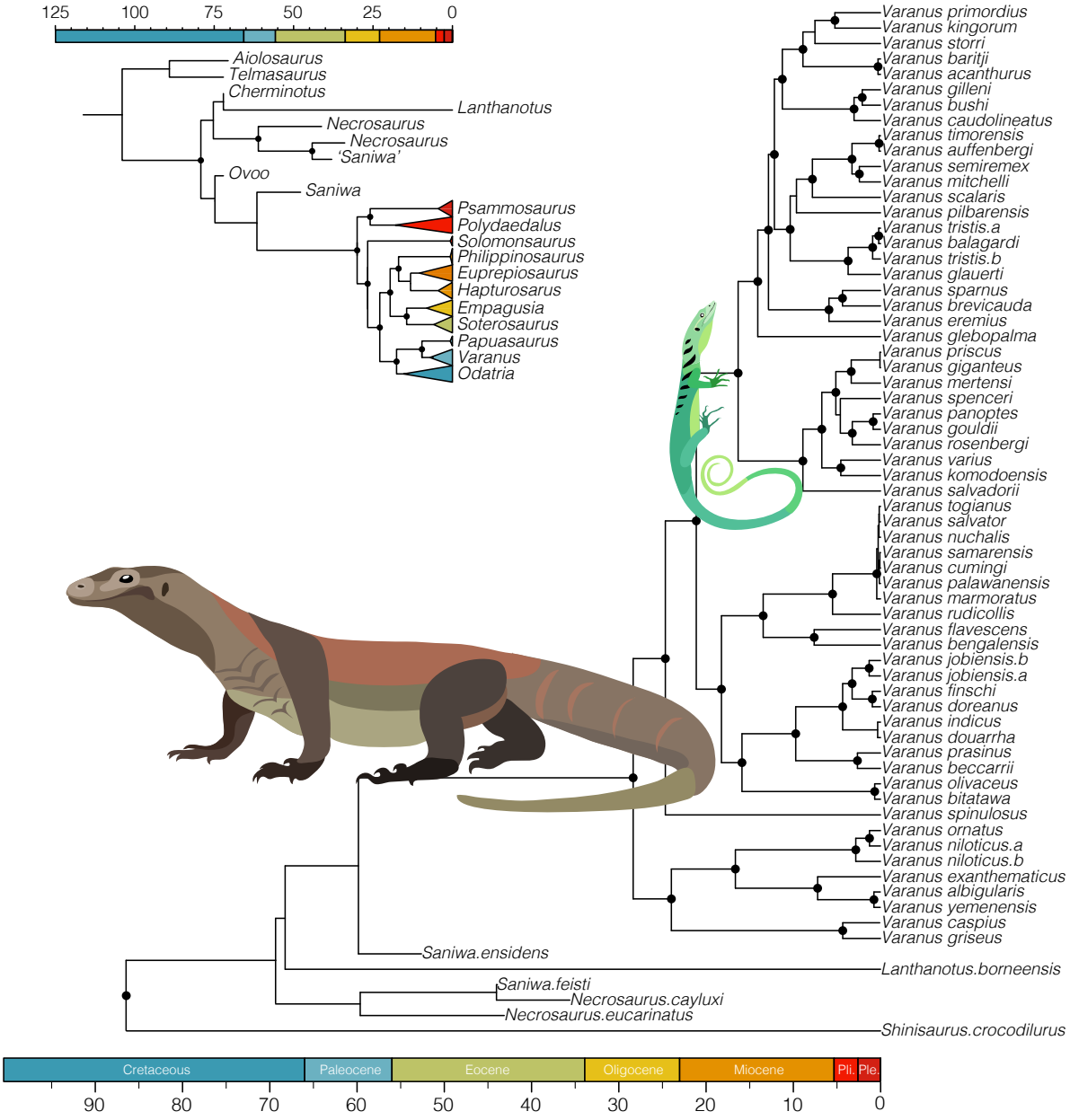

Figure 2: Relationships among living and extinct varaniforme lizards and relatives, as a result of total evidence dating (molecular and morphological data). The resolution of fossil anguimorph taxa is volatile and appears highly sensitive to the fragmentary remains of many of these taxa. Varanids emerge in the Eocene, and extant Varanus appear in the Oligocene. Support values for relationships among *Varanus* subgenera as well as interspecific relationships are consistently high, though extinct *Varanus* are again difficult to place in our phylogeny. Nodes denoted by a • black circle are supported by posterior probabilities >0.90, all others are equivocal (<0.90).

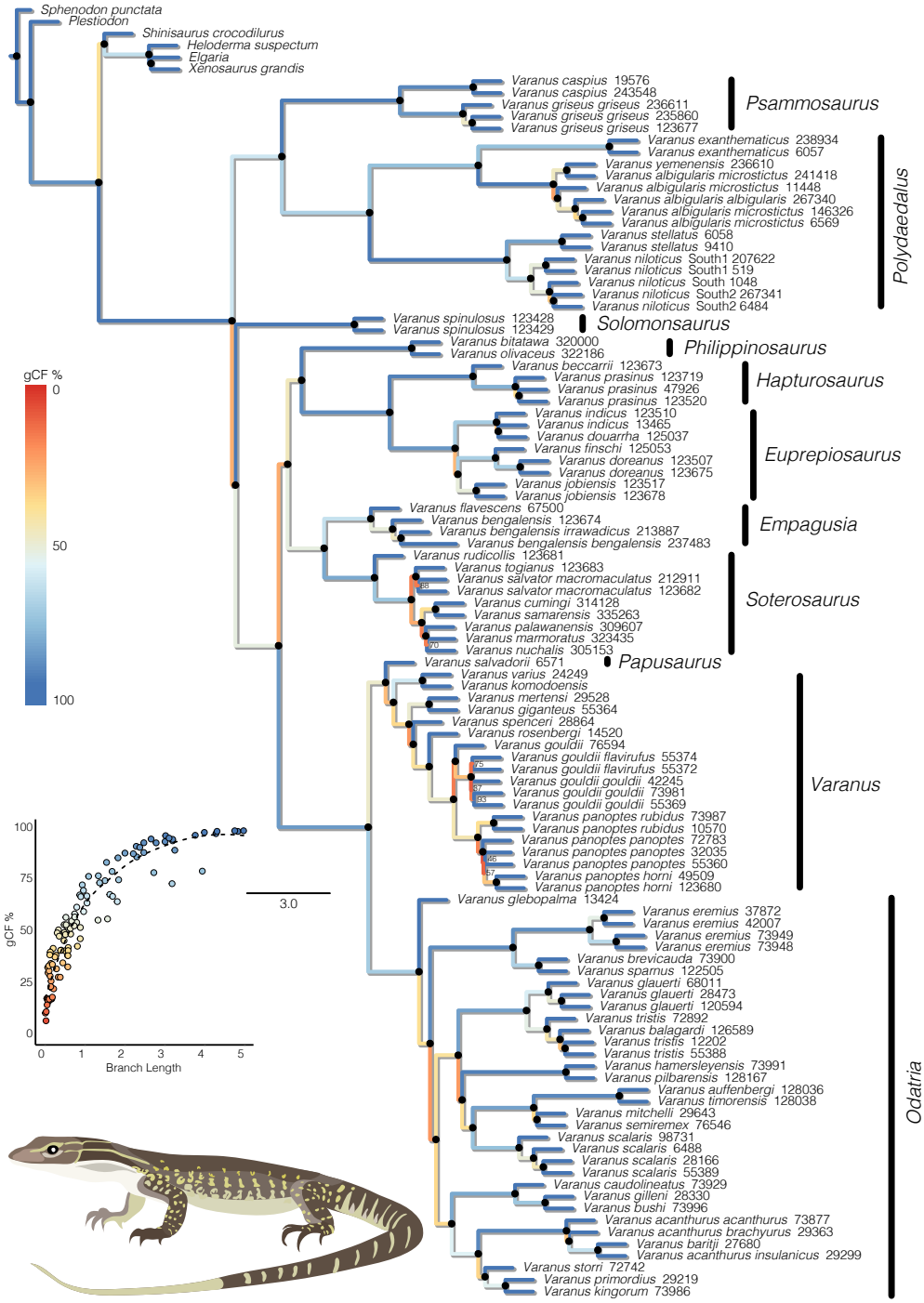

Figure 3: The fully sampled ASTRAL tree is largely concordant with our total evidence species tree. Nodes denoted by a • black circle are supported by local posterior probability values >0.90, all others (<0.90) are considered equivocal and designated by lpp values. Branch colors correspond to gene concordance factors, and represent the percent of gene trees which decisively support the presented bifurcation. Inset plot shows that as expected, gCF values increase with increasing branch lengths, shown in coalescent units. Subgeneric names are listed to the right of each group.

Multidimensional scaling (MDS) of gene-trees reveals that nuclear loci constitute two topological clusters. The larger cluster (n=264 loci) supports a sister relationship between *Empagusia* and *Soterosaurus*, and the smaller cluster (n=76 loci) supports a sister relationship between *Empagusia* and *Polydaedalus* (Fig.4). Looking at fully-sampled gene trees we see that these patterns are driven by a sister relationship between *V.bengalensis* and *V.flavescens* (both *Empagusia*) in the larger cluster, and a sister relationship between *V.bengalensis* and *V.albigularis/V.yemenensis* in the smaller cluster.

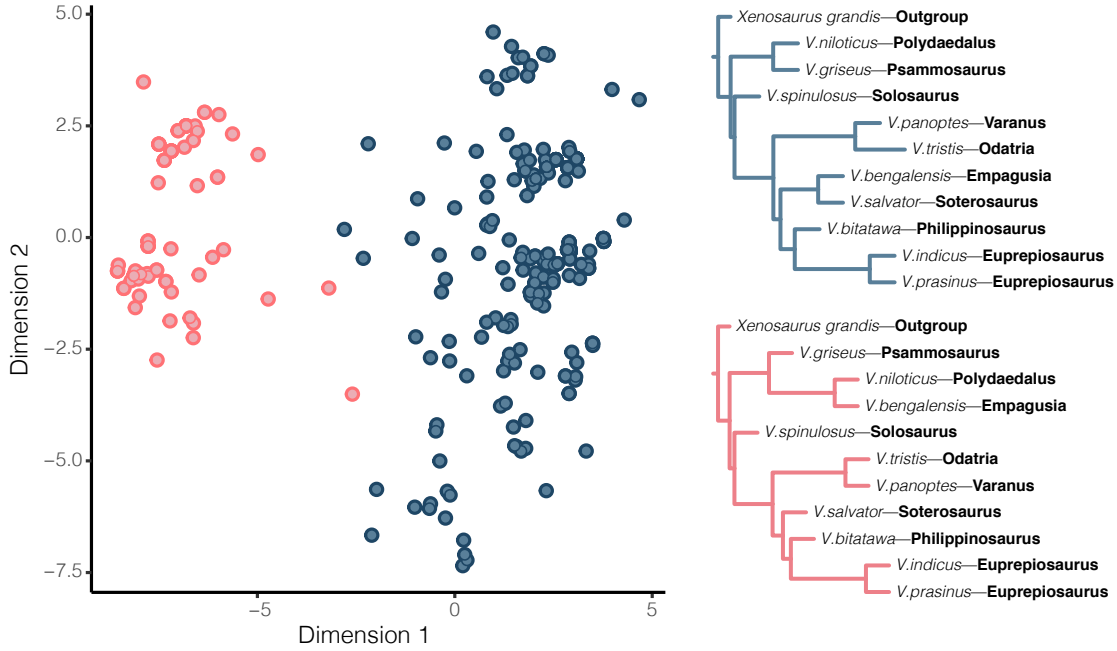

Figure 4: Two dimensional representation of multidimensional scaling (MDS) of gene tree space, colored by optimal clustering scheme (k=2), and their associated topologies inferred using ASTRAL. Analysis in both two and three dimensions supported the same optimum number of clusters, and cluster compositions. Each point represents a single gene tree, colored clusters match colored trees displayed to the right. Bootstrap support of all nodes was 1. The general topology of the clusters differ only in the placement of *V.bengalensis*—*Empagusia* as sister to the African group *Polydaedalus*, or to the Asian group *Soterosaurus*.

The phylogenetic affinities of fossil taxa in our total evidence analyses are highly volatile. It appears this is may be correlated with the number of available characters, with more fragmentary fossils being harder to assign phylogenetically. By comparing the placement of fossil taxa in prior and posterior analyses using Bayes Factors, we find support for the majority of these taxa as terminals in our trees (BF < -1) (Fig.S2). Two taxa *Cherminotus* and *Bahndwivici* are ambiguous, but the former shows evidence for being a tip, which the latter shows evidence of being a sampled ancestor of *Shinisaurus*. Of particular interest are the fossil varanids including *V.priscus*, *V.mytilini*,

V.marathonensis, *V.hooijeri*, *V.rusingensis*, *V.cf.bengalensis*, and a number of north African taxa. With the exception of *V.priscus*, their phylogenetic placement is equivocal and highly inconsistent between analyses, despite previous evidence of the placement of these taxa (Conrad et al. 2012; Ivanov et al. 2017). A number were removed from subsequent analyses because of disruptive RogueNaRok scores (Table S3). *V.priscus*, which is generally considered an extinct relative of the Indo-AustraloPapuan clade of giant monitors including *V.varius*, *V.komodoensis*, and *V.salvadorii*, is consistently placed in the Australian radiation, but in some runs is instead affiliated with the dwarf monitors *Odatria*.

Dating estimates from our reduced-sampling total evidence analysis and molecular and node dating analysis in MCMCTree provide similar timing for *Varanus* divergences. They suggest an origin of varanids (split between Varanidae and Lanthanotidae) in the late Cretaceous, and an early-to-mid Oligocene (StarBEAST) or late Eocene (MCMCTree) origin for the crown divergence of extant *Varanus*. These dates are comparable with existing estimates from the literature (Lin and Wiens 2017; Pyron 2017).

Biogeography and Community Assembly

Global biogeographic analysis of *Varanus* and allies suggests an origin of varaniforme lizards in East Asia, with dispersals west across Laurasia into Europe, and east into North America. The origin of the genus *Varanus* itself is equivocal (Fig.S3), but likely followed a similar pattern, with independent clades dispersing west through the Middle East and into Africa and Europe, and south and east through Southeast Asia, Sundaland, and into IndoAustralia. After reaching the western and eastern extents of their range, both the African and AustraloPapuan clades appear to have begun dispersals back towards their origins. This has resulted in *V.yemenensis* extending across the Red Sea into the Arabian Peninsula, and *V.komodoensis* and members of the *V.scalaris* complex reaching back into Wallacea. The DEC model incorporating dispersal probability as a function of distance is strongly preferred (AIC = 170.66, x = -0.682) over the traditional DEC model (AIC = 186.04, ΔAIC = 15.38).

Phylogeographic reconstruction of Australian *Varanus* reveals an origin spread across much of northern and central Australia (Fig.5). Ancestral and contemporary species ranges and patterns of dispersal are plotted at cladogenetic events and available as a .gif file in *Supplementary Material*. Considering northern Australia was the most likely colonization point for monitors, it makes sense that our analyses of community structure highlight this area as the center of greatest species richness

for *Varanus*, with up to eleven species recorded in some half-degree grid cells. Taken together with dasyuromorphian marsupials, we again recognize the richness in the Top End, but also note species richness hotspots in the Central Deserts and the Pilbara. These regions are functionally diverse for monitors as well, but much less so for communities of marsupials *and* monitors analyzed jointly. Overall, we find support for overdispersion in trait values in both datasets, with functional diversity of most communities greater than expected under our null model (mean SES across all cells for monitors = 0.57 ± 0.07; monitors and marsupials = 1.2 ± 0.26).

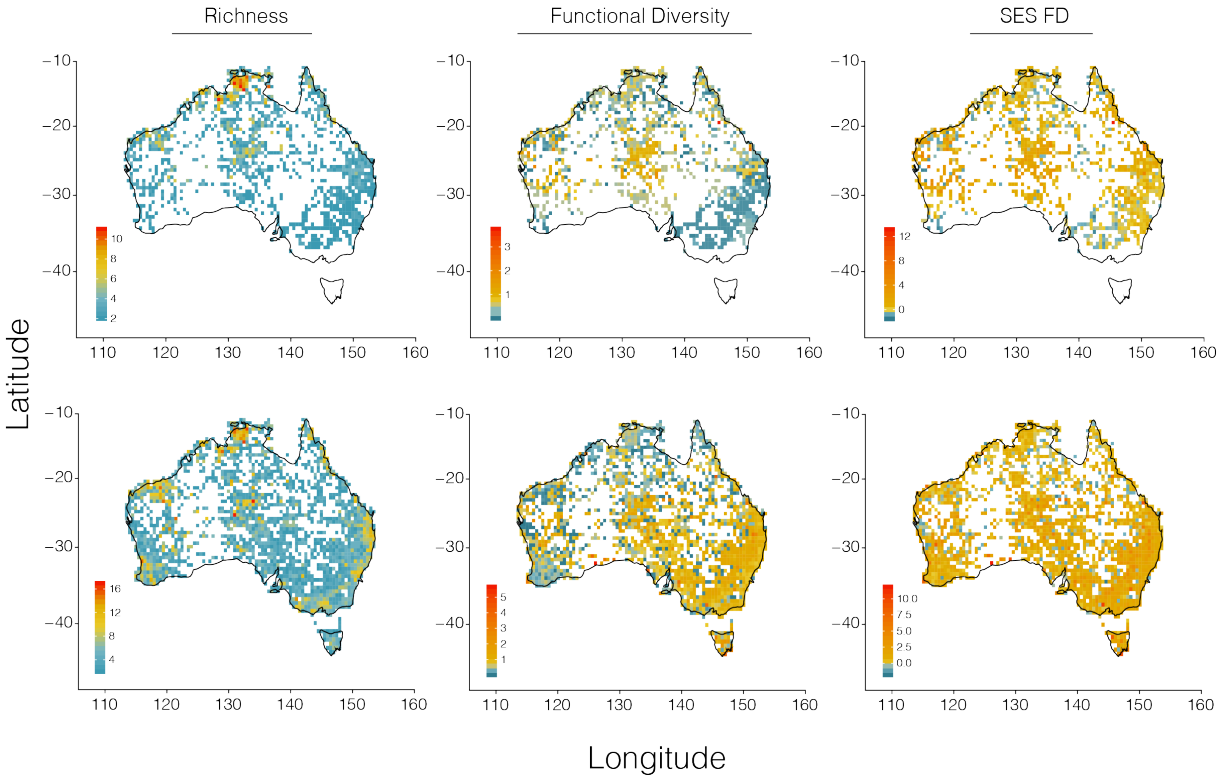

Figure 5: Maps of Australia showing patterns of richness and functional diversity for monitor lizards and faunivorous marsupials. The top row shows results for monitor lizards, and the bottom monitors and marsupials together. Values were calculated and plotted for half-degree squares, with warmer colors indicating greater values—but note different scales for each plot. The left plots display species richness across the landscape, center plots show absolute values for functional diversity (Rao's Q), and the right plots show the standardized effect size of functional diversity when compared to the dispersal-corrected null model.

Modelling Body Size Evolution

Comparison of traditional models of trait evolution with those that incorporate interactions among lineages decisively favors interactive models (AICc weight 94%) (Figs.6b, S4). These models can be broadly divided into those which estimate the interaction parameter S from occurrences (**1**) within clades (S_{intra}), (**2**) between clades (S_{inter}), or (**3**) both. We find greatest support for models

that estimate interactions only within a clade or clades (Fig.6c), such as the best fitting model **CoPM$_{\mathbf{geo}}$** (Fig.6a). Support for the **CoPM$_{\mathbf{geo}}$** model—which fits only a single S_{intra} parameter for *both* trees—suggests that the strength of intraclade interactions is indistinguishable between the two groups. Across those models that estimate S_{intra}, inferred negative values of S support **competitive** interactions in both monitors and marsupials, S_{intra} = -0.043 ± 0.005.

Support for the **CoPM$_{\mathbf{geo}}$** model also comes indirectly from parameter estimates of the **CoEvo$_{\mathbf{split}}$** model. In fitting the **CoEvo$_{\mathbf{split}}$** model, which estimates separate inter- and intraclade interaction parameters (S_{inter}, S_{intra}), we estimate a weak positive S_{inter} parameter of 0.0043, suggesting that interclade interactions between marsupials and varanids are indistinguishable from these data, as depicted in the preferred **CoPM$_{\mathbf{geo}}$** model.

Results of our model identifiability exercise indicate that all proposed models can be recovered under realistic circumstances (Fig.S5). Because a number of these are nested forms of one variety or another, when simulated values of S (as S_1 or S_2) approach 0, some models may be incorrectly conflated (see *Supplementary Material—Nested Models*). This happens most commonly with the CoEvo$_{\text{split}}$ model, which is identical to the models: CoPM$_{\text{geo}}$ if S_1=0, CoEvo if S_2=0, and CoEvo$_{\text{all}}$ if S_1=S_2. This also occurs with the JointPM$_{\text{geo}}$ model which may be confused with the CoPM$_{\text{geo}}$ model as S_1 approaches S_2. Although not explicitly tested here, in situations where S is large (positive), OU models may be preferred, as the α parameter may mimic the effect of low amounts of drift and attraction towards shared theta values. Consistent with previous assessment (Drury et al. 2016), we also find that the accuracy of estimated S is directly related to the absolute value of S, with greater values of S being more precisely recovered (Fig.S6).

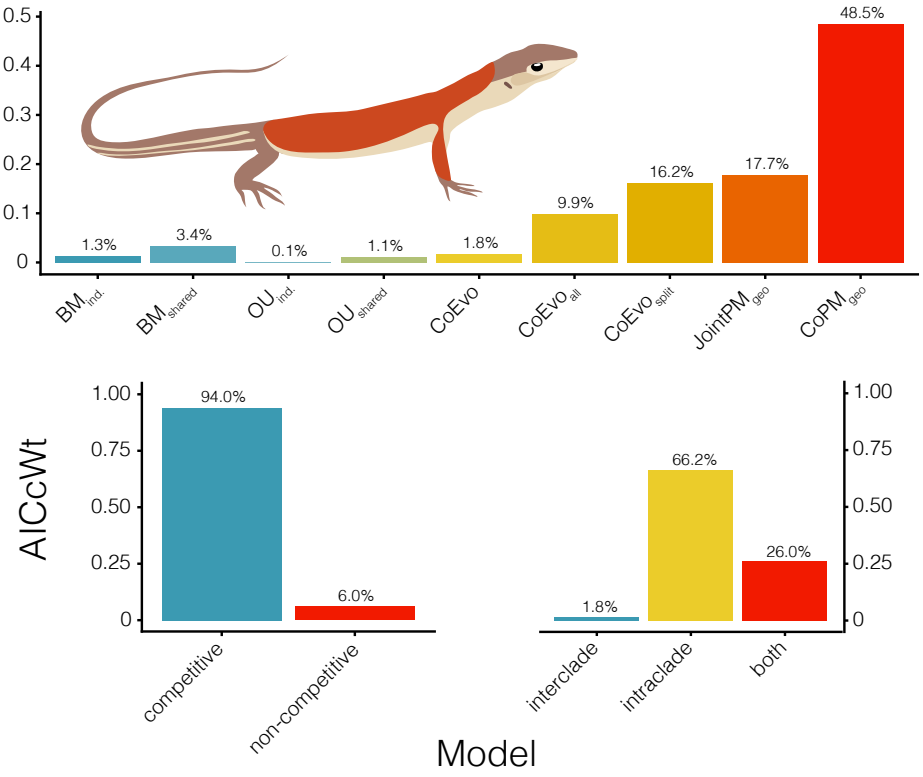

Figure 6: Comparative model fitting highlights the importance of incorporating interactions when modelling body size evolution of monitor lizards and dasyuromorphian marsupials. Modelling competition vastly improves model fit, but size evolution appears largely driven by intraclade evolution and not competition between monitors and mammals.

Discussion

Competitive interactions are expected to impact diversity by influencing species ranges, and influence phenotypic and behavioral evolution through character displacement (Brown and Wilson 1956; Benton 1987). *Varanus* represent a diverse group of lizards with exceptional variation in body size and ecologies. To investigate the role of competition in size evolution in monitors, we started by building a phylogenomic hypothesis of living and extinct varanids and their allies. By using a total evidence dating approach we were able to take advantage of both molecular and morphological data to incorporate fossil taxa, and reconstruct the global biogeography of varaniforme lizards. After focusing on the Australian continent, we used a temporally dynamic Brownian Motion dispersal process to infer ancestral ranges for monitor lizards and co-occurring marsupial predators. We then quantified the functional diversity of monitor communities, and monitor–marsupial communities to address how these assemblages are structured. Finally, we developed and implemented a number of comparative models to account for interspecific interactions and estimate competition among monitors *and* with dasyuromorphian marsupials. Results of our comparative modelling provide a compelling case for considering competition in phylogenetic comparative methods (PCMs) of trait evolution.

Phylogenetic Relationships and Origins

Relationships between anguimorph lizard groups have been contentious, particularly with regard to the placement of fossil taxa (Conrad 2008; Conrad et al. 2011; Pyron 2017). Different datasets have supported strongly competing hypotheses including a monophyletic Varanoidea (Varanidae, Shinisauridae, Monstersauria) (Gauthier et al. 2012), paraphyly of Varanoidea with regards to Anguidae, and even sister relationships between Varanidae and Mosasauria (Conrad 2008) or Varanidae and Serpentes (Hejnol et al. 2018). Existing hypotheses about relationships among these groups appear highly sensitive to the data used, with conflicting molecular and morphological signals (Pyron 2017; Hejnol et al. 2018), and even incongruences between different morphological datasets (Conrad 2008; Conrad et al. 2011; Gauthier et al. 2012; Pyron 2017). Much of this likely has to do with the fragmentary nature of many fossil taxa, morphological models of character evolution, and previous reliance on mitochondrial DNA of extant taxa. Unfortunately our reanalysis of existing morphological data alongside new phylogenomic data do not provide any strong answers that have not already been considered regarding anguimorph origins.

Fortunately our nuclear data do provide some new insights into the phylogenetics of the *living*

members of *Varanus*. Interestingly, much of our tree is consistent with the first molecular phylogenies of *Varanus* proposed by Fuller et al. (1998) and Ast (2001) two decades ago. Our results verify the monophyly of African and Arabian monitor lizards, and contrary to other recent studies (Lin and Wiens 2017), support the recognition of *Psammosaurus* and *Polydaedalus* subgenera. Our data support a geographically widespread clade composed of Philippines (*Philippinosaurus*) and tree(*Hapturosaurus*) and mangrove monitors (*Euprepiosaurus*), with water monitors (*Soterosaurus*) and species from the subcontinent (*Empagusia*). Finally, we return a well resolved clade of Indo-AustraloPapuan monitors comprising the crocodile monitor (*Papuasaurus*), and the subgenera *Varanus* and *Odatria* (the dwarf monitors).

One of the most intriguing results from our data is the the phylogenetic placement of *V.spinulosus*. Although it is not wholly unexpected [**Ziegler et al. 2007a; 2007b; 2010; Bucklitsch**), it is not affiliated with the subgenus *Varanus* (Sweet and Pianka 2007) or with *Euprepiosaurus* (Harvey and Barker 1998), from which it was recently distinguished by hemipenial characteristics. Instead, the phylogenetic position of *V.spinulosus* is remarkable given that it is a Solomon Islands endemic, meaning it likely made a considerable over-water dispersal or island hopped to the Solomons only shortly after their formation ~30 Ma (Hall 2002). This corroborates the idea that Melanesian islands have long been sources for ancient endemic diversity (Oliver et al. 2018). It also suggests at least two independent dispersals of *Varanus* across Wallace's line, and a convoluted history of movement throughout the Indo-Australian region. We agree with the unique assessment of (**Bucklitsch et al**) in identifying a distinct subgenus *Solomonsaurus*, for *V.spinulosus*.

In addition to movement throughout Asia, the large ranges of some African and Middle Eastern *Varanus* highlights their dispersal capabilities. Previous research has found that at least one member of the African varanids *Polydaedalus*—*V.yemenensis* has since dispersed back across the Red Sea into the Arabian Peninsula (Portik and Papenfuss 2012). On a similar time frame, *V.bengalensis* appears to have dispersed west back across Asia, and the subcontinent, into the Middle East. This is relevant because we find signature of introgression (Fig.4) between one sample of *V.bengalensis* and members of the *V.albigularis* group, to which *V.yemenensis* belongs. Though this result is tentative, it remains an exciting concept that secondary contact between distantly related *Varanus* could result in hybridization, perhaps facilitated by the noted chromosomal conservatism of this genus (King and King 1975).

Our phylogeny of *Varanus* also highlights the adaptive capacity of these amazing lizards. Note the sister relationship between *V.giganteus* and *V.mertensi* for example. The perentie *V.giganteus* is

the largest extant Australian lizard, reaching well over two meters long, while remaining extremely thin. Its sister species *V.mertensi* in contrast, is a heavy bodied semiaquatic lizard built for the watercourses of northern Australia. Together, these species are sister to a group of sturdy terrestrial wanderers—the sand goannas—*V.gouldii*, *V.panoptes*, *V.rosenbergi*, and *V.spenceri*. In roughly five million years, these monitors diverged broadly both ecologically and morphologically, to spread across Australia's landscape. In the process of diversifying, monitor lizards have also converged repeatedly on ecological niches and body plans. There are at least three different origins of amphibious monitors (*V.salvator*, *V.mertensi*, *V.mitchelli* groups), and four or more origins of arboreal species (*V.prasinus*, *V.gilleni*, *V.salvadorii*, *V.olivaceous*, *V.dumerilii* groups), emphasizing the ability of monitors to fill available niches.

A number of phylogenetic questions evade our sampling, and largely concern the population genetics of known species complexes. These include the *V.acanthurus*, *V.doreanus*, *V.griseus*, *V.indicus*, *V.jobiensis*, *V.prasinus*, *V.salvator*, *V.scalaris*, and *V.tristis* groups, of which most have recognized subspecies, very closely related species, or are paraphyletic in our data (Fig.3). Some of these taxa have experienced dramatic taxonomic growth in recent years as a result of more extensive sampling, and are sure to present exciting phylogeographic and systematic stories when the right data and sampling are paired together.

Overall, we suggest a younger timeline for the diversification of modern varanid lizards, with a crown age possibly in the early-to-mid Oligocene. This timing suggests *Varanus* potentially dispersed into the Indo-Australian region shortly after the collision of the Australian and Asian plates. If this is true, the connection of Sahul to Sundaland likely facilitated the dispersal of monitor lizards across an Indonesian island bridge, and extensive over-water dispersals seem less probable. Similarly, this proximity has also allowed small AustraloPapuan *Varanus* like the *V.scalaris* complex, as well as the largest extant monitor *V.komodoensis* to disperse back into the Indonesian archipelago (at least Wallacea). This pattern is consistent with the adaptive radiation of AustraloPapuan elapid snakes (Keogh 1998) and pythons (Reynolds et al. 2014; Esquerre et al. 2019), from Asian origins, and may underlie a more common diversification trend.

Competition, Character Displacement & Size Evolution

Despite a relatively conservative body form, *Varanus* lizards have diverged into a number of ecologies and an astonishing array of body sizes. These include highly crytpozooic pygmy monitors like *V.primordius*, slender canopy dwellers like *V.prasinus*, the stout-bodied semiaquatic *V.mertensi*

and *V.salvator* complex, and monstrous apex predators like the Komodo dragon *V.komodoensis* and extinct *V.priscus*. Across their range, monitors have also converged ecomorphologically with a number of mammalian predators, potentially putting them in direct competition for resources. Competition is expected to influence interacting lineages by driving similar organisms apart in geographic space (exclusion), or in phenotypic or behavioral traits (character displacement) (Brown and Wilson 1956). In Australia, the diversity of varanids is matched by that of carnivorous marsupials, which vary from tenacious shrew-sized planigales (*Planigale*) up to the recently extinct wolf-like *Thylacine*.

By modelling the body sizes of Australian monitors and dasyuromorphian marsupials using lineage interaction-informed PCMs, we find strong support for a narrative in which body size of these two groups evolved as a result of character displacement. This is corroborated by greater than expected functional diversity of monitor and marsupial assemblages (over dispersion). However, our results are somewhat surprising in that we do not find evidence of competition between marsupials and monitors. Instead, size evolution appears to have been dictated by within-clade character displacement, meaning monitors most strongly influence other monitors, and marsupials influence marsupials. Cursorily, this may seem counterintuitive, considering carnivorous marsupials and monitors largely overlap in diet and size, with small animals—monitors and marsupials alike—eating large invertebrates and small lizards, and larger animals taking larger vertebrate prey. Dasyuromorphian marsupials and monitors differ in one very basic way, which is their activity period. Both are active foragers, covering wide tracks of land in search of food, but while monitors are almost exclusively diurnal, often roaming during the hottest part of the day, nearly all dasyuromorphians are nocturnal. In this way, perhaps these two groups have come to coexist. While this sounds like a just-so story, consider other regions where monitors exist, but have not radiated in the same way as in Australia. Across Africa, the Indian subcontinent, and throughout Southeast Asia, monitor lizards compete with other diurnal carnivorans, such as herpestids (mongooses), viverrids (civets), canids (dogs), mustelids (weasels), and felids (cats). The possibility of competitive release upon reaching Australia provides a plausible explanation for the diversification of dwarf monitor species (Sweet and Pianka 2007).

While monitor lizards and marsupial predators appear to have diversified without outwardly influencing each others' trait evolution, both groups appear to have diverged according to character displacement occurring *within* their respective radiations. Character displacement has long been associated with trait divergence, and was principally described on shallow scales from observable

interactions among extant lineages (Vaurie 1951; Brown and Wilson 1956). The practice of extrapolating this idea to fit evolution on geological timescales fits the concept of a micro-to-macro evolutionary spectrum that is dictated by the same processes. The concept of competition as an impetus for evolution however, has been difficult to show explicitly from the fossil or phylogenetic record, and has been criticized for an unnecessarily "progressive" view of the process of evolution (Benton 1987). With the recent development of more appropriate process-generating models, we are now capable of better testing the influence of lineage interactions on evolutionary outcomes (Drury et al. 2016, 2018b; Manceau et al. 2017; Quintero and Landis 2019). In the case of monitor lizards, the exaggerated disparity in body sizes of Australian species is best described by an evolutionary model which accounts for competition among taxa in both space and time. This finding is further supported by evidence of overdispersion in body size variation within monitor communities, suggesting niche partitioning by body size is prevalent across the continent.

Conclusion

Monitors are an exceptional radiation of lizards capable of traversing sandy deserts and open ocean, living in the canopy and below ground. Here we present a comprehensive phylogenomic hypothesis of the genus, and place them among related varaniforme and anguimorph lizards. In agreement with previous study, we find that varanids likely originated in Eurasia in the late Cretaceous or early Paleocene, but have long been spread across Europe, North America, and Africa. Their greatest richness is found throughout Indo-Australia, and we suggest that the diversity of sizes of Australian monitors may be the result of a combination of competitive release from carnivorans, and character displacement among other monitor species. The methods used here to investigate the role of coevolutionary interactions on trait evolution can be broadly applied to any co-occuring lineages. We look forward to the further development of ecologically-aware comparative methods.

Supplementary Material

Equation 1. Following Manceau et al. (2017), we can estimate if lineage k is repelled from (-S) or attracted to (+S) the average trait value of the lineages it interacts with. S represents the the *strength* of the interaction on trait evolution. d_1 and d_2 represent the shift values for lineages from clade 1 and 2 respectively, with the expectation that d_1+d_2=0. δ_k equals one if lineage k belongs to clade 1, and zero it if belongs to clade 2, and $p_{k,l}$ equals one if lineages k and l interact (in our case it is assumed if they are sympatric) and zero otherwise. $n_k = \sum_l p_{k,l}$ is the number of lineages interacting with lineage k, and n is the total number of lineages.

$$dX_t^{(k)} = S\left(\delta_k d + (1-\delta_k)d_2 + \frac{1}{n_k}\sum_{l=1}^{n} p_{k,l}X_t^{(l)} - X_t^{(k)}\right)dt + \sigma dW_t^{(k)}$$

Table S1. Taxon sampling for this project.

Taxon	Tree ID	Accession Number	Locality
Elgaria	76547	ABTC 76547	Oregon, USA
Heloderma suspectum	—	SAMAR 55982	—
Plestiodon	81170	ABTC81170	—
Shinisaurus crocodilurus	—	—	—
Sphenodon punctata	—	—	—
Varanus acanthurus acanthurus	73877	WAMR 117242	Yilbrinna Pool, Australia
Varanus acanthurus brachyurus	29363	NTMR 20528	Cape Crawford, Australia
Varanus acanthurus insulanicus	29299	NTMR 19073	Guluwuru Island, Australia
Varanus albigularis albigularis	276340	MVZ 267340	Limpopo, South Africa
Varanus albigularis microstictus	6569	—	—
Varanus albigularis microstictus	146326	MVZ 146326	Gorongosa NP, Mozambique
Varanus albigularis microstictus	241148	UMFS 11448	Dodoma, Tanzania
Varanus albigularis microstictus	11448	UMFS 11448	Dodoma, Tanzania
Varanus auffenbergi	128036	WAMR 105802	Rote Ndau, Indonesia
Varanus balagardi	12689	NTMR 36799	Arnhemland, Australia
Varanus baritji	27680	NTMR 13150	Donydji, Australia
Varanus beccarrii	123673	UMMZ 225561	Aru Islands, Indonesia
Varanus bengalensis	123674	ABTC 123674	Captive (Baltimore Zoo)
Varanus bengalensis bengalensis	237483	MVZ 237483	Laghman Province, Afghanistan
Varanus bengalensis irrawadicus	213887	CAS 213887	Magwe Division, Myanmar
Varanus bitatawa	320000	KU 320000	Barangay Casapsipan, Philippines
Varanus brevicauda	73900	WAMR 90898	Woodstock Station, Australia
Varanus bushi	73996	WAMR 108999	Marandoo, Australia
Varanus caudolineatus	73929	WAMR 122576	Australia
Varanus cumingi	314128	KU 314128	Barangay San Marcos, Philippines
Varanus doreanus	123507	BPBM 19509	Mount Obree, Papua New Guinea
Varanus doreanus	123675	UMMZ 227117	Merauke, Indonesia
Varanus douarrha	125037	ABTC 125037	New Ireland, Papua New Guinea
Varanus eremius	37872	SAMAR 49961	Purni Bore, Australia
Varanus eremius	42007	SAMAR 48779	Mt. Lindsay, Australia
Varanus eremius	73948	WAMR 121347	Australia
Varanus eremius	73949	WAMR 121348	Australia
Varanus exanthematicus	238934	MVZ 238934	Gbele Resource Reserve, Ghana
Varanus exanthematicus	6057	UWBM 6057	Duidan Iddar, Nigeria
Varanus finschi	125053	ABTC 125053	Kokopo, Papua New Guinea
Varanus flavescens	67500	UF 67500	Sindh Province, Pakistan
Varanus giganteus	55364	SAMAR 20988	Oodnadatta, Australia
Varanus gilleni	28330	NTMR 13778	Australia
Varanus glauerti	28473	ABTC 28473	Bungle Bungles, Australia
Varanus glauerti	68011	NTMR 24867	Bradshaw Station, Australia
Varanus glauerti	120594	ABTC 120594	Mt. Elizabeth Station, Australia
Varanus glebopalma	13424	ABTC 13424	Adelaide River, Australia
Varanus gouldii	76594	ABTC 76594	Katherine, Australia
Varanus gouldii flavirufus	55372	SAMAR 24554	Etadunna Station, Australia
Varanus gouldii flavirufus	55374	SAMAR 24717	Australia
Varanus gouldii gouldii	42245	SAMAR 50146	Sentinel Hill, Australia
Varanus gouldii gouldii	55369	SAMAR 22941	Perth, Australia
Varanus gouldii gouldii	73981	WAMR 117288	Doole Island, Australia
Varanus griseus caspius	19576	ZISP 19576	Chardjou Region, Turkmenistan
Varanus griseus caspius	243548	MVZ 243548	Sistan and Baluchistan Province, Iran
Varanus griseus griseus	123677	UMMZ 238881	-
Varanus griseus griseus	235860	MVZ 235860	Nouakchott, Mauritania
Varanus griseus griseus	236611	MVZ 236611	Al Hudaydah, Yemen
Varanus hamersleyensis	73991	WAMR 125100	Newman, Australia
Varanus indicus	13465	ABTC 13465	Maningrida, Australia

Taxon	Tree ID	Accession Number	Locality
Varanus indicus	123510	BPBM 20841	Rossel Island, Papua New Guinea
Varanus jobiensis	123517	BPBM 19510	Dorobisoro, Papua New Guinea
Varanus jobiensis	123678	ABTC 123678	Papua, Indonesia
Varanus kingorum	73986	WAMR 136382	Turkey Creek, Australia
Varanus komodoensis	75731	—	Captive (Taronga Zoo)
Varanus komodoensis	genome	—	—
Varanus marmoratus	323435	KU 323435	Barangay Villa Aurora, Philippines
Varanus mertensi	29528	NTMR 21389	Musselbrook Reservoir, Australia
Varanus mitchelli	29643	NTMR 21745	Litchfield NP, Australia
Varanus niloticus South	6484	ABTC 6484	—
Varanus niloticus South	1048	ELI 1048	Rumonge, Burundi
Varanus niloticus South	267341	MVZ 267341	Limpopo, South Africa
Varanus niloticus South	519	DMP 519	Edea, Cameroon
Varanus niloticus South	207622	CAS 207622	Bioko Id, Equatorial Guinea
Varanus stellatus	19410	PEM R 19410	Sierra Leone
Varanus stellatus	6058	UWBM 6058	Bvi NP, Ghana
Varanus nuchalis	305153	KU 305153	Barangay Camalanda-an, Philippines
Varanus olivaceus	322186	ABTC 126105	Philippines
Varanus palawanensis	309607	KU 309607	Palawan, Philippines
Varanus panoptes horni	49509	AMSR 121162	Wipim, Papua New Guinea
Varanus panoptes horni	123680	UMMZ 227307	Merauke, Indonesia
Varanus panoptes panoptes	32035	ABTC 32035	Rosebank Station, Australia
Varanus panoptes panoptes	55360	NTMR 10690	Alligator Head, Australia
Varanus panoptes panoptes	72783	—	Smithburne River, Australia
Varanus panoptes rubidus	10570	ABTC 10570	Yuinmery Station, Australia
Varanus panoptes rubidus	73987	WAMR 102099	Mt. Cotton, Australia
Varanus pilbarensis	128167	WAMR 163916	Goldsworthy, Australia
Varanus prasinus	47926	ABTC 47926	Wau, Papua New Guinea
Varanus prasinus	123520	BPBM 18696	Apele, Papua New Guinea
Varanus prasinus	123719	BPBM 18695	Dorobisoro, Papua New Guinea
Varanus primordius	29219	NTMR 17884	Elizabeth Downs Station, Australia
Varanus rosenbergi	14520	AMSR 123331	Kulnura, Australia
Varanus rudicollis	123681	R OM24456	Kalimantan, Indonesia
Varanus salvadorii	6571	ABTC 6571	Papua New Guinea
Varanus salvator macromaculatus	123682	UMMZ 225562	Rantra Prapat, Indonesia
Varanus salvator macromaculatus	212911	CAS 212911	Ayeyarwade Division, Myanmar
Varanus samarensis	335263	KU 335263	Barangay Danicop, Philippines
Varanus scalaris	6488	WAMR 77223	Mitchell Plateau, Australia
Varanus scalaris	28166	ABTC 28166	Katherine Gorge, Australia
Varanus scalaris	98731	ABTC 98731	Wegamu, Papua New Guinea
Varanus scalaris	55389	ABTC 55389	Scotts Creek, Australia
Varanus semiremex	76546	ANWCR 6121	Cooktown, Australia
Varanus sparnus	122505	WAMR 168475	Coulomb Point, Australia
Varanus spenceri	28864	ABTC 28864	Tablelands Highway, Australia
Varanus spinulosus	123428	ABTC 123428	Isabel, Solomon Islands
Varanus spinulosus	123429	ABTC 123429	Isabel, Solomon Islands
Varanus storri	72742	SAMAR 54351	Mount Isa, Australia
Varanus timorensis	128038	WAMR 105914	Semau, Indonesia
Varanus togianus	123683	ABTC 123683	Sulawesi, Indonesia
Varanus tristis	12202	SAMAR 38779	Tennant Creek, Australia
Varanus tristis	55388	SAMAR 32491	Coongie, Australia
Varanus tristis	72892	SAMAR 54476	Torrens Creek, Australia
Varanus varius	24249	ABTC 24249	Kroombit Tops, Australia
Varanus yemenensis	236610	MVZ 236610	Al Hudaydah, Yemen
Xenosaurus grandis	137786	—	—

Table S2. Per locus best fitting models of molecular evolution, determined by IQ-TREE and the Bayesian Information Criterion (BIC). Independent gene trees were estimated using the preferred model, and 1,000 ultrafast bootstraps.

Locus	Site Model	Locus	Site Model	Locus	Site Model
L1	K3Pu+F+R3	L131	HKY+F+G4	L260	TIM2e+R3
L2	K3Pu+F+R3	L132	K3Pu+F+R3	L261	K2P+R3
L3	TIM+F+R3	L133	HKY+F+G4	L262	GTR+F+R3
L4	TN+F+R2	L134	K3Pu+F+R3	L263	HKY+F+G4
L5	TVM+F+R3	L135	HKY+F+R3	L264	TIM+F+R3
L6	TIMe+G4	L136	TPM3u+F+G4	L265	HKY+F+R3
L7	TIM+F+R3	L137	TIM3e+G4	L266	K3P+R3
L8	HKY+F+R3	L138	HKY+F+G4	L267	TVM+F+I+G4
L9	K2P+R2	L139	K2P+G4	L268	HKY+F+R2
L10	K3Pu+F+G4	L140	K2P+R3	L269	TIM+F+R3
L11	HKY+F+G4	L141	K2P+R2	L270	K3P+R3
L12	HKY+F+G4	L142	TIM2e+R3	L271	TPM2u+F+I+G4
L13	TIM+F+R3	L143	TN+F+R3	L272	TNe+G4
L14	K2P+G4	L144	HKY+F+G4	L273	TIM+F+R3
L15	K2P+G4	L145	HKY+F+G4	L274	TPM2u+F+R3
L16	HKY+F+R2	L146	K2P+R3	L275	TPM2u+F+R3
L17	TNe+R2	L147	TIM+F+R3	L276	TIM3+F+R2
L18	TNe+I	L148	TN+F+R2	L277	TN+F+G4
L19	HKY+F+I+G4	L149	HKY+F+R3	L278	K3P+I+G4
L20	HKY+F+G4	L150	HKY+F+G4	L279	HKY+F+G4
L21	TNe+R2	L151	HKY+F+G4	L281	K2P+G4
L22	TIM2e+R3	L152	K2P+R2	L282	TVMe+I+G4
L23	K2P+R3	L153	TN+F+R2	L283	TIM2e+R2
L24	TIM+F+R3	L154	K2P+G4	L284	TN+F+R2
L25	K3Pu+F+R3	L155	TN+F+G4	L285	HKY+F+G4
L27	HKY+F+G4	L156	K3Pu+F+G4	L286	TPM2u+F+R3
L28	HKY+F+G4	L157	HKY+F+G4	L287	HKY+F+G4
L29	K3Pu+F+R2	L158	TIM2+F+I+G4	L288	TN+F+R3
L30	K3Pu+F+G4	L159	HKY+F+R3	L289	K2P+R3
L31	K3Pu+F+I+G4	L160	TIM2+F+G4	L290	GTR+F+R2
L32	TN+F+R3	L161	TPM3u+F+R3	L291	TIM2+F+I+G4
L33	HKY+F+G4	L162	K2P+G4	L292	TN+F+G4
L34	HKY+F+G4	L163	HKY+F+G4	L293	HKY+F+R3
L35	TPM3u+F+R3	L164	K3Pu+F+R2	L294	TPM2+F+G4
L36	TIM2+F+G4	L165	K3P+G4	L295	HKY+F+I
L37	TIM3e+R2	L166	HKY+F+G4	L296	TNe+R2
L38	TIM3+F+R3	L167	HKY+F+R2	L297	TVMe+I+G4
L39	K3P+R3	L168	HKY+F+I	L298	K3P+I+G4
L40	HKY+F+R3	L169	HKY+F+G4	L299	HKY+F+R2
L41	TPM2u+F+I+G4	L170	K3P+R3	L300	HKY+F+R3
L42	TIM+F+R3	L171	K3Pu+F+R3	L301	TPM2+F+G4
L43	TIM+F+R2	L172	TIM3+F+G4	L302	TN+F+R3
L44	TPM3+F+G4	L173	HKY+F+R3	L303	K3P+R3
L45	HKY+F+G4	L174	HKY+F+G4	L304	HKY+F+G4
L46	HKY+F+G4	L175	TIM+F+G4	L305	JC
L47	HKY+F+R3	L176	K3Pu+F+I	L306	TIM3+F+G4
L48	HKY+F+R3	L177	TVM+F+R4	L307	SYM+R3
L49	TIM+F+R3	L178	TN+F+R2	L308	K2P+G4
L50	K2P+R2	L179	TIM3+F+R3	L309	TNe+R3
L51	TN+F+R3	L180	K2P+G4	L310	K3P+G4
L52	K3Pu+F+R3	L181	HKY+F+G4	L311	HKY+F+R3
L53	TIM2e+R2	L182	HKY+F+G4	L312	HKY+F+G4
L54	TPM2+F+G4	L183	HKY+F+R2	L313	TIM+F+R3

Locus	Site Model	Locus	Site Model	Locus	Site Model
L55	HKY+F+G4	L184	TPM3u+F+G4	L314	K3Pu+F+R2
L56	HKY+F+G4	L185	K3Pu+F+G4	L315	TIMe+R3
L57	HKY+F+R2	L186	TIMe+R3	L316	TVMe+R3
L58	K3Pu+F+R2	L187	F81+F+G4	L317	K3Pu+F+G4
L59	TIM+F+R3	L188	TIM3+F+R2	L318	TN+F+I+G4
L60	TN+F+R3	L189	HKY+F+R3	L319	TN+F+G4
L61	TIM3+F+R3	L190	HKY+F+G4	L320	HKY+F+I+G4
L62	TIM3+F+R3	L191	TPM3u+F+R3	L321	TNe+R2
L63	TN+F+R3	L192	HKY+F+G4	L322	TVM+F+R3
L64	HKY+F+G4	L193	TN+F+G4	L323	K3P+R3
L65	HKY+F+G4	L194	HKY+F+R2	L324	HKY+F+R2
L66	TIM2+F+R3	L195	HKY+F+G4	L325	TIM+F+R3
L67	HKY+F+G4	L196	HKY+F+R2	L326	TIMe+R3
L68	HKY+F+G4	L197	TNe+R2	L327	TN+F+G4
L69	TPM3u+F+R3	L198	TPM2u+F+G4	L328	TN+F+I
L70	TN+F+R2	L199	HKY+F+G4	L329	K3Pu+F+I+G4
L71	GTR+F+I+G4	L200	TIM2+F+R3	L330	GTR+F+R3
L72	HKY+F+R3	L201	K3Pu+F+R3	L331	GTR+F+R3
L73	TPM2u+F+I+G4	L202	TIM+F+R3	L332	HKY+F+G4
L74	HKY+F+G4	L203	K2P+G4	L333	TVMe+R3
L75	TN+F+G4	L204	TPM3u+F+R2	L334	K2P+R2
L76	HKY+F+I+G4	L205	TN+F+R3	L335	K3P+G4
L77	HKY+F+G4	L206	HKY+F+G4	L336	HKY+F+G4
L78	TPM3u+F+R3	L207	HKY+F+R3	L337	K2P+G4
L79	TN+F+G4	L208	TN+F+G4	L338	HKY+F+R2
L80	TIM+F+R3	L209	K2P+R2	L339	HKY+F+R2
L81	K2P+G4	L210	K3P+G4	L340	TIM+F+R3
L82	TIM2+F+G4	L211	HKY+F+G4	L341	K2P+G4
L83	K3Pu+F+R3	L212	K3Pu+F+G4	L342	K2P+R3
L84	TIM3e+I+G4	L213	K3Pu+F+G4	L343	TIM+F+R3
L85	TPM2u+F+G4	L214	K3Pu+F+G4	L344	HKY+F+G4
L86	HKY+F+R3	L215	TPM2+F+I	L345	TIM2+F+G4
L87	K3Pu+F+R3	L216	TIMe+R2	L346	K3P+R2
L88	K2P+R2	L217	HKY+F+I+G4	L347	TIM3+F+G4
L89	K2P+I	L218	TPM3u+F+R3	L348	TPM3u+F+R2
L90	TN+F+R2	L219	GTR+F+I+G4	L349	K3Pu+F+R2
L91	TIM2+F+R3	L220	TVM+F+R2	L350	TIM+F+R3
L92	TN+F+R2	L221	TIMe+I+G4	L351	K2P+G4
L93	TN+F+R3	L222	GTR+F+G4	L352	TPM2+F+G4
L94	TN+F+G4	L223	K3P+R3	L353	K3Pu+F+R3
L95	HKY+F+R2	L224	K2P+R3	L354	TPM2u+F+R3
L96	K2P+G4	L225	TNe+G4	L355	HKY+F+R3
L97	HKY+F+R2	L226	K2P+R3	L356	TIM+F+R2
L98	K2P+G4	L227	K3P+R3	L357	HKY+F+G4
L99	TIM+F+G4	L228	TIM+F+G4	L358	HKY+F+G4
L100	TN+F+R2	L229	TPM3u+F+R3	L359	K3P+R3
L101	HKY+F+R3	L230	TIM+F+R3	L360	TIM+F+R3
L102	K2P+I+G4	L231	K3Pu+F+R3	L361	HKY+F+G4
L103	K3P+R2	L232	TIM+F+G4	L362	TPM3u+F+R2
L104	TPM2u+F+R3	L233	HKY+F+I	L363	TIM+F+R3
L105	HKY+F+R3	L234	K2P+G4	L364	K3P+G4
L106	HKY+F+R3	L235	K2P+I	L365	HKY+F+R2
L107	HKY+F+G4	L236	TN+F+G4	L366	TPM3+F+G4
L108	K2P+I+G4	L237	TPM3+F+R3	L367	TN+F+R4
L109	K2P+G4	L238	K3P+G4	L368	TN+F+G4
L110	TIM+F+I+G4	L239	K2P+G4	L369	HKY+F+R2
L111	TN+F+R3	L240	TN+F+R3	L370	K3Pu+F+R2

Locus	Site Model	Locus	Site Model	Locus	Site Model
L112	TN+F+R3	L241	HKY+F+G4	L371	K3P+R3
L113	K3Pu+F+G4	L242	HKY+F+G4	L372	K3Pu+F+G4
L114	HKY+F+G4	L243	TPM2u+F+R2	L373	K2P+G4
L115	HKY+F+G4	L244	HKY+F+G4	L374	HKY+F+G4
L116	K3Pu+F+G4	L245	K3Pu+F+G4	L375	HKY+F+R2
L117	HKY+F+R3	L246	HKY+F+G4	L376	HKY+F+R3
L118	HKY+F+R3	L247	HKY+F+G4	L377	K3Pu+F+G4
L119	TN+F+R3	L248	TPM3+F+G4	L378	HKY+F+G4
L120	TN+F+R3	L249	TN+F+R3	L379	HKY+F+G4
L121	HKY+F+G4	L250	TNe+R2	L380	HKY+F+R3
L122	HKY+F+G4	L251	K2P+G4	L381	K2P+R3
L123	K3Pu+F+G4	L252	K3P+G4	L382	TNe+R3
L124	HKY+F+R2	L253	TIMe+G4	L383	HKY+F+R3
L125	K3Pu+F+R3	L254	K2P+G4	L384	TPM2u+F+R3
L126	TVM+F+G4	L255	HKY+F+G4	L385	TN+F+G4
L127	TVMe+R2	L256	HKY+F+R2	L386	K3Pu+F+I
L128	K2P+G4	L257	TVMe+R3	L387	HKY+F+R2
L129	TPM2u+F+R3	L258	SYM+R3	L388	TIM+F+R3
L130	HKY+F+G4	L259	TNe+R3	L389	TN+F+R2
				L390	HKY+F+I+G4

Table S3. RogueNaRok scores for disruptive samples, which were ultimately pruned from final dating analyses.

taxon	rawImprovement	RBIC
Aiolosaurus oriens	0.611000	0.840256
Paravaranus angustifrons	0.441300	0.852011
Palaeosaniwa	0.505000	0.811362
Varanus rusingensis	0.512000	0.836463
Varanus dumerilii	0.672919	0.895830

Simulation Exercise

Table S4. We simulated traits onto our empirical trees under the parameters below.

Model	σ	α
Brownian Motion	0.003, 0.03, 0.3	0
Ornstein-Uhlenbeck	0.3	0.03, 0.06, 0.12

Model	m_0	v_0	d_1	d_2	σ	S_1	S_2
CoEvo	0	0	-0.01	0.01	0.3	-0.001, -0.01, -0.1, -1	—
$\text{CoEvo}_{\text{all}}$	0	0	-0.01	0.01	0.3	-0.001, -0.01, -0.1, -1	—
CoPM_{geo}	0	0	-0.01	0.01	0.3	-0.001, -0.01, -0.1, -1	—
$\text{JointPM}_{\text{geo}}$	0	0	-0.01	0.01	0.3	-0.001, -0.01, -0.1, -1	-0.005, -0.05, -0.5, -5
$\text{CoEvo}_{\text{split}}$	0	0	-0.01	0.01	0.3	-0.001, -0.01, -0.1, -1	-0.005, -0.05, -0.5, -5

Empirical Model Fitting

Table S5. Model fitting results to accompany Figure 6.

Model	logLik	Param.	AIC	AICc	deltaAICc	AICcWt
$CoPM_{geo}$	-23.90383	6	59.80767	60.78441	0.000000	0.484718461
$JointPM_{geo}$	-23.73944	7	61.47888	62.79653	2.012117	0.177240890
$CoEvo_{Split}$	-23.83223	7	61.66447	62.98212	2.197701	0.161534338
$CoEvo_{all}$	-25.49440	6	62.98880	63.96554	3.181127	0.098790805
BM_{shared}	-29.90901	3	65.81802	66.08768	5.303269	0.034190017
CoEvo	-27.22316	6	66.44632	67.42307	6.638654	0.017535744
BM_{ind}	-29.77132	4	67.54264	67.99719	7.212771	0.013160008
OU_{shared}	-29.90844	4	67.81688	68.27142	7.487007	0.011473783
OU_{ind}	-29.78290	6	71.56580	72.54254	11.75812	0.001355954

Table S6. Model fitting results to accompany Figure S4.

Model	logLik	Param.	AIC	AICc	deltaAICc	AICcWt
$CoPM_{geo}$	-23.90383	6	59.80767	60.78441	0.0000000	0.2750436948
CoPM	-24.00661	6	60.01322	60.98997	0.2055527	0.2481798347
$JointPM_{geo}$	-23.73944	7	61.47888	62.79653	2.0121169	0.1005717613
JointPM	-23.81588	7	61.63177	62.94942	2.1650026	0.0931702707
$CoEvo_{Split}$	-23.83223	7	61.66447	62.98212	2.1977010	0.0916593953
GMM_{all}	-25.28098	6	62.56195	63.53870	2.7542820	0.0693932078
$CoEvo_{all}$	-25.49440	6	62.98880	63.96554	3.1811274	0.0560568457
GMM	-26.43762	6	64.87524	65.85199	5.0675740	0.0218268965
BM_{shared}	-29.90901	3	65.81802	66.08768	5.3032690	0.0194004344
CoEvo	-27.22316	6	66.44632	67.42307	6.6386539	0.0099503035
BM_{ind}	-29.77132	4	67.54264	67.99719	7.2127713	0.0074673808
OU_{shared}	-29.90844	4	67.81688	68.27142	7.4870071	0.0065105660
OU_{ind}	-29.78290	6	71.56580	72.54254	11.758126	0.0007694085

Table S7. Model fitting results for *Varanus* only analyses. The $PMOU_{geo}$ model is identical to the PM_{geo} model, but without the alpha/psi parameter of the OU process, meaning traits are not constrained to evolve around a single optimum value.

Model	logLik	Param.	AIC	AICc	deltaAICc	AICcWt
$PMOU_{geo}$	-6.503810	4	21.00762	22.54608	0.000000	0.67565891
BM	-7.963686	4	23.92737	25.46583	2.919753	0.15693186
OU	-7.367979	5	24.73596	27.13596	4.589877	0.06808452
PM_{geo}	-5.955623	6	23.91125	27.41125	4.865166	0.05932944
OUM	-6.349967	6	24.69993	28.19993	5.653854	0.03999527

Table S8. Node prior information. Bolded clades indicate priors which were constrained to be monophyletic. In our taxon sampling: **Lepidosauria** represents the root (all taxa—Rhynchocephalians + Squamata); **Anguimorpha** comprises all taxa to the exclusion of *Sphenodon* and *Plestiodon*; Neoanguimorpha comprises *Heloderma*, *Xenosaurus*, and *Elgaria*; *Saniwa feisti* represents the split between *Lanthanotus* and *Varanus*; and *Varanus rusingensis* is the oldest discernible crown *Varanus*.

Fossil Taxon	Min.Age	Max.Age	Clade	Calibration
Vellberg Jaw	238	—	**Lepidosauria**	Exp.; M=10, Off=238
Dalinghosaurus	113	—	**Anguimorpha**	Log; M=2, S=1, Off=113
Primaderma	98	—	Neoanguimorph	Exp.; M=4, Off=98
Saniwa ensidens	48	—	*Lan.* + *Varanus*	Gamma; A=2, B=8, Off=45
Varanus rusingensis	16	—	Crown *Varanus*	Gamma; A=2, B=8, Off=16

Node Priors and *Varanus* in the Fossil Record

Monitor lizards and their relatives are not rare in the fossil record, however the phylogenetic affinities of fossil taxa have been difficult to resolve. This is perhaps best captured by Ralph Molnar in his chapter titled *The Long and Honorable History of Monitors and their Kin* (Molnar 2004):

> "Although some of the Cretaceous monitors, particularly those from Mongolia, are known from nice skulls, words like 'fragmentary' and 'frustrating' involuntarily spring to mind when conisdering the fossil record of varanids, particularly of *Varanus* itself."

To calibrate our phylogeny, we used a combination of node and tip priors to incorporate fossil taxa that were directly sampled (tips) in morphological data or indirectly sampled (nodes) using estimated fossil ages. Previous studies of monitor lizards have used varied calibration schemes to estimate divergence times. The most influential of these has been the application of a hard minimum prior on the crown age of *Varanus* (Vidal et al. 2012; Portik and Papenfuss 2012). This minimum bound is either attributed to the age of the 'Jebel Qatrani *Varanus*' (Holmes et al. 2010), or the 'Yale Quarry *Varanus*' (Smith et al. 2008). Based on morphological analyses of monitors and their kin (Conrad et al. 2012; Ivanov et al. 2017), these fragmentary fossils are not recovered within the crown of *Varanus* and are more likely stem varanids, suggesting that they should not be used to constrain the minimum age of extant *Varanus*.

There are however rumors of additional *Varanus* fossil material. Stirton (1961) mentioned varanid material from the Etadunna formation, however this material was misattributed, and appears to actually have been a snake (Estes 1984). Estes (1984) further went on to briefly discuss the existence of *Varanus* fossil material from the Mid Miocene Lake Ngapakaldi area, though these vertebrae have not since been described. The same goes for Oligo-Miocene material mentioned by Scanlon (2014), which comes from the Hiatus and White Hunter sites of Riversleigh World Heritage Area (Scanlon 2014). Interestingly, the Riversleigh material contains "the occasional isolated tooth, jaw element, or limb or girdle bone" in addition to the more common vertebrae. Hiatus and White Hunter sites have been dated via biocorrelation (15–25 mya), but could not be radiometrically dated (Woodhead et al. 2016). Finally, also mentioned by Scanlon (2014) are Miocene fossils from Bullock Creek and Alcoota, which are roughly 11-16 mya and 5-12 mya respectively (Murray & Megirian, 1992), but have not been described, evaluated, or scored. Many of these fossils would be

particularly valuable for dating the Australian radiation of *Varanus*, but again cannot be placed within the crown of Australian *Varanus* (*Odatria* + *Varanus*), and so should probably only be used to provide a minimum age on the divergence between the Australian radiation and the Asian clade (*Soterosaurus*, *Empagusia*, *Euprepriosuarus*, *Hapturosaurus*, et al.). We outline the node calibrations we did apply in our analyses in Table S8.

Nested Models

We can show that some of the proposed models are nested. We start by simulating data under the simplest intraclade interaction model CoPM_{geo}.

```
simCoPM_geo <- simulateTipData(modelCoPM_geo, method=1,
                  c(m0=0, v0=0, d1=-0.001, d2=0.001, S=-0.1, sigma=0.1))
```

We can then fit the $\text{JointPM}_{\text{geo}}$, CoPM_{geo}, and $\text{CoEvo}_{\text{split}}$ models, using the *getDataLikelihood* function, keeping all other parameters the same.

```
getDataLikelihood(modelCoPM_geo, simCoPM_geo,
                  c(m0=0, v0=0, d1=-0.001, d2=0.001, S=-0.1, sigma=0.1))
getDataLikelihood(modelJointPM_geo, simCoPM_geo,
                  c(m0=0, v0=0, d1=-0.001, d2=0.001, S=-0.1, sigma=0.1, S2=-0.1))
getDataLikelihood(modelCoEvo_Split, simCoPM_geo,
                  c(m0=0, v0=0, d1=-0.001, d2=0.001, S=0, sigma=0.1, S2=-0.1))
```

These result in near identical log-likelihood values, showing that the $\text{JointPM}_{\text{geo}}$ and $\text{CoEvo}_{\text{split}}$ models collapse into the CoPM_{geo} model when $S_1{=}S_2$, and when $S_1{=}0$, respectively.

We can further show that the CoEvo and $\text{CoEvo}_{\text{all}}$ models are special cases of the $\text{CoEvo}_{\text{split}}$ model.

```
simCoEvo <- simulateTipData(modelCoEvo_Split, method=1,
                  c(m0=0, v0=0, d1=-0.001, d2=0.001, S=-0.1, sigma=0.1))
simCoEvo_all <- simulateTipData(modelCoEvo_all, method=1,
                  c(m0=0, v0=0, d1=-0.001, d2=0.001, S=-0.1, sigma=0.1))
```

We then estimate the likelihood for CoEvo and $\text{CoEvo}_{\text{split}}$ models to the first dataset, and $\text{CoEvo}_{\text{all}}$ and $\text{CoEvo}_{\text{split}}$ models to the second dataset.

```
getDataLikelihood(modelCoEvo, simCoEvo,
                  c(m0=0, v0=0, d1=-0.001, d2=0.001, S=-0.1, sigma=0.1))
getDataLikelihood(modelCoEvo_Split, simCoEvo,
                  c(m0=0, v0=0, d1=-0.001, d2=0.001, S=-0.1, sigma=0.1, S2=0))

getDataLikelihood(modelCoEvo_all, simCoEvo_all,
                  c(m0=0, v0=0, d1=-0.001, d2=0.001, S=-0.1, sigma=0.1))
getDataLikelihood(modelCoEvo_Split, simCoEvo_all,
                  c(m0=0, v0=0, d1=-0.001, d2=0.001, S=-0.1, sigma=0.1, S2=-0.1))
```

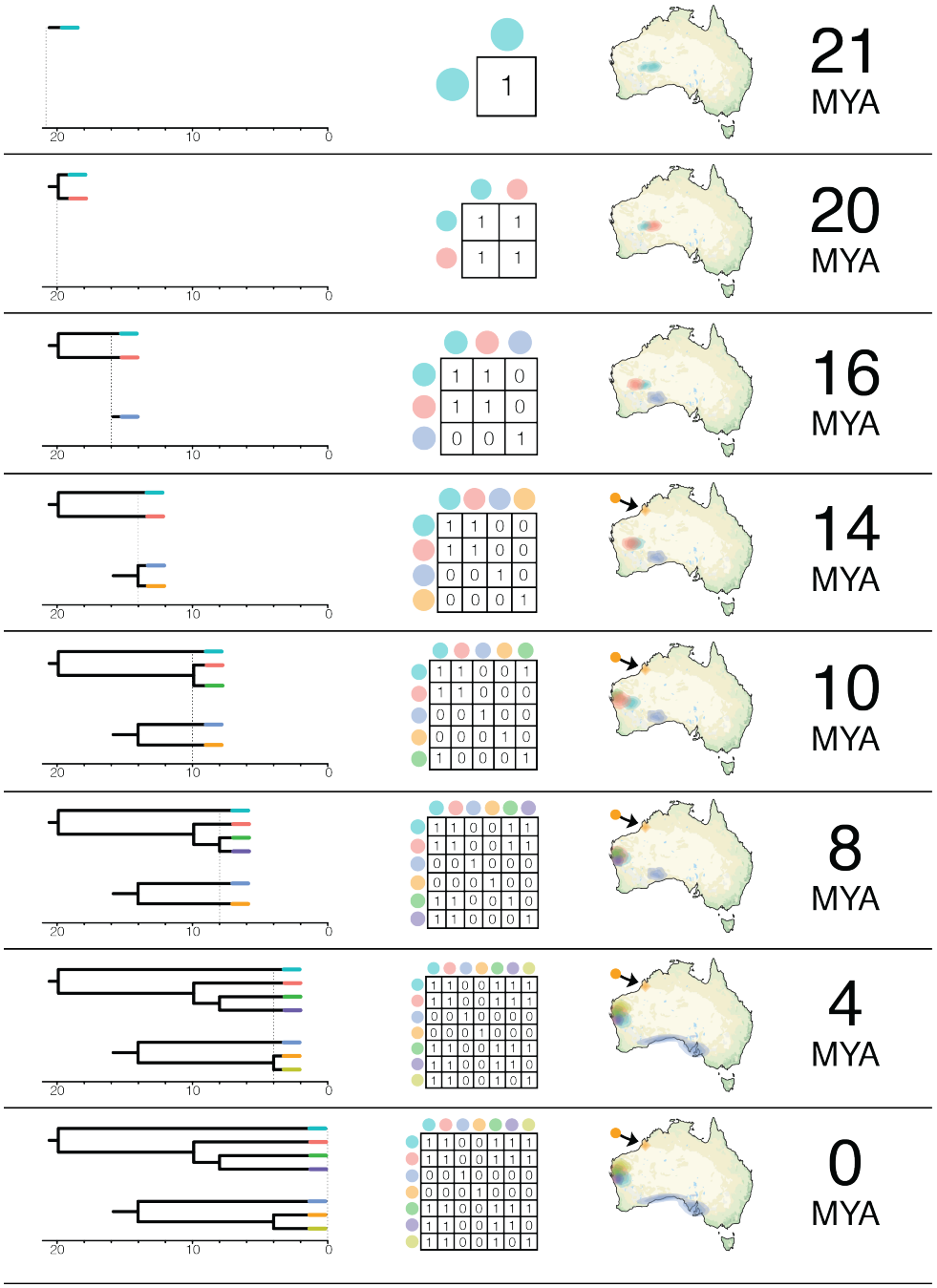

Figure S1: Diagram of the construction of interaction matrices P through time in geographically-informed models, using the CoEvo-all model as an example. Ancestral ranges were estimated using *rase*. The process of constructing these matrices is incorporated into the function CreateCoEvoGeoObject-SP, which takes as input the the trees, and two processed *rase* objects—one for each clade.

Investigating Data Completeness and Informativeness

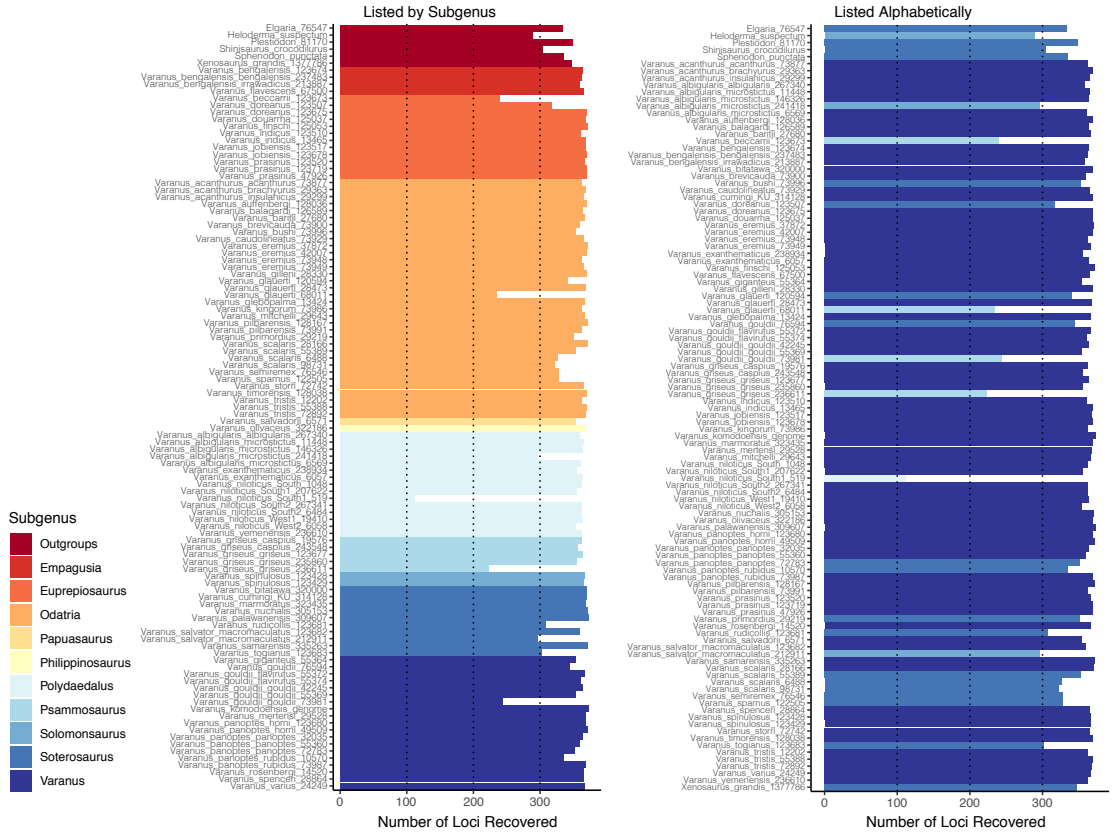

Figure S2: Number of loci recovered per sample for all *Varanus* and outgroup taxa included in the molecular data.

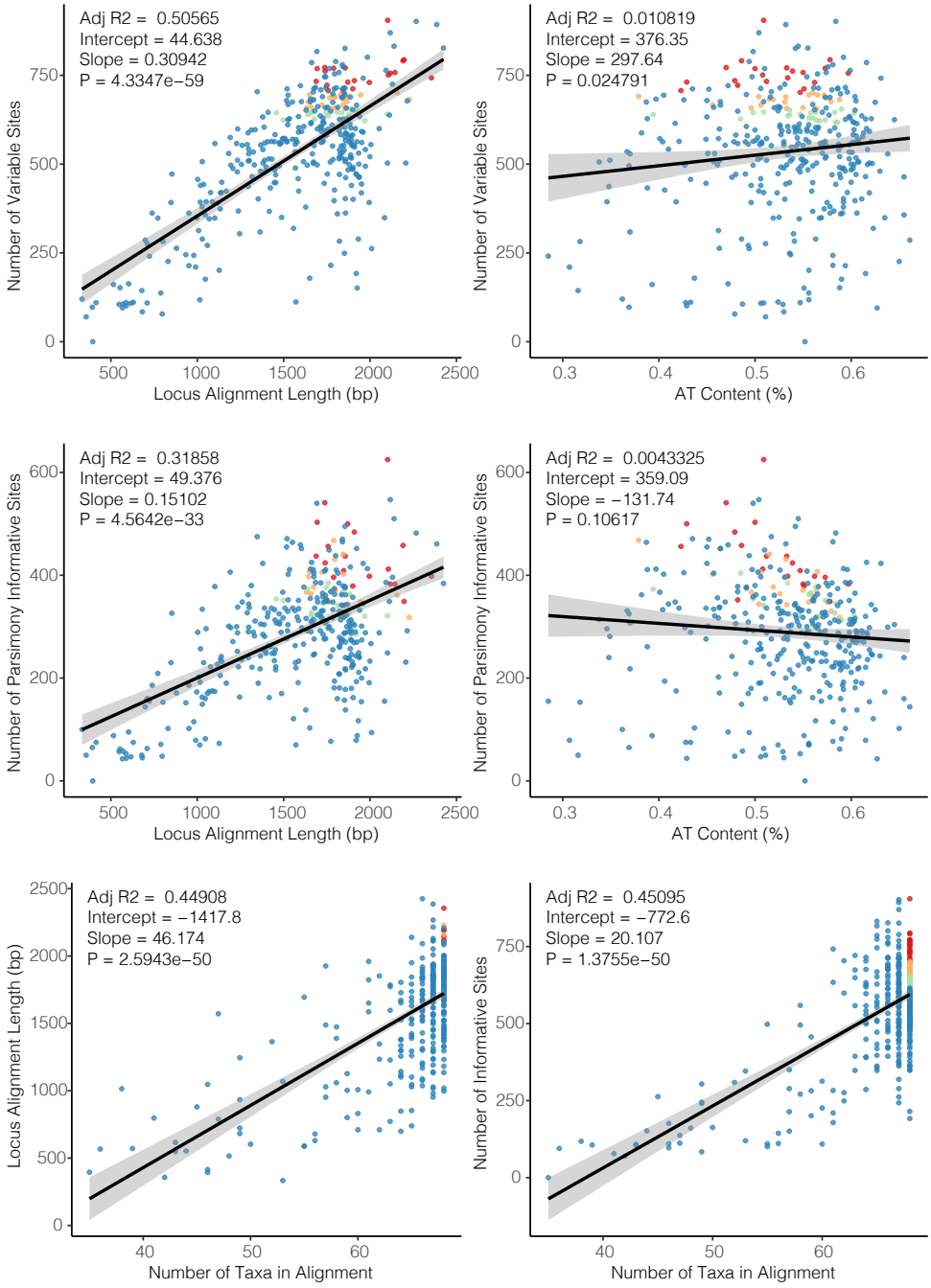

Figure S3: Plots of individual locus completeness and informativeness. For the StarBEAST2 species tree analyses, loci were ordered first by completeness (number of taxa in alignment), then by variable sites. They were then partitioned into 3 sets of twenty loci, and are color coded in these plots: 'top twenty' (1-20: red), 'second twenty' (21-40: orange), 'third twenty' (41-60: green), and all others (blue). Top row shows the number of variable sites in each alignment as a function of alignment length and AT content. The middle row shows the number of parsimony informative sites as a function of alignment length and AT content. The bottom row shows alignment length and number of variable sites as a function of completeness.

Testing for Fossil Taxa as Sampled Ancestors

Given that we place a prior on the age of each taxon (τ) and are jointly estimating their position among the phylogeny, including a model (M) of the molecular and morphological evolution, we can sample exclusively from both the prior and posterior of our starBEAST2 analyses. We used a threshold of log(BF) > 1 to identify sampled ancestors, log(BF) < -1 to recognize terminal taxa, and -1 < log(BF) < 1 taxa were categorized as equivocal. To calculate Bayes Factors for fossil taxa as sampled ancestors:

$$BF = \frac{P(H_1|D,\tau,M)P(H_2|\tau,M)}{P(H_2|D,\tau,M)P(H_1|\tau,M)} = \frac{P(Posterior_{ancestor})P(Prior_{tip})}{P(Posterior_{tip})P(Prior_{ancestor})}$$

Figure S4: Bayes Factors support the position of nearly all fossil taxa as terminals. Green circles are strongly supported as terminal taxa, and black circles denote equivocal assignment. Very low log BF scores (taxa nearly always sampled as terminals) are reported arbitrarily as -5 to facilitate visualization.

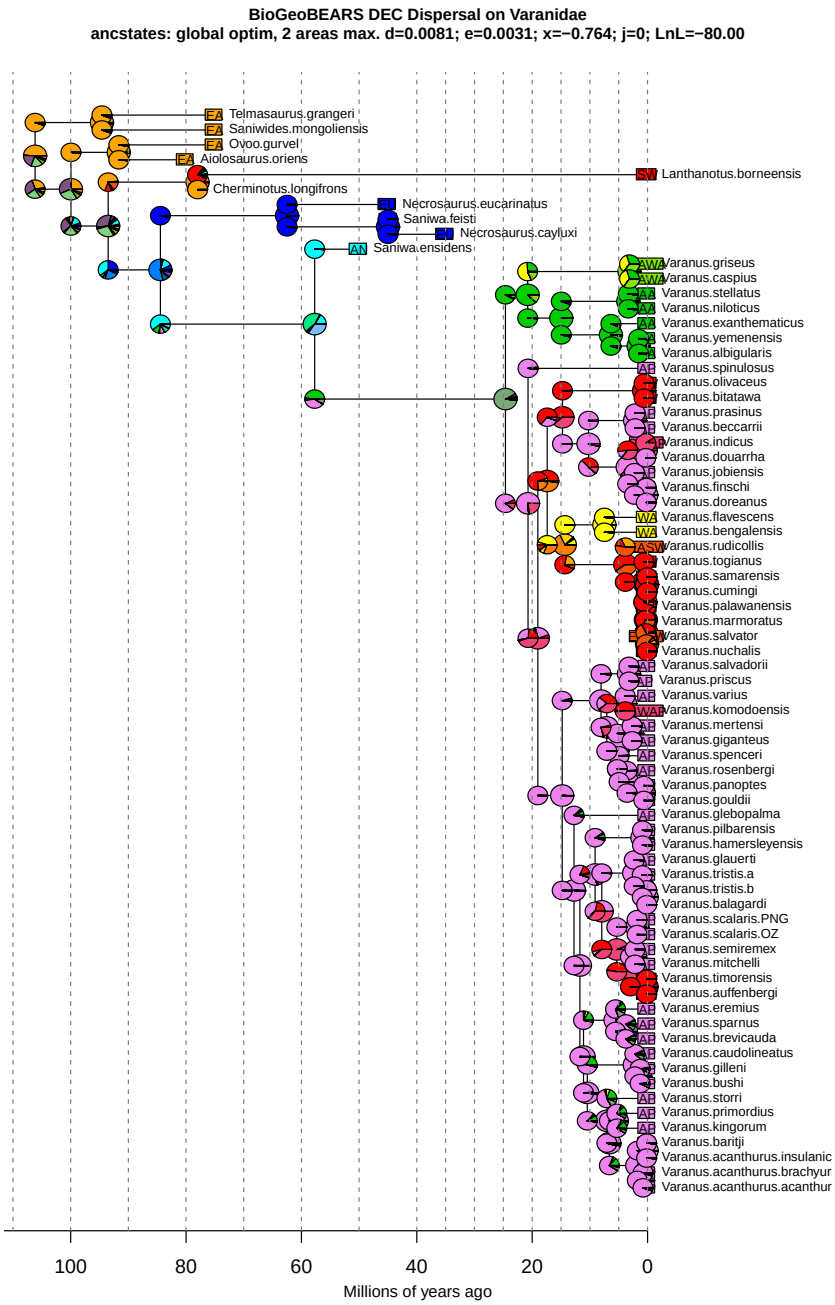

Figure S5: BioGeoBEARS ancestral state reconstruction under the DEC model with dispersal probability modelled as a function of distance among areas.

Model Fitting Results

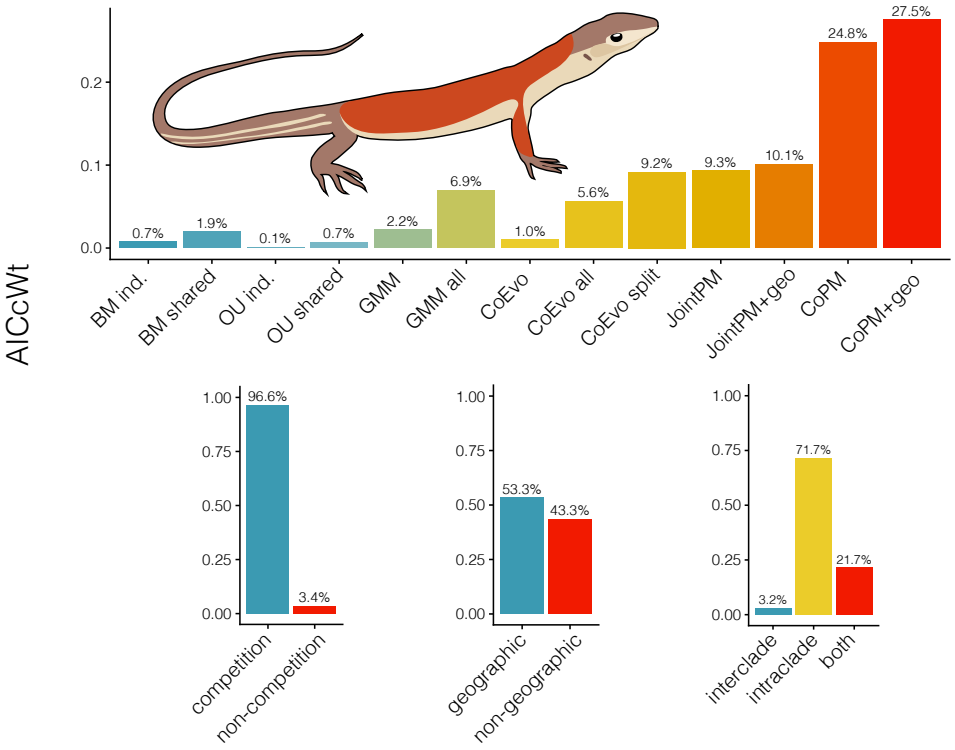

Figure S6: Comparative model fitting highlights the importance of incorporating interactions when modelling body size evolution of monitor lizards and dasyuromorphian marsupials. Modelling competition vastly improves model fit, but size evolution appears largely driven by intraclade evolution and not competition between monitors and mammals. Incorporating historical biogeography only narrowly improves model inference.

Model Identifiability

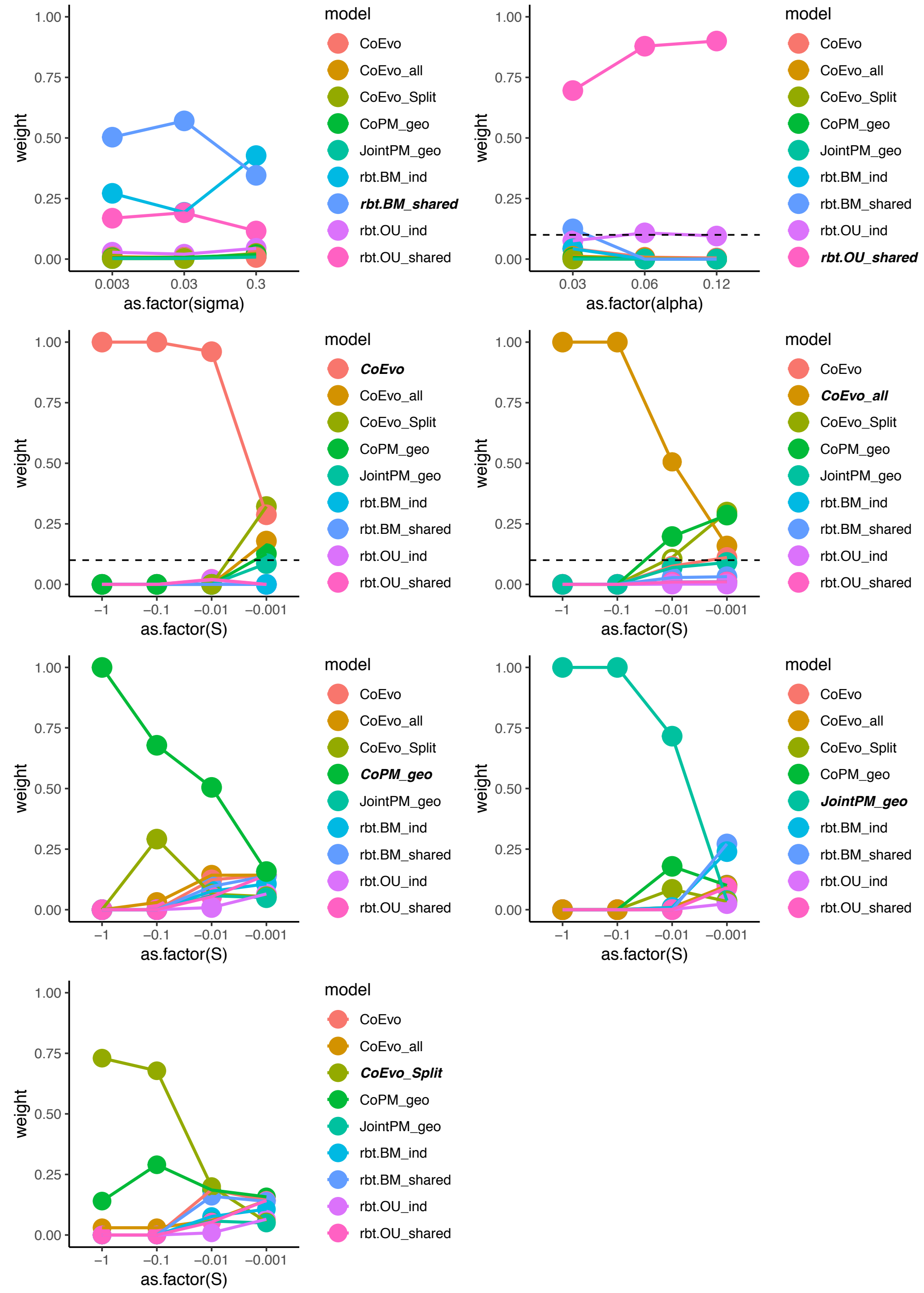

Figure S7: As the strength of competition S increases, model selection becomes more reliable. Results of model identifiability simulations as a function of varying parameter values. Identifiability (presented as AICCweight) of interaction models is uniformly poor for extremely small absolute values of S, but increases considerably at values of -0.01 and beyond. Values for simulations are included in Table SX.

Parameter Estimation Under GMM-type Models

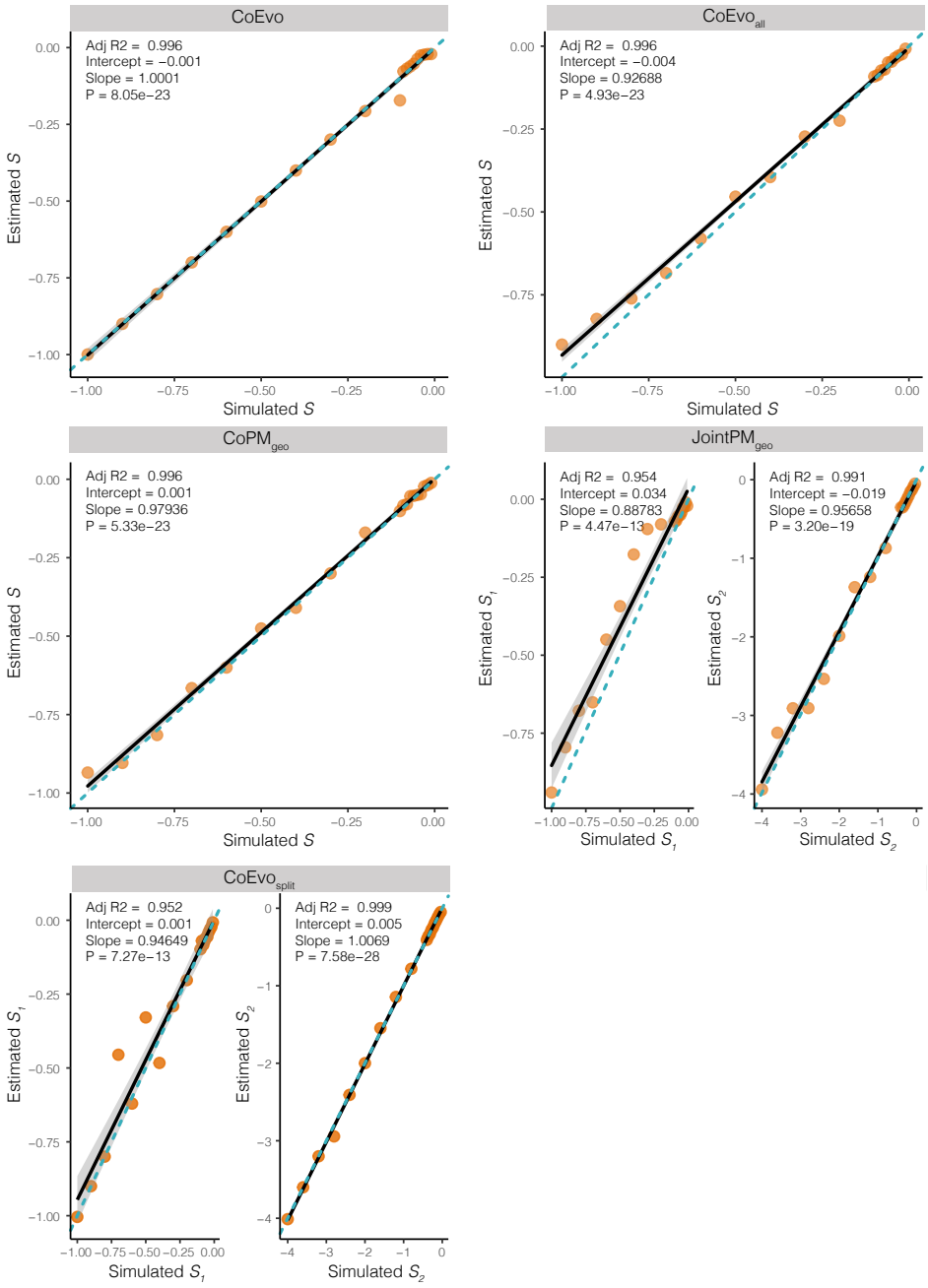

Figure S8: The competition parameter S can be accurately estimated under competitive models. Simulated values were -0.01, -0.02, -0.03, -0.04, -0.05, -0.06, -0.07, -0.08, -0.09, -0.1, -0.2, -0.3, -0.4, -0.5, -0.6, -0.7, -0.9, -1. Estimated values are consistently accurate between these limits.

Interaction Model Summaries

The Generalist Matching Mutualism (**GMM**) model. Assumes equal interaction (S) between all inter-clade lineages, but no interaction (0) among lineages within a tree (intra-clade). We embrace a broad description of the GMM mdoel, where S can be positive indicating attraction towards the mean trait value of interacting lineages, or negative indicating repulsion away from the mean trait value of interacting lineages. Because interactions are estimated only **between** clades, $p_{k,l}$=1 if lineages k and l are from different clades (trees), and $p_{k,l}$=0 for any two lineages k and l from the same clade (tree).

The Generalist Matching Mutualism All (**GMM$_{\mathbf{all}}$**) model. Assumes equal interaction (S) between all taxa in both trees (inter- and intra-clade). S can be positive indicating attraction towards the mean trait value of interacting lineages, or negative indicating repulsion away from the mean trait value of interacting lineages, but $p_{k,l}$=1 always.

The **CoEvo** model. An extension of the GMM model, accounting for interactions only between geographic co-occurring lineages. As with the GMM model, it only estimates interaction (S) between taxa across trees (inter-clade, *not* intra-clade). This model also properly accounts for the number of co-occuring lineages by dividing S (Pk/l) using rowsums (see Manceau et al. pg.559, equation 7).

The **CoEvo$_{\mathbf{all}}$** model. This is a CoEvo extension of the GMM$_{\text{all}}$ model, estimating interaction (S) between all co-occurring taxa (inter-clade *and* intra-clade). $p_{k,l}$=1 always. In calculating the interaction matrices, this model accounts for the number of co-occuring lineages by dividing $S/p_{k,l}$, assuming an equal strength of interaction with each cohabiting lineage.

The **CoEvo$_{\mathbf{split}}$** model. Again, an extension of the GMM model, accounting for interactions only between geographic co-occurring lineages. It accounts for interactions between all taxa like the CoEvo$_{\text{all}}$ model, but estimates a different interaction parameter for intra-clade (S2) and inter-clade (S1) interactions. In calculating the interaction matrices, this model accounts for the number of co-occuring lineages by dividing $S/p_{k,l}$, assuming an equal strength of interaction with each cohabiting lineage. This model is identical to the models: CoPM$_{\text{geo}}$ if S_1=0, CoEvo if S_2=0, and CoEvo$_{\text{all}}$ if S_1=S_2.

The **CoPM** model. This is a joint estimation of the PM model for two trees. It estimates single interaction (S) and rate (σ) values for both trees, but S is estimated solely from intra-clade

interactions (no interaction between trees). All lineages in a tree are assumed to interact with *all* other lineages in that tree

The **CoPM$_{\mathbf{geo}}$** model. This is an extension of the CoPM model, which is a joint estimation of the PM model for two trees. It estimates single interaction (S) and rate (σ) values for both trees, but S is estimated solely from intra-clade interactions (no interaction between trees). It correctly accounts for interaction only among geographic overlapping lineages, and corrects the interaction estimate for the number of overlapping lineages.

The **JointPM** model. This is a joint estimation of the PM model for two trees. It differs from the CoPM model by estimating separate interaction values for each clade ($\text{tree}_1 = S_1$; $\text{tree}_2 = S_2$). All lineages in a tree are assumed to interact with *all* other lineages in that tree.

The **JointPM$_{\mathbf{geo}}$** model. This is a joint estimation of the PM model for two trees. It differs from the CoPM$_{\text{geo}}$ model by estimating separate interaction values for each clade ($\text{tree}_1 = S_1$; $\text{tree}_2 = S_2$). Like the CoPM$_{\text{geo}}$ (unlike JointPM) it correctly estimates the interaction parameters (S_1,S_2) for only geographic overlapping taxa (it also corrects for the number of taxa overlapping). This model is identical to the CoPM$_{\text{geo}}$ model if S_1=S_2.

Funding

This work was supported by an International Postgraduate Research Scholarship at the Australian National University to IGB.

Acknowledgments

We would like to thank the Keogh and Moritz lab groups at ANU for discussion and comments throughout the development of this project. Thanks to Alex Skeels for a crash-course in methods of spatial data and functional diversity, and as always Zoe K.M. Reynolds for troubleshotting scripts. We appreciate the opportunity provided by the Society for Systematic Biology to present this research in the Ernst Mayr symposium at the 2018 Evolution meeting in France. A considerable thank you to the the curators and staff of the many Australian and international museums and databases (Australian Museum, Museum and Art Gallery of the Northern Territory, South Australian Museum, Australian Biological Tissue Collection, Queensland Museum, Western Australian Museum, Australian National Wildlife Council, University of Michigan Museum of Zoology, Bernice P.Bishop Museum, California Academy of Sciences, Museum of Vertebrate Zoology at Berkeley, Port Elizabeth Museum, Royal Ontario Museum, and University of Kansas Natural History Museum) for access to tissues and locality data that made this work possible.

References

Aberer A.J., Krompass D., Stamatakis A. 2012. Pruning rogue taxa improves phylogenetic accuracy: An efficient algorithm and webservice. Systematic Biology. 62:162–166.

Adams D.C., Nason J.D. 2018. A phylogenetic comparative method for evaluating trait coevolution across two phylogenies for sets of interacting species. Evolution. 72:234–243.

Amer S.A.M., Kumazawa Y. 2008. Timing of a mtDNA gene rearrangement and intercontinental dispersal of varanid lizards. Genes & Genetic Systems. 83:275–280.

Barido-Sottani J., Aguirre-Fernandez G., Hopkins M.J., Stadler T., Warnock R. 2019. Ignoring stratigraphic age uncertainty leads to erroneous estimates of species divergence times under the fossilized birth-death process. Proc Biol Sci. 286:20190685.

Baum D.A., Donoghue M.J. 2002. Transference of Function, heterotopy and the evolution of plant development. Systematics Association Special Volume. 65:52–69.

Beaulieu J.M., Jhwueng D.-C., Boettiger C., O'Meara B.C. 2012. Modeling stabilizing selection: Expanding the Ornstein-Uhlenbeck model of adaptive evolution. Evolution. 66:2369–2383.

Beck R.M., Lee M.S. 2014. Ancient dates or accelerated rates? Morphological clocks and the antiquity of placental mammals. Proc Biol Sci. 281.

Benton M.J. 1987. Progress and competition in macroevolution. Biological Reviews. 62:305–338.

Billet G., Bardin J. 2018. Serial Homology and Correlated Characters in Morphological Phylogenetics: Modeling the Evolution of Dental Crests in Placentals. Systematic Biology. 68:267–280.

Borowiec M.L. 2016. AMAS: A fast tool for alignment manipulation and computing of summary statistics. PeerJ. 4:e1660.

Boyden J.A., Müller R.D., Gurnis M., Torsvik T.H., Clark J.A., Turner M., Ivey-Law H., Watson R.J., Cannon J.S. 2011. Next-generation plate-tectonic reconstructions using GPlates..

Brennan I.G., Keogh J.S. 2018. Miocene biome turnover drove conservative body size evolution across Australian vertebrates. Proceedings of the Royal Society B: Biological Sciences. 285.

Brown W.L., Wilson E.O. 1956. Character displacement. Systematic Zoology. 5:49–64.

Collar D.C., Schulte Ii J.A., Losos J.B. 2011. Evolution of extreme body size disparity in monitor lizards (*Varanus*). Evolution. 65:2664–2680.

Conrad J.L. 2008. Phylogeny and systematics of Squamata (Reptilia) based on morphology.

SPIE.

Conrad J.L., Ast J.C., Montanari S., Norell M.A. 2011. A combined evidence phylogenetic analysis of Anguimorpha (Reptilia: Squamata). Cladistics. 27:230–277.

Conrad J.L., Balcarcel A.M., Mehling C.M. 2012. Earliest example of a giant monitor lizard (*Varanus*, Varanidae, Squamata). PLoS ONE. 7:e41767.

Darwin C. 1859. On the origin of species by means of natural selection, or preservation of favoured races in the struggle for life. London : John Murray, 1859.

Drury J.P., Clavel J., Manceau M., Morlon H. 2016. Estimating the effect of competition on trait evolution using maximum likelihood inference. Systematic Biology. 65:700–710.

Drury J.P., Grether G.F., Garland T. Jr., Morlon H. 2018a. An assessment of phylogenetic tools for analyzing the interplay between interspecific interactions and phenotypic evolution. Systematic Biology. 67:413–427.

Drury J.P., Tobias J.A., Burns K.J., Mason N.A., Shultz A.J., Morlon H. 2018b. Contrasting impacts of competition on ecological and social trait evolution in songbirds. PLOS Biology. 16:1–23.

Duchene D.A., Bragg J.G., Duchene S., Neaves L.E., Potter S., Moritz C., Johnson R.N., Ho S.Y.W., Eldridge M.D.B. 2018. Analysis of phylogenomic tree space resolves relationships among marsupial families. Syst Biol. 67:400–412.

Esquerre D., Donnellan S., Brennan I.G., Lemmon A.R., Lemmon E.M., Zaher H., Grazziotin F., Keogh J.S. 2019. Phylogenomics, biogeography, and morphometrics reveal rapdi phenotypic evolution in pythons after crossing Wallace's line. in press.

Estes R. 1983. The fossil record and early distribution of lizards. Advances in herpetology and evolutionary biology. 365:398.

Estes R. 1984. Fish, amphibians and reptiles from the Etadunna Formation, Miocene of South Australia. Australian Zoologist. 21:335–343.

Fuller S., Baverstock P., King D. 1998. Biogeographic origins of goannas (Varanidae): A molecular perspective. Molecular Phylogenetics and Evolution. 9:294–307.

Gauthier J.A., Kearney M., Maisano J.A., Rieppel O., Behlke A.D.B. 2012. Assembling the squamate tree of life: Perspectives from the phenotype and the fossil record. Bulletin of the Peabody Museum of Natural History. 53:3–308.

Gavryushkina A., Heath T.A., Ksepka D.T., Stadler T., Welch D., Drummond A.J. 2017.

Bayesian Total-Evidence Dating Reveals the Recent Crown Radiation of Penguins. Syst Biol. 66:57–73.

Georgalis G.L. 2017. *Necrosaurus* or *Palaeovaranus*? Appropriate nomenclature and taxonomic content of an enigmatic fossil lizard clade (Squamata). Annales de Paléontologie. 103:293–303.

Goloboff P.A., Pittman M., Pol D., Xu X. 2018. Morphological Data Sets Fit a Common Mechanism Much More Poorly than DNA Sequences and Call Into Question the Mkv Model. Systematic Biology. 68:494–504.

Grant P.R., Grant B.R. 2006. Evolution of character displacement in Darwin's finches. Science. 313:224–226.

Haeseler A. von, Minh B.Q., Nguyen M.A.T. 2013. Ultrafast approximation for phylogenetic bootstrap. Molecular Biology and Evolution. 30:1188–1195.

Hall R. 2002. Cenozoic geological and plate tectonic evolution of SE Asia and the SW Pacific: computer-based reconstructions, model and animations. Journal of Asian Earth Sciences. 20:353–431.

Harvey M.B., Barker D.G. 1998. A New Species of Blue-Tailed Monitor Lizard (Genus *Varanus*) from Halmahera Island, Indonesia. Herpetologica. 54:34–44.

Heath T.A., Huelsenbeck J.P., Stadler T. 2014. The fossilized birth–death process for coherent calibration of divergence-time estimates. Proceedings of the National Academy of Sciences. 111:E2957–E2966.

Hejnol A., Mongiardino Koch N., Gauthier J.A. 2018. Noise and biases in genomic data may underlie radically different hypotheses for the position of Iguania within Squamata. Plos One. 13.

Hijmans R. 2016. geosphere: spherical trigonometryR package version 1.5-5 https://CRAN. R-project. org/package= geosphere.

Hillis D.M., Heath T.A., John K.S. 2005. Analysis and visualization of tree space. Systematic Biology. 54:471–482.

Ho S.Y.W., Phillips M.J. 2009. Accounting for Calibration Uncertainty in Phylogenetic Estimation of Evolutionary Divergence Times. Systematic Biology. 58:367–380.

Holmes R.B., Murray A.M., Attia Y.S., Simons E.L., Chatrath P. 2010. Oldest known *Varanus* (Squamata: Varanidae) from the Upper Eocene and Lower Oligocene of Egypt: Support for an African origin of the genus. Palaeontology. 53:1099–1110.

Ivanov M., Ruta M., Klembara J., Böhme M. 2017. A new species of *Varanus* (Anguimorpha: Varanidae) from the early Miocene of the Czech Republic, and its relationships and palaeoecology. Journal of Systematic Palaeontology. 16:767–797.

Jennings W., Pianka E. 2004. Tempo and timing of the Australian *Varanus* radiation. Varanoid Lizards of the World. Indiana University Press, Bloomington, Indiana.:77–87.

Jones K.E., Bielby J., Cardillo M., Fritz S.A., O'Dell J., Orme C.D.L., Safi K., Sechrest W., Boakes E.H., Carbone C., Connolly C., Cutts M.J., Foster J.K., Grenyer R., Habib M., Plaster C.A., Price S.A., Rigby E.A., Rist J., Teacher A., Bininda-Emonds O.R.P., Gittleman J.L., Mace G.M., Purvis A. 2009. PanTHERIA: A species-level database of life history, ecology, and geography of extant and recently extinct mammals. Ecology. 90:2648–2648.

Keast A. 1971. Continental drift and the evolution of the biota on southern continents. The Quarterly Review of Biology. 46:335–378.

Keogh J.S. 1998. Molecular phylogeny of elapid snakes and a consideration of their biogeographic history. Biological Journal of the Linnean Society. 63:177–203.

King M., King D. 1975. Chromosomal Evolution in the Lizard Genus *Varanus* (Reptilia). Australian Journal of Biological Sciences. 28:89–108.

Kubatko L.S., Degnan J.H. 2007. Inconsistency of Phylogenetic Estimates from Concatenated Data under Coalescence. Systematic Biology. 56:17–24.

Laliberté E., Legendre P., Shipley B., Laliberté M.E. 2014. Package "fd". Measuring functional diversity from multiple traits, and other tools for functional ecology.

Lee M.S.Y., Oliver P.M., Hutchinson M.N. 2009. Phylogenetic uncertainty and molecular clock calibrations: A case study of legless lizards (Pygopodidae, Gekkota). Molecular Phylogenetics and Evolution. 50:661–666.

Lemmon A.R., Emme S.A., Lemmon E.M. 2012. Anchored hybrid enrichment for massively high-throughput phylogenomics. Syst Biol. 61:727–44.

Lewis P.O. 2001. A Likelihood Approach to Estimating Phylogeny from Discrete Morphological Character Data. Systematic Biology. 50:913–925.

Lin L.-H., Wiens J.J. 2017. Comparing macroecological patterns across continents: Evolution of climatic niche breadth in varanid lizards. Ecography. 40:960–970.

Lind A.L., Lai Y.Y., Mostovoy Y., Holloway A.K., Iannucci A., Mak A.C., Fondi M., Orlandini

V., Eckalbar W.L., Milan M., others. 2019. Genome of the Komodo dragon reveals adaptations in the cardiovascular and chemosensory systems of monitor lizards. Nature ecology & evolution. 3:1241.

Losos J.B. 1990. A phylogenetic analysis of character displacement in Caribbean *Anolis* lizards. Evolution. 44:558–569.

Luo A., Duchêne D.A., Zhang C., Zhu C.-D., Ho S.Y. 2018. A Simulation-Based Evaluation of Total-Evidence Dating Under the Fossilized Birth-Death Process. bioRxiv.

Maechler M., Rousseeuw P., Struyf A., Hubert M., Hornik K. 2018. Cluster: Cluster analysis basics and extensions..

Manceau M., Lambert A., Morlon H. 2017. A unifying comparative phylogenetic framework including traits coevolving across interacting lineages. Systematic Biology. 66:551–568.

Matzke N.J. 2014. Model selection in historical biogeography reveals that founder-event speciation is a crucial process in island clades. Systematic Biology. 63:951–970.

Molnar R. 2004. The long and honorable history of monitors and their kin. Varanoid lizards of the world.:10–67.

Morlon H., Lewitus E., Condamine F.L., Manceau M., Clavel J., Drury J. 2016. RPANDA: An r package for macroevolutionary analyses on phylogenetic trees. Methods in Ecology and Evolution. 7:589–597.

Nuismer S.L., Harmon L.J. 2015. Predicting rates of interspecific interaction from phylogenetic trees. Ecology Letters. 18:17–27.

Ogilvie H.A., Heled J., Xie D., Drummond A.J. 2016. Computational performance and statistical accuracy of *BEAST and comparisons with other methods. Systematic Biology.

Ogilvie H.A., Vaughan T.G., Matzke N.J., Slater G.J., Stadler T., Welch D., Drummond A.J. 2018. Inferring species trees using integrative models of species evolution. bioRxiv.

Oliver P.M., Brown R.M., Kraus F., Rittmeyer E., Travers S.L., Siler C.D. 2018. Lizards of the lost arcs: mid-Cenozoic diversification, persistence and ecological marginalization in the West Pacific. Proceedings of the Royal Society B: Biological Sciences. 285.

O'Reilly J.E., Donoghue P.C. 2016. Tips and nodes are complementary not competing approaches to the calibration of molecular clocks. Biol Lett. 12.

Paradis E., Claude J., Strimmer K. 2004. APE: Analyses of phylogenetics and evolution in R

language. Bioinformatics. 20:289–290.

Pennell M.W., Slater G.J., Eastman J.M., Uyeda J.C., Brown J.W., Harmon L.J., Alfaro M.E., FitzJohn R.G. 2014. geiger v2.0: an expanded suite of methods for fitting macroevolutionary models to phylogenetic trees. Bioinformatics. 30:2216–2218.

Peters R.H., Peters R.H. 1986. The ecological implications of body size. Cambridge University Press.

Pianka E.R. 1995. Evolution of body size: Varanid lizards as a model system. The American Naturalist. 146:398–414.

Plummer M., Best N., Cowles K., Vines K. 2006. CODA: Convergence diagnosis and output analysis for MCMC. R news. 6:7–11.

Portik D.M., Papenfuss T.J. 2012. Monitors cross the Red Sea: the biogeographic history of Varanus yemenensis. Mol Phylogenet Evol. 62:561–5.

Puttick M.N., O'Reilly J.E., Tanner A.R., Fleming J.F., Clark J., Holloway L., Lozano-Fernandez J., Parry L.A., Tarver J.E., Pisani D., Donoghue P.C. 2017. Uncertain-tree: discriminating among competing approaches to the phylogenetic analysis of phenotype data. Proc Biol Sci. 284.

Pyron R.A. 2011. Divergence Time Estimation Using Fossils as Terminal Taxa and the Origins of Lissamphibia. Systematic Biology. 60:466–481.

Pyron R.A. 2017. Novel approaches for phylogenetic inference from morphological data and total-evidence dating in squamate reptiles (lizards, snakes, and amphisbaenians). Systematic Biology. 66:38–56.

Quintero I., Keil P., Jetz W., Crawford F.W. 2015. Historical biogeography using species geographical ranges. Syst Biol. 64:1059–73.

Quintero I., Landis M.J. 2019. Interdependent Phenotypic and Biogeographic Evolution Driven by Biotic Interactions. bioRxiv.

Rambaut A., Drummond A.J., Xie D., Baele G., Suchard M.A. 2018. Posterior Summarization in Bayesian Phylogenetics Using Tracer 1.7. Systematic Biology. 67:901–904.

Ree R.H., Sanmartín I. 2018. Conceptual and statistical problems with the DEC+J model of founder-event speciation and its comparison with DEC via model selection. Journal of Biogeography. 45:741–749.

Reynolds G.R., Niemiller M.L., Revell L.J. 2014. Toward a Tree-of-Life for the boas and

pythons: multilocus species-level phylogeny with unprecedented taxon sampling. Mol Phylogenet Evol. 71:201–13.

Ronquist F., Klopfstein S., Vilhelmsen L., Schulmeister S., Murray D.L., Rasnitsyn A.P. 2012. A Total-Evidence Approach to Dating with Fossils, Applied to the Early Radiation of the Hymenoptera. Systematic Biology. 61:973–999.

Scanlon J.D. 2014. Giant terrestrial reptilian carnivores of Cenozoic Australia. Carnivores of Australia: Past, Present and Future.:27.

Schluter D., Price T.D., Grant P.R. 1985. Ecological character displacement in Darwin's finches. Science. 227:1056–1059.

Schmidt H.A., Minh B.Q., Haeseler A. von, Nguyen L.-T. 2014. IQ-tree: A fast and effective stochastic algorithm for estimating maximum-likelihood phylogenies. Molecular Biology and Evolution. 32:268–274.

Schulte 2. J. A., Melville J., Larson A. 2003. Molecular phylogenetic evidence for ancient divergence of lizard taxa on either side of Wallace's Line. Proc Biol Sci. 270:597–603.

Sepkoski Jr J.J. 1996. Competition in macroevolution: The double wedge revisited. Evolutionary paleobiology.:211–255.

Smith K.T., Bhullar B.-A.S., Holroyd P.A. 2008. Earliest African record of the Varanus stem-clade (Squamata: Varanidae) from the Early Oligocene of Egypt. Journal of Vertebrate Paleontology. 28:909–913.

Sweet S.S., Pianka E.R. 2007. Monitors, mammals and Wallace's Line. Mertensiella. 16:79–99.

Vaurie C. 1951. Adaptive differences between two sympatric species of nuthatches (Sitta). Proc. Xth int. Ornith. Congress, uppsala.:163–166.

Vidal N., Marin J., Sassi J., Battistuzzi F.U., Donnellan S., Fitch A.J., Fry B.G., Vonk F.J., Rodriguez de la Vega R.C., Couloux A., Hedges S.B. 2012. Molecular evidence for an Asian origin of monitor lizards followed by tertiary dispersals to Africa and Australasia. Biology Letters. 8:853–855.

Wilson D.S. 1975. The adequacy of body size as a niche difference. The American Naturalist. 109:769–784.

Wilson S., Swan G. 2013. A complete guide to reptiles of Australia. Chatswood, New South Wales: New Holland Publishers.

Woodhead J., Hand S.J., Archer M., Graham I., Sniderman K., Arena D.A., Black K.H.,

Synthesis

Identifying evolutionary patterns is the first step in linking diversity with the processes dictating it. While it is often difficult to disentangle the many forces shaping diversity, recognizing these patterns is inherently exciting because it helps us to better understand the world around us. Evolutionary trajectories that we *are* able to explain tell us incredible stories about evolution's successes and failures. We learn tales of profilic diversifiers like rodents and beetles, and others about the boom-and-bust history of trilobites and ammonites. We also revel in those that have just managed to hang on like the coelacanth and *Ginkgo*. By identifying these trends, and linking them across disparate groups, we are able to identify commonalities, and recognize fruitful and austere periods of diversity through time.

Over the course of earth's history, a handful of mass extinction events have threatened to snuff out all life [11]. The dramatic climate change of the Eocene-Oligocene boundary (EOb) is not one of those catastrophic events, but this period does show evidence of considerable turnover in floral and faunal records [9,12–14]. Our research suggests that pygopodoid geckos—one of Australia's oldest endemic groups—exhibit a similar signal of turnover found elsewhere. In the absence of an informative fossil record for this group, we used phylogenetic comparative models to test the idea that long stem branches for each of the families is a signature of mass turnover early in the group's history. This pattern is temporally concordant with the EOb, and suggests that mass extinction in these families may have been the result of the rapid cooling and habitat restructuring of this period [15].

The impacts of climatic change are not always so intense however. Periods of gradual climate change may result in environmental forcing and protracted filtering, instead of elevated extinction [16,17]. This can result in diversification trends that do not appear anomalous, but may affect phenotypic traits or biogeographic history. We find evidence of these processes in a number of Australian vertebrate lineages during the Miocene

aridification of Australia. This period, marked by gradual cooling and drying of the Australian continent, appears correlated with slowdowns in phenotypic evolution and increasing speciation by allopatry. We suggest that these patterns are linked, and the Miocene fragmentation of mesic habitats resulted in elevated niche conservatism among agamid lizards, skinks, geckos, birds, and mammals.

The expansion of arid habitas across Australia in the Miocene has also long been associated with the proliferation of arid-adapted lineages [18–20]. We add to the literature by describing elevated rates of speciation in arid-zone geckos, and suggest that this biome has acted as a source for Australian continental diversity. The radiation of Australia's vertebrate groups is not all about reptiles and deserts however. Recent research has enthusiastically linked the rise of Plio-Pleistocene grasses with the rapid radiation of macropod marsupials [21,22]. Though this trend is intuitive, morphological and molecular dating methods disagree on the timing of divergences in this group. By incorporating known error around fossil age estimates, and estimated error around divergence times, we show that drawing the link between the diversification of modern kangaroos and the spread of Australian grasslands is not so clear. We do not disagree that this is a plausible scenario, but instead encourage macroevolutionary biologists to account for both uncertainty in their data, as well as their conclusions.

Of course not all macroevolutionary patterns are dictated by extrinsic environmental forces. Changes in the rate of speciation or phenotypic evolution may also be driven by intrinsic factors, or ecological interactions, among other causes [23,24]. Interactions among lineages have been considered a particularly strong selective force on the morphology and distribution of species [25,26]. In a classic anecdote, Darwin and Wallace each considered a Madagascan orchid with a foot long nectary. Independently, they determined there must be a moth pollinator with an equally long proboscis to match. The later discovery of just such a moth was ultimately less of a surprise than it was a fulfillment of the expectation that organismal interactions can dictate phenotypic evolution, even to absurd extremes. These interactions may also cause organismal phenotypes to diverge to extremes as well, as a result of character displacement [25]. We investigated whether the immense disparity in body sizes—multiple orders of magnitude—among Australian monitor lizards may be the result of interaction among species of *Varanus*, or as a result of competition with Australian marsupial predators. We found that monitors assemble communities with

considerable functional diversity in the body size of members, and that size extremes have evolved as the result of competition. These results suggest that monitors do appear to have competitively displaced one another in geographic space as well as evolutionarily, but we do not find an influence of marsupials on this process.

Australia's rich floral and faunal diversity, isolation, and scientific community make it an amazing place to study phylogenetics and macroevolution. I would be remiss to ignore that Australia's 1,000+ reptile and amphibian species are what has drawn me —like many other biologists—here to study the evolution of these animals. Uncovering the patterns of their diversification through time has provided insight into how and when the continent's fauna appeared and became so rich. While Australia's plants and animals are unique, the broad processes dictating their radiation are similar to those occurring on other continents around the globe.

Appendix 1:

Barcoding utility in a mega-diverse cross-continental genus: Keeping pace with Cyrtodactylus geckos

www.nature.com/scientificreports

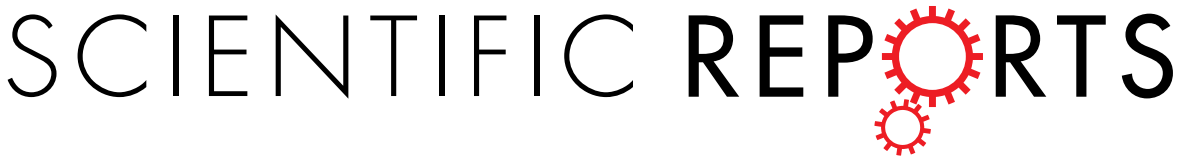

OPEN

Barcoding utility in a mega-diverse, cross-continental genus: keeping pace with *Cyrtodactylus* geckos

Received: 9 December 2016
Accepted: 25 May 2017
Published online: 17 July 2017

Ian G. Brennan[1], Aaron M. Bauer[1], Ngo Van Tri[2], Yun-yu Wang[3,4], Wen-zhi Wang[3,4], Ya-Ping Zhang[3,5] & Robert W. Murphy[3,6]

Over the past decade, DNA barcoding has become a staple of low-cost molecular systematic investigations. The availability of universal primers and subsidized sequencing projects (PolarBOL, SharkBOL, SpongeBOL) have driven this popularity, often without appropriate investigation into the utility of barcoding data for the taxonomic group of interest. Here, our primary aim is to determine the phylogenetic value of DNA barcoding (mitochondrial locus *COI*) within the gecko genus *Cyrtodactylus*. With >40 new species described since last systematic investigation, *Cyrtodactylus* represents one of the most diverse extant squamate genera, and their contemporary distribution spans the Indian subcontinent, eastward through Indochina, and into AustraloPapua. The complex biogeographic history of this group, and morphology-only designation of many species have complicated our phylogenetic understanding of *Cyrtodactylus*. To highlight the need for continued inclusive molecular assessment, we use Vietnamese *Cyrtodactylus* as a case study showing the geopolitically paraphyletic nature of their history. We compare *COI* to the legacy marker *ND2*, and discuss the value of *COI* as an interspecific marker, as well as its shortcomings at deeper evolutionary scales. We draw attention back to the Cold Code as a subsidized method for incorporating molecular methods into species descriptions in the effort to maintain accurate phylogenies.

Barcoding the Tree of Life

Barcoding initiatives across the tree of life have helped document and describe thousands of species of bony fishes, birds, sharks, and sponges, among many other groups[1–5]. Cold Code[6], the barcoding initiative for amphibians and non-avian reptiles, has similarly produced an immense quantity of sequence data for the mitochondrial locus encoding cytochrome c oxidase subunit I (*COI*). Cold Code and other barcoding initiatives provide a cost-free sequencing service for up to ten individuals of any species. In conjunction with databases such as the Barcode of Life Data Systems (BOLD), GenBank, and Dryad, researchers without access to sequencing facilities can produce and visualize novel sequences before adding preexisting data and running analyses. Implementation of Cold Code has contributed considerably to taxonomic resolution in Third World nations, and has been applied for conservation efforts in these regions that most need them[7]. Although Cold Code instigated barcoding on the grounds of species identification and discovery[8], recent studies have increasingly used barcoding data for phylogenetic inference and to answer phylogeographic questions[9,10]. This practice is often undertaken without sufficient assessment of the utility of barcoding for the taxonomic group of interest. Inference at deep timescales, may be severely compromised by the rapid mutational rate and limited size of the *COI* fragment used for barcoding. At shallower timescales, and in narrower phylogenetic contexts, DNA barcoding remains valuable[11].

[1]Division of Ecology & Evolution, Research School of Biology, The Australian National University, Canberra, ACT 2602, Australia. [2]National Key Laboratory, Institute of Tropical Biology, Vietnamese Academy of Sciences and Technology, 9/621 Hanoi Highway, Linh Trung District, Ho Chi Minh City, Vietnam. [3]State Key Laboratory of Genetic Resources and Evolution State, and Yunnan Laboratory of Molecular Biology of Domestic Animals, Kunming Institute of Zoology, Chinese Academy of Sciences, Kunming, 650223, China. [4]South China DNA Barcoding Center, Kunming Institute of Zoology, Chinese Academy of Sciences, Kunming, 650223, China. [5]Laboratory for Conservation and Utilization of Bio-resource and Key Laboratory for Microbial Resources of the Ministry of Education, Yunnan University, 2 Cuihu N. Rd., Kunming, 650091, China. [6]Centre for Biodiversity and Conservation Biology, Royal Ontario Museum, 100 Queen's Park, Toronto, M5S 2C6, Canada. Correspondence and requests for materials should be addressed to I.G.B. (email: Ian.Brennan@anu.edu.au)

Limitations to Barcoding

Despite ease of amplification, subsidized sequencing, and fast mutational rates making for high informativeness, mtDNA species-level inference via barcoding has its drawbacks. Mitochondrial phylogenetic reconstruction may be hampered by introgression and hybridization, male-biased gene flow, and selection on the linked mitochondrial genome, among other limitations[12]. Specifically, in several taxonomic groups—blowflies[13]; birds[14]; orthopterans[15]; dipterans[16]—mtDNA divergence and barcoding have been shown to be insufficient in delineating rapidly evolving species lineages, or those likely to introgress mitogenomes. However, these cases are interesting exceptions and when barcoding is used in concert with alternative methodologies such as ecology, morphology, and nuclear genomic data, barcoding is a powerful tool[17–19]. These integrative approaches facilitate pluralistic assessments of species delimitation and enhance accuracy. Requisite morphological diagnosis as part of species descriptions can quickly and easily pair with molecular data produced by DNA barcoding[20,21].

Systematics of *Cyrtodactylus* Gray 1827

Since the last extensive molecular phylogenetic assessment of *Cyrtodactylus*[22], more than 40 new species have been described using morphological, molecular, or integrative methods[21,23–25]. Indeed, as of 2016, several species[26–31] and many lineages await description[23,32,33]. These add to the more than 200 formally described species[34], and contribute to the growing number of publications (100+ per year) discussing *Cyrtodactylus* (Supplemental Fig. 1). In lieu of costly molecular methods, many of these species descriptions rely solely on a morphological framework. These analyses distinguish species from their closest congener(s), diagnose species within their local region, and leave them unassigned or ambiguously assigned to a more inclusive species-group. This is compounded by rapid species discovery which outpaces a phylogenetic understanding of this immensely successful genus.

Cyrtodactylus ranges from Pakistan and western India eastward to the Solomon Islands and in doing so covers an enormous expanse of ecoregions and global biodiversity hotspots[35]. Given the distributional spread across geopolitical borders, the number of researchers involved, and methods of specimen collection, it remains a challenge to keep current with the systematics of this group. Biodiversity estimates are consistently underreported for a number of countries within the range of *Cyrtodactylus*. With increased attention and sampling throughout Southeast Asia, specifically in the Indochinese, Sundaic, Philippine, Wallacean, and Papuan regions, it remains vital to maintain consistency in methods for accurate records of species diversity. Where barcoding datasets do exist for *Cyrtodactylus*, they have been created almost exclusively for species descriptions[21,24,25]. Often these barcoding phylogenies are carried out within the confines of a single country, such as for Laos[36] and Vietnam[20,37]. The complex geological histories of the regions across which *Cyrtodactylus* occurs, and the convoluted biogeographic history of the genus itself, make these 'barcode-by-country' reviews potentially misleading in their phylogenetic conclusions. Indeed, more inclusive molecular phylogenies are already beginning to resolve the synonymy of a number of bent-toed gecko species[38]. And while we are aware of no researchers who would agree with a geopolitically monophyletic hypothesis (clades are restricted to country borders) for *Cyrtodactylus*, 'barcode-by-country' reviews continue to unintentionally make just such phylogenetic assumptions.

Herein, we highlight the utility of the barcoding marker *COI* for intraspecific and shallow interspecific phylogenetic use, and encourage its use as an alternative to morphology-only systematic comparison. Additionally, we hope to draw attention to the potentially damaging practice of "barcoding-by-country," by elucidating the fractured biogeographic history of *Cyrtodactylus* throughout the Indochinese region. We use Vietnam as an explicit example of a geopolitical boundary thought to be inhabited by three independent lineages[22], to encourage a broader comparison of *Cyrtodactylus* in taxonomic and systematic works. Ultimately, for researchers without access to funding or sequencing facilities, DNA barcoding with the Cold Code continues to allow us all to work towards more complete sampling of *Cyrtodactylus*, providing a more accurate picture of the taxonomic and morphological diversity of this genus.

Results

Phylogenetic Inference using COI and ND2. New sequences and those acquired from GenBank included a total of 63 individuals sampled for both mitochondrial markers. In the fully sampled *COI* (Fig. 1) and the *COI*/*ND2*-standardized genealogies (Fig. 2), deeper relationships within *Cyrtodactylus* obtained very little support. However, nearly all (37/39) intraspecific relationships were strongly supported (BSS $\geq$ 90%). Sister-taxa relationships are also well supported ($\geq$70%) in both full and standardized genealogies. As expected, no support existed for reciprocal monophyly of current geopolitical regions.

The genealogy based on *ND2* and standardized to our *COI* sampling strongly supported the majority of intraspecific relationships (Fig. 2). Analyses of sampling-standardized *ND2* obtained greater and more frequent support for sister-taxa relationships, as well as strong support ($\geq$90%) at a number of deeper nodes that denoted species-groups of *Cyrtodactylus* (Fig. 2; colored boxes denote geographic region). Biogeographic matrilines returned by analysis of *ND2* were largely consistent with those presented by Wood *et al.*[22], albeit with reduced support.

Congruence in Mitochondrial Markers. Prior phylogenetic reconstructions (combined mitonuclear) of *Cyrtodactylus* found mtDNA matrilineal genealogies and nDNA phylogenies were largely congruent[22,23,32]. Matrilineal phylogeny as inferred by *ND2* has been valuable in predicting accurate phylogenetic relationships within *Cyrtodactylus*[22]. Both *ND2* and *COI* genealogies strongly supported the monophyly of several species groups that were obtained consistently in other investigations of *Cyrtodactylus*[23,32,39–41]. Exclusive of *C. battalensis*—the sole representative of the West Himalayan group—there was strong support (91-*ND2*/72-*COI*) for the monophyly of an India-Myanmar (IM) sister-group to the remaining species of *Cyrtodactylus*. Both genealogies supported three independent Indochinese groups: (A; IA) *C. chanhomae*, *C. lomyenensis*, and

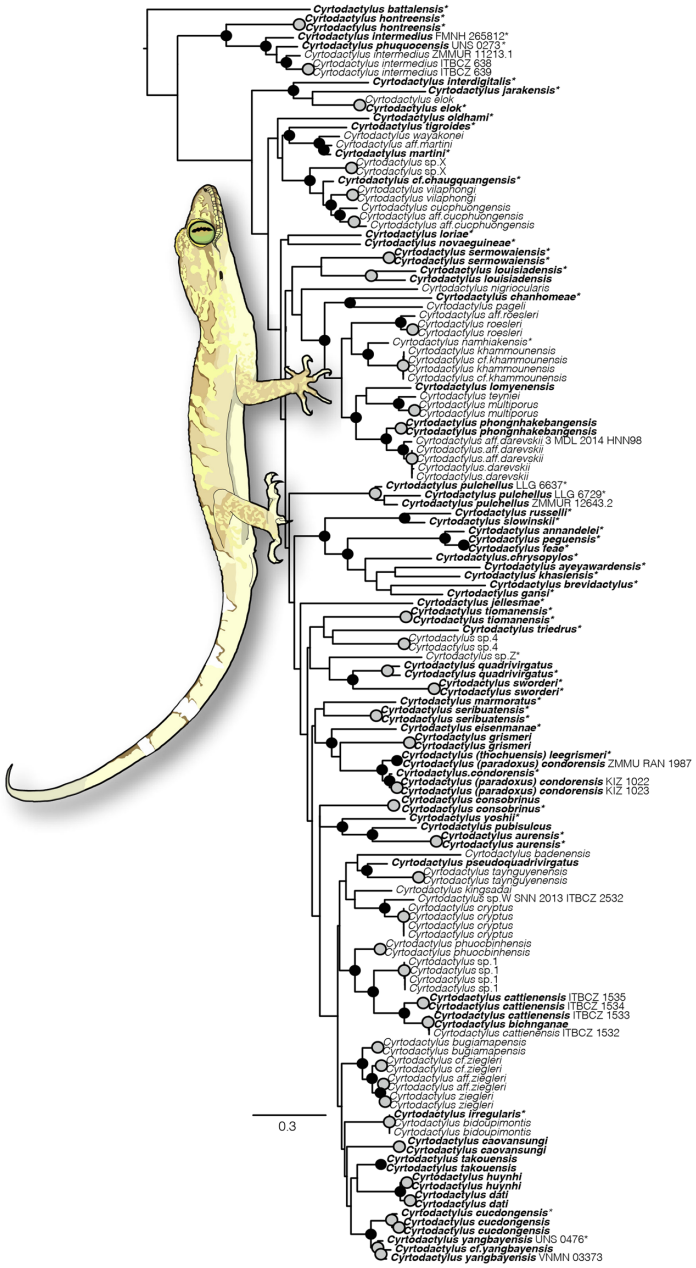

Figure 1. 'Fully-sampled' maximum likelihood phylogeny of *Cyrtodactylus* as inferred from mitochondrial locus *COI*, including novel sequences contributed by this study (51) indicated by asterisks. Circles at nodes indicate BSS values of ≥70: grey indicate intraspecific sampling and black interspecific sampling. Bolded names indicate samples also included in the 'Standardized *ND2*' phylogeny (Fig. 2). Sample numbers are included to aid in determining relationships in cases where more than 2 samples were used for a given species, or species are reconstructed as paraphyletic. *Cyrtodactylus pubisulcus* image drawn by IGB from photograph courtesy of Ben Karin.

C. phongnhakebangensis (96/83); (B; IB) *C. hontreensis*, *C. intermedius*, and *C. phuquocensis* (98/72); and (C; IC) *C. tigroides*, *C. bichnganae*, and *C. cf. chauquangensis* (99/70). These matrilines included residents of Thailand, Laos, and Vietnam, without geopolitical monophyly. Members of the '*C. sworderi* complex' (WM)[39,40] varied in

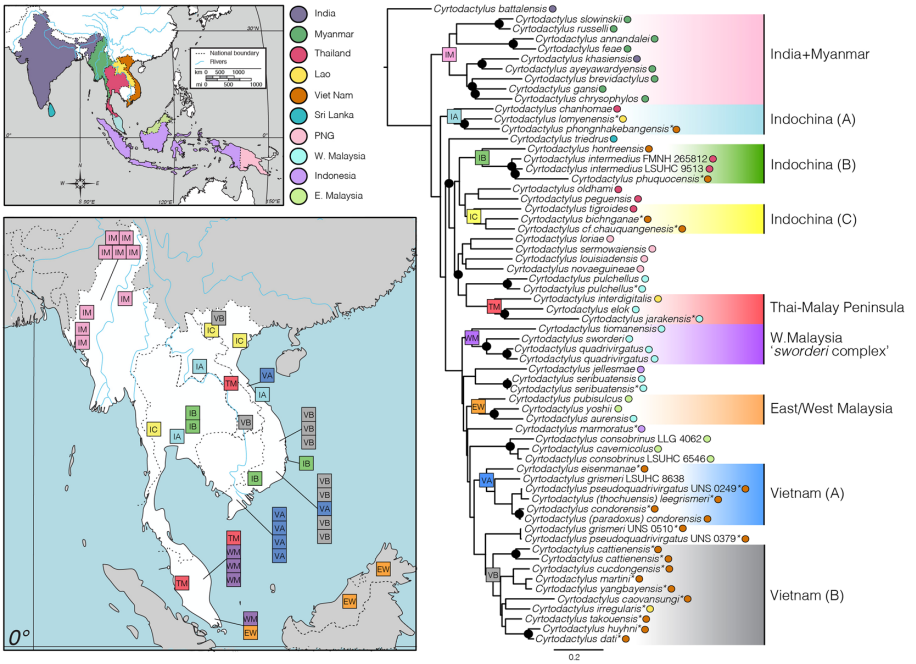

Figure 2. 'Standardized *ND2*' Maximum likelihood genealogy of *ND2* including only taxa for which *COI* sequence data also exist. Circles at nodes indicate clade congruence between *ND2* and *COI* loci, with BSS values of ≥70: blue indicate species groups, black interspecific sampling. Asterisks indicate new *ND2* sequences contributed by this study. Upper map shows the geopolitical distribution of samples included in this phylogeny, and colored circles associated with tree tips correspond to this map. Lower map highlights the Indochinese region, and boxes represent generalized sampling localities of species groups (IM, IA, IB, IC, TM, WM, EW, VA, VB; denoted by blue circles at nodes). Sampled country localities indicated by colored circles at the tree tips highlight the interdigitated nature of geographic relationships within phylogenetic species groups. Maps drawn and adapted by IGB in Adobe Illustrator CS6 from public domain image provided by Wikimedia Commons (https://commons.wikimedia.org/wiki/File:Location_Map_Asia.svg).

support (100/65), as did an East/West Malaysian (EW) group composed of *C. pubisulcus*, *C. yoshii*, and *C. aurensis* (88/72). Moderate support existed for a Thai/Malay Peninsula (TM) matriline comprised of *C. interdigitalis*, *C. elok*, and *C. jarakensis*. Additionally, there was strong support for distinct Vietnamese groups A (VA) (100/73) and B (VB) (85/75), although no consistent support united them into a monophyletic group (55/40). Indochinese species from Vietnam, Thailand, and Laos were assigned to multiple clades (5, 3, and 3, respectively), which were strongly supported across both molecular datasets.

Discussion

As in any field, assessing the appropriateness of the data to resolve the question of interest is paramount. In molecular systematics studies, this means addressing the ability of the data to provide phylogenetic information at the evolutionary depth or depths of interest. DNA barcoding has been lauded as a way to cheaply and rapidly include molecular data into species descriptions and phylogenetic studies. However, the evolutionary scale of the group of interest often resides outside the limits of barcoding's phylogenetic reconstruction abilities. We find that *COI* alone can not replace phylogenetic assessment by multilocus mitonuclear study, nor does it resolve relationships as accurately as another, single mitochondrial locus (*ND2*). What it does provide however, is valuable information for shallow scale interspecific and intraspecific systematics, which are invaluable to species discovery.

When viewed in its entirety, instead of by geopolitical boundaries, *Cyrtodactylus* show a general West to East biogeographic trend[22]. A number of eastward dispersals of Indochinese origin into the Sundaic, Wallacean, Papuan, and Philippine regions punctuate this overall pattern[22]. These dispersal events account for the distribution of geographically proximate species interspersed across the tree of *Cyrtodactylus*. This is particularly relevant to the appropriate differential diagnosis of novel taxa. Some groups of *Cyrtodactylus* are easy to identify morphologically from geographic congeners, such as ground-dwelling members of the subgenus *Geckoella* from India and Sri Lanka[23], Papuan giants[42], and Sundaic dwarves[43]. In contrast, however, Vietnamese bent-toed geckos represent a prime example of a morphologically conservative body plan involving multiple species groups. Our trees depict five well supported matrilines of Vietnamese *Cyrtodactylus* (Fig. 2; orange circles) interspersed with inhabitants of

other Indochinese and Sundaic nations. This convoluted biogeographic history highlights the necessity of molecular and morphological comparison against closest phylogenetic and not solely political congeners.

Barcoding initiatives across the tree of life largely coincide with an interest in species discovery and delimitation. At least 12 species of *Cyrtodactylus* have been described since 2012 using a combination of morphological means and barcoding data. However, during that same period, several other species have been described based solely on morphological assessments[26,44–48]. Prior to the initiation of DNA barcoding and Cold Code, the inclusion of molecular data into species descriptions was time-intensive, costly, and limited significantly by access to sequencing resources. The advent of Cold Code and the introduction of subsidized genetic barcoding makes it possible to include molecular results in species descriptions. Notwithstanding, barcoding is not the ultimate phylogenetic tool because it offers a matrilineal perspective on the history of species only, and the rapid evolution of barcoding genes often precludes the resolution of deep relationships.

DNA barcoding in other taxa has, unfortunately, unsuccessfully resolved interspecific relationships, identified independently evolving lineages, and, worse, misidentified interspecific relationships as a result of mitogenome introgression[13–16]. Our analyses address the use of genetic barcoding as a method for inferring historical associations among species of *Cyrtodactylus* via direct comparison with another popular mitochondrial marker *ND2*. Prior to the implementation of Cold Code, alternative mitochondrial markers such as *ND2*, *16S*, and *cytb* have been used more frequently as markers for identifying independently evolving units for taxonomic description. However, as DNA barcoding has become more popular, *COI* has supplanted alternatives due to its near-universal applicability. *COI* also is the dominant marker for describing and inferring relationships between novel taxa within this genus. As a result, many species of *Cyrtodactylus* have been described using morphology in combination with either *COI* or *ND2*, but rarely both molecular markers. Here, our assessment adds 46 additional samples to allow for direct comparison of both loci, to assess the value of *COI* as a phylogenetic tool in *Cyrtodactylus*.

Neither *COI* nor *ND2* successfully resolve deeper relationships within *Cyrtodactylus* with much support. This result likely owes to the phylogenetic depth, i.e. age of the genus, and the limitations of employing a single locus. Notwithstanding, the matrilineal phylogeny as inferred using *ND2* is largely concordant with the nuclear DNA phylogeny of Wood *et al.*[22]. Moderate to strong levels of support for a series of species-groups in Fig. 2 highlights the value of *COI* at resolving shallow interspecific relationships that are consistent with those of *ND2*. The smaller fragment of *COI* (658 bp) and slower mutational rate when compared to *ND2* (1047 bp + 400 bp of tRNAs) hamper phylogenetic inference beyond close relationships (Fig. 1). As an identifier of species groups, *COI* performs moderately well by providing support for 9 of 12 matrilines obtained with strong support by analysis of *ND2*.

DNA barcoding has been used most frequently in *Cyrtodactylus* as a method for describing and inferring relationships between novel taxa. Most of these investigations have used *COI* exclusively, and because of this, *COI* and *ND2* datasets are largely non-overlapping. The standardizing of datasets across mitochondrial loci serves to evaluate the phylogenetic utility of *COI* as a tool for genealogical inference relative to *ND2*. Ultimately, many sister-taxa and some higher level relationships as suggested by our fully sampled *COI* tree cannot be tested against *ND2* due to sampling. While *COI* plays a valuable role in species discovery and as a tool for informing other comparative methods (morphology, ecology, biogeography), we also recognize its shortcomings. When possible, we encourage the use of additional molecular markers (*ND2*, *RAG1*, *PDC*, *MXRA5*) for inferring relationships within this ultra-diverse genus. Ultimately, confident resolution may require massive amounts of data that next generation genomic sequencing yields, either complete mitogenomes, or SNPs from nuclear DNA. In addition to Cold Code-funded barcode sequencing, we encourage potential descriptors of new species of *Cyrtodactylus* to contact IGB and AMB regarding the possibility of additional molecular sequencing.

When used as the sole molecular marker for phylogenetic inference of a group of any considerable depth, or as an intraspecific marker for tracking matrilineal history, *COI* is unlikely to provide the resolution desired to confidently support or refute hypotheses. When appropriately used as part of a pluralistic methodology, however, DNA barcoding may prove extremely useful. Prior molecular assessment or "genetic screening" can help accurately place a novel species into a species group for the most useful morphological comparison. While it is important to diagnose new taxa in reference to geographic congeners, it is also necessary to distinguish it from its closest evolutionary congeners, to help develop a more complete image of its history. The high expense of DNA sequencers and satellite equipment and time-intensive methods continue to impede the inclusion of genetic data in species' descriptions. In response, Cold Code provides cost-free sequencing of the DNA barcoding locus *COI* for up to 10 individuals of any species.

Materials and Methods

Ethics. Field and laboratory experimental protocol for NSF subaward 13–0632 and DEB 0844532 were approved by Villanova University IACUC (approval: 16-14 and 11-04 respectively). *Cyrtodactylus* samples were collected in compliance with permits to NVT at the Institute of Tropical Biology, under the Vietnam Academy of Science and Technology, following guidelines of the Institutional Animal Care and Use Committee (IACUC).

Taxon Sampling and Molecular Methods. New sampling for this project was built upon molecular datasets assembled for investigations into inter- and intraspecific relationships within *Cyrtodactylus*[21–25,36,37,39–41,49]. A large number of sequences were acquired from GenBank, but to this growing dataset we have sequenced 51 additional samples for *COI*, and a further 25 samples sequenced for the mitochondrial locus *ND2*. Due to its comparatively fast mutation rate, length, history in the literature, and ease of amplification, *ND2* has been used consistently in studies of squamate phylogenetics (>20,900 GenBank records), and as the primary locus for the systematics of *Cyrtodactylus* (>900 GenBank records). For these reasons we have chosen to compare *COI* directly to *ND2*, for use in bent-toed gecko phylogenetics. All samples are accompanied by locality data, voucher information, and GenBank accession numbers, recorded in Table 1.

Genus & species	Collection #	Locality	Country	Genbank #	
				COI	ND2
Cyrtodactylus aff. cucphuongensis	MDL 2014 AT 2013 2	NA	Vietnam	KJ817428	—
Cyrtodactylus puhuensis	SNN 2013a KIZ 11665	Houphan Province	Laos	KF929529	—
Cyrtodactylus aff. darevskii	3 MDL 2014 HNN 98	Khammouane Province	Laos	KJ817429	—
Cyrtodactylus aff. darevskii	SNN 2013d ZISPFN 185	Na Hom Village, Khammouan Province	Laos	KF929542	—
Cyrtodactylus aff. darevskii	SNN 2013d ZISPFN 186	Na Hom Village, Khammouan Province	Laos	KF929543	—
Cyrtodactylus aff. martini	SNN 2013c KIZ 2011.03	Xishuangbanna, Yunnan Province	China	KF929537	—
Cyrtodactylus aff. roesleri	4 MDL 2014 HNN 68	Khammouane Province	Laos	KJ817437	—
Cyrtodactylus aff. ziegleri	SNN 2013 VNMN 2014	Na Nung, Dak Nong Province	Vietnam	KF169975	—
Cyrtodactylus aff. ziegleri	SNN 2013 VNMN 2015	Na Nung, Dak Nong Province	Vietnam	KF169976	—
Cyrtodactylus annadalei	CAS 215722	Alaung Daw Kathapa NP	Myanmar	MF169899	JX440524
Cyrtodactylus aurensis	LSUHC 7286	Pulau Aur, Johor	W. Malaysia	MF169900	JX440525
Cyrtodactylus aurensis	LSUHC 7300	Pulau Aur, Johor	W. Malaysia	MF169901	—
Cyrtodactylus ayeyawardensis	CAS 216459	Than Dawe District, Rakhine State	Myanmar	MF169902	JX440526
Cyrtodactylus badenensis	KIZ 13689	Mt. Ba Den, Tay Ninh Province	Vietnam	KF929505	—
Cyrtodactylus battalensis	PMNH 2301	Battagram City, NWFP	Pakistan	MF169903	KC152035
Cyrtodactylus bichnganae	UNS 0473	Son La Urban, Son La Province	Vietnam	MF169904	MF169953
Cyrtodactylus bidoupimontis	ITBCZ 1536	Bi Doup, Nui Ba NP, Lam Dong Province	Vietnam	KF169958	—
Cyrtodactylus bidoupimontis	ITBCZ 1537	Bi Doup, Nui Ba NP, Lam Dong Province	Vietnam	KF169959	—
Cyrtodactylus brevidactylus	CAS 214104	Popa Mountain Park, Mandalay Division	Myanmar	MF169905	JX440527
Cyrtodactylus bugiamapensis	ITBCZ 1562	Bu Gia Map NP	Vietnam	KF169961	—
Cyrtodactylus bugiamapensis	KIZ 45	Bu Gia Map NP	Vietnam	KF169965	—
Cyrtodactylus caovansungi	ITBCZ 2305; UNS 0304	Nui Chua NP, Ninh Thuan Province	Vietnam	—	MF169954
Cyrtodactylus caovansungi	ITBCZ 1113	Nui Chua NP, Ninh Thuan Province	Vietnam	KF219680	—
Cyrtodactylus caovansungi	ITBCZ 932	Nui Chua NP, Ninh Thuan Province	Vietnam	KF219679	—
Cyrtodactylus cattienensis	UNS 0368	Ma Da SFE, Dong Nai Province	Vietnam	—	MF169955
Cyrtodactylus cattienensis	UNS 0389	Ma Da SFE, Dong Nai Province	Vietnam	—	MF169956
Cyrtodactylus cattienensis	ITBCZ 1532	Cat Tien NP	Vietnam	KF169956	—
Cyrtodactylus cattienensis	ITBCZ 1533	Cat Tien NP	Vietnam	KF169957	—
Cyrtodactylus cattienensis	ITBCZ 1534	Cat Tien NP	Vietnam	KF929506	—
Cyrtodactylus cattienensis	ITBCZ 1535	Cat Tien NP	Vietnam	KF929507	—
Cyrtodactylus cavernicolus	LSUHC 4056	Niah Cave, Sarawak	E. Malaysia	—	JX440528
Cyrtodactylus cavernicolus	LLG 4055	Niah Cave, Sarawak	E. Malaysia	MF169906	—
Cyrtodactylus cf. chaquangensis	UNS 0505	Chau Quang Commune, Nghe An Province	Vietnam	MF169907	MF169957
Cyrtodactylus cf. khammounensis	SNN 2013e ZISPFN 191	Na Hom Village, Khammouan Province	Laos	KF169958	—
Cyrtodactylus cf. khammounensis	SNN 2013e ZISPFN 192	Na Hom Village, Khammouan Province	Laos	KF169959	—
Cyrtodactylus cf. yangbayensis	RuHF ZMMU R 13090.1	Ba Ho cascade, Khanh Hoa Province	Vietnam	KC016081	—
Cyrtodactylus cf. ziegleri	ITBCZ 2051; UNS 5006	Chu Yang Sin NP, Dak Lak Province	Vietnam	KF169946	—
Cyrtodactylus cf. ziegleri	ITBCZ 2052; UNS 5007	Chu Yang Sin NP, Dak Lak Province	Vietnam	KF169945	—
Cyrtodactylus chanhomae	CUM Z 2003.62	Thep Nimit Cave, Saraburi Province	Thailand	MF169908	JX440529
Cyrtodactylus chrysophylos	CAS 226141	Panlaung-Pyadalin Cave, Shan State	Myanmar	MF169909	JX440530
Cyrtodactylus condorensis	ITBCZ 2231; UNS 0431	Con Dao NP, Ba Ria-Vung Tau Province	Vietnam	MF169910	MF169958
Cyrtodactylus consobrinus	LSUHC 4062	Niah Cave, Sarawak	E. Malaysia	—	EU268349
Cyrtodactylus consobrinus	LSUHC 6546	Selangor	W. Malaysia	MF169911	JX440532
Cyrtodactylus consobrinus	ZMMUR 12644.1	"without precise locality"	Malaysia	HQ967204	—
Cyrtodactylus cryptus	PNKB 1	Phong Nha-Ke Bang NP	Vietnam	KF169969	—
Cyrtodactylus cryptus	PNKB 2	Phong Nha-Ke Bang NP	Vietnam	KF169970	—
Cyrtodactylus cryptus	PNKB 3	Phong Nha-Ke Bang NP	Vietnam	KF169971	—
Cyrtodactylus cryptus	PNKB 4	Phong Nha-Ke Bang NP	Vietnam	KF169972	—
Cyrtodactylus cucdongensis	ITBCZ 2344; UNS 0544	Hon Heo Mountain, Khanh Hoa Province	Vietnam	Awaiting accession	MF169959

Continued

Genus & species	Collection #	Locality	Country	Genbank #	
				COI	ND2
Cyrtodactylus cucdongensis	VNMN A 2013 18	Cuc Dong Cape, Khanh Hoa Province	Vietnam	KJ403845	—
Cyrtodactylus cucdongensis	ZFMK 95513	Cuc Dong Cape, Khanh Hoa Province	Vietnam	KJ403847	—
Cyrtodactylus cucphuongensis	ITBCZ 2206; UNS 0406	Cuc Phuong NP, Ninh Binh Province	Vietnam	MF169912	—
Cyrtodactylus darevskii	RN 2012 ZISP FN 187	Na Home, Boulapha, Khammouane Province	Laos	HQ967223	—
Cyrtodactylus darevskii	RN 2012 ZISP FN 188	Na Home, Boulapha, Khammouane Province	Laos	HQ967225	—
Cyrtodactylus dati	ITBCZ 2343; UNS 0543	Bu Dop, Binh Phuoc Province	Vietnam	—	MF169960
Cyrtodactylus dati	ITBCZ 2537	Bu Dop, Binh Phuoc Province	Vietnam	KF929508	—
Cyrtodactylus dati	ITBCZ 2538	Bu Dop, Binh Phuoc Province	Vietnam	KF929509	—
Cyrtodactylus eisenmanae	LSUHC 8598	Hon Son Island, Kien Giang Province	Vietnam	—	JX440534
Cyrtodactylus eisenmanae	UNS 0479	Hon Son Island, Kien Giang Province	Vietnam	MF169913	MF169961
Cyrtodactylus elok	LSUHC 6471	Fraser's Hill, Pahang	W. Malaysia	—	JQ889180
Cyrtodactylus elok	JB 14	Captive	NA	MF169914	—
Cyrtodactylus elok	ZMMU RAN 1991	"without precise locality"	Malaysia	HM888478	—
Cyrtodactylus feae	USNM 559805	Popa Mountain Park, Mandalay Division	Myanmar	MF169915	JX440536
Cyrtodactylus gansi	CAS 222412	Min Dat District, Chin State	Myanmar	MF169916	JX440537
Cyrtodactylus grismeri	LSUHC 8638	Tuc Dup Hill, An Giang Province	Vietnam	—	JX440538
Cyrtodactylus grismeri	UNS 0510	Tuc Dup Hill, An Giang Province	Vietnam	—	MF169962
Cyrtodactylus grismeri	ITBCZ 683	Mt. Tuc Dup, An Giang Province	Vietnam	KF929512	—
Cyrtodactylus grismeri	ITBCZ 684	Mt. Tuc Dup, An Giang Province	Vietnam	KF929513	—
Cyrtodactylus hontreensis	LSUHC 8583	Hon Tre Island, Kien Giang Province	Vietnam	MF169917	JX440539
Cyrtodactylus huynhi	UNS 0413	Chua Chan Mountain, Dong Nai Province	Vietnam	—	MF169963
Cyrtodactylus huynhi	ITBCZ 511	Mt. Chua Chan, Dong Nai Province	Vietnam	KF169947	—
Cyrtodactylus interdigitalis	FMNH 255454	Nakai District, Khammouan Province	Lao PDR	MF169919	JQ889181
Cyrtodactylus intermedius	FMNH 265812	Muang Sa Kaeo, Sa Kaeo	Thailand	MF169920	JQ889182
Cyrtodactylus intermedius	LSUHC 9513	Khao Khitchakut, Chantaburi Province	Thailand	—	JX519469
Cyrtodactylus intermedius	ITBCZ 638	Mt. Nui Cam, An Giang Province	Vietnam	KF929521	—
Cyrtodactylus intermedius	ITBCZ 639	Mt. Nui Cam, An Giang Province	Vietnam	KF929522	—
Cyrtodactylus intermedius	ZMMU R 11213 1	Phnom Bakor NP	Cambodia	KC016076	—
Cyrtodactylus irregularis	FMNH 258697	Pakxong District, Champasak Province	Lao PDR	—	JX440540
Cyrtodactylus irregularis	UNS 0269	Bi Doup, Nui Ba NP, Lam Dong Province	Vietnam	MF169921	MF169964
Cyrtodactylus jarakensis	LSUHC 8990	Pulau Jarak, Perak	W. Malaysia	MF169922	MF169965
Cyrtodactylus jellesmae	MVZ 239337	Propinsi Sulawesi Selatan, Sulawesi	Indonesia	MF169923	JX440542
Cyrtodactylus khammounensis	RN 2012 ZISP FN 191	Na Hom Village, Khammouan Province	Laos	HM888467	—
Cyrtodactylus khammounensis	RN 2012 ZISP FN 192	Na Hom Village, Khammouan Province	Laos	HM888468	—
Cyrtodactylus khasiensis	MFA 50083	Kaziranga, Assam	India	MF169924	JX440543
Cyrtodactylus kingsadai	IEBRA 2013 3	Dai Lanh, Phu Yen Province	Vietnam	KF188432	—
Cyrtodactylus lomyenensis	UNS 0534	Lom Yen Cave, Khammouane Province	Laos	—	MF169966
Cyrtodactylus lomyenensis	IEBR KM 2012.54	Lom Yen, Gnommalath, Khammouane Province	Laos	KP199942	—
Cyrtodactylus loriae	FK 7709	Mt. Simpson, Milne Bay Province	Papua New Guinea	MF169925	EU268350
Cyrtodactylus louisiadensis	NA	Sudest Island	Papua New Guinea	—	HQ401190
Cyrtodactylus louisiadensis	BPBM 15434	Mt. Pekopekowana, Milne Bay Province	Papua New Guinea	MF169926	—
Cyrtodactylus louisiadensis	BPBM 18654	Apele, Morobe Province	Papua New Guinea	MF169927	—
Cyrtodactylus marmoratus	ABTC 48075	Java	Indonesia	—	GQ257747

Continued

Genus & species	Collection #	Locality	Country	Genbank #	
				COI	ND2
Cyrtodactylus marmoratus	JAM 2242	NA	NA	MF169928	MF169967
Cyrtodactylus martini	UNS 0471	Lai Chau Province	Vietnam	MF169929	MF169968
Cyrtodactylus multiporus	RN 2012 ZMMU RAN 1996 2	Na Hom Village, Khammouan Province	Laos	HQ967193	—
Cyrtodactylus multiporus	RN 2012 ZMMU RAN 1998	Na Hom Village, Khammouan Province	Laos	HQ543943	—
Cyrtodactylus namhiakensis	UNS 0529	Nam Hiak Cave, Khammouane Province	Vietnam	MF169930	—
Cyrtodactylus nigriocularis	VNMN 2187	Mt. Ba Den, Tay Ninh Province	Vietnam	KF929523	—
Cyrtodactylus novaeguineae	BPM 23316	Toricelli Mountains, West Sepik Province	Papua New Guinea	—	JX440547
Cyrtodactylus novaeguineae	BMBM 18655	Mt. Shungoi, Morobe Province	Papua New Guinea	MF169931	—
Cyrtodactylus oldhami	JB 126	captive	NA	MF169932	JX440548
Cyrtodactylus pageli	ZFMK 91827	Vientiane Province	Laos	KJ817431	—
Cyrtodactylus (*paradoxus*) *condorensis*	LSUHC 8672	Hon Nghe Island	Vietnam	—	JX440549
Cyrtodactylus (*paradoxus*) *condorensis*	KIZ 1022	Hon Chong, Kien Giang Province	Vietnam	KF929524	—
Cyrtodactylus (*paradoxus*) *condorensis*	KIZ 1023	Hon Chong, Kien Giang Province	Vietnam	KF929525	—
Cyrtodactylus (*paradoxus*) *condorensis*	ZMMU RAN 1987	Koh Tang Island	Cambodia	HM888464	—
Cyrtodactylus peguensis	CUM Z R2005.07.30.54	Khao Luang NP	Thailand	—	GU550727
Cyrtodactylus peguensis	CAS 214029	Popa Mountain Park, Mandalay Division	Myanmar	MF169933	—
Cyrtodactylus phongnhakebangensis	UNS 0347	Phong Nha-Ke Bang NP, Quang Binh Province	Vietnam	—	MF169970
Cyrtodactylus phongnhakebangensis	PNKN 2011.30	Phong Nha-Ke Bang NP, Quang Binh Province	Vietnam	KF929526	—
Cyrtodactylus phongnhakebangensis	PNKN 2011.32	Phong Nha-Ke Bang NP, Quang Binh Province	Vietnam	KF929527	—
Cyrtodactylus phuquocensis	UNS 0273	Phu Quoc NP, Kien Giang Province	Vietnam	MF169934	MF169971
Cyrtodactylus pseudoquadrivirgatus	UNS 0249	Ba Na NR, Da Nang City	Vietnam	—	MF169972
Cyrtodactylus pseudoquadrivirgatus	UNS 0379	Son Tra NR, Da Nang City	Vietnam	—	MF169973
Cyrtodactylus pseudoquadrivirgatus	ITBCZ 30001	A Luoi, Hue Province	Vietnam	KF169963	—
Cyrtodactylus pubisulcus	LSUHC 4069	Niah Cave, Sarawak	E. Malaysia	—	JX4405510
Cyrtodactylus pubisulcus	ZMMUR 13091.3	near Tondong, Sarawak	E. Malaysia	HQ967199	—
Cyrtodactylus pulchellus	LSUHC 6637	Genting Highlands, Selangor	NA	MF169935	—
Cyrtodactylus pulchellus	LSUHC 6729	Moongate Trail, Pulau Pinang	W. Malaysia	MF169936	MF169974
Cyrtodactylus pulchellus	ZMMU R 12643.2	"without precise locality"	Malaysia	HQ967201	—
Cyrtodactylus quadrivirgatus	LSUHC 4813	Pulau Tioman, Pahang	W. Malaysia	—	JX440553
Cyrtodactylus quadrivirgatus	LSUHC 9869	Bukit Larut, Perak	W. Malaysia	—	JQ889252
Cyrtodactylus quadrivirgatus	JB 78	Captive	NA	MF169937	—
Cyrtodactylus quadrivirgatus	ZMMUR AN 1990	"without precise locality"	Malaysia	HM888466	—
Cyrtodactylus roesleri	PNKB 20111	Phong Nha-Ke Bang NP	Vietnam	KF929530	—
Cyrtodactylus roesleri	PNKB 20113	Phong Nha-Ke Bang NP	Vietnam	KF929531	—
Cyrtodactylus russelli	CAS 226137	Htamanthi Wildlife Sanctuary, Sagaing Division	Myanmar	MF169938	JX440555
Cyrtodactylus seribuatensis	LSUHC 6348	Pulau Mentigi, Johor	W. Malaysia	MF169939	JX440557
Cyrtodactylus seribuatensis	LSUHC 6349	Pulau Mentigi, Johor	W. Malaysia	MF169940	MF169976
Cyrtodactylus sermowaiensis	BPM 23317	Toricelli Mountains, West Sepik Province	Papua New Guinea	—	JX440558
Cyrtodactylus sermowaiensis	BMBM 23317	Toricelli Mountains, West Sepik Province	Papua New Guinea	MF169941	—
Cyrtodactylus sermowaiensis	BPBM 23320	Toricelli Mountains, West Sepik Province	Papua New Guinea	MF169942	—
Cyrtodactylus slowinskii	CAS 210205	Alaung Daw Kathapa NP	Myanmar	MF169943	JX440559
Cyrtodactylus sp. 1	RuHF ZMMU R 11503.2	Mt. Nui Chua NP, Ninh Thuan Province	Vietnam	KC016080	—
Cyrtodactylus sp. 1	SNN 2013 ITBCZ 1150	Mt. Nui Chua NP, Ninh Thuan Province	Vietnam	KF929540	—
Cyrtodactylus sp. 1	SNN 2013 ITBCZ 965	Mt. Nui Chua NP, Ninh Thuan Province	Vietnam	KF929538	—
Cyrtodactylus sp. 1	SNN 2013b ITBCZ 1117	Mt. Nui Chua NP, Ninh Thuan Province	Vietnam	KF929539	
Cyrtodactylus sp. W	SNN 2013 ITBCZ 2532	Ba Na Resort, Da Nang City	Vietnam	KF169962	—
Cyrtodactylus phuocbinhensis	SNN 2013 ITBCZ 1518	Phuoc Binh NP	Vietnam	KF169953	—

Continued

Genus & species	Collection #	Locality	Country	Genbank #	
				COI	ND2
Cyrtodactylus phuocbinhensis	SNN 2013 ITBCZ 1529	Phuoc Binh NP	Vietnam	KF169954	—
Cyrtodactylus taynguyenensis	SNN 2013 ROM 32119	Krongpa Village, Gia Lai Province	Vietnam	KF169978	—
Cyrtodactylus taynguyenensis	SNN 2013 ROM 32120	Krongpa Village, Gia Lai Province	Vietnam	KF169979	—
Cyrtodactylus sp. 4	RuHF ZMMU RAN 1994	NA	NA	KC016078	—
Cyrtodactylus sp. 4	RuHF ZMMU RAN 1995	NA	NA	KC016079	—
Cyrtodactylus sp. X	MDL 2014 LPB 62	Luang Prabang Province	Laos	KJ817432	—
Cyrtodactylus sp. X	MDL 2014 LPB 63	Luang Prabang Province	Laos	KJ817433	—
Cyrtodactylus sp. Z	ENS 7764	Sumatra	Indonesia	MF169944	—
Cyrtodactylus sworderi	LSUHC 7685	Endau-Rompin, Johor	W. Malaysia	MF169945	JQ889189
Cyrtodactylus sworderi	LSUHC 7700	Endau-Rompin, Johor	W. Malaysia	MF169946	—
Cyrtodactylus takouensis	UNS 0486	Ta Kou NR, Binh Thuan Province	Vietnam	—	MF169978
Cyrtodactylus takouensis	ITBCZ 2527	Ta Kou NR, Binh Thuan Province	Vietnam	KF929533	—
Cyrtodactylus takouensis	ITBCZ 2528	Ta Kou NR, Binh Thuan Province	Vietnam	KF929534	—
Cyrtodactylus teyniei	KM 2012.77	Khammouane Province	Laos	KP199945	—
Cyrtodactylus (*thochuensis*) *leegrismeri*	UNS 0498	Tho Chu Island, Kien Giang Province	Vietnam	MF169947	MF169979
Cyrtodactylus tigroides	IRSNB 2380	Sai-Yok District, Kanchanaburi Province	Thailand	MF169948	JX440562
Cyrtodactylus tiomanensis	LSUHC 6251	Pulau Tioman, Pahan	W. Malaysia	MF169949	JX440563
Cyrtodactylus tiomanensis	LSUHC 6268	Pulau Tioman, Pahan	W. Malaysia	MF169950	—
Cyrtodactylus triedrus	Anslem de Silva 35 A	Yakkunehela	Sri Lanka	MF169951	JX440522
Cyrtodactylus vilaphongi	IEBRA 2013 103	Luang Prabang Province	Laos	KJ817435	—
Cyrtodactylus vilaphongi	NUOL R 2013 5	Luang Prabang Province	Laos	KJ817434	—
Cyrtodactylus wayakonei	ZFMK 91016	Luang Nam Tha Province	Laos	KJ817438	—
Cyrtodactylus yangbayensis	UNS 0407	Hon Ba NR, Khanh Hoa Province	Vietnam	—	MF169980
Cyrtodactylus yangbayensis	UNS 0476	Yang Bay Waterfall, Khanh Hoa Province	Vietnam	MF169952	—
Cyrtodactylus yoshii	ZRC 2.4851	Poring Hot Spring, Sabah	E. Malaysia	Awaiting accession	JX440565
Cyrtodactylus ziegleri	ZMMU R 13116 3	NA	NA	HQ967210	—
Cyrtodactylus ziegleri	ZMMU R 13116.4	NA	NA	HQ967211	—

Table 1. List of samples used in this study with appropriate voucher (museum or field) numbers, locality data, and GenBank accession numbers. *Abbreviations*: Eric N Smith, University of Texas, Arlington, USA (ENS); Kunming Institute of Zoology, China (KIZ); California Academy of Sciences, USA (CAS); La Sierra University Herpetological Collection, USA (LSUHC); L. Lee Grismer field series (LLG); United States National Museum, USA (UNS); Institute of Tropical Biology Zoological Collection, Vietnam (ITBCZ); Pakistan Museum of Natural History Museum, Pakistan (PMNH); Zoological Institute, St. Petersburg (ZISPFN); Chulalongkorn University Museum of Zoology, Thailand (CUMZ); Zoological Museum Moscow State University, Russia (ZMMUR); Phong Nha-Ke Bang, Vietnam (PNKB); Zoologisches Forschungsmuseum Alexander Koenig, Germany (ZFMK); Jon Boone captive series (JB); Field Museum of Natural History, USA (FMNH); Museum of Vertebrate Zoology, University of California, Berkeley, USA (MVZ); Institute of Ecology and Biological Resources, Vietnam (IEBRA); M. Firoz Ahmed field series (MFA); Fred Kraus field series (FK); Australian Biological Tissue Collection, Australia (ABTC); Bernice P. Bishop Museum (BPBM); Royal Ontario Museum, Canada (ROM); Institute des Sciences Naturelles du Belgique, Belgium (IRSNB); National University of Laos, Laos (NUOL); Zoological Research Collection, Raffles Museum of Biodiversity, National University of Singapore (ZRC); Jimmy A. McGuire (JAM).

After extracting genomic DNA from liver, heart, or tail tissue preserved in 95–100% ethanol via Qiagen DNeasy Blood and Tissue kits (Qiagen), isolated DNA was quantified using a NanoDrop spectrophotometer (Thermo Scientific). Samples for *COI* amplification and sequencing were sent to South China DNA Barcoding Center at the Kunming Institute of Zoology. *ND2* samples were amplified via polymerase chain reaction using standard primers and protocols[22]. All sequences were assembled, edited, and aligned in Geneious v.7, and protein-coding regions were translated to amino acid sequences to maintain proper reading frames and avoid premature stop codons. tRNA secondary structure was addressed and adjusted by eye for consistency. Final *COI* and *ND2* alignments stretched 677 and 1,512 bp, respectively.

Phylogenetic Analyses. Datasets of mitochondrial loci *COI* and *ND2* were analyzed independently via the maximum likelihood (ML) framework for phylogenetic inference. The alignments of both genes were standardized to include the same species and wherever possible, the same specimens, to allow for direct comparison of results. An additional *COI* alignment of two samples per species for all available species (GenBank accession numbers of some recently described species remain unavailable) were combined to create a matrilineal genealogy representing all currently barcoded *Cyrtodactylus*.

We used the Akaike Information Criterion (AIC) in PartitionFinder[50] to establish the most accurate models of evolution based on locus and codon position, specific to our analytical program (RAxML). ML analyses were carried out in RAxML 8.0[51] via the CIPRES supercomputing portal[52]. *COI* was analyzed as a single locus, and *ND2* was partitioned into the protein coding region and tRNAs. We employed the GTR+I+Γ model of evolution, and ran the program for 100 independent tree searches to find the best topology, and 5000 bootstrap replicates to retrieve topological support values.

Accession Codes (Data Availability). All accession numbers are included in Table 1, except where pending acceptance to GenBank (noted as 'Awaiting accession').

References

1. Ward, R. D., Zemlak, T. S., Innes, B. H., Last, P. R. & Hebert, P. D. N. DNA barcoding Australia's fish species. *Philos. Trans. R. Soc. Lond. B. Biol. Sci* **360**, 1847–1857 (2005).
2. Steinke, D., Zemlak, T. S. & Hebert, P. D. N. Barcoding Nemo: DNA-based identifications for the ornamental fish trade. *PLoS. ONE* **4**, e6300 (2009).
3. Aliabadian, M., Kaboli, M., Nijman, V. & Vences, M. Molecular identification of birds: Performance of distance-based DNA barcoding in three genes to delimit parapatric species. *PLoS. ONE* **4**, e4119 (2009).
4. Holmes, B. H., Steinke, D. & Ward, R. D. Identification of shark and ray fins using DNA barcoding. *Fisheries Research* **95**, 280–288 (2009).
5. Bucklin, A., Steinke, D. & Blanco-Bercial, L. DNA barcoding of marine Metazoa. *Ann. Rev. Marine Sci* **3**, 471–508 (2011).
6. Murphy, R. W. *et al*. Cold Code: the global initiative to DNA barcode amphibians and nonavian reptiles. *Mol. Ecol.* **13**, 161–167 (2013).
7. Vernooy, R. *et al*. Barcoding Life to Conserve Biological Diversity: Beyond the Taxonomic Imperative. *PLoS. Biol* **8**, e1000417 (2010).
8. Shen, Y.-Y., Chen, X. & Murphy, R. W. Assessing DNA Barcoding as a Tool for Species Identification and Data Quality Control. *PLoS. ONE* **8**, e57125 (2013).
9. Strutzenberger, P., Brehm, G. & Fiedler, K. DNA barcoding-based species delimitation increases species count of *Eois* (Geometridae) moths in a well-studied tropical mountain forest by up to 50%. *Insect Sci* **18**, 349–362 (2011).
10. Johnsen, A. *et al*. DNA barcoding of Scandinavian birds reveals divergent lineages in trans-Atlantic species. *J. Ornithol.* **151**, 565–578 (2010).
11. Hajibabaei, M., Singer, G. A. C., Hebert, P. D. N. & Hickey, D. A. DNA barcoding: how it complements taxonomy, molecular phylogenetics and population genetics. *Trends Genet.* **23**, 167–172 (2007).
12. Moritz, C. & Cicero, C. DNA Barcoding: Promise and Pitfalls. *PLoS. Biol* **2**, e354 (2004).
13. Whitworth, T., Dawson, R., Magalon, H. & Baudry, E. DNA barcoding cannot reliably identify species of the blowfly genus *Protocalliphora* (Diptera: Calliphoridae). *ProC.R. Soc. B Biol. Sci.* **274**, 1731–1739 (2007).
14. Johnson, N. K. & Cicero, C. New mitochondrial DNA data affirm the importance of Pleistocene speciation in North American birds. *Evolution* **58**, 1122–1130 (2004).
15. Trewick, S. A. DNA Barcoding is not enough: mismatch of taxonomy and genealogy in New Zealand grasshoppers (Orthoptera: Acrididae). *Cladistics* **24**, 240–254 (2008).
16. Meier, R., Shiyang, K., Vaidya, G. & Ng, P. K. DNA barcoding and taxonomy in Diptera: a tale of high intraspecific variability and low identification success. *Syst. Biol* **55**, 715–728 (2006).
17. Smith, M. A. *et al*. Extreme diversity of tropical parasitoid wasps exposed by iterative integration of natural history, DNA barcoding, morphology, and collections. *Proc. Natl. Acad. Sci. U.* **105**, 12359–12364 (2008).
18. Wilson, J. *et al*. Identity of the ailanthus webworm moth (Lepidoptera, Yponomeutidae), a complex of two species: evidence from DNA barcoding, morphology and ecology. *ZooKeys* **46**, 41–60 (2010).
19. Will, K. W., Mishler, B. D. & Wheeler, Q. D. The perils of DNA barcoding and the need for integrative taxonomy. *Syst. Biol* **54**, 844–851 (2005).
20. Nguyen, N. S. *et al*. Phylogeny of the *Cyrtodactylus irregularis* species complex (Squamata: Gekkonidae) from Vietnam with the description of two new species. *Zootaxa* **3737**, 399–414 (2013).
21. Nazarov, R. *et al*. Two new cryptic species of the *Cyrtodactylus irregularis* complex (Squamata: Gekkonidae) from southern Vietnam. *Zootaxa* **3302**, 1–24 (2012).
22. Wood, P. L. Jr., Heinicke, M. P., Jackman, T. R. & Bauer, A. M. Phylogeny of bent-toed geckos (*Cyrtodactylus*) reveals a west to east pattern of diversification. *Mol. Phylogenet. Evol.* **65**, 992–1003 (2012).
23. Agarwal, I. & Karanth, K. P. A phylogeny of the only ground-dwelling radiation of *Cyrtodactylus* (Squamata, Gekkonidae): diversification of *Geckoella* across peninsular India and Sri Lanka. *Mol. Phylogenet. Evol.* **82**(Part A), 193–199 (2015).
24. Ziegler, T., Phung, M. T., Le, D. M. & Nguyen, Q. T. A new Cyrtodactylus (Squamata: Gekkonidae) from Phu Yen Province, southern Vietnam. *Zootaxa* **3686**, 432–446 (2013).
25. Schneider, N., Phung, M. T., Le, D. M., Nguyen, Q. T. & Ziegler, T. A new Cyrtodactylus (Squamata: Gekkonidae) from Khanh Hoa Province, southern Vietnam. *Zootaxa* **3785**, 518–532 (2014).
26. Sumontha, M., Pauwels, O. S., Panitvong, N., Kunya, K. & Grismer, L. L. A new lowland forest Bent-toed Gecko (Squamata: Gekkonidae: Cyrtodactylus) from Ranong Province, peninsular Thailand. *Zootaxa* **3911**, 106–118 (2015).
27. Kunya, K. *et al*. A new forest-dwelling Bent-toed Gecko (Squamata: Gekkonidae: *Cyrtodactylus*) from Doi Inthanon, Chiang Mai Province, northern Thailand. *Zootaxa* **3905**, 573–584 (2015).
28. Grismer, L. L., Anuar, S., Davis, H., Cobos, A. & Murdoch, M. A new species of karst forest Bent-toed Gecko (genus *Cyrtodactylus* Gray) not yet threatened by foreign cement companies and a summary of Peninsular Malaysia's endemic karst forest herpetofauna and the need for its conservation. *Zootaxa* **4061**, 1–17 (2016).
29. Luu, Q. V. *et al*. *Cyrtodactylus rufford*, a new cave-dwelling Bent-Toed Gecko (Squamata: Gekkonidae) from Khammouane Province, central Laos. *2016* **4067**, 15 (2016).
30. Pauwels, O. S. G., Sumontha, M. & Bauer, A. M. A new Bent-Toed Gecko (Squamata: Gekkonidae: *Cyrtodactylus*) from Phetchaburi Province. *Thailand. 2016* **4088**, 11 (2016).
31. Oliver, P. M., Richards, J., Mumpuni, M. & Rösler, H. The Knight and the King: two new species of giant Bent-Toed Gecko (*Cyrtodactylus*, Gekkonidae, Squamata) from northern New Guinea, with comments on endemism in the North Papuan Mountains. *ZooKeys* 105–130 (2016).
32. Agarwal, I., Bauer, A. M., Jackman, T. R. & Karanth, K. P. Insights into Himalayan biogeography from geckos: A molecular phylogeny of *Cyrtodactylus* (Squamata: Gekkonidae). *Mol. Phylogenet. Evol.* **80**, 145–155 (2014).
33. Wilmer, J. W. & Couper, P. Phylogeography of north-eastern Australia's *Cyrtodactylus* radiation: a habitat switch highlights adaptive capacity at a generic level. *Aust. J. Zool.* **63**, 398–410 (2016).
34. Uetz, P. & Hošek, J. *The Reptile Database*, http://www.reptile-database.reptarium.cz/ (11/11/2016) (2016).
35. de Bruyn, M. *et al*. Borneo and Indochina are major evolutionary hotspots for Southeast Asian biodiversity. *Syst. Biol* **63**, 879–901 (2014).

36. Nazarov, R. *et al*. A review of genus *Cyrtodactylus* (Reptilia: Sauria: Gekkonidae) in fauna of Laos with description of four new species. *Proc. Zool. Inst. Russian Acad. Sci.* **318**, 391–423 (2014).
37. Nguyen, N. S. *et al*. DNA barcoding of Vietnamese bent-toed geckos (Squamata: Gekkonidae: Cyrtodactylus) and the description of a new species. *Zootaxa* **3784**, 48–66 (2014).
38. Grismer, L. L., Wood, P. L. J., Ngo, V. T. & Murdoch, M. L. The systematics and independent evolution of cave ecomorphology in distantly related clades of Bent-toed Geckos (Genus *Cyrtodactylus* Gray, 1827) from the Mekong Delta and islands in the Gulf of Thailand. *2015* **3980**, 21 (2015).
39. Grismer, L. L., Anuar, S., Muin, M. A., Quah, E. & Wood, P. Phylogenetic relationships and description of a new upland species of Bent-Toed Gecko (*Cyrtodactylus* Gray, 1827) of the *C. sworderi* complex from northeastern Peninsular Malaysia. *Zootaxa* **3616**, 239–252 (2012).
40. Grismer, L. L., Belabut, D. M., Quah, E. S., Onn, C. K. & Wood, P. L. Jr. A new species of karst forest-adapted Bent-Toed Gecko (genus *Cyrtodactylus* Gray, 1827) belonging to the C. sworderi complex from a threatened karst forest in Perak, Peninsular Malaysia. *Zootaxa* **3755**, 434–446 (2014).
41. Grismer, L. L. *et al*. A phylogeny and taxonomy of the Thai-Malay Peninsula Bent-Toed Geckos of the *Cyrtodactylus pulchellus* complex (Squamata: Gekkonidae): combined morphological and molecular analyses with descriptions of seven new species. *Zootaxa* **3520**, 1–55 (2012).
42. Oliver, P. M., Skipwith, P. & Lee, M. S. Crossing the line: increasing body size in a trans-Wallacean lizard radiation (*Cyrtodactylus*, Gekkota). *Biol. Lett.* **10**, 20140479 (2014).
43. Bauer, A. M. & Doughty, P. A new Bent-Toed Gecko (Squamata: Gekkonidae: *Cyrtodactylus*) from the Kimberley region, Western Australia. *Zootaxa* **3187**, 32–42 (2012).
44. Nguyen, N. S., Orlov, N. L. & Darevsky, I. S. Descriptions of two new species of the genus *Cyrtodactylus* Gray, 1827 (Squamata: Sauria: Gekkonidae) from southern Vietnam. *Russ. J. Herpetol* **13**, 215–226 (2013).
45. Pauwels, O. S. G. & Sumontha, M. *Cyrtodactylus samroiyot*, a new limestone-dwelling Bent-Toed Gecko (Squamata: Gekkonidae) from Prachuap Khiri Khan Province, peninsular Thailand. *Zootaxa* **3755**, 573–583 (2014).
46. Pauwels, O. S. G., Sumontha, M., Latinne, A. & Grismer, L. L. *Cyrtodactylus sanook* (Squamata: Gekkonidae), a new cave-dwelling gecko from Chumphon Province, southern Thailand. *Zootaxa* 275–285 (2013).
47. Pauwels, O. S. G., Sumontha, M., Panitvong, N. & Varaguttanonda, V. *Cyrtodactylus khelangensis*, a new cave-dwelling Bent-Toed Gecko (Squamata: Gekkonidae) from Lampang Province, northern Thailand. *Zootaxa* **3755**, 584–594 (2014).
48. Sumontha, M. *et al*. A new forest-dwelling gecko from Phuket Island, Southern Thailand, related to *Cyrtodactylus macrotuberculatus* (Squamata: Gekkonidae). *Zootaxa* **3522**, 61–72 (2012).
49. Schneider, N. *et al*. A new species of karst dwelling *Cyrtodactylus* (Squamata: Gekkonidae) from northwestern Laos. *Zootaxa* **2930**, 1–21 (2011).
50. Lanfear, R., Calcott, B., Ho, S. Y. W. & Guindon, S. PartitionFinder: Combined selection of partitioning schemes and substitution models for phylogenetic analyses. *Mol. Biol. Evol.* **29**, 1695–1701 (2012).
51. Stamatakis, A. RAxML Version 8: A tool for phylogenetic analysis and post-analysis of large phylogenies. *Bioinformatics*, 1093 (2014).
52. Miller, M. A., Pfeiffer, W. & Schwartz, T. Creating the CIPRES Science Gateway for inference of large phylogenetic trees. In *Gateway Computing Environments Workshop* (*GCE*). 1–8 (IEEE, 2010).

Acknowledgements

This work was supported by the National Natural Science Foundation of China (NSFC grant no. 31090251 to Y.Z.), the Ministry of Science and Technology of China (MOST no. 2012FY110800 to W.W.), and the Joint Grant of CAS Kunming Branch and Guizhou Academy of Sciences (CASKMB no. 2014-001 to W.W.). This work was also supported by the Animal Branch of the Germplasm Bank of Wild Species, Chinese Academy of Sciences (the Large Research Infrastructure Funding, Funding code: GBOWS to W.W. and Y.Z.), an Australian American Association Fellowship to I.G.B, and National Science Foundation (USA) grants DEB 0844523 and EF 1241885 (sub-award 13-0632) to A.M.B.

Author Contributions

I.G.B. conceived the study, and analyzed the data; I.G.B., A.M.B, and R.W.M. wrote, edited, and guided the paper; N.V.T. provided necessary tissue samples; Y.y.W., W.z.W., and Y.P.Z. collected the barcoding data that made this project possible.

Additional Information

Supplementary information accompanies this paper at doi:10.1038/s41598-017-05261-9

Competing Interests: The authors declare that they have no competing interests.

Publisher's note: Springer Nature remains neutral with regard to jurisdictional claims in published maps and institutional affiliations.

References

1. Filipchenko J. 1927 *Variabilität und variation.* Berlin: Gebrunder Bortraeger.

2. Felsenstein J. 1985 Phylogenies and the comparative method. *The American Naturalist* **125**, 1–15. (doi:10.1086/284325)

3. Harvey PH, Pagel MD, others. 1991 *The comparative method in evolutionary biology.* Oxford university press Oxford.

4. Levinton JS. 1983 Stasis in progress: The empirical basis of macroevolution. *Annual Review of Ecology and Systematics* **14**, 103–137.

5. Jablonski D. 1986 Background and mass extinctions: The alternation of macroevolutionary regimes. *Science* **231**, 129–133. (doi:10.1126/science.231.4734.129)

6. Benton MJ. 1987 Progress and competition in macroevolution. *Biological Reviews* **62**, 305–338. (doi:10.1111/j.1469-185X.1987.tb00666.x)

7. Levinton JS. 2001 *Genetics, paleontology, and macroevolution.* Cambridge University Press.

8. Futuyma DJ, Agrawal AA. 2009 Macroevolution and the biological diversity of plants and herbivores. *Proceedings of the National Academy of Sciences* **106**, 18054–18061. (doi:10.1073/pnas.0904106106)

9. Stadler T. 2011 Mammalian phylogeny reveals recent diversification rate shifts. *Proceedings of the National Academy of Sciences* **108**, 6187–6192. (doi:10.1073/pnas.1016876108)

10. Crottini A, Madsen O, Poux C, Strauß A, Vieites DR, Vences M. 2012 Vertebrate time-tree elucidates the biogeographic pattern of a major biotic change around the K–T boundary in Madagascar. *Proceedings of the National Academy of Sciences* **109**, 5358–5363. (doi:10.1073/pnas.1112487109)

11. Raup D. 1986 Biological extinction in earth history. *Science* **231**, 1528–1533. (doi:10.1126/science.11542058)

12. Prothero DR. 1994 The late Eocene-Oligocene extinctions. *Annual Review of Earth and Planetary Sciences* **22**, 145–165.

13. Zanazzi A, Kohn MJ, MacFadden BJ, Terry DO. 2007 Large temperature drop across the Eocene-Oligocene transition in central North America. *Nature* **445**, 639–642. (doi:http://www.nature.com/nature/journal/v445/n7128/suppinfo/nature05551_S1.html)

14. Sun J, Ni X, Bi S, Wu W, Ye J, Meng J, Windley BF. 2014 Synchronous turnover of flora, fauna, and climate at the Eocene–Oligocene boundary in Asia. *Scientific Reports* **4**, 7463. (doi:10.1038/srep07463 http://www.nature.com/articles/srep07463#supplementary-information)

15. Hill RS. 2004 Origins of the southeastern Australian vegetation. *Philosophical Transactions of the Royal Society of London. Series B: Biological Sciences* **359**, 1537–1549.

16. Badgley C, Barry JC, Morgan ME, Nelson SV, Behrensmeyer AK, Cerling TE, Pilbeam D. 2008 Ecological changes in miocene mammalian record show impact of prolonged climatic forcing. *Proceedings of the National Academy of Sciences* **105**, 12145–12149. (doi:10.1073/pnas.0805592105)

17. Fortelius M, Eronen JT, Kaya F, Tang H, Raia P, Puolamäki K. 2014 Evolution of neogene mammals in eurasia: Environmental forcing and biotic interactions. *Annual Review of Earth and Planetary Sciences* **42**, 579–604. (doi:10.1146/annurev-earth-050212-124030)

18. Jennings WB, Pianka ER, Donnellan S. 2003 Systematics of the lizard Family Pygopodidae with implications for the diversification of Australian temperate biotas. *Systematic Biology* **52**, 757–780. (doi:10.1080/10635150390250974)

19. Rabosky DL, Donnellan SC, Talaba AL, Lovette IJ. 2007 Exceptional among-lineage variation in diversification rates during the radiation of Australia's most diverse vertebrate clade. *Proceedings of the Royal Society B Biological Sciences* **274**, 2915–2923.

20. Byrne M *et al.* 2008 Birth of a biome: Insights into the assembly and maintenance of the Australian arid zone biota. *Molecular Ecology* **17**, 4398–4417. (doi:10.1111/j.1365-294X.2008.03899.x)

21. Couzens AMC, Prideaux GJ. 2018 Rapid Pliocene adaptive radiation of modern kangaroos. *Science* **362**, 72–75. (doi:10.1126/science.aas8788)

22. Nilsson MA, Zheng Y, Kumar V, Phillips MJ, Janke A. 2018 Speciation generates mosaic genomes in kangaroos. *Genome Biol Evol* **10**, 33–44. (doi:10.1093/gbe/evx245)

23. Glor RE. 2010 Phylogenetic insights on adaptive radiation. *Annual Review of Ecol-*

ogy, Evolution, and Systematics **41**, 251–270. (doi:10.1146/annurev.ecolsys.39.110707.173447)

24. Losos JB. 2010 Adaptive radiation, ecological opportunity, and evolutionary determinism. *The American Naturalist* **175**, 623–639. (doi:10.1086/652433)

25. Brown WL, Wilson EO. 1956 Character displacement. *Systematic Zoology* **5**, 49–64. (doi:10.2307/2411924)

26. Sepkoski Jr JJ. 1996 Competition in macroevolution: The double wedge revisited. *Evolutionary paleobiology*, 211–255.